

Controls on organic-rich mudstone deposition: The Devonian Duvernay Formation, Alberta,  
Canada

by

Levi J. Knapp

A thesis submitted in partial fulfillment of the requirements for the degree of

Master of Science

Department of Earth and Atmospheric Sciences  
University of Alberta

© Levi J. Knapp, 2016

**Abstract:**

The Upper Devonian Duvernay Formation of Western Canada is a prolific source rock that in recent years has become an exploration target for shale gas and liquids. Development of the Duvernay Formation has demonstrated the importance of robust models for rock properties such as porosity, permeability, organic richness, and fracturability. Depositional processes and conditions govern the character and distribution of mudstone lithofacies, which are directly linked to variations in rock properties. The depositional and sequence stratigraphic models presented here are based on a detailed sedimentology and stratigraphy study.

Twelve lithofacies were characterized based on lithology, sedimentary and biogenic structures, fossil type and abundance, and type and abundance of cement. Significant variation exists between organic-rich lithofacies, indicating that organic-rich mudstones were deposited in variably energetic and oxygenated environments, rather than within persistently anoxic, stagnant bottom waters.

Correlation of core descriptions to a network of 759 wells with wireline logs led to the creation of a basin-scale sequence stratigraphic framework with 3 third order sequences. The sequence stratigraphic model shows a strong sea level and basin morphology control on basinal lithofacies. Transgression, and subsequent highstand normal regression in sequence 1 (oldest) resulted in significant platform construction in the northeast side of the basin. Sediments become consistently finer-grained and organic-rich away from the platform. Major transgression at the start of sequence 2 resulted in flooding of the platform and significant upslope trapping of sediments, locally so significant that no sediment reached the platform edge and large zones of non-deposition developed. Lithofacies basinward of these zones are especially clay mineral-poor and organic-rich. A sea level stillstand or lowstand at the base of sequence 3 resulted in

progradation of basin-margin facies, reduction in the extent of organic-rich mudstone deposition, and an influx of clay minerals into the basin.

The geographic extent of organic-rich, siliceous mudstone deposition was greatest during transgressive and highstand systems tracts. Sustained highstands resulted in increased carbonate sedimentation, which diluted organic matter. Sea level stillstands resulted in progradation of argillaceous sediment, and reduction of TOC values due to dilution and oxygenation.

## PREFACE:

This thesis is part of a larger study that examines the sedimentology, stratigraphy, geochemistry, petrophysics, and geomechanics of Devonian shales of Western Canada. The sedimentology and sequence stratigraphy of the Duvernay Formation are presented here.

The study presented in this thesis was undertaken in order to examine the depositional processes and conditions responsible for organic-rich mudstone deposition, and to generate a predictive capability for lithofacies and rock properties by developing a sequence stratigraphic model. The need for a greater understanding of mudstone deposition and rock property variation has been recognized by the oil and gas industry as it attempts to produce hydrocarbons from fine-grained reservoirs. More generally, robust sequence stratigraphic models for mudstones allow for the prediction of the distribution of sediment bodies and lithologies, and also explain how sea level change and basin morphology affect the character of fine-grained sediments.

The thesis is divided into two main chapters. Chapter 1 examines the lithologies and sedimentary facies of the Duvernay Formation and presents a depositional model that explains the processes and conditions present upon deposition of the sediments. Lithofacies defined in Chapter 1 are integrated with total organic carbon data collected by Julia McMillan to examine the factors governing organic enrichment. Examination of drill core was carried out at the AER Core Research Center and TerraTek Labs in Calgary, and at the University of Alberta in Edmonton. Sedimentology discussions with Dr. Korhan Ayranci and comparison to his results

from the Horn River Basin were very valuable in developing interpretations. Chapter 1 will be submitted to *Sedimentary Geology* as Knapp, L.J., McMillan, J.M, and Harris, N.B., 2016a. Lithofacies variations in organic-rich Duvernay Formation mudstones.

Chapter 2 presents a sequence stratigraphic model that explains variations in the lithologies and sedimentary facies from Chapter 1 in the context of sea level variation. Depositional units and surfaces identified in core were correlated through a network of wireline logs on GeoScout. Chapter 2 will be submitted to the *AAPG Bulletin or Marine and Petroleum Geology* as Knapp, L.J., McMillan, J.M, and Harris, N.B., 2016b. Sea level and basin morphology control on distribution and character of organic-rich mudstones: A sequence stratigraphic model for the Duvernay Formation, Alberta, Canada

A parallel MSc. thesis was completed by Julia McMillan to analyze geochemical and petrophysical properties of the Duvernay Formation. Samples for geochemical and petrophysical analysis were taken from the same cores that were used for the sedimentology study so that multiple datasets were available for every sample. Julia sampled cores at 1 meter spacing and at points of interest so that all major lithofacies and stratigraphic intervals were represented. By integrating our data we have created more robust depositional models to explain rock property variation. Sedimentological observations combined with geochemical analysis provide the opportunity to characterize the depositional environment in greater detail. The integration of sedimentological, geochemical, and petrophysical analyses on the same set of samples allows us to comprehensively characterize the properties of the rock, and predict the nature of one data set based on the character of another.

## Table of Contents

Abstract:.....	ii
PREFACE: .....	iii
CHAPTER 1: LITHOFACIES VARIATIONS IN ORGANIC-RICH DUVERNAY FORMATION MUDSTONES .....	1
1.1 Introduction:.....	1
1.2 Geologic Setting: .....	2
1.3 Methods: .....	5
1.4 Results:.....	8
1.5 Discussion:.....	30
1.5.1 Lithofacies Interpretations .....	32
1.5.2 Transport and Deposition of Fine-Grained, Organic-Rich Sediment .....	43
1.5.3 Depositional Model.....	47
1.6 Conclusion: .....	51
CHAPTER 2: SEA LEVEL AND BASIN MORPHOLOGY CONTROL ON DISTRIBUTION AND CHARACTER OF ORGANIC-RICH MUDSTONES: A SEQUENCE STRATIGRAPHIC MODEL FOR THE DUVERNAY FORMATION, ALBERTA, CANADA .....	53
2.1 Introduction:.....	53
2.2 Geological Setting:.....	54
2.3 Methods: .....	58
2.4 Results:.....	60
2.4.1 Lithofacies Analysis.....	60
2.4.2 Lithofacies Stacking Patterns and Cyclicity .....	60
2.4.3 Geographic Variation in Lithofacies and Stratal Thickness Variations .....	69
2.5 Discussion:.....	81
2.5.1 Sequence Stratigraphic Method .....	81
2.5.2 Sequence Stratigraphy in Mudstones .....	83
2.5.3 Duvernay Formation Sequence Stratigraphic Model.....	84
2.5.4 Recognizing Sequence Stratigraphic Surfaces and Systems Tracts in Organic-Rich Mudstones .....	95
2.6 Conclusion: .....	103
CHAPTER 3: CONCLUSIONS .....	106
3.1 Sediment Transport Mechanisms and Organic Enrichment.....	106
3.2 Lithofacies Variation in a Sequence Stratigraphic Context .....	107
ACKNOWLEDGEMENTS: .....	108

REFERENCES: .....	109
Appendix A: Thin Section Descriptions .....	130
SCL Kaybob 02-22 .....	130
GuideX Gvillee 09-06 .....	137
ECA Cecilia 11-04 .....	139
EOG Cygnet 08-20 .....	141
Appendix B: Additional Core Descriptions .....	148
Figure 1.1: Map of study area .....	3
Figure 1.2: Late Devonian stratigraphy of Central Alberta .....	4
Table 1.1: Name and location of described cores .....	7
Figure 1.3: LF1 planar-laminated mudstone .....	9
Figure 1.4: Types of sedimentary aggregates in LF1 .....	9
Figure 1.5: Core description of the SCL Kaybob 02-22 core .....	11
Figure 1.6: LF2 planar-laminated pyritic mudstone .....	12
Figure 1.7: Core description of the ECA Cecilia 11-04 core .....	13
Figure 1.8: LF3 planar-laminated silty mudstone .....	15
Figure 1.9: LF4 wavy-laminated mudstone .....	16
Figure 1.10: Core description of the Chevron Chickadee 03-05 core .....	17
Figure 1.11: LF4 in the NE West Shale Basin .....	18
Figure 1.12: LF7 siliceous-calcareous wackestone-floatstone .....	19
Figure 1.13: LF6 bioturbated pyritic mudstone .....	20
Figure 1.14: Benthic life in LF6 .....	21
Figure 1.15: LF7 bioturbated calcareous mudstone .....	22
Figure 1.16: EOG Cygnet 08-20 core description .....	23
Figure 1.17: LF8 nodular limestone .....	24
Figure 1.18: LF9 intraclastic packstone and LF10 limestone breccia .....	26
Figure 1.19: LF11 argillaceous-dolomitic mudstone .....	28
Figure 1.20: Core description of the Imperial Virginia Hills 06-36 core .....	29
Figure 1.21: LF12 nodular dolostone .....	30
Figure 1.22: Core description of the Sarcee et al. Pibroch 10-16 core .....	31
Figure 1.23: Depositional models .....	48
Figure 2.1: Map of study area .....	55
Figure 2.2: Late Devonian stratigraphy of the Western Canadian Sedimentary Basin in central Alberta .....	56
Table 2.1: Name and location of described cores .....	60
Table 2.2: Lithofacies characteristics for LF1-12 .....	62
Figure 2.3: Photo plate summary of lithofacies .....	63
Figure 2.4: Core description and cyclicity summary of ECA Cecilia 11-04 .....	65
Figure 2.5: Core photos of the top Majeau Lake Formation / base Duvernay Formation surface .....	66
Figure 2.6: DS1-DS2 contact .....	67
Figure 2.7: Core photos of DS2-DS3 contact .....	68

Figure 2.8: Core photos of the top of DS3 .....	69
Figure 2.9: Imperial Figure Lake 11-19 core description. ....	73
Figure 2.10: Gamma log, deep resistivity, lithofacies, TOC, and sequence stratigraphic interpretation for SCL Kaybob 02-22. ....	73
Figure 2.11: Gamma log, deep resistivity, lithofacies, TOC, and sequence stratigraphic interpretation for EOG Cygnet 08-28. ....	74
Figure 2.12: Dip section from Wild River Sub Basin, through Kaybob, towards Grosmont. ....	75
Figure 2.13: DS1 isopach.....	76
Figure 2.14: Dip section through the East Shale Basin.....	77
Figure 2.15: Dip section through the eastern West Shale Basin. ....	78
Figure 2.17: DS2 isopach.....	80
Figure 2.19: DS1 lithofacies distribution.....	91
Figure 2.20: DS2 lithofacies distribution.....	91
Figure 2.21: DS3 lowstand/stillstand lithofacies distribution.....	95
Figure 2.22: DS3 TST and HST lithofacies distribution.....	95
Figure 2.23: SCL Kaybob 02-22 core description with potassium, thorium and uranium abundances.....	98

## CHAPTER 1: LITHOFACIES VARIATIONS IN ORGANIC-RICH DUVERNAY FORMATION MUDSTONES

### 1.1 Introduction:

Recent petrographic studies of mudstone successions have identified fabrics that are attributed to a wide variety of depositional processes. Processes such as gravity flows (e.g. Macquaker et al., 2010a), storm dispersal and reworking (e.g. Schieber et al., 2010), and contour currents (e.g. Loucks and Ruppel, 2007) have been suggested to explain mudstone fabrics and contrast with traditional views on mud deposition. High energy deposition of clays as a result of flocculation and pelletization has been demonstrated in laboratory flume experiments (Schieber et al., 2007b; Schieber and Southard, 2009; Schieber, 2011) and ancient deposits (e.g. Macquaker and Keller, 2005; Macquaker et al., 2010b; Aplin and Macquaker, 2011). The presence of bioturbation challenges interpretations that infer persistent anoxia during organic-rich mudstone deposition (Macquaker and Gawthorpe, 1993; Macquaker et al., 2007; Schieber, 1999, 2003; Macquaker et al., 2010a; Egenhoff and Fishman, 2013).

The recognition of these processes has important implications for hydrocarbon exploration, which has revealed the need to understand and predict small-scale heterogeneity of rock properties in mudstones. Small-scale variations in components such as biogenic silica and carbonate minerals have been demonstrated to significantly influence petrophysical and geomechanical properties of the rock (Schieber, 1996; Schröder-Adams et al., 1996; Loucks and Ruppel, 2007; Aoudia et al., 2010). Additionally, organic matter distribution is variable both vertically and laterally and is associated with variations in textural characteristics of mudstones (Bohacs, 1998; Macquaker and Howell 1999; Passey et al., 2010).

This study characterizes lithofacies of the organic-rich Duvernay Formation – a prolific source rock (Fowler et al., 2001) and recent target for liquids-rich gas in the Western Canadian Sedimentary Basin (Rokosh et al., 2012). A core-scale sedimentological study of the Duvernay

Formation has not been published since Stoakes (1980), and no detailed petrographic study exists. The Duvernay Formation represents an outstanding opportunity to study the depositional processes and conditions of fine-grained, organic-rich mudstones within a stratigraphic and paleogeographic context. A growing volume of Duvernay Formation drill cores and data are available as the result of intense exploration since 2009. The presence of well-studied shallow water carbonates of the Leduc Formation (e.g. Mountjoy, 1980; Weissenberger 1994; Van Buchem, 1996a, 2000a; Whalen et al., 2000; Potma et al., 2001) and Grosmont Formation (e.g. Cutler, 1983) allows for correlation of basinal mudstones to their shallow water equivalents.

## **1.2 Geologic Setting:**

Duvernay Formation sediments were deposited during the Late Devonian in Western Canada (Fig. 1.1, 1.2), roughly time-equivalent to several other major black shale deposits across North America. During the Middle to Late Devonian, global sea level was significantly higher than present day (Johnson et al., 1985; Savoy and Mountjoy, 1995; Haq and Schutter, 2008), resulting in widespread flooding of continental margins. It is within these epicontinental settings that many organic-rich Devonian successions were deposited, such the Duvernay, Horn River, Bakken, Marcellus, Chattanooga, Ohio, New Albany, and Woodford shales.

The Western Canadian Sedimentary Basin during the Frasnian was a passive margin at the western edge of North America. The northwest margin of North America was generally dominated by open marine shales in British Columbia and the Northwest Territories, transitioning to shallow water carbonates in Alberta, and restricted dolomites and evaporites in Saskatchewan and Manitoba to the southeast (Ziegler, 1967; Switzer et al., 1994). During deposition of the Woodbend Group, the rate of accumulation and preservation of sediment increased dramatically (Switzer et al., 1994). In Alberta, the section is characterized by thick accumulations of basin-filling shales, including hydrocarbon source rocks, and thick, extensive reef complexes (Switzer et al., 1994).

Tectonic features that influenced sedimentation during deposition of Duvernay Formation sediments include the Peace River Arch, West Alberta Ridge, Rimbey Arc (overlain by Rimbey-Meadowbrook reef trend), and Meadow Lake Escarpment (overlain by the Killiam Barrier Reef)

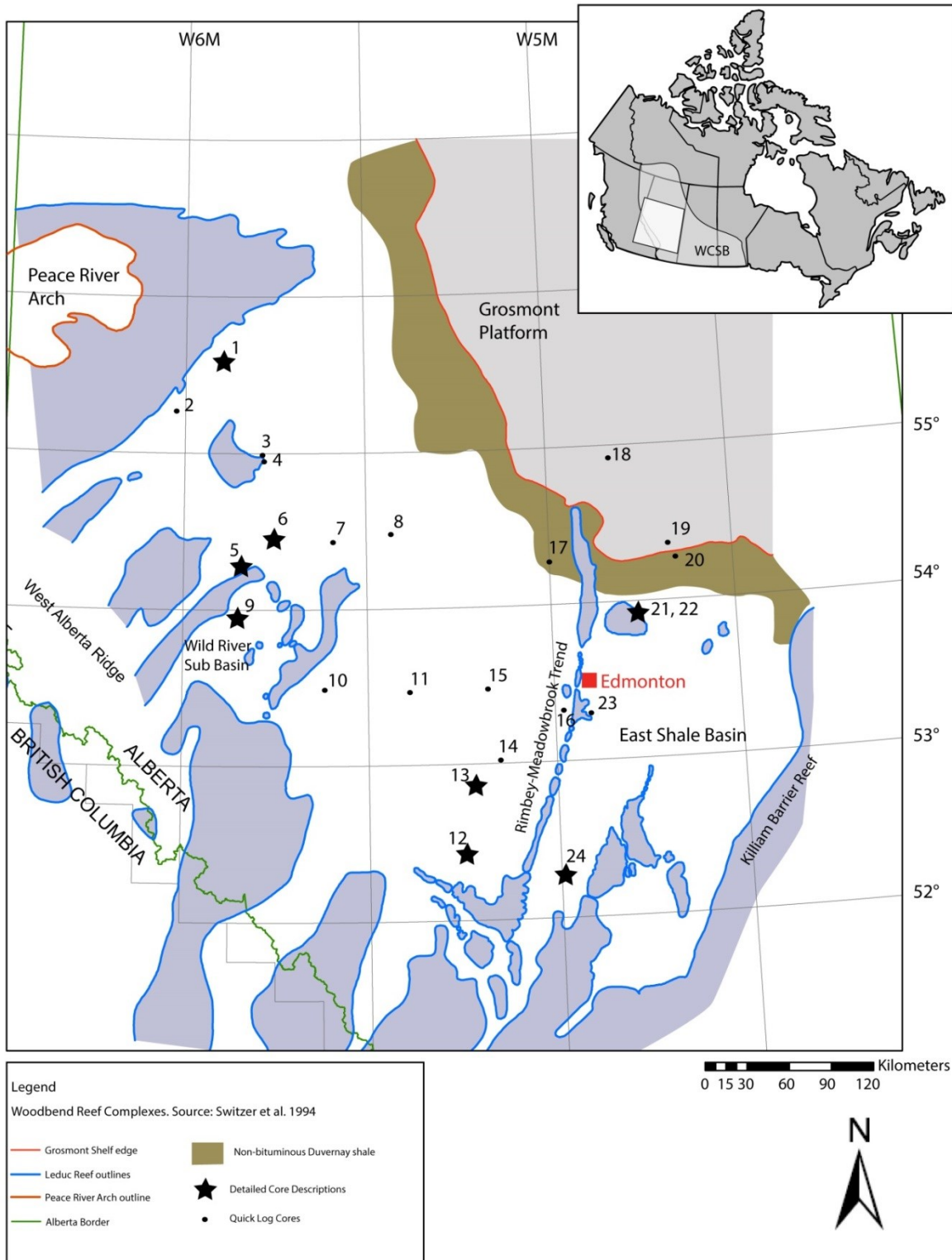


Figure 1.1: Map of study area. Duvernay Formation organic-rich mudstones are the basinal equivalent of Leduc Formation reefs. Organic-lean mudstones are deposited adjacent to the Grosmont Platform. The Peace River Arch was an emergent land mass during the Late Devonian, and was fringed by Leduc Formation reefs. Data from Switzer et al., 1994.

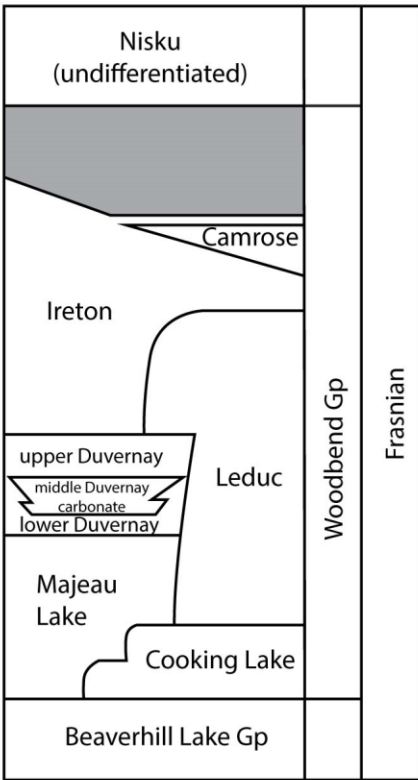


Figure 1.2: Late Devonian stratigraphy of Central Alberta. The Duvernay Formation is informally divided into lower, middle, and upper members. Modified from Switzer et al., 1994.

(Fig. 1.1). The Peace River Arch was an emergent landmass on the west side of the basin, fringed by Leduc Formation reefs (Dix, 1990; O’Connell et al., 1990). The West Alberta Ridge was flooded, but formed a base for extensive Leduc reef complexes (Switzer et al., 1994). The Rimbey Arc was a southwest-northeast trending basement lineament that exerted a strong control on accommodation space during Woodbend Group deposition (Ross and Stephenson, 1989). During deposition of Duvernay Formation sediments, the lineament was marked by a chain of Leduc Formation reefs

called the Rimbey-Meadowbrook trend. This reef chain divides the basin into a West Shale Basin and East Shale Basin. Accommodation space was limited in the East Shale Basin with respect to the West Shale Basin due to differences in tectonic subsidence on either side of the Rimbey Arc (Switzer et al., 1994). This effect was compounded by differential compaction, because the West Shale Basin was a major site of shale deposition, whereas the East Shale Basin was underlain by the Cooking Lake Carbonate Platform (Switzer et al., 1994). The Meadow Lake Escarpment is a pre-Devonian erosional and structural feature (Oldale and Munday, 1994). During deposition of Duvernay Formation sediments, the Killiam Barrier Reef roughly coincided with the underlying Meadow Lake Escarpment, and marks the furthest eastward extent of Duvernay Formation shales and argillaceous limestones (Switzer et al., 1994).

The Duvernay Formation conformably overlies the Majeau Lake Formation throughout most of the basin (Fig. 1.2). In the far south and west, Majeau Lake Formation sediments were not deposited and Duvernay Formation strata onlap Swan Hills Formation platform carbonates and older Devonian strata (Switzer et al., 1994). The Ireton Formation conformably overlies the Duvernay Formation across much of the basin. Near reef complexes and the Grosmont Platform,

Leduc Formation reef-margin strata and Grosmont Formation platform carbonates, respectively, overlie the Duvernay Formation. An informal stratigraphy, introduced by Andrichuk (1961) and used by industry, separates the Duvernay Formation into lower, middle, and upper members.

The Duvernay Formation is predominantly composed of organic-rich, siliceous-calcareous mudstones over much of the basin. East Shale Basin deposits are notably more calcareous than equivalent West Shale Basin sediments (Rokosh et al., 2012). Towards the northeast, adjacent to the Grosmont Platform, mudstones become argillaceous and organic-lean (Stoakes, 1980). Limestones and dolostones occur proximal to reef complexes. Stratigraphically, organic-rich siliceous-calcareous mudstones are common within the lower and upper Duvernay members, while organic-lean limestones dominate the middle Duvernay member (Andrichuk, 1961). Member boundaries are lithostratigraphic.

### **1.3 Methods:**

Eight drill cores (Table 1.1) were selected for detailed description. Cores were described at a scale of 1:10, paying special attention to lithology, grain size, sedimentary structure, bioturbation, and presence of cements. Core selection was primarily based on total thickness of formation cored, core quality, and geographic distribution across the basin. An additional 16 cores were described in less detail to observe facies variations and stratigraphic surfaces over a greater extent of the basin. Few of the 16 additional cores covered the entire Duvernay Formation interval. A total of 108 thin sections were cut from 4 cores, covering the major lithofacies and intervals of interest. Thin sections were cut to 20  $\mu\text{m}$  rather than the standard 30  $\mu\text{m}$ , so that finer detail could be observed in fine-grained facies. Most thin sections were cut perpendicular to bedding but a subset was selected for bed-parallel thin sections to further examine the nature of potential bioturbation features. Thin sections were scanned using a Nikon Super Coolscan 5000 ED scanner to observe centimeter- to millimeter-scale features. Millimeter- to micrometer-scale features were analyzed under transmitted and reflected white light using a Zeiss Axio Scope.A1 petrographic microscope.

Samples for geochemical analysis were cut every 1 meter from 5 of the 8 cores. These 5 cores were chosen for their geographic coverage of the basin and range of thermal maturity.

Detailed analysis of these samples is presented in McMillan (2016). A 10 cm long by 2 cm thick slab was cut from the back of the core at each sample location. Vertical splits were cut along the length of the slabs for separate analyses. Samples were sent to Weatherford Geochemical Services Group in Shanandoah, TX for Leco-TOC analysis. Total organic carbon values reported here are averages for each sampled facies from the SCL Kaybob 02-22, ECA Cecilia 11-04, GuideX Gvillee 09-06, and EOG Cygnet 08-20 cores. Esso Redwater 16-28 was also sampled for TOC but was removed from average TOC calculations because it is much less thermally mature than the other sampled wells and as such has much higher TOC values for all facies.

<b>Map #</b>	<b>Well Name</b>	<b>UWI</b>	<b>Sampled</b>	<b>Detailed Description</b>
<b>1</b>	GuideX Gvillee 09-06	100/09-06-076-23W5/00	Y	Y
<b>2</b>	BPC et al. Smoky HT 04-36	100/05-36-072-01W6/00	N	N
<b>3</b>	Xerex SturLks 07-22	100/07-22-069-21W5/00	N	N
<b>4</b>	Enermax Panther SturLs 14-02	100/14-02-069-21W5/00	N	N
<b>5</b>	AOSC Grizzly 01-24	100/01-24-061-23W5/00	N	Y
<b>6</b>	SCL HZ Kaybob 02-22	100/02-22-063-20W5/00	Y	Y
<b>7</b>	Chevron Chickadee 03-05	100/03-05-062-16W5/00	N	N
<b>8</b>	Imperial Virginia Hills 06-36	100/06-36-063-12W5/00	N	N
<b>9</b>	ECA Cecilia 11-04	100/11-04-058-23W5/00	Y	Y
<b>10</b>	CNRL HZ Edson 01-10	100/01-10-052-17W5/00	N	N
<b>11</b>	Imperial Cynthia No. 09-06	100/09-06-052-11W5/00	N	N
<b>12</b>	SCL HZ Ferrier 03-21	100/03-21-040-07W5/00	N	Y
<b>13</b>	Penn West Pembina 10-17	100/10-17-045-06W5/00	N	Y
<b>14</b>	Imp Cdn-Sup Norbuck 02-06	100/02-06-047-04W5/00	N	N
<b>15</b>	Imp Cdn-Sup	100/16-18-052-	N	N

	Tomahawk 16-18	05W5/00		
<b>16</b>	Forgotson Burk SGSpike 10-04	100/10-04-051- 27W4/00	N	N
<b>17</b>	Sarcee et al. Pibroch 10- 16	100/10-16-061- 26W4/00	N	N
<b>18</b>	Imperial Deep Creek 04- 33	100/04-33-068- 22W4/00	N	N
<b>19</b>	Imperial Figure Lake 11-19	100/11-19-062- 18W4/00	N	N
<b>20</b>	Tex et al. Lucky 09-09	100/09-09-061- 18W4/00	N	N
<b>21</b>	Esso Redwater 10-27	102/10-27-057- 21W4/00	N	N
<b>22</b>	Esso Redwater 16-28	102/16-28-057- 21W4/00	Y	Y
<b>23</b>	Nexxtep 07-05	102/07-05-050- 25W4/00	N	N
<b>24</b>	EOG Cygnet 08-20	100/08-20-038- 28W4/00	Y	Y

Table 1.1: Name and location of described cores.

## 1.4 Results:

Twelve lithofacies comprise Duvernay Formation sediments over most of the basin. Lithofacies were characterized on the basis of composition, grain size, sedimentary structure, bioturbation, and presence of cements and are described here in order of decreasing TOC.

### *LF1: Planar laminated siliceous mudstone*

LF1 is dark grey-brown, faintly planar-laminated siliceous-calcareous mudstone (Fig. 1.3A). Lamination is commonly difficult to recognize in core samples but in thin section can be seen as sub-millimeter-thick alternating silt-rich and silt-poor mud-supported laminae (Fig 3B). Grading is generally absent, although rare, vague normal grading has been observed (Fig. 1.3C). Rare grain-supported silt laminae are commonly only 1 or 2 silt grains thick, show no grading, and are commonly cemented with calcite or silica cement (Fig. 1.3D). Silt is primarily carbonate, with some quartz and rare chert. Laminae may contain calcareous styliolinid tests. Laminae are locally partially cemented with calcite or quartz.

Except for the silty laminae, LF1 is composed of an unstructured mixture of clay- and silt-sized detrital grains and organic matter. Detrital grains are calcite, dolomite, and quartz, with a very low abundance of clay minerals. Individual grains are identified as detrital when they are present in graded or grain-supported laminae, but calcite and dolomite grains in unstructured mud-supported laminae are possibly authigenic. Clay minerals are sometimes observed as small aggregates, generally between 100 and 300  $\mu\text{m}$  long and  $\sim 20$   $\mu\text{m}$  thick (Fig. 1.4A, 1.4C). Fragments or complete tests of calcareous styliolinids and tentaculitids are present but uncommon. Siliceous planktonic radiolaria are uncommon to common, are crushed and recrystallized, and appear as cherty masses ( $\sim 50 \times 10$   $\mu\text{m}$ ). Amorphous organic matter occurs intimately mixed with matrix grains. Boundaries of organic matter aggregates can sometimes be observed (Fig. 1.4B). Individual organic matter aggregates appear as dark brown stringers (commonly 50-200  $\mu\text{m}$  long and less than 10  $\mu\text{m}$  thick) in bed-normal thin sections and appear equidimensional to ovoid with irregular edges in bed-parallel thin sections (Fig. 1.4D). The average TOC for LF1 is 3.6 wt% (SD=1.8, n=26).

LF1 is most common in the western and southern West Shale Basin, where it can be the dominant lithofacies, for example, in the SCL Kaybob 02-22 core (Fig. 1.5). At GuideX Gvillee 09-06, near the Peace River Arch, planar-laminated mudstones are more argillaceous and clay mineral aggregates are more commonly observed. In East Shale Basin cores, calcareous styliolinid tests are much more common in LF1 laminae, and siliceous planktonic radiolaria are not observed.

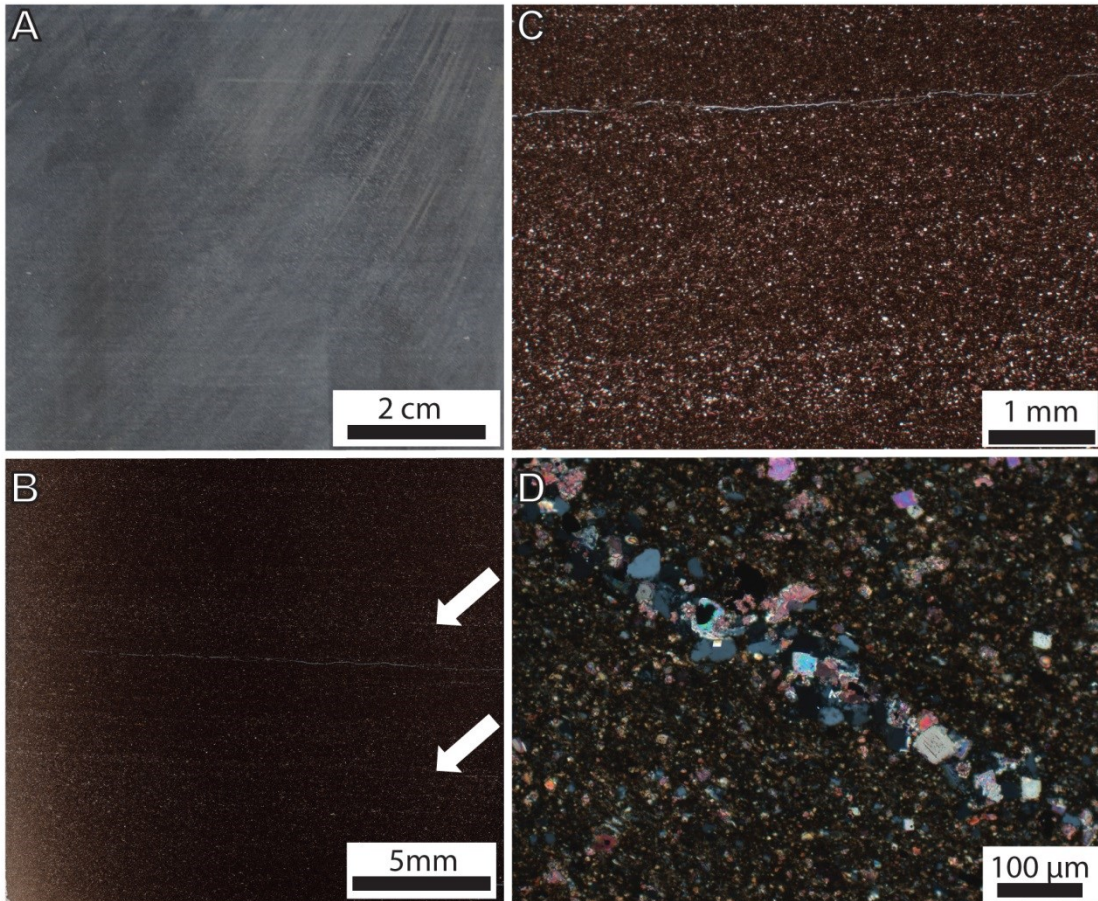
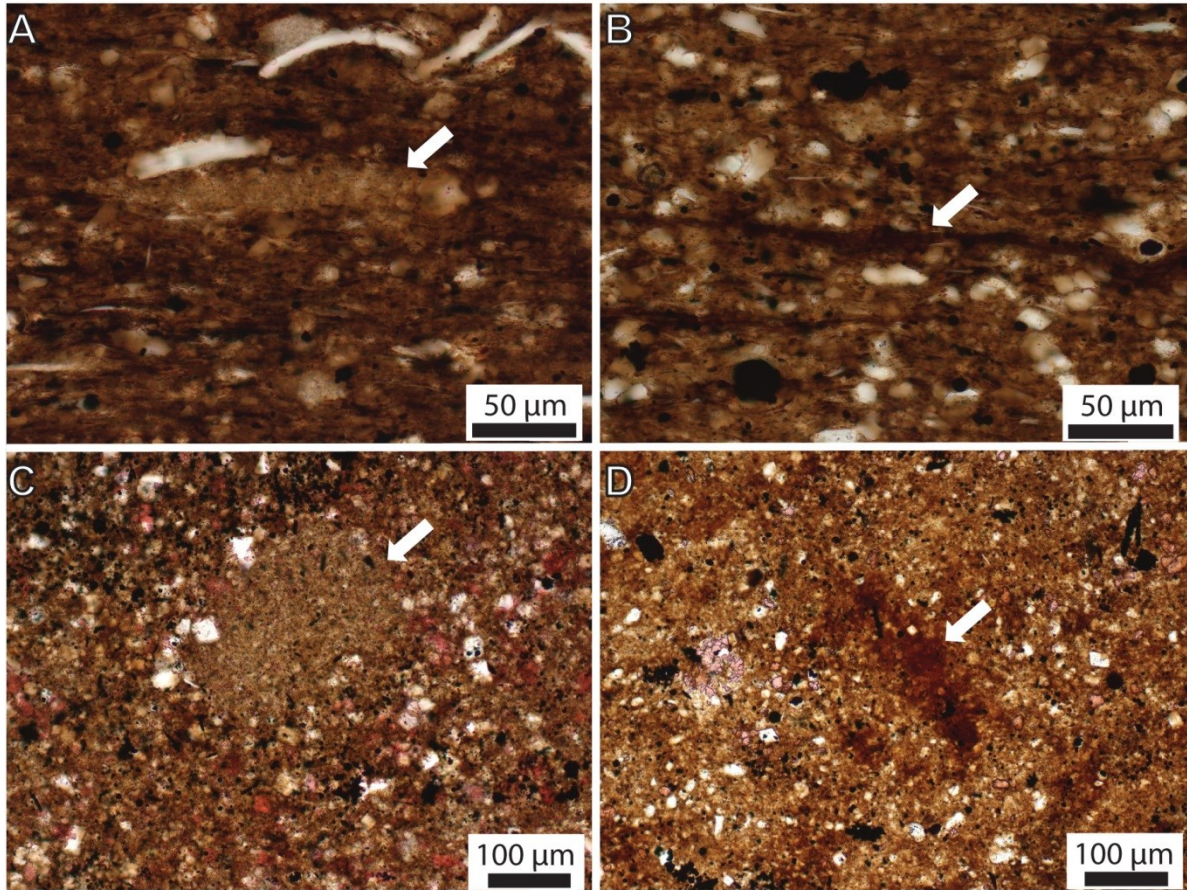


Figure 1.3: LF1 planar-laminated mudstone. A) Planar laminae are very subtle in core. Core photo. B) Laminae are faintly defined by increases in silt (arrow). Most silty laminae are mud-supported. Thin section scan. C) Rare vague normal grading observed in silty laminae. Calcite is stained pink. Thin section photomicrograph, plane-polarized light. D) Rare grain-supported silt lamina. Silt is a combination of calcite, dolomite, quartz, and rare chert clasts. Thin section photomicrograph, cross-polarized light. All samples from SCL Kaybob 02-22.

Figure 1.4: Types of sedimentary aggregates in LF1. A) Clay mineral aggregate in bed-normal thin section. Thin section photomicrograph. B) Organic matter aggregate in bed-normal thin section. Thin section photomicrograph. C) Clay mineral aggregate in bed-parallel thin section. Clay mineral aggregates are round to ovoid in plan view and contain much less silt than surrounding sediment. Thin section photomicrograph. D) Organic matter aggregate in bed-parallel thin section. Organic matter aggregates are round to ovoid in plan view and have wispy edges. Thin section photomicrograph. All samples from GuideX Gvillee 09-06.



*LF2: Planar-laminated pyritic mudstone*

LF2 is dark grey-brown mudstone with discontinuous pyritic laminae and planar silt laminae (Fig. 1.6). Pyritic laminae are typically less than 1mm thick, and are a few millimeters to several centimeters long. Pinching and swelling of these laminae is observed in thin section. Pyrite in laminae occurs as both framboidal and euhedral pyrite with varying abundances of pyrite-replaced carbonate silt grains and fossil fragments. Mud-supported silty laminae are seen in thin section as alternating sub-millimeter thick variations in silt abundance. No grading was observed in silt laminae or pyritic laminae.

Except for the silty or pyritic laminae, LF2 is composed of an unstructured mixture of clay- and silt-sized detrital grains and organic matter, similar to LF1. Detrital grains are primarily

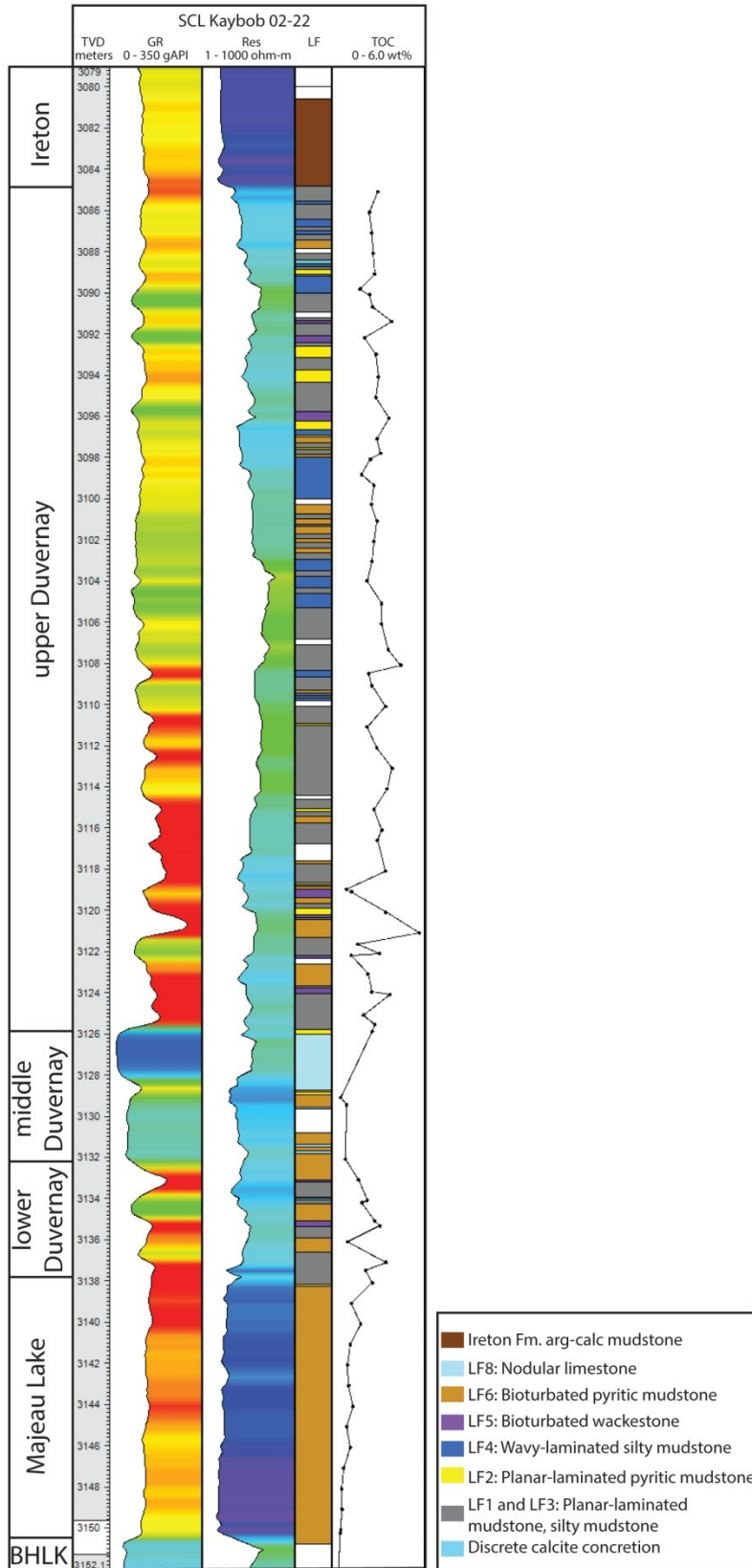


Figure 1.5: Core description of the SCL Kaybob 02-22 core. Note the dominance of LF1, LF3 (dark grey) organic-rich mudstones. LF8 nodular limestone is dominant in the middle Duvernay member.

calcite, dolomite, and quartz, with a low abundance of clay minerals. LF1 and LF2 have similar compositions but clay minerals are more abundant in LF2. Clay minerals occur locally as small aggregates generally between 100 and 300  $\mu\text{m}$  long and  $\sim 20$   $\mu\text{m}$  thick. Fossil fragments are uncommon but may include calcareous styliolinid and tentaculitid tests. Amorphous organic matter occurs intimately mixed with matrix grains. Boundaries of organic matter aggregates can sometimes be observed. Individual organic matter aggregates appear as dark brown stringers (commonly 50-200  $\mu\text{m}$  long and less than 10  $\mu\text{m}$  thick) in bed-normal thin sections and appear equidimensional to ovoid with irregular edges in bed-parallel thin sections. The average TOC for LF2 is 3.2 wt% (SD=0.6, n=6).

LF2 is more common in the West Shale Basin than the East Shale Basin; an example from the Encana Cecilia well is provided in Fig. 1.7, where LF2 is commonly associated with LF6 bioturbated pyritic mudstones. LF2 commonly overlies flooding surfaces.

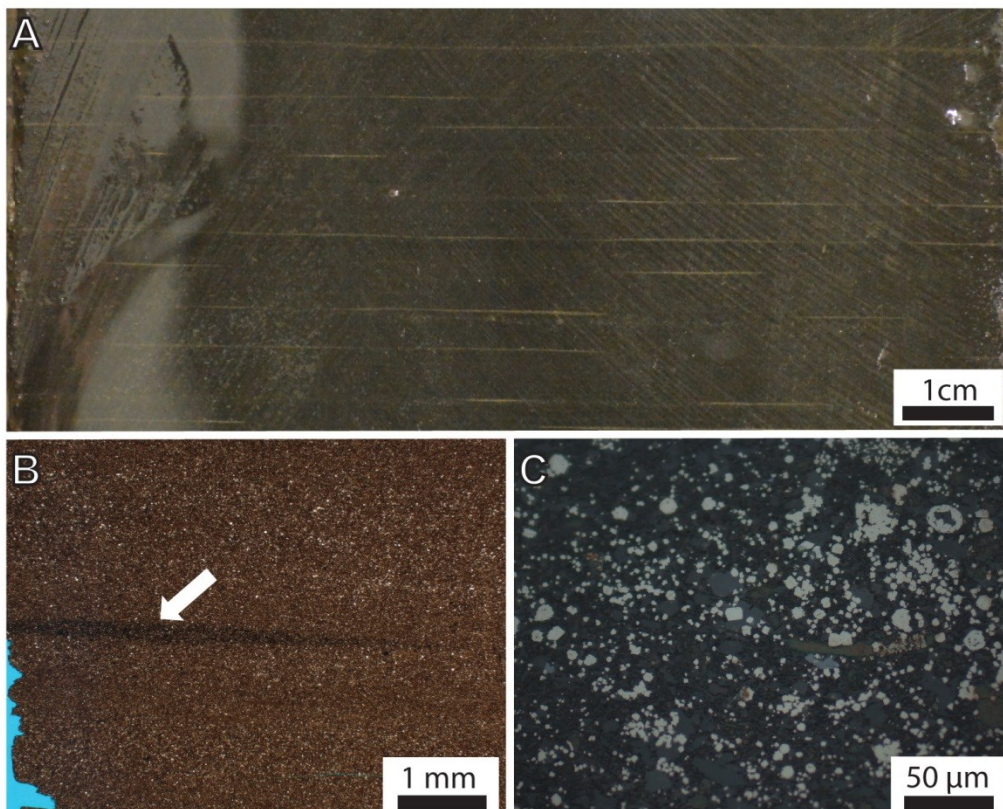
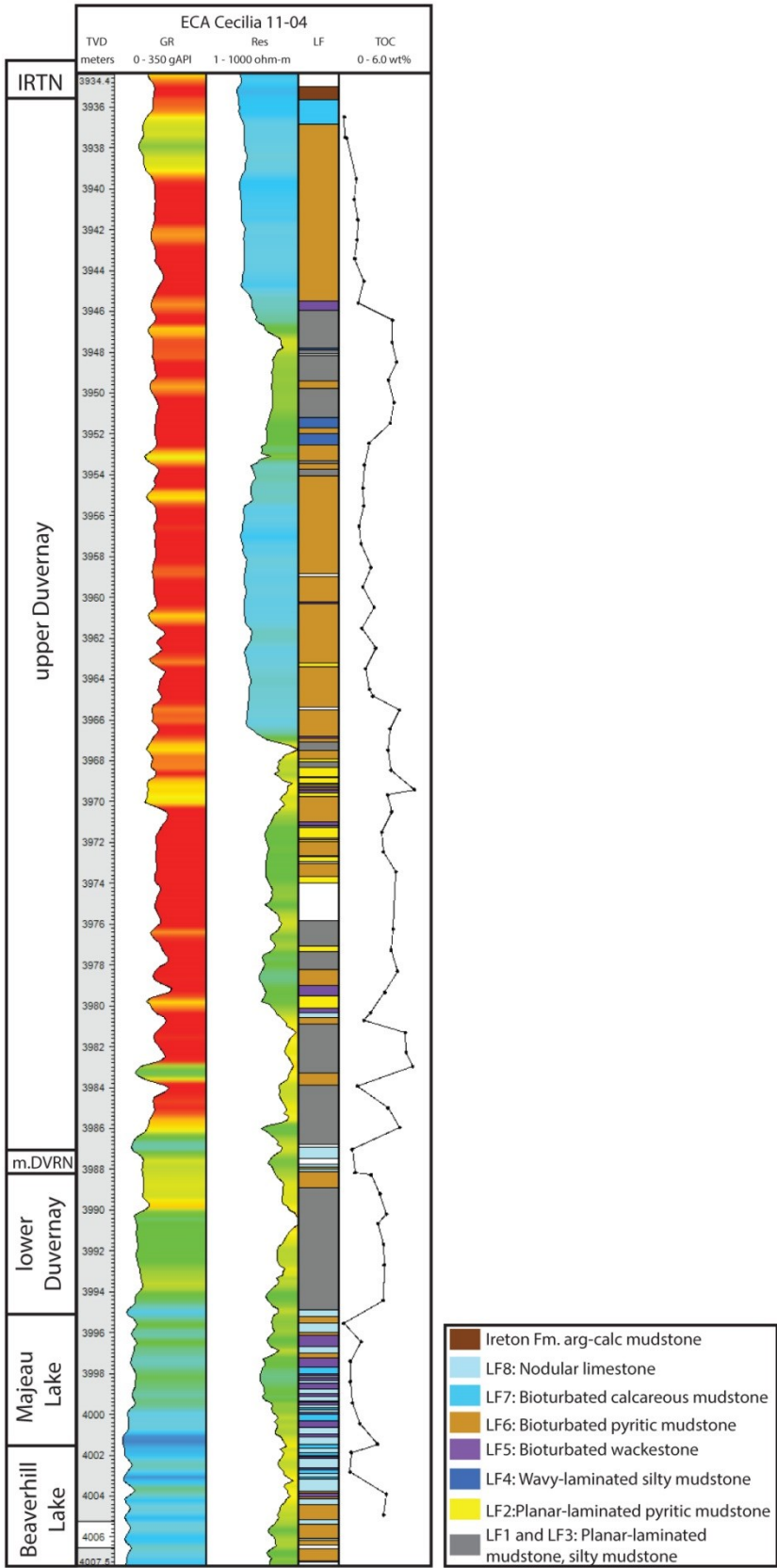


Figure 1.6: LF2 planar-laminated pyritic mudstone. A) Discontinuous planar laminae are enriched in framboidal and euhedral pyrite as well as pyritized fossil fragments and carbonate silt. Core photo, CNRL Edson 01-10. B) Lamination is defined by discontinuous pyrite laminae (arrow) and continuous silt-rich and silt-poor laminae. Discontinuous pyrite laminae pinch and swell. Thin section photomicrograph, plane polarized light, SCL Kaybob



02-22. C) Pyrite (bright reflectance) in laminae is present most commonly as euhedral crystals and framboids, but also as full and partial replacement of calcareous grains and fossil fragments. Thin section photomicrograph, reflected white light, SCL Kaybob 02-22.

Figure 1.7: Core description of the ECA Cecilia 11-04 core. Note the tendency of LF2 laminated pyritic mudstones to occur in association with bioturbated pyritic mudstones of LF6. LF6 is especially dominant in the upper Duvernay member in wells in the Wild River Sub Basin.

### *LF3: Planar-laminated silty mudstone*

LF3 consists of dark grey-brown silty mudstones that display planar-parallel lamination (Fig. 1.8). Laminae are easily visible at hand sample scale, and normal and inverse grading is observed in thin section. Lamina bases and tops may be sharp or gradational. Laminae are composed primarily of carbonate silt with less common quartz and rare chert clasts. Laminae contain varying abundances of calcareous styliolinid and tentaculitid tests, depending on location within the basin. Laminae are locally partially cemented with calcite or quartz. Bioturbation is rare, but was observed as gaps in silty laminae, and horizontal, silt-filled burrows.

Silt-poor laminae alternate with silt-rich laminae and are composed of an unstructured mixture of clay- and silt-sized detrital grains and organic matter, similar to LF1 and LF2. Detrital grains include calcite, dolomite, and quartz, with a very low abundance of clay minerals. Clay minerals are sometimes observed as small aggregates generally between 100 and 300  $\mu\text{m}$  long and  $\sim 20$   $\mu\text{m}$  thick. Fragments or complete tests of calcareous styliolinids and tentaculitids are uncommon. Siliceous planktonic radiolaria are uncommon to common, are crushed and recrystallized, and appear as cherty masses ( $\sim 50 \times 10$   $\mu\text{m}$ ). Amorphous organic matter occurs intimately mixed with matrix grains. Boundaries of organic matter aggregates can sometimes be observed. Individual organic matter aggregates appear as dark brown stringers (commonly 50-200  $\mu\text{m}$  long and less than 10  $\mu\text{m}$  thick) in bed-normal thin sections and appear equidimensional to ovoid with irregular edges in bed-parallel thin sections. The average TOC for LF3 is 3.2 wt% (SD=1.3, n=31).

LF3 is common throughout the basin and along with LF1, comprises a significant proportion of West Shale Basin cores (Fig. 1.5) LF3 is commonly found associated with LF1 but is more common than LF1 near reef complexes. In the East Shale Basin, styliolinid tests are common in LF3 laminae. Near the Redwater reef, carbonate silt is dominantly peloidal. Cherty masses are common in LF3 matrix of West Shale Basin cores, but unobserved in East Shale Basin cores.

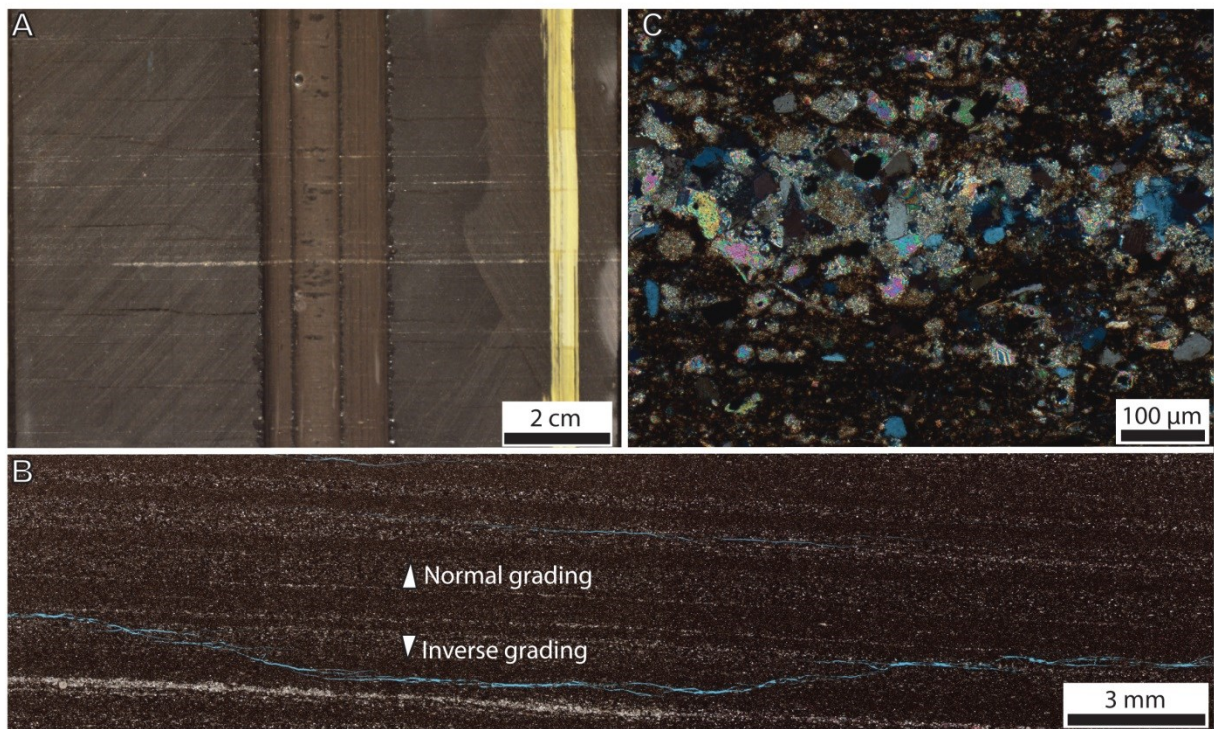


Figure 1.8: LF3 planar-laminated silty mudstone. A) Silty laminae are clearly visible in hand sample. Core photo, ECA Cecilia 11-04. B) Silty laminae show both normal and inverse grading. Grain-supported laminae are more common and prominent than LF1-2. Thin section scan, SCL Kaybob 02-22. C) Silt is dominantly calcite and dolomite with lesser amounts of quartz and rare chert clasts. Thin section photomicrograph, cross-polarized light, SCL Kaybob 02-22.

*LF4: Wavy-laminated silty mudstone*

LF4 consists of dark grey-brown mudstone with light to medium grey wavy-laminated silty-sandy laminae (Fig. 1.9). Silt abundance is higher in LF4 than LF1-3. Laminae typically show wavy to lenticular lamination, but sedimentary structures also include planar parallel lamination, low angle cross-lamination, starved ripples, loading structures, and flame structures. Laminae are typically grain-supported and show both normal and inverse grading (Fig. 1.9B). Normally graded laminae commonly have sharp bases while inversely graded laminae typically have sharp upper contacts. Grain size in silty-sandy laminae is typically fine silt to medium sand, and is primarily carbonate with minor quartz and rare chert clasts. Laminae may contain uncommon bioclast fragments including styliolinids, tentaculitids. In cores where LF4 is abundant, distinctly coarser-grained, and more fossiliferous beds are intermittently present (Fig.

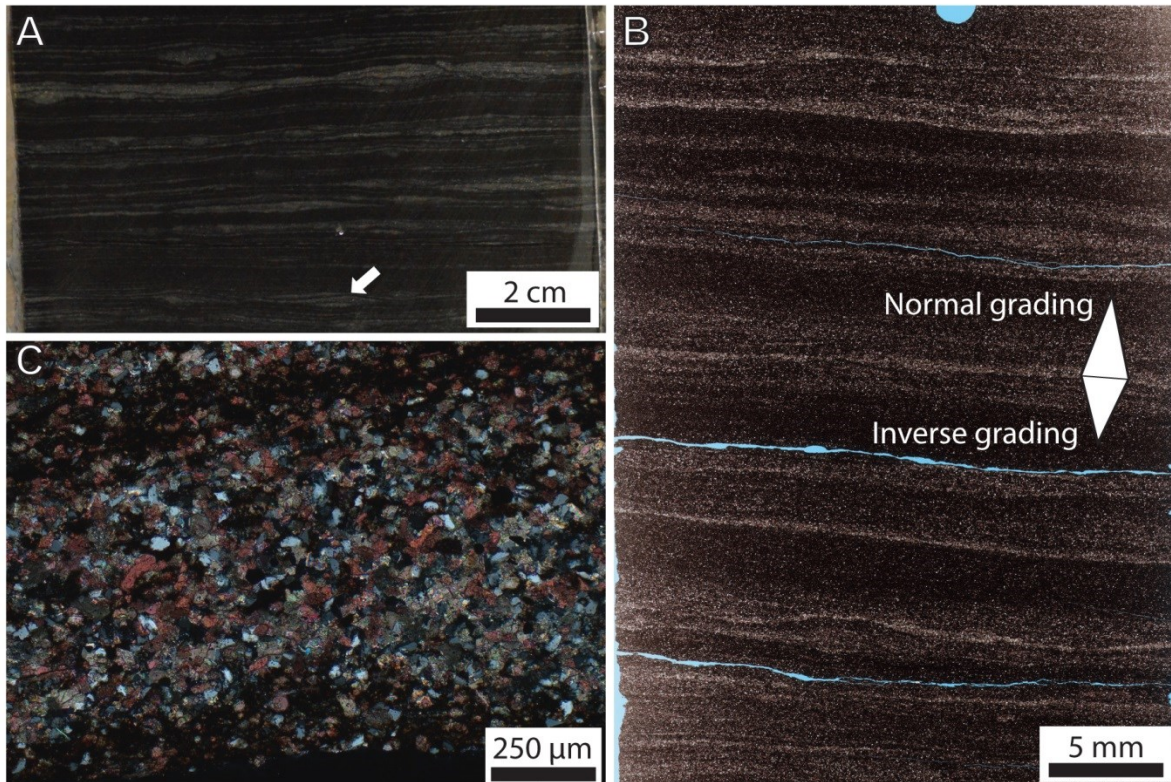


Figure 1.9: LF4 wavy-laminated mudstone. A) Lenticular silt laminae pinch and swell and contain starved ripples (arrow). Core photo, Chevron Chickadee 62-16. B) Silty laminae show normal and inverse grading. Thin section scan, SCL Kaybob 02-22. C) Silt is a mixture of calcite, dolomite, quartz, and uncommon chert clasts. Dark, silt-poor laminae are rich in clay-sized grains and organic matter. Thin section photomicrograph, cross-polarized light, SCL Kaybob 02-22

1.10). These beds are 1-6 cm thick and are always normally graded, with sharp, erosive bases. Fossil fragments commonly include brachiopods and crinoids. Bioturbation is minor to moderate in LF4 and is seen as gaps in silt laminae, silt-filled horizontal burrows, and homogenization of silt-rich and silt-poor laminae.

Silt-poor laminae alternate with silt-rich laminae and are composed of an unstructured mixture of clay- and silt-sized detrital grains and organic matter, similar to LF1-3. Detrital grains are calcite, dolomite, and quartz, with a very low abundance of clay minerals. Fragments or complete tests of calcareous styliolinids and tentaculitids are uncommon. Siliceous planktonic radiolaria are uncommon to common, are crushed and recrystallized, and appear as cherty masses (~50x10 μm). Amorphous organic matter occurs intimately mixed with matrix grains. Boundaries of organic matter aggregates can sometimes be observed. Individual organic matter aggregates appear as dark brown stringers (commonly 50-200 μm long and less than 10 μm

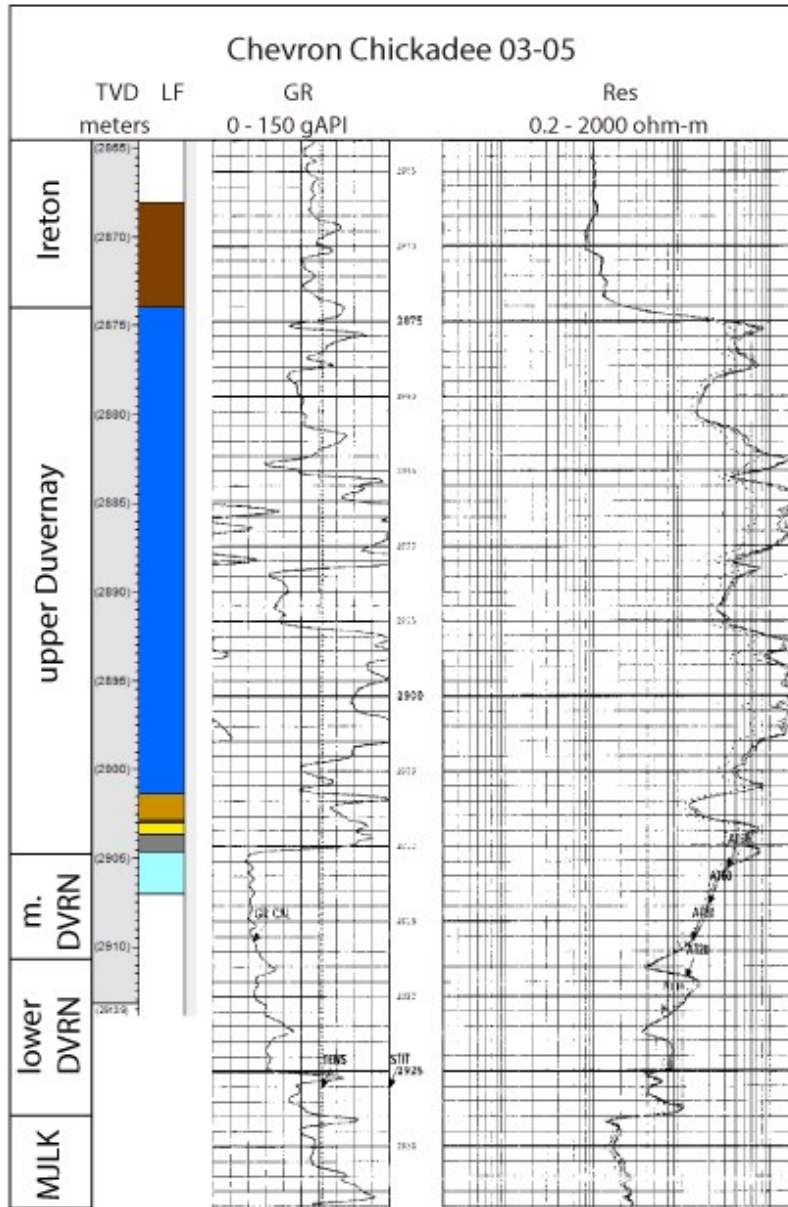
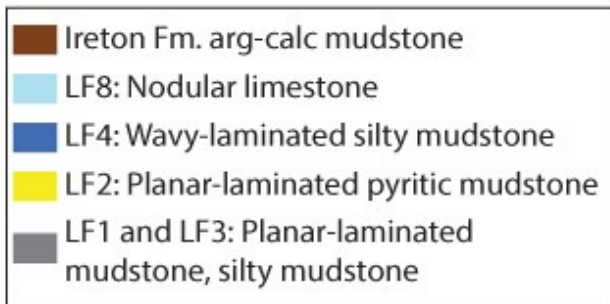


Figure 1.10: Core description of the Chevron Chickadee 03-05 core. LF4 is dominant in the upper Duvernay member.



thick) in bed-normal thin sections and appear equidimensional to ovoid with irregular edges in bed-parallel thin sections. The average TOC for LF4 is 2.4 wt% (SD=0.5, n=10)

LF4 is most common in the West Shale Basin and is especially common and coarse-grained towards the northeast (Fig. 1.10, 1.11). LF4 is uncommonly found in the East Shale Basin where primary sedimentary structures are often disrupted.

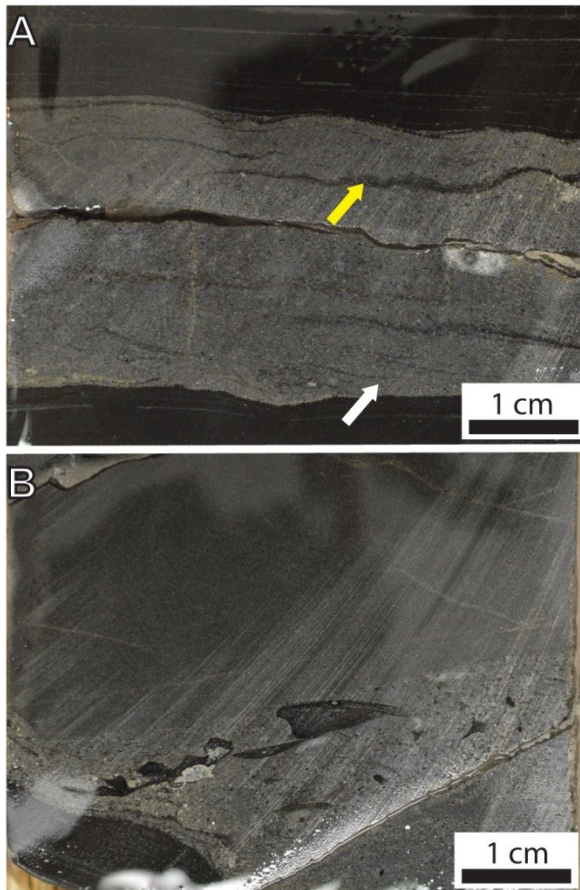


Figure 1.11: LF4 in the NE West Shale Basin. A) Silt-sand beds are coarser, more prominent, often with sharp, erosive bases, and sharp, non-erosive tops. Contourite bed shows low angle cross lamination near base (white arrow) and mud drapes (yellow arrow) near the top of the bed. Thin section photograph. B) Sharp-based, normally graded turbidite beds have especially coarse, fossiliferous bases and become more common. Core photograph. Both images from Chevron Chickadee 03-05.

*LF5: Siliceous-calcareous wackestones and floatstones*

LF5 is comprised of siliceous-calcareous wackestones and floatstones in beds that are a few millimeters to several centimeters thick. LF5 is usually poorly-bedded to structureless, although uncommon sharp bases and normal grading can be observed (Fig. 1.12). Bioclasts include whole or fragmented styliolinids, tentaculitids (Fig. 1.12B), and radiolaria. Less commonly, fragments of brachiopods, bivalves (Fig. 1.12C), and crinoids are observed. Rarely, brachiopod fossils are disarticulated rather than fragmented. Bioturbation is minor to intense, based on disruption of primary sedimentary structures

The matrix of LF5 is composed dominantly of clay- to silt- sized carbonate grains and amorphous organic matter, with less common quartz and clay minerals. Amorphous organic

matter occurs intimately mixed with matrix grains. Boundaries of organic matter aggregates are rarely observed. Individual organic matter aggregates appear as dark brown stringers (commonly 50-200  $\mu\text{m}$  long and less than 10  $\mu\text{m}$  thick) in bed-normal thin sections and appear equidimensional to ovoid with irregular edges in bed-parallel thin sections. Organic matter abundance is greatest in fine-grained, less calcareous beds. The average TOC for LF5 is 2.3 wt% (SD=1.2, n=19).

LF5 is more common in the East Shale Basin than the West Shale Basin, although it is consistently a relatively minor facies. In the East Shale Basin, LF5 beds are more fossiliferous, more commonly contain larger taxa such as brachiopods and bivalves, and contain more abundant clay- and silt-sized carbonate grains.

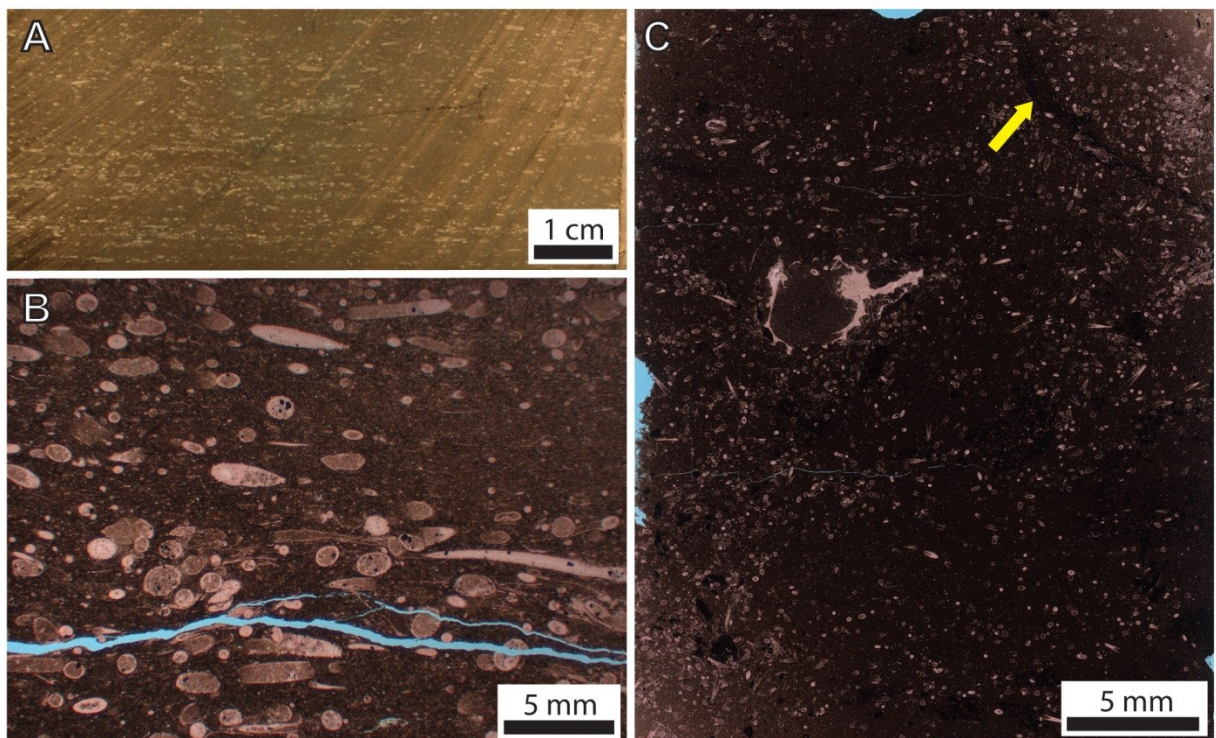


Figure 1.12: LF7 siliceous-calcareous wackestone-floatstone. A) Poorly bedded styliolinid wackestone. Calcareous styliolinid fossils in medium grey, organic-rich calcareous-siliceous mudstone. Core photo, EOG Cygnet 08-20. B) Styliolinid and tentaculitid fossils are unevenly distributed. Matrix contains abundant fine grain calcite debris. EOG Cygnet 08-20. C) Intensely bioturbated styliolinid wackestone. Uncommon larger fossils include brachiopods. Pyrite preferentially precipitates in traces (yellow). Thin section scan, SCL Kaybob 02-22.

*LF6: Bioturbated pyritic mudstone*

LF6 is composed of dark grey-brown poorly-bedded mudstone with pyritic burrows. Where bedding is preserved, it appears as wispy, wavy laminae, although commonly no bedding is evident (Fig. 1.13). Laminae are observed as subtle variations in color due to varying silt abundance. Bedding is disrupted by subhorizontal to subvertical burrows that are enriched in pyrite.

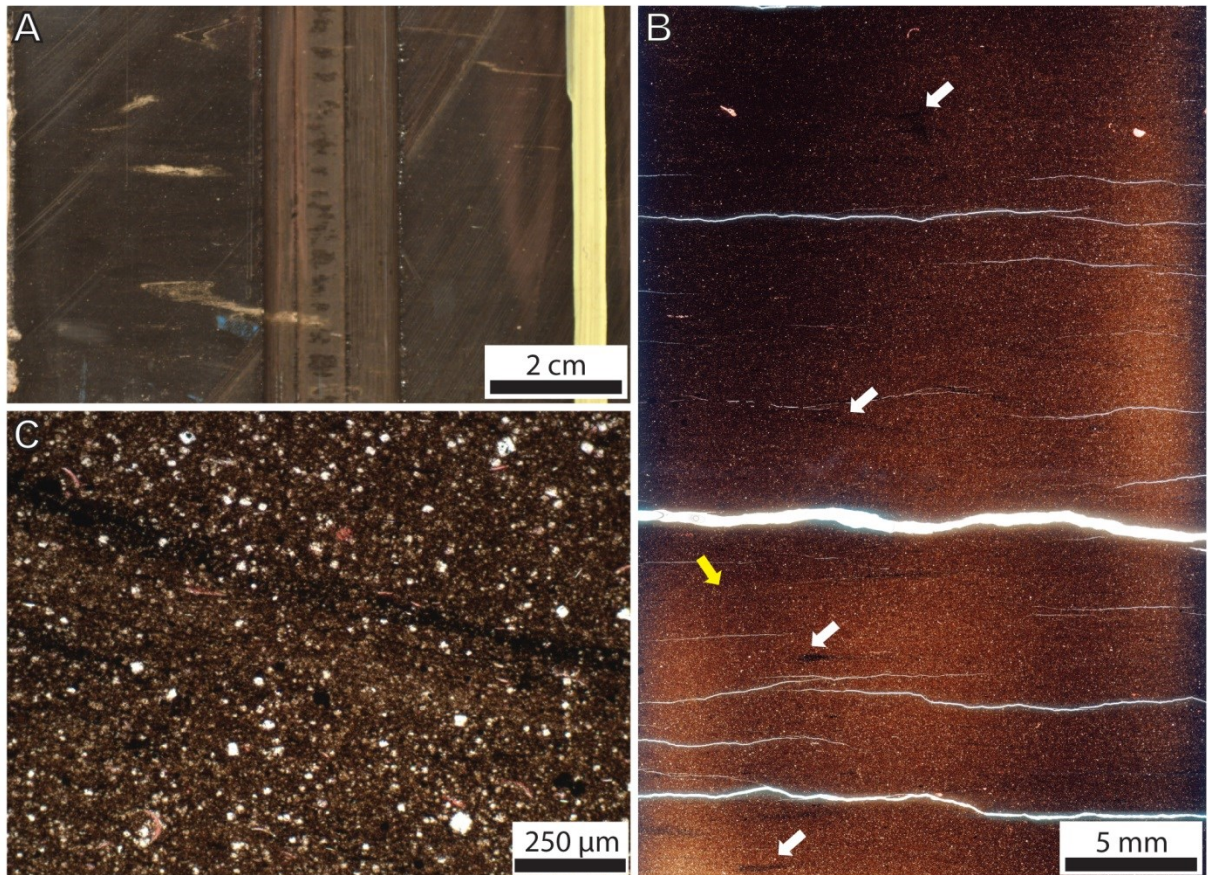


Figure 1.13: LF6 bioturbated pyritic mudstone. A) Intensely bioturbated mudstone. Pyrite preferentially precipitates in traces. Core photo, ECA Cecilia 11-04. B) Most of the sample is structureless but a faint bedding contact (yellow arrow) can be seen in the lower half of the image. White arrows point to pyrite-rich burrows. Thin section scan, adjusted brightness and contrast, ECA Cecilia 11-04. C) An inclined burrow in structureless mudstone is lined with pyrite (black). Burrow fill is less silty than surrounding sediment. Silt grains are dolomite, calcite and quartz. Brown matrix contains clay minerals and organic matter. Thin section photomicrograph, ECA Cecilia 11-04.

Clay- and silt-sized carbonate, quartz, clay minerals, and organic matter comprise most of the rock. Clay minerals and amorphous organic matter are sometimes observed as aggregates. Both clay mineral aggregates (~100-300 μm long, ~20 μm thick) and organic matter aggregates

(~50-200  $\mu\text{m}$  long, <10  $\mu\text{m}$  thick) appear as elongate stringers in bed-normal thin sections, and are approximately equidimensional in bed-parallel thin section. The average TOC for LF6 is 2.1 wt%. (SD=1.3, n=69). Calcareous radiolaria are uncommon to common. *In-situ* benthic macrofossils such as brachiopods and gastropods are common (Fig. 1.14) and *in-situ* benthic agglutinated foraminifera are uncommon to common. Fossils were identified as *in-situ* based on preservation, position, and presence within mudstone beds that do not show traction structures (i.e. no evidence for transport of grains/clasts or fossil fragments either).

LF6 is most common in the western and southern West Shale Basin. LF6 mudstones are particularly thick in the Wild River Sub Basin (Fig. 1.7).

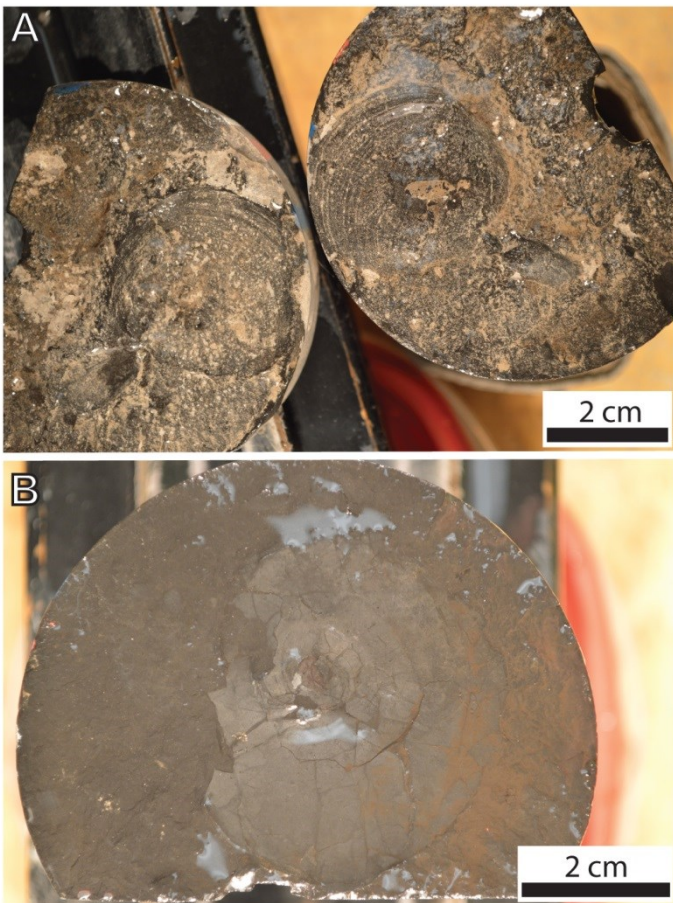


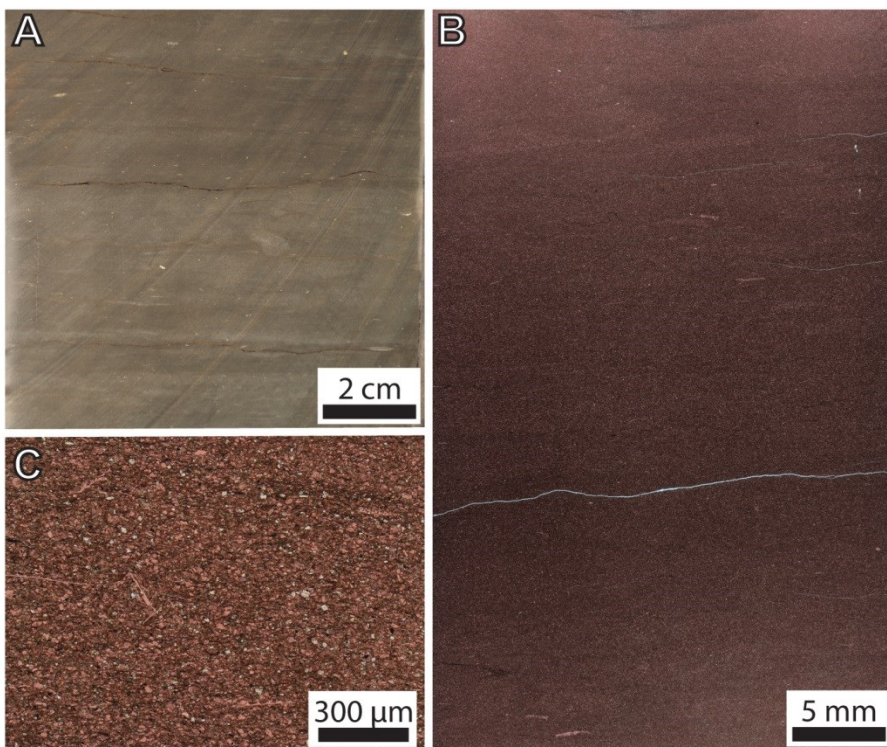
Figure 1.14: Benthic life in LF6. A) *In-situ* bivalve in bedding surface of core. Core photo. B) *In-situ* gastropod on bedding surface of core. Gastropod fossils larger than core diameter are common in LF6 of ECA Cecilia 11-04. Both photos from ECA Cecilia 11-04.

*LF7: Bioturbated calcareous mudstone*

LF7 is composed of medium grey-brown poorly-bedded calcareous mudstone. Bedding, where present, appears as wispy, wavy laminae that are generally less than 8 mm thick (Fig. 1.15). Laminae are observed as subtle variations in color. Lighter-colored laminae contain more fine-grained calcite than darker laminae. LF7 is moderately to intensely bioturbated and burrows are horizontal to subhorizontal.

Clay- and silt-sized calcite comprises most of the rock. Fine calcareous fossil fragments are common. Dark brown, amorphous organic matter fills space between grains. Rarely, organic matter appears as dark brown stringers in bed-normal thin sections (~50-200  $\mu\text{m}$  long, <10  $\mu\text{m}$  thick). In bed-parallel thin sections, uncommon organic matter masses appear approximately equidimensional. The average TOC for LF7 is 1.8 wt% (SD=1.6, n=24). No *in-situ* benthic macrofossils were observed but *in-situ* benthic agglutinated foraminifera are moderately common.

LF7 is most common in the East Shale Basin and is only a minor facies in the West Shale Basin. LF7 is the dominant lithofacies in the EOG 08-20 core, especially in the upper Duvernay member (Fig. 1.16).



LF7 is the dominant lithofacies in the EOG 08-20 core, especially in the upper Duvernay member (Fig. 1.16).

Figure 1.15: LF7 bioturbated calcareous mudstone. A) Poorly bedded, moderately bioturbated calcareous mudstone. Lighter colored beds have greater calcite abundance. Core photo. B) Structureless calcareous mudstone. Clay- and silt-sized calcite

is abundant. A lesser amount of quartz silt is present. Thin section scan. C) A large percentage of the rock is composed of calcite silt and calcareous fossil fragments. Minor organic matter is present between grains. Thin section photomicrograph, plane-polarized light, calcite is stained pink. All samples from EOG Cygnet 08-20.

#### LF8: Nodular limestone

LF8 is composed of nodular to burrow-mottled lime mudstone and wackestone. Light grey calcite nodules are hosted in dark grey mudstones to wackestones (Fig. 1.17). Nodules range from very irregular and burrow-mottled to ovoid to near-planar, and commonly contain

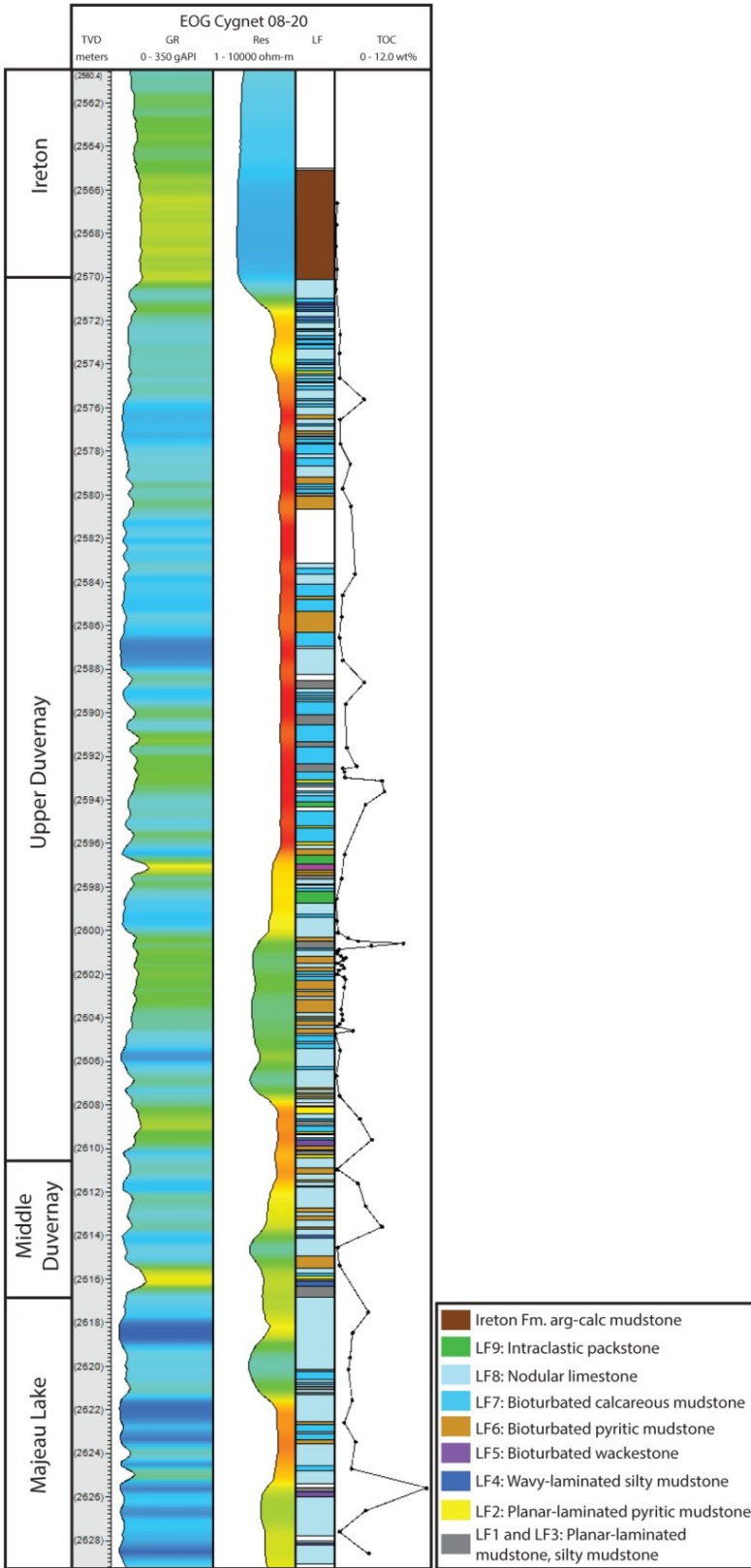


Figure 1.16: EOG Cygnet 08-20 core description. The core is dominated by calcareous facies LF7 and LF8. LF7 is especially dominant in the upper Duvernay member.

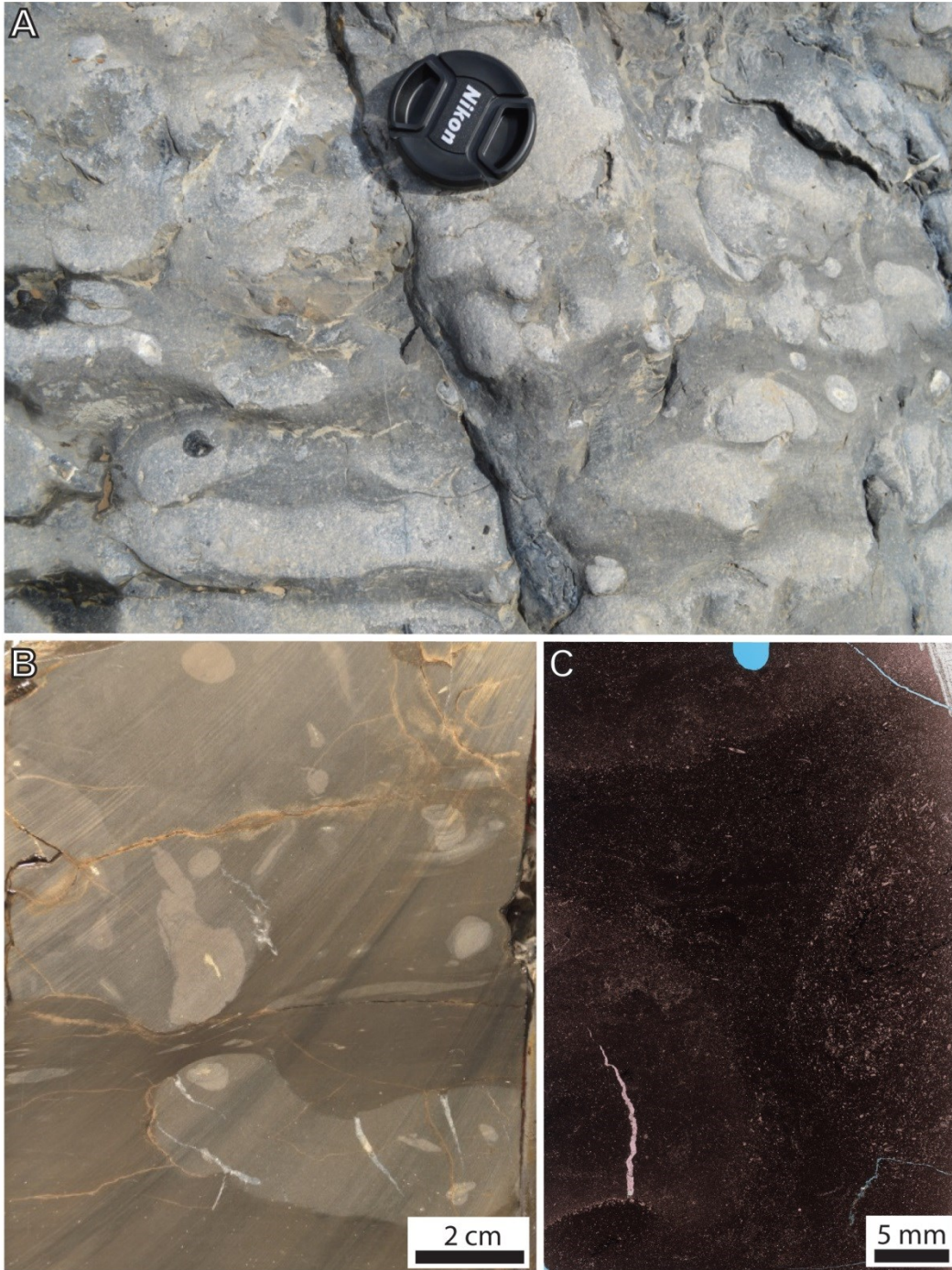


Figure 1.17: LF8 nodular limestone. A) Nodular limestone in Perdrix Formation outcrop (outcrop nomenclature for Duvernay Formation). Nodule size and morphology is variable and ranges from ovoid to irregular. Outcrop location: Nigel Peak / Wilcox Creek, Alberta, Canada. Lense cap diameter = 5cm. B) Uncemented dark grey mudstone is plastically deformed around calcite nodules. Calcite nodules contain spar-filled, wedge-shaped fractures. Burrows are preferentially cemented. Core photo, EOG Cygnet 08-20. C) Intensely bioturbated nodular lime wackestone. Fine calcite fossil fragments are abundant. Thin section scan, SCL Kaybob 02-22.

spar-filled, wedge-shaped fractures. Burrows are preferentially cemented with calcite. Detrital grains within nodules are predominantly clay- and silt-sized calcite and calcareous fossil fragments, most commonly styliolinids, tentaculitids, and brachiopods.

Nodules are surrounded by more ductile, uncemented mudstone, which deforms and drapes around nodules. Dark grey mudstone is structureless to poorly bedded, and is calcareous to argillaceous. Where calcareous, mudstones may not show significant compositional differences from nodules, aside from a lack of cementation. Where clay content is high, mudstones are fissile and tend to physically separate from nodules. The average TOC for LF8 is 1.1 wt% (SD=1.2, n=34), and was measured as a combination of nodule and mudstone.

LF8 is dominant within the middle Duvernay member (Fig. 1.5)

#### *LF9: Intraclastic packstone*

LF9 is composed of light grey intraclastic packstone. Bedding is structureless to planar-laminated and ungraded to normally-graded (Fig. 1.18A). Cross lamination is uncommonly observed. Grains are most commonly sand-sized calcite clasts and fossil fragments but generally also include a small amount of quartz and dolomite silt, and siliceous, phosphatic, or pyritic clasts and fossil fragments (Fig. 1.18B). Mud rip-up clasts are common. Fossil fragments include crinoids, gastropods, brachiopods, bivalves, styliolinids, tentaculitids and uncommon amphipora coral. Beds are significantly bioturbated where bedding is poorly preserved.

LF9 is very organic-lean. LF9 samples only contained notable organic matter when other organic-rich facies were included in the sample. For this reason, TOC values are not reported here. Only very rare wispy organic matter is observed in thin section between grains.

LF9 was only observed in the East Shale Basin (Fig. 1.16) and proximal to reef complexes in the West Shale Basin.

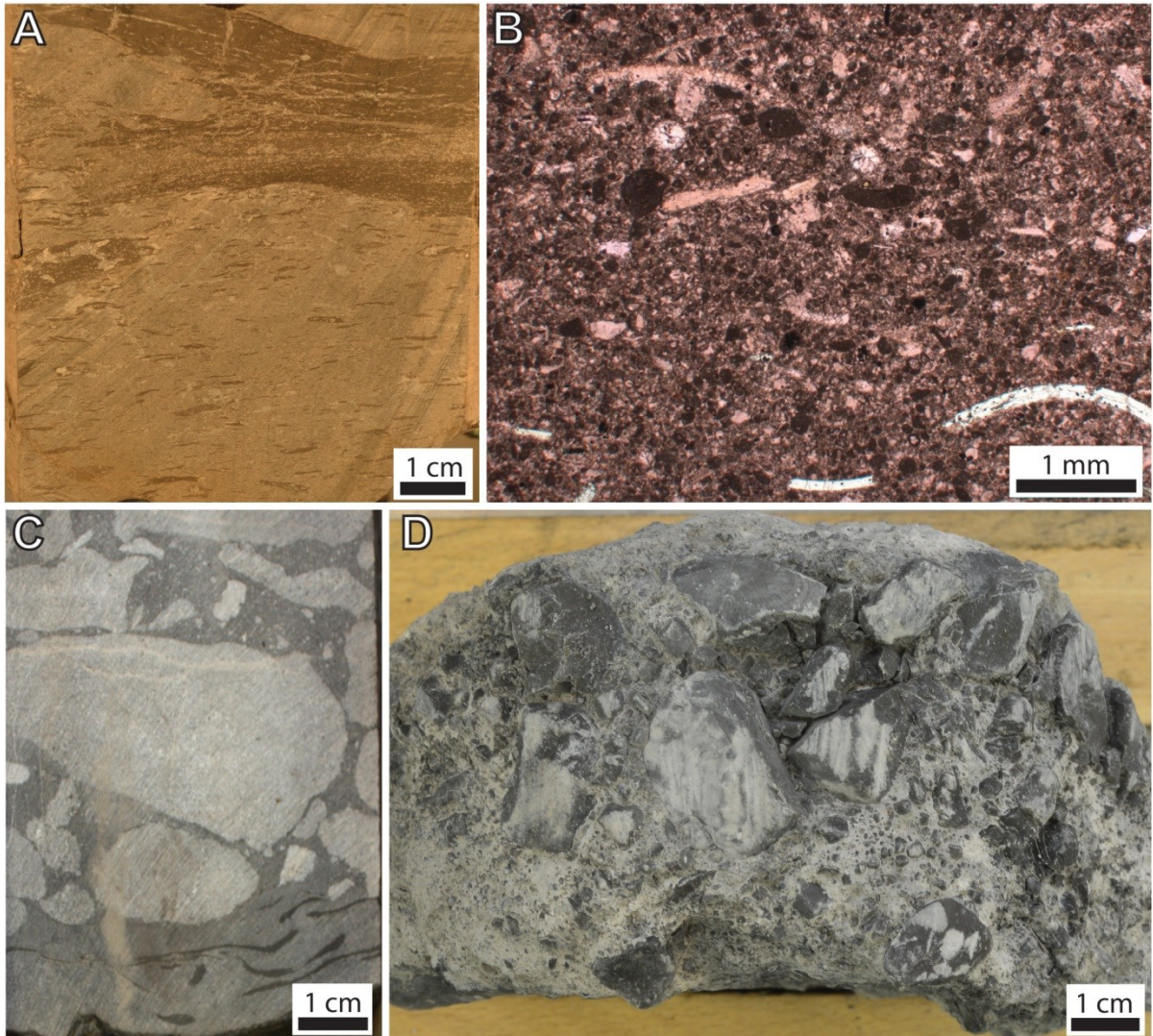


Figure 1.18: LF9 intraclastic packstone and LF10 limestone breccia. A) LF9 packstones are light grey and composed dominantly of sand-sized calcite with common mud rip up clasts. Core photo. B) Calcite clasts and fossil fragments are dominant but phosphatic, siliceous, and pyritic clasts and fossil fragments are present as well. Thin section photomicrograph. Both samples are from EOG Cygnet 08-20. C) Subangular limestone clasts are surrounded by packstone matrix. Bed has a sharp base and includes dark grey mudstone rip up clasts. Core photograph, AOSC Grizzly 01-24. D) Limestone clasts are poorly sorted in mudstone-packstone matrix. This core photo of a LF10 breccia is in the Swan Hills Formation underlying the Duvernay Formation in the Enermax Panther SturLs 14-02 core.

*LF10: Limestone breccia*

LF10 consists of angular limestone clasts in a calcareous mudstone to packstone matrix (Fig. 1.18C, D). Beds are generally 10-20cm thick, fine upwards or, less commonly, are

ungraded. LF10 intervals may contain several stacked fining upwards beds. Bases of beds are erosive and commonly contain dark to medium grey mudstone rip up clasts. Limestone clasts are angular to poorly rounded and range in size from pebble- to boulder-sized. Clasts larger than core diameter were identified as clasts rather than beds based on their angular edges, and because they had the same composition and textures as clasts that were smaller than core diameter.

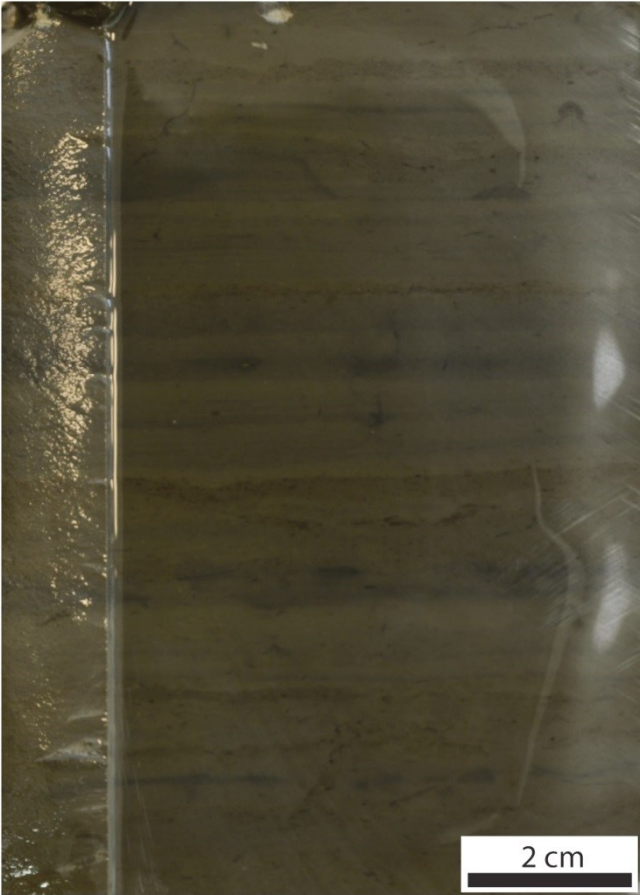
The matrix of LF10 is composed of calcareous mudstone to packstone. Mudstone ranges from dark grey and organic-rich to light grey, calcareous, organic-lean, and cemented. Matrix may be coarser-grained, up to granule-sized (above which grains were not considered matrix), consisting of calcite detritus. No thin sections were cut so no microscopic detail of LF10 is reported here.

Overall, LF10 is organic-lean, although no samples were taken for TOC analysis. Estimation of relative organic enrichment is primarily based on color, with dark grey matrix mudstone being the most organic rich.

The only core in which LF10 limestone breccias were found within the Duvernay Formation was the AOSC Grizzly 01-24 core, located adjacent to the northern margin of a reef complex in the West Shale Basin. No LF10 breccias were observed in East Shale Basin cores. LF10 intervals in the Duvernay Formation are immediately over- and underlain by organic-rich mudstones of LF1-4.

#### *LF11: Argillaceous-dolomitic mudstone*

LF11 is composed of organic-lean argillaceous-dolomitic mudstones. Mudstones are laminated to thinly-bedded and bedding quality ranges from moderately well-laminated to burrow-mottled (Fig. 1.19). Millimeter- to centimeter-scale light grey-brown organic lean laminae/beds alternate with 1-2mm thick dark grey-brown, more organic-rich laminae, or blue-grey, anhydrite- rich laminae. Laminae/beds are most commonly ungraded or normally graded, and are less commonly inversely graded. Bedding contacts may be sharp but are most commonly gradational over 1-2 mm, and are usually irregular due to bioturbation. Bioturbation ranges from moderate to intense. Horizontal to subhorizontal burrows are more common than subvertical



burrows. Subvertical burrows are rarely more than a few millimeters to one centimeter long. No fossiliferous material was observed in core.

LF11 was not sampled, analyzed for TOC, or thin sectioned so no microscopic detail is reported here. Relative organic richness is estimated based on color.

LF11 was only found in cores in the northeastern and eastern West Shale Basin (Fig. 1.20) and northern to northeastern East Shale Basin. LF11 is commonly associated with LF12 nodular dolostone.

Figure 1.19: LF11 argillaceous-dolomitic mudstone. Mudstones are laminated to thinly-bedded and significantly bioturbated. Core photo, Imperial Virginia Hills 06-36.

### *LF12: Nodular dolostone*

LF12 is nodular to burrow-mottled buff-colored dolomitic mudstone. Bedding is nodular to irregular and burrow-mottled (Fig. 1.21). Poorly bedded dolomitic-argillaceous mudstone is deformed around nodules. Fossils are rarely observable in core but include brachiopod and crinoid fragments. Anhydrite is common within burrows. Uncommonly, nodules contain wedge-shaped fractures filled with calcite, dolomite and/or anhydrite. Rarely, anhydrite nodules are observed. LF12 is organic-lean.

LF12 was not sampled, analyzed for TOC, or thin sectioned, so no microscopic detail is reported here. Relative organic richness is estimated based on color.

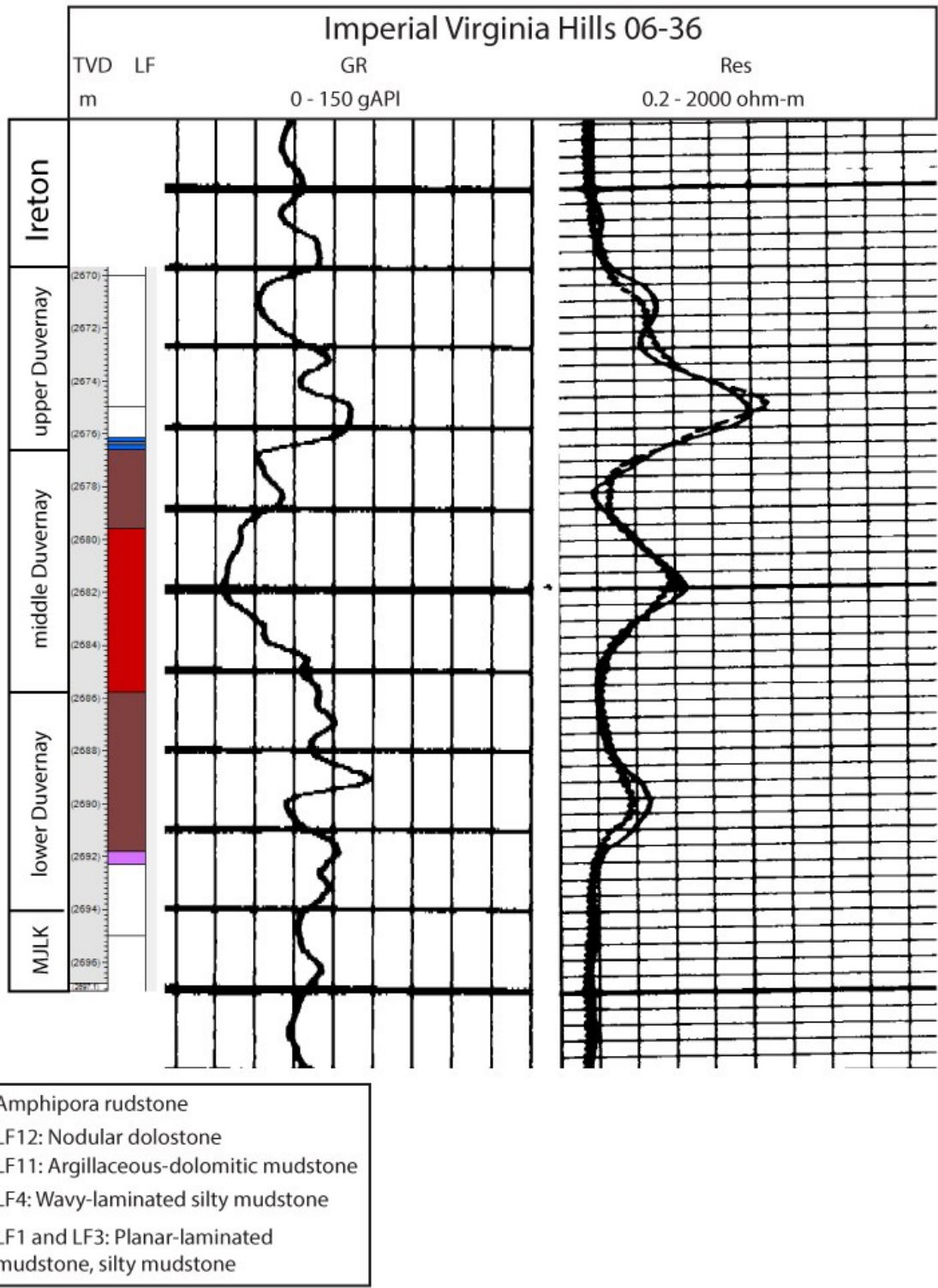


Figure 1.20: Core description of the Imperial Virginia Hills 06-36 core. LF11 and LF12 dominate the lower and middle Duvernay.

LF12 was only found in cores in the northeastern and eastern West Shale Basin and northern to northeastern East Shale Basin. LF12 is commonly associated with LF11 (Fig. 1.22)

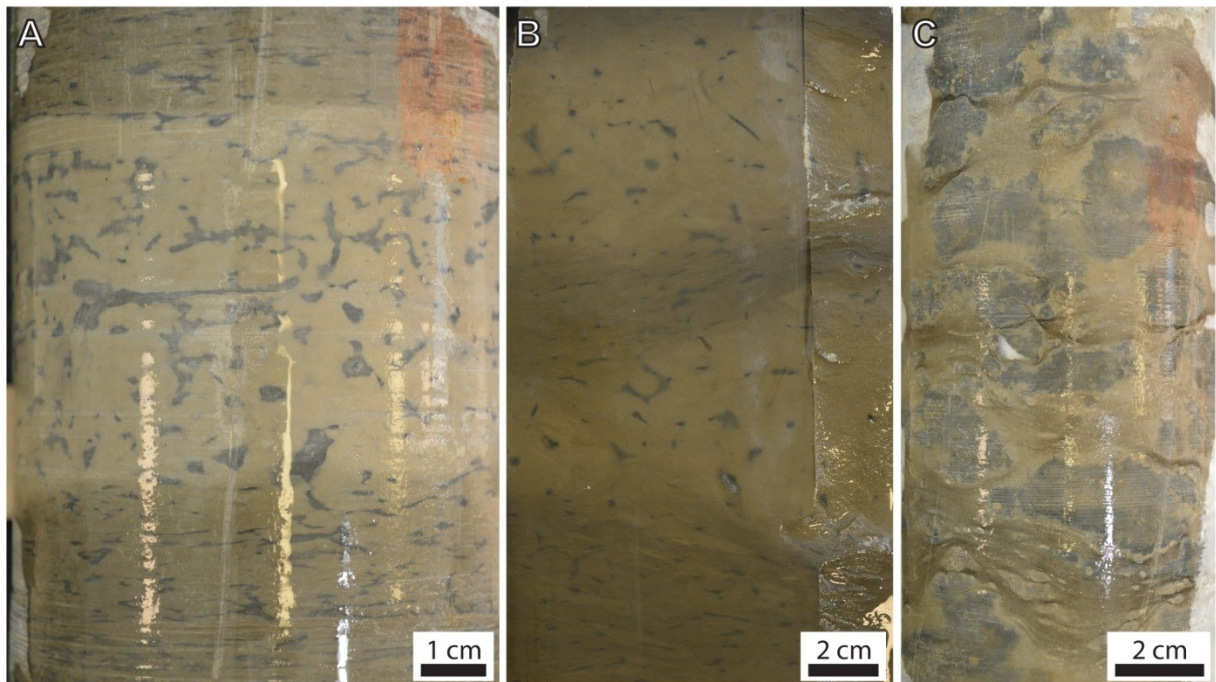


Figure 1.21: LF12 nodular dolostone. Nodules range from near-planar (A), to ovoid (B), to irregular (C), with varying abundance of anhydrite. All images are core photos. A) Sun IOE 10-09. B) Sarcee et al. Pibroch 10-16. C) Sun IOE 10-09

### 1.5 Discussion:

By examining lithofacies character and distribution in detail, we are able to interpret the depositional conditions responsible for each lithofacies. By examining sedimentary structures, we can determine mechanisms for the transport of both inorganic and organic sediment. Sedimentary structures, bioturbation fabrics, benthic fossils, and the presence of authigenic minerals such as pyrite, allow for the characterization of relative bottom water oxygen concentrations during the time of deposition. The relative compositions of each lithofacies, combined with their spatial distributions and sedimentary structures enable us to determine locations of lithofacies with respect to sediment sources.

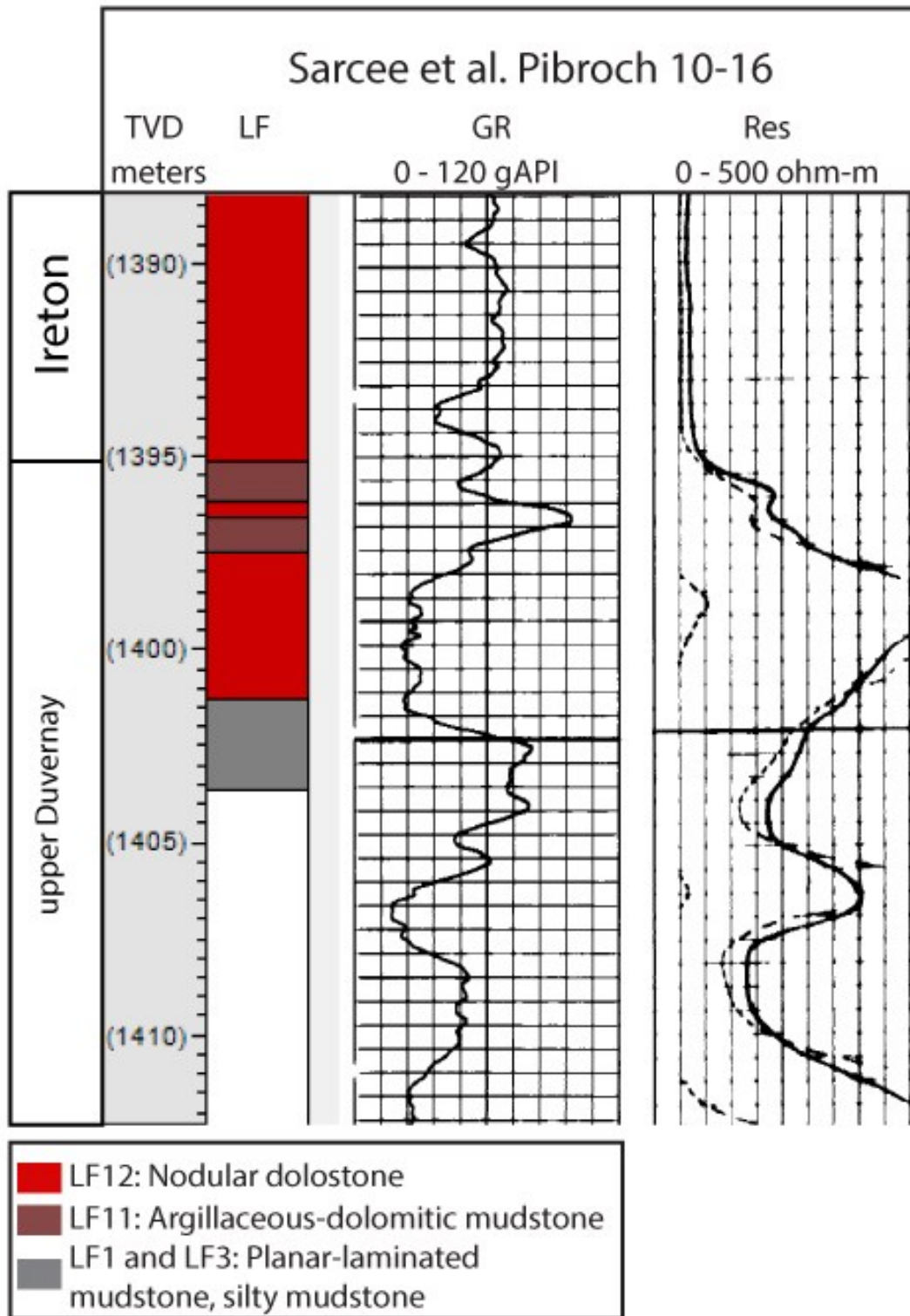


Figure 1.22: Core description of the Sarcee et al. Pibroch 10-16 core. LF12 is the dominant lithofacies.

### ***1.5.1 Lithofacies Interpretations***

#### *LF1-2 planar laminated mudstones:*

LF1 and LF2 contain the highest average TOC, and are the finest-grained facies. Most of the rock is mud-supported, dominated by amorphous organic matter and clay- and very fine silt-sized grains. Sedimentary structures are generally absent, and randomly dispersed planktonic radiolaria are moderately common. Subtle, mud-supported silty laminae, which represent ~50% of the facies, are generally ungraded, but rarely, poorly-defined normal grading is observed.

We conclude that hemipelagic suspension settling was the dominant but only depositional process for these facies, based on the general absence of sedimentary structures and the mud-supported fabric. Graded laminae represent deposition by weak turbidity currents or bottom water currents. Rare grain-supported silt laminae are interpreted to be lag deposits. Similar laminae are found within LF3 and LF4, interbedded with silty-sandy laminae that contain a variety of traction-type sedimentary structures, most of which are attributed to contour currents (see discussion below). Because of this association, the grain-supported and possibly the mud-supported silt laminae of LF1 and LF2 are interpreted to be the result of very weak contour currents that winnow away clay-sized sediment. Winnowing of fines by bottom current flow is a common occurrence in other formations (e.g. Shanmuggam, 2000; Martin-Chivelet et al., 2008).

Amorphous organic matter is present as organic matter aggregates. Organic matter aggregates are interpreted to be “marine snow” (Macquaker et al., 2010b). Organic matter aggregates form in the upper water column due to random collision or the activities of organisms (e.g., Alldredge 1976; McCave 1984; Alldredge and Silver 1988; Macquaker et al., 2010b), then settle through the water column. Aggregation of organic matter in modern environments increases settling velocity (Shanks, 2002), more rapidly removing aggregates from the water column. In modern oceans, marine snow is most common where primary productivity in the upper column is high (Alldredge, 1976; Billett et al., 1983; Lampitt, 1985; Thiel, 1995; Grimm et al., 1997; Fortier et al., 2002), and some authors have interpreted ancient beds rich in organic matter aggregates to be the result of enhanced productivity or algal blooms (Macquaker et al., 2010b). Organic matter aggregates in LF1 and LF2 of this study are not notably enriched in individual beds or laminae, but are randomly dispersed in the matrix, suggesting that enhanced

productivity events such as algal blooms were not frequent. Chow et al. (1995) reached a similar conclusion by mapping organic facies and depositional facies in Duvernay Formation sediments near the Redwater reef complex. The authors concluded that a lack of algal bloom facies (defined by algal akinete cells and large, thick-walled Prasinophyte phycomas) in Duvernay Formation sediments was an indicator that normal productivity and low oxygen conditions were the norm, rather than episodic high productivity.

Clay minerals are in low abundance in LF2 and especially LF1. Near the Peace River Arch, where clay minerals are more abundant within LF1 and LF2 mudstones, clay mineral aggregates are more common. The morphology of clay mineral aggregates is similar to the organic matter aggregates, suggesting a similar origin as floccules or fecal pellets in the upper water column and deposition through suspension settling. Konitzer et al. (2014) identified similar features late Mississippian mudstones of the Widmer Gulf, UK, attributing them to suspension settling of aggregates. Konitzer et al. (2014) also recognized slightly larger clay mineral aggregates with sharper edges and tapered ends, which they attributed to erosion and transport of mud clasts. Clay mineral aggregates observed in LF1 and LF2 Duvernay Formation mudstones are ovoid, some with irregular to wispy edges, and are interpreted to be a product of suspension settling of aggregates rather than erosion and transport of mud clasts.

LF2 is distinguished from LF1 by the presence of laminae defined by enrichments of framboidal and euhedral pyrite, and varying amounts of pyrite-replaced carbonate silt and fossil fragments. The limiting factors in pyrite formation in marine sediments are the availability of metabolizable organic matter, the diffusion of sulfate into sediments, and the total concentration and reactivity of iron minerals (Berner, 1970). In epicontinental settings  $\text{Fe}^{2+}$  is sourced primarily from terrigenous minerals (Berner, 1970), and in the Duvernay Formation, especially in LF1-4, terrigenous mineral supply is low. Pyritic laminae of LF2 are interpreted to be the result of slightly increased clay mineral abundance. In environments where the availability of metabolizable organic matter and the diffusion of sulfate in the sediment are not limiting factors for pyrite formation, the limiting factor may be  $\text{Fe}^{2+}$  from clay minerals. Most commonly, LF2 is seen overlying flooding surfaces, in which case the clay minerals are interpreted to be the result of transgressive reworking of more clay mineral-rich regressive deposits (see Chapter 2 for

sequence stratigraphic discussion). Additionally, LF2 is common within intervals of abundant (and more argillaceous) LF6 bioturbated pyritic mudstone (Fig. 1.7), suggesting iron from terrigenous clay minerals is the limiting factor in pyrite formation. Pyrite laminae in LF2 commonly pinch and swell and include pyritized fossil fragments suggesting that pyrite formation occurred during early diagenesis.

*LF3-4 planar to wavy laminated silty mudstones:*

Sedimentary structures in LF3 and LF4 include planar parallel lamination, low angle cross-lamination, lenticular- to wavy-bedding, starved ripples, gradational to sharp erosive bases, both normal and inverse grading, sharp (non-erosional) upper contacts, flame structures and soft sediment loading deformation. Shanmugam (2000) identified many of these features and others as evidence for reworking and transport by bottom water currents when several are observed in combination. Critically, most silty-sandy beds and laminae of LF3 and LF4 show no regular vertical stacking of structures such as those recognized in the Bouma (1962) sequence. While some authors argue that a characteristic set of traction current structures are diagnostic of contourites (Martín-Chivelet et al., 2008; Shanmugam, 2008), other authors suggest that pervasive bioturbation that destroys primary sedimentary structures is a diagnostic criteria (Stow and Faugères, 2008; Wetzel et al., 2008). Pervasive bioturbation is a common phenomenon in some recent and modern contourite systems (for example, the Faro Drift in the Gulf of Cadiz; Gonthier et al., 1984; Stow and Holbrook, 1984; Stow and Piper, 1984) due to oxygen-rich bottom currents, but the same conditions may not have been present throughout the rock record, especially during the Devonian when global sea level was much higher and black shale deposition was widespread. Contourite studies from recent and ancient successions show that bioturbation in contourites can be highly variable or non-existent (Dalrymple and Narbonne, 1996; Ito, 1996). Contourite beds in the Duvernay Formation are recognized by their diagnostic set of traction current structures, as per Shanmugam (2000). Some contourite beds in this study are bioturbated, but in general, bioturbation is minimal, which likely reflects low-oxygen conditions at the sediment-water interface.

While most of the silty laminae in LF3-4 are interpreted to have been deposited by contour currents, turbidite beds are present as well. Thin turbidite beds are most commonly found within LF4 and are identified by their sharp, erosive bases, normal grading, and presence of coarser fossil fragments than in surrounding beds. The grain size in contourite beds is silt to sand, while turbidite beds often contain fossil fragments greater than 1mm in length and uncommonly greater than 1cm. Importantly, turbidite beds do not contain sedimentary structures such as inverse grading, wavy to lenticular bedding, starved ripples, or sharp (non-erosional) upper contacts, which have been used as diagnostic criteria for contourite deposits. Contourite and turbidite beds are commonly interbedded in continental slope, rise, and abyssal plain settings (Rebesco and Camerlenghi, 2008; He et al., 2008; Mulder et al., 2008; Gao et al., 1995; Stow et al., 2002d; Moraes et al., 2007; Stow et al., 2002f; Viana and Rebesco, 2007); in these settings, bottom water currents may rework turbidite beds or more rarely, pirate sediment directly from turbidity currents (Rebesco et al., 2002; 2007). Turbidites probably provided a source of sediment for contourites in LF3 and LF4.

The mudstone interbeds in LF3 and LF4 are very similar to LF1 and LF2, in that they are very fine-grained, organic-rich, lack sedimentary structures, and contain randomly dispersed planktonic radiolaria. This implies that mudstone interbeds in LF3 and LF4 were deposited through suspension in a low energy environment, when contour currents were weak or nonexistent. A lack of bioturbation and *in-situ* benthic macrofossils suggests that anoxia was the norm during periods of minimal bottom current activity. Organic matter in LF3 and LF4 is found primarily in the mudstone laminae/beds. Amorphous organic matter is observed as aggregates, as in LF1 and LF2, similarly leading to the conclusion that organic matter formed aggregates in the water column and settled from suspension.

The interbedded nature of organic-rich mudstone with silty-sandy contourite beds is interpreted to reflect long-term fluctuations in bottom-current strength. Stow et al. (2008) noted that bottom water currents show variability in strength over periods of tens of years to thousands of years, which can be linked to climatic cycles and sea level cycles, and in some cases to the morphology of basins and their connection to open ocean currents. Similarly, Hemmesch et al., (2014) documented systematic variability in carbonate beds in the Woodford Shale that they related to third order sea level cycles. While surface currents in the Alberta Basin during

deposition of Duvernay Formation sediments have been studied (e.g. McLean and Mountjoy, 1993; Mallamo, 1995), no documentation of bottom water currents exists. It is hypothesized here that basin morphology had a strong control on bottom water current development, and that the evolution of the northeast portion of the basin from ramp to platform focused contour currents and fed carbonate sediment to the contour current system (see discussion in Chapter 2).

#### *LF5 bioturbated wackestones and floatstones*

LF5 is fossiliferous and structureless to poorly-bedded. LF5 beds are interpreted to be the product of turbidity currents, based on the presence of sharp bases and normal grading, although these features are commonly destroyed during bioturbation. The abundance of fossils and fossil fragments represents an increase in energy as fossils and fossil fragments are often much larger than LF5 matrix grains and the clay to silt grain size of under- and overlying beds.

The fossiliferous nature of LF5 beds may simply be due to grain size sorting within turbidity currents and the concentration of fossils and fossil fragments that are significantly larger than matrix grains. This is likely the case as beds that are not significantly bioturbated show a concentration of bioclasts near the base of the bed and bioclasts become finer and less concentrated upwards. Stasiuk and Fowler (2004), in a study of the Duvernay Formation and other Devonian and Mississippian source rocks of Western Canada, suggested that their radiolarian-rich organic facies D may be the result of increased basin circulation and connection to open ocean, and pointed to the modern occurrence of siliceous planktonic organisms in association with upwelling systems (Barron, 1993; Jones, 1996). If the presence of radiolaria is indicative of increased productivity events such as algal blooms, LF5 beds may have formed in response to an influx of organic and biologic sediment to the sea floor. Importantly however, increased organic matter is not petrographically observed in association with LF5 beds. Common bioturbation in LF5 beds may have destroyed evidence of increased organic matter deposition, but this is not likely the case. Algal bloom events result in a rapid influx of organic matter to the sea floor. Anoxia can be induced by the oxygen demand of decaying organic matter (e.g. Pedersen and Calvert, 1990), and as such, an algal bloom is not likely to produce a significantly bioturbated bed in an otherwise unbioturbated or minimally bioturbated succession of mudstones

(e.g. Wetzel, 2010). LF5 beds in this study are interpreted to be the result of turbidity currents and resultant temporary increase in bottom water oxygen concentration rather than increased upper water column biological productivity.

#### *LF6 bioturbated pyritic mudstone*

LF6 is moderately to intensely bioturbated, often contains *in-situ* benthic macrofossils, but contains much more organic matter (average 2.1% TOC) than similarly bioturbated LF7 and LF8. While organic matter preservation in organic rich facies LF1-4 can generally be explained by anoxic conditions at the sediment-water interface, the same interpretations cannot be applied to LF6 due to the abundance of bioturbation and *in-situ* benthic macrofossils that imply oxygenation. There is no evidence for persistent anoxia, and anoxia may not have developed at all. Bottom waters are interpreted to be dysoxic based on moderate to intense bioturbation but low trace fossil diversity as predicted by studies of modern sediments (e.g. Bromley and Ekdale, 1984; Ekdale and Mason, 1988). Total organic carbon values are lower in LF6 than LF1-4, which is likely due to an increase in bottom water oxygenation and increased aeration of sediment due to burrowing activity (e.g. Rhoads, 1974; Aller, 1978; Demaison and Moore, 1980). However, similarly bioturbated sediments of LF7 and LF8 are considerably less organic-rich than LF6, indicating that organic matter in LF6 was enriched due to some factor.

One possible factor in organic matter enrichment in LF6 is increased sedimentation rates. A slight increase in sedimentation rate due to a greater flux of clay minerals in LF6 with respect to LF1-4 may have more rapidly buried organic matter below the reach of oxidants. While an increase in rates of inorganic sediment can dilute organic matter, slight increases in sedimentation rates have been shown to result in enhanced organic carbon preservation in depositional settings that are not persistently anoxic (Tyson, 2005; Bohacs et al., 2005; Macquaker et al., 2010b)

A second factor in organic matter preservation in LF6 may be increased organic matter aggregation or armoring of organic matter by clay minerals. LF6 contains an increase in clay minerals with respect to LF1-4, which may have resulted in more common formation of organo-minerallic aggregates and more efficient transportation of organic matter to the sea floor.

Macquaker et al. (2010b) have linked increased organic matter preservation to an increase in aggregation of organic matter and clay-sized minerals in oxygenated settings. Aggregation of organic matter increases settling velocity (Shanks, 2002), and reduces the time that organic matter is exposed to oxidants in the water column. Kennedy et al. (2002) demonstrated that increased preservation of organic matter can be associated with the high surface area in clay minerals.

#### *LF7 bioturbated calcareous mudstone*

LF7 is structureless to poorly bedded, with observable bedding characterized by wispy-wavy laminae of varying calcite abundance. Bioturbation commonly destroyed much of the primary sedimentary structures in LF7, making it difficult to characterize sediment transport mechanisms with confidence. The lack of primary sedimentary structures also suggests that episodes of rapid sedimentation were uncommon and that persistently slow sedimentation rates provided ample time for infaunal organisms to homogenize the sediment. Interlaminated layers of variable calcite silt may be the remains of thin turbidite or contourite beds.

Bioturbation in LF7 is moderate to intense, but only horizontal to sub-horizontal burrows are observed, suggesting that only the surface millimeters of sediment were habitable for burrowing organisms. Additionally, moderate to intense bioturbation combined with shallow burrow depth and low diversity of trace fossils is a likely indicator of dysoxic bottom waters (e.g. Bromley and Ekdale, 1984; Ekdale and Mason, 1988; Savrda and Bottjer, 1987, 1989; Wignall, 1991; Wignall and Pickering, 1993; Savrda 1995, 2007). *In-situ* benthic macrofossils are not observed. Low oxygen concentration rather than soft substrate is interpreted to be the cause of the absence of benthic macrofossils, as soft substrate will only reduce benthic diversity, not eliminate it (Rhoads and Morse, 1971; Byers, 1977; Wignall, 1993). Additionally, low-oxygen-tolerant benthic agglutinated foraminifera are observed in LF6. In other organic-rich mudstone formations, the presence of benthic agglutinated foraminifera has been used to infer the presence of dysoxic rather than anoxic bottom waters (Milliken et al., 2007; Schieber, 2009). Benthic agglutinated foraminifera have a high tolerance for low oxygen conditions but cannot survive in anoxic bottom waters (Bernhard and Reimers, 1991; Bernhard et al., 2003). LF7

mudstones are interpreted to be deposited in dysoxic but not anoxic bottom waters due to the presence of a diminutive set of trace fossils, lack of benthic macrofossils, and presence of low-oxygen-tolerant benthic agglutinated foraminifera.

LF7 is not significantly enriched in organic matter, which is likely due to dysoxic rather than anoxic bottom waters, the activity of burrowing organisms, and an increased rate of carbonate sedimentation resulting in dilution of organic matter.

#### *LF8 nodular limestone*

LF8 is typically organic-lean, with irregular to ovoid calcite nodules encased in medium to dark grey-brown mudstone and wackestone. Increased bioturbation is the result of increased bottom water oxygen concentration. An abundance of fine calcareous fossil fragments within nodules may be the result of event bed deposition, although any sedimentary structures diagnostic of turbidity currents have largely been destroyed by bioturbation. Where LF8 is not considerably burrow-mottled, calcite nodules form semi-continuous beds that alternate with uncemented mudstone beds, and may reflect changes in the sedimentation rate of carbonate detritus. Mudstone-wackestone beds between nodular horizons likely accumulated during prolonged periods of lower sedimentation rates and dysoxic bottom waters. These beds are variably bioturbated but sometimes contain crude lamination and are more organic-rich than calcite nodules.

Uncemented mudstones and wackestones are deformed around calcite nodules, suggesting that nodule formation predates complete compaction. Additionally, wedge-shaped, calcite spar-filled fractures in calcite nodules suggest that brittle fracturing of nodules occurred, likely due to compaction post-dating early lithification. Stoakes (1980) came to the same conclusion, as have other authors studying similar deposits (Tucker, 1973; Noble and Howells, 1974; Kennedy and Garrison, 1975; Mullins et al., 1980).

### *LF9-10 packstones and breccias*

LF9-10 packstones and breccias contain angular clasts and display poor sorting and normal grading, suggesting deposition from turbidity currents and debris flows. Debris flows were likely caused by slope instability of reef margins (e.g. Braithwaite, 2014). McLean and Mountjoy (1993) suggested that northeastern sides of reef complexes in the Alberta Basin had steeper slopes due to the northeast to southwest direction of wind and surface water currents. Southwestern sides of reef complexes and areas protected from wave energy had more gently dipping reef margins due to the accumulation of fine-grained carbonate detritus. Leeward sides of reef complexes commonly have steeper margins because wave energy does not allow for the accumulation of fine-grained calcareous sediment. Duvernay Formation LF10 breccias were only observed in the AOSC Grizzly 01-24 core which is located adjacent to the northern margin of the Bigstone reef complex. LF9 packstones were also likely generated by slope failure events, as suggested by the wide range of clasts, and presence of shallower water taxa than organic-rich mudstones. Their presence near reef complexes suggests origin from reef-margin deposits.

Breccias and packstones are commonly overlain by dark grey, organic rich mudstones of LF1, indicating that they were deposited as event beds in an environment that was suitable for the accumulation of fine-grained, organic rich sediment. This environment is described in the discussion for LF1 and LF2.

LF10 breccias were likely not geographically widespread, occurring only very close to reef margins, as suggested by their presence in only 1 of the 26 cores examined. Additionally, authors such as Mountjoy (1980), McLean and Mountjoy (1993), Van Buchem et al. (1996a), and Whalen et al. (2000) have documented in time-equivalent reef margin strata in outcrop that limestone breccias and conglomerates extend a few hundred meters to a few kilometers into the basin from reef margins. LF9 packstones are more widespread and were deposited further from reef complexes than LF10 breccias (i.e. EOG Cygnet 08-20 core). However, LF9 packstones are not observed in the vast majority of the West Shale Basin due to longer transport distances from reef complexes.

### *LF11 argillaceous mudstone*

LF11 is argillaceous to dolomitic, organic-lean, and bioturbated mudstone. Light brown laminae comprise most of the rock, and represent periods of increased sedimentation rate of argillaceous and dolomitic detritus. Light brown laminae are often sharp based when not significantly bioturbated, and grade upwards into darker colored laminae. Dark brown laminae are interpreted to be more organic-rich, based on color, and may represent periods of reduced inorganic sediment supply and increased concentration of preserved organic matter. Similarly, where grey-blue, anhydrite-rich laminae alternate with light brown laminae, evaporite precipitation seems to have occurred between increased sedimentation events. Anhydrite-rich laminae are more common when LF11 is interbedded with LF12, likely representing a position further upslope than instances of LF11 with more common dark grey-brown laminae. The bulk of the sediment resides in light brown laminae most of which are interpreted to be deposited from sediment-gravity flows based on the abundance of sharp-based, normally graded beds. Similar graded mud beds have been outlined in other studies (e.g. Bhattacharya and MacEachern, 2009; Macquaker et al., 2010a; Macquaker et al., 2010b; Aplin and Macquaker, 2011), although this study does not present any microscopic observation of LF11 for direct comparison of results. The presence of beds showing inverse grading or both inverse and normal grading suggests some deposition during waxing and waning flow energies. These conditions can be created by density-driven deep-water contour currents (e.g. Rebesco, 2014) or currents driven by climatic factors such as wind, runoff, precipitation and evaporation rates, temperature gradients, and mixing of water bodies (e.g. Kump and Slingerland, 1999). Basin-filling patterns in the Duvernay Formation (Stoakes, 1980; Chapter 2 of this thesis) and overlying Ireton Formation (Stoakes, 1980) suggest that currents flowing parallel to the Grosmont Platform significantly affected sedimentation patterns.

Bioturbation is moderate to intense, with greater trace fossil diversity than seen in previously described lithofacies, suggesting dysoxic to oxic bottom water conditions. This interpretation is supported by the lack of organic matter in LF11. No benthic macrofossils were observed in LF11, which may be the result of soft substrates, rapid rates of sedimentation, or inadequate oxygenation. Subvertical burrows are present but are only uncommonly more than 1 cm in length, which may be a result of rapid sedimentation rates or variable oxygen or salinity

conditions. Oxygen variability is more likely the case when light brown laminae alternate with dark grey-brown, more organic-rich laminae, which reflect deposition further downslope. Such variability in oxygen conditions has been suggested to deter colonization of shelly benthic fauna, and act to preserve lamination from disruption by burrowers (Savrda et al., 1984). Salinity fluctuations seem to have been more common in upslope positions where LF11 and LF12 are interbedded and grey-blue, more anhydrite-enriched laminae are common.

#### *LF12 nodular, burrow-mottled dolostone*

LF12 is an organic-lean, dolomitic, and intensely bioturbated dolostone. The nodular fabric, similar to LF8 nodular limestones, results from early cementation. Ductile, more argillaceous mudstone between nodules is deformed around nodules, indicating that nodules had formed before significant compaction and lithification of the mudstone. Rare wedge-shaped fractures in nodules are filled with calcite, dolomite and/or anhydrite and are the result of brittle fracture – another indicator of early cementation (Tucker, 1973; Noble and Howells, 1974; Kennedy and Garrison, 1975; Mullins et al., 1980; Stoakes, 1980). The presence of nodules may indicate that overall sedimentation rates were low, allowing time for nodule formation before significant burial and compaction.

Intense bioturbation and scarcity of organic carbon indicate that LF12 was deposited in an oxic to dysoxic environment. Anhydrite is very common in burrows, and uncommonly as nodules, which may indicate that salinity levels were high. High or fluctuating salinity may explain the scarcity of benthic macrofossils. Alternatively, benthic taxa may have been deterred by variable oxygen levels, as in LF11, however, no organic-rich laminae were observed, and bioturbation is consistently intense.

LF12 is interpreted to be deposited on the carbonate platform margin or upper foreslope, in relatively oxic bottom waters. Deposition of clay minerals was limited by increased wave energy and increased carbonate sediment supply (Stoakes, 1980).

### ***1.5.2 Transport and Deposition of Fine-Grained, Organic-Rich Sediment***

Interpretations of the depositional processes responsible for mud transport and deposition of organic-rich sediment have changed significantly since the 1980s, particularly since the recognition of high wave and tidal energies in mud-dominated environments (e.g. Nittrouer and Sternberg 1981; Rine and Ginsburg 1985). Higher energy deposition of clays as a result of flocculation has also been demonstrated in laboratory flume experiments (Scheiber et al., 2007b; Scheiber and Southard, 2009; Schieber, 2011) and ancient deposits (e.g. Wignall, 1994; Macquaker and Keller, 2005; Macquaker et al., 2010b; Aplin and Macquaker, 2011). Bottom water currents in modern oceans and ancient marine deposits have also been observed in mud-dominated settings (Rebesco et al., 2014). These studies demonstrate that the presence of mud or shale does not necessarily imply a dominance of suspension settling in deep, quiet water. Traction transport of fine sediment by bottom water currents have been observed within organic-rich strata as well (Hernández-Molina et al., 2013; Stow et al., 2013b), indicating that black shale deposition does not necessarily depend on a persistently stagnant water body.

#### *Aggregate Grains and Suspension Settling*

In the Duvernay Formation, clay minerals and organic matter are commonly deposited as aggregate grains. In clay-poor facies such as LF1-4, aggregates are primarily composed of amorphous organic matter, whereas more clay-rich facies such as LF6 contain more clay-mineral aggregates; this also characterizes occurrences of LF1 and LF2 near the Peace River Arch. Both organic matter aggregates and clay mineral aggregates are interpreted to have formed in the upper water column due to random collision or the activities of organisms (e.g., Alldredge 1976; McCave 1984; Alldredge and Silver 1988; Macquaker, 2010b)

Bioturbated facies generally lack aggregate grains, which is interpreted to primarily be the result of disaggregation during sediment disturbance. LF6 bioturbated pyritic mudstones are more argillaceous than both LF1 and LF2 but clay mineral aggregates are less common than would be expected if the abundance of aggregates was simply a function of clay mineral abundance. The presence of a bioturbating infauna suggests oxygenation of bottom waters, which may also imply periodic sediment agitation by wave or current action that would cause

disaggregation. While it is conceivable that sediment agitation by soup-ground-style bioturbation may cause disaggregation, no support for this hypothesis was found in the literature. Aggregate grains are uncommon in calcareous bioturbated facies LF7 and LF8. This may be partially due to the reduced potential for electrochemical flocculation of clay-sized carbonate grains as compared to platy clay minerals. Clay minerals have greater flocculation potential than carbonates due to their high surface area to volume ratios and potential for their surfaces to carry strong electrochemical charges (Grabowski et al., 2011). Rarely, calcareous aggregates are observed, and are interpreted to be calcareous fecal pellets, rather than floccules. The lack of organic matter aggregates in bioturbated calcareous facies is likely due to a combination of increased oxygenation resulting in increased organic matter decay, disaggregation due to sediment reworking by burrowers and wave/bottom current energy, and less common aggregation in the water column because clay minerals are scarce.

Clay mineral aggregates and organic matter aggregates observed in Duvernay Formation sediments are interpreted to have been deposited through suspension and not subsequently reworked or transported by bottom water currents. Schieber et al. (2007b), and Schieber and Southard (2009) used flume experiments to show that flocculated clay minerals can be transported as bedload without disaggregating, and can form sedimentary structures such as ripples. This phenomenon has not been observed in Duvernay Formation mudstones. While it is possible that some aggregate grains were reworked by contour currents such as those responsible for sedimentary structures in LF3 and LF4, these aggregates must have been disaggregated during transport, as no aggregate grains are found in association with any traction-deposited bed. Schieber et al. (2010) detailed the transport of mud rip up clasts in flume experiments, but noted that these rip up clasts show irregular outlines in plan view and are poorly sorted. Clay mineral aggregates in Duvernay Formation sediments tend to have ovoid outlines in plan view, and have a relatively narrow size range. These results are consistent with fecal pellets observed by Cuomo and Bartholomew (1991) and Roehl et al. (2001). A lack of elongate morphologies in plan view eliminates an interpretation of aggregates as burrows.

### *Bottom Water Currents in Organic-Rich Facies*

Early interpretations of black shales postulated that deposition occurred in deep, quiet, anoxic bottom waters; recent detailed sedimentological studies have been breaking down this paradigm. The recognition of event beds and traction-derived sedimentary structures in black shales (e.g. Schieber, 1999; Macquaker and Bohacs, 2007; Macquaker et al., 2010b; Ghadeer and Macquaker, 2011, 2012; Abouelresh and Slatt, 2012; Hemmesch et al., 2014) indicates that bottom waters were not persistently stagnant and that in some cases, much of the sediment may have been deposited from sediment-gravity flows, or bottom water currents, rather than predominantly through suspension settling from the upper water column.

In the Duvernay Formation, the presence of contourite and turbidite beds within black shale units of LF3 and LF4 indicates that quiet water deposition was not persistent. Silty-sandy beds and laminae are commonly interbedded/interlaminated with organic-rich mudstone beds and laminae, indicating that periodically, bottom water energy was high enough to transport larger grains and rework and winnow previously deposited sediment. Some turbidite beds exist within LF3 and LF4 and represent very short-term events that introduce fresh sediment. However, the majority of the coarser grained material has been reworked and deposited by contour currents, which represent longer-term fluctuations in bottom water energy (Stow et al., 2008). In LF1 and LF2, the most organic-rich facies, suspension settling was the dominant depositional process, however some of the silt-sized material in these facies was transported by weak turbidity currents and bottom water currents as evidenced by weakly graded laminae, and rare grain-supported silt-laminae. This dual role of suspension settling and bottom current/turbidity current transport is important to note, as suspension-deposited sediment in some organic-rich mudstones is actually a very minor component of the rock (e.g. Ghadeer and Macquaker, 2011, 2012)

Bioturbation in LF3 and LF4 is absent to moderate, indicating that bottom water currents carried low but variable concentrations of dissolved oxygen. Some authors (Stow and Faugères, 2008; Wetzel et al., 2008) have suggested that ubiquitous bioturbation is diagnostic of contourites, although others disagree (Martin-Chivelet et al., 2008; Shanmugam, 2008), and have identified unbioturbated contourite deposits. While many bottom water currents in modern oceans occur in oxygenated environments, paleoceanographic conditions were likely much

different during the Late Devonian. Eustatic sea level was roughly 150m higher during the Frasnian than today (Haq and Schutter, 2008; see Johnson et al., 1985 and Savoy and Mountjoy, 1995 for alternative estimates of the magnitude of sea level rise), an epicontinental seaway covered much of North America, and black shale deposition was widespread. Bottom water oxygen concentration seems to have been minimal (although not necessarily anoxic), during deposition of many Devonian black shales, even though evidence for traction currents is becoming commonly recognized (e.g. Schieber, 1999; Macquaker and Bohacs, 2007; Macquaker et al., 2010b; Ghadeer and Macquaker, 2011, 2012; Abouelresh and Slatt, 2012; Hemmesch et al., 2014). It is not unreasonable to suggest that contour currents during deposition of Duvernay Formation sediments had only a minimal effect on bottom water oxygenation, and that between periods of contour current activity, anoxia was likely the norm during LF3 and LF4 deposition. Alternatively, minimally bioturbated contourite beds may be the result of increased sedimentation rates that deterred organisms from completely bioturbating a contourite bed. Even during contourite deposition, the dysoxic-anoxic boundary likely occurred just below the sediment-water interface, as bioturbation rarely extends more than a few millimeters below contourite beds.

Contourite deposits in the Duvernay Formation are found primarily in the northeast portion of the West Shale Basin, adjacent to the Grosmont Platform. It is likely that the flow of bottom water currents was at least partially governed by the morphology of the platform slope. Stoakes (1980) invoked a similar model of slope-parallel transport for terrigenous clays that make up much of the thickness of the Grosmont Platform margin. Stoakes (1980) suggested that currents transported terrigenous clays (LF11 of this study) parallel to the Grosmont Platform slope where they were subsequently deposited, forming clinoforms of Duvernay Formation and Ireton Formation strata. These palaeocurrents likely would have been most effective in the upper portions of the water column, as they would have been driven by interactions with the atmosphere. These types of currents may have been driven by climatic factors such as wind, runoff, precipitation and evaporation rates, temperature gradients, and mixing of water bodies (e.g. Slingerland et al., 1996; Kump and Slingerland, 1999). Drivers for basin circulation are not the focus of this paper and little work has been published on the subject for the Alberta Basin (Mallamo, 1995), so sediment distribution patterns are currently the strongest line of evidence for the character of basin circulation (see Chapter 2 of this thesis; Andrichuk and Wonfor, 1954;

Newland, 1954; Andrichuk, 1958, 1961; Staplin, 1961; McCrossan, 1961; Klovan, 1964; Wendte, 1974; Stoakes, 1980; McLean and Mountjoy, 1993). Contour currents responsible for silty-sandy beds within LF3 and LF4 and slope-parallel currents that deposited argillaceous muds of LF11 (as proposed by Stoakes, 1980) may have had different drivers. Contour currents responsible for contourite beds of LF3 and LF4 were present at the base of the Grosmont Platform slope in deeper water than LF11 sediments and may have been driven by contrasts in water density, which is the driver of many modern and ancient contour currents (Rebesco et al., 2014)

### ***1.5.3 Depositional Model***

This section describes a depositional model created from the summation of our observations and interpretations outlined above. Analysis of lithofacies distribution, along with the characterization of depositional processes and conditions, allows us to understand the drivers that controlled the deposition and character of Duvernay Formation sediments. The depositional model is separated into two phases: a period of platform-building (Fig. 1.23A), which largely describes lower and middle members of Duvernay Formation strata, and a period of time when the platform was flooded (Fig. 1.23B), which generally describes the upper Duvernay member.

#### *Platform Construction*

In the northeast part of the basin, adjacent to the Grosmont Platform, LF11 argillaceous-dolomitic mudstones and LF12 nodular dolostones are dominant, representing a well-oxygenated platform-margin and oxic to dysoxic slope environment. During deposition of lower and middle Duvernay member sediments, thick packages of LF11 were deposited and capped by LF12 during a phase of platform-building (Fig. 1.23A) LF11 is enriched in terrigenous clay minerals, and represents slope deposition. Clastic deposition was a result of slope-parallel current transport of clays from the north, parallel to the Grosmont Platform edge, followed by deposition on the slope (Stoakes, 1980; Chapter 2 of this thesis). Slope-parallel transport of clastics is primarily based on the pattern of basin filling observed in the Duvernay Formation and Ireton Formation.

Clastic abundance decreases upslope towards the platform as a result of increased wave energy, and decreases downslope towards the basin as clastic supply wanes (Stoakes, 1980).

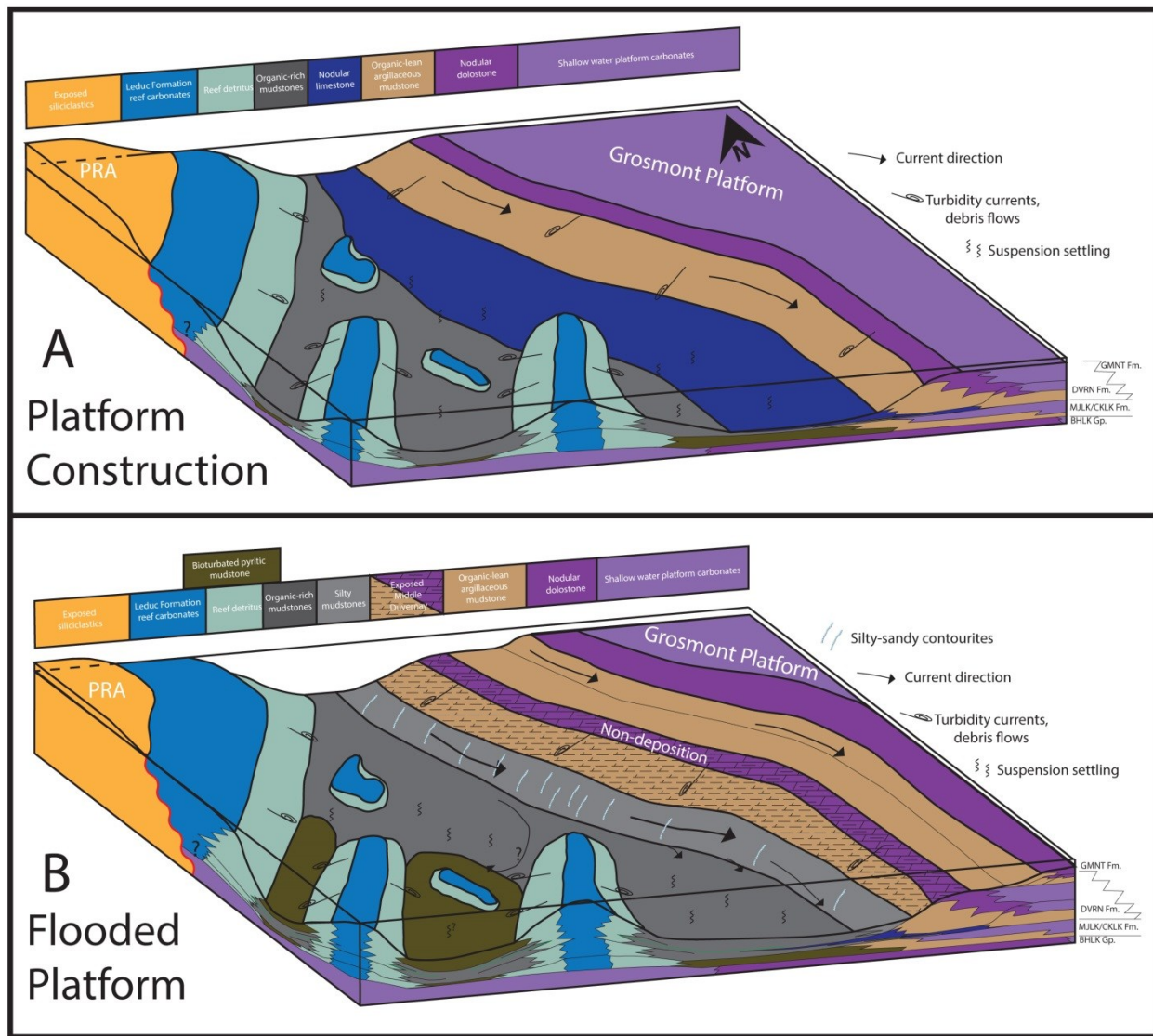


Figure 1.23: Depositional models. A) During deposition of the lower and middle Duvernay members lithofacies distribution is best explained by a platform construction model. A continuous dolomitic-argillaceous-calcareous-siliceous transition of lithofacies occurs basinward from the Grosmont Platform. Sediment is primarily sourced from the northeast. Clastic sediment was transported parallel to slope by currents (Stoakes, 1980). Organic-rich mudstones of LF1-3 are only prominent in distal parts of the basin. B) Deposition of upper Duvernay member sediments is best explained by a flooded platform model. LF11 and LF12 argillaceous-dolomitic facies occur further to the northeast, and are separated from basinal organic-rich facies by a zone of non-deposition. Contour currents flow parallel to the previously developed platform slope, depositing silty contourites of LF4. Organic-rich facies of LF1-3 are prominent over much of the basin. Clay mineral supply increases to the west (reverse of platform construction model) as a result of NE-derived clastics being trapped upslope, and the Peace River Arch becoming a more significant supply of clastics.

Southward and westward, organic-rich lithofacies become more common as a result of decreasing bottom water oxygen concentrations and reduced sediment supply. In the East Shale Basin, bottom water anoxia was rare due to decreased bathymetry, which is supported by the dominance of bioturbated lithofacies, especially LF7 bioturbated calcareous mudstones and LF8 nodular limestones. The East Shale Basin was shallower than the West Shale Basin due to the presence of the underlying Cooking Lake Platform and older tectonic features (Switzer et al., 1994). Organic carbon accumulation in East Shale Basin sediments was hampered by higher oxygen levels, and diluted by increased carbonate sediment supply.

In the West Shale Basin, during platform construction, LF8 nodular limestones are the dominant lithofacies immediately basinward of the major platform-building sediments (LF11 and LF12). Nodular limestones of LF8 are moderately to intensely bioturbated, suggesting dysoxic rather than anoxic bottom waters and variable abundance of fragmented shell material suggests periodic downslope transport of coarser carbonates.

Further westward and southward into the West Shale Basin, bottom water anoxia was much more persistent and organic rich sediments were dominant. In areas of the basin such as Kaybob, Edson, and Willesden Green, thick packages of organic rich mudstones accumulated, dominated by LF1-3. In these areas, much of the clay-sized sediment was deposited from suspension, but silt- and sand-sized detritus shows evidence for transport by bottom water currents and turbidity currents. Organic matter formed aggregates in the upper water column, settling to an anoxic sediment-water interface, which inhibited the breakdown of organic matter. Dilution of organic-rich sediments by northeast-derived clastics was minimal.

### *Flooded Platform*

The flooded platform model, depicted in figure 24B, is most applicable to the upper Duvernay member. The order of facies transitions from platform to basin, as described above, still generally applies during the flooded platform phase, but distinct differences are noted and are important to understand the lithofacies distribution.

The northeast part of the basin is once again dominated by LF11 and LF12, representing the oxygenated platform margin, however the thickness of these deposits is greatly reduced and the areal extent of deposition of these lithofacies is shifted to the north and east (detailed in Chapter 2 of this thesis). This backstepping of facies resulted in the formation of a zone of non-deposition over older platform margin and slope sediments that were deposited during the platform-building phase. The creation of a non-deposition zone was likely aided by NW-SE-flowing currents, which encouraged NE-derived sediments to prograde parallel to the Grosmont Platform edge, rather than perpendicular to it (Chapter 2). This relationship has important implications for the distribution of basinal lithofacies.

Accentuated by the backstepping of LF11 clastics during major transgression and the flooding of the Grosmont Platform, the extent of siliceous, organic-rich lithofacies LF1-3 is greatly increased during the flooded platform phase with respect to the platform construction phase (Fig. 1.23B; Chapter 2). Dilution of organic sediment by carbonate detritus was only significant near Leduc reef complexes and at the base of the Grosmont Platform. At the base of the Grosmont Platform, contour currents transported silt- and sand-sized carbonate detritus (LF3 and LF4) which was sourced from reefs, eroded from exposed and cemented platform-building strata, and potentially washed into the basin from areas of platform growth further to the northeast (bathymetrically upslope). LF3 and LF4 record interbedded black shale and silty-sandy contourite deposition in a variably energetic, but oxygen-deprived environment.

In the far west of the West Shale Basin, the Wild River Sub Basin is dominated by LF6 bioturbated pyritic mudstones. The dominance of a more clastic-enriched facies so far removed from the northeasterly-derived clastic sediment source, suggests that a second, more minor source of clastics existed (Fig. 1.23B). The most likely source was the subaerially-exposed Peace River Arch on the northwestern corner of the basin. Organic carbon values in LF6 are unexpectedly high, given that the sediments are thoroughly bioturbated, for which an increased supply of clay minerals from the Peace River Arch may be responsible. Increased sedimentation rates may have more rapidly buried organic matter below the sediment-water interface, which was clearly not anoxic. This process has been shown to increase organic matter preservation (Tyson, 2005; Bohacs et al., 2005; Macquaker et al., 2010b). Additionally, the aggregation of organic matter and clay minerals (e.g. Macquaker et al., 2010b) and/or adsorption of organic

matter onto clay minerals (e.g. Kennedy et al., 2002) seems to be enhanced with increased clay mineral supply, as given by more abundant aggregates in LF1 and LF2 near the Peace River Arch. Aggregation of organic matter and clay minerals would have increased the settling velocity of individual aggregates (Shanks, 2002) and decreased the time organic matter was exposed to oxidants in the water column.

## **1.6 Conclusion:**

In this study, we develop a lithofacies analysis that characterizes the heterogeneity in Duvernay Formation mudstones, especially in areas of the basin that are prospective for hydrocarbon exploration. The detailed lithofacies analysis presented in this study describes the fine-scale variability of lithofacies in Duvernay Formation mudstones, and is the foundation for a basin-scale depositional model.

While suspension-deposited sediment is significant in the most organic-rich Duvernay Formation lithofacies, we present evidence of other processes based on the variety of sedimentary structures present in drill cores. Unlike some other organic-rich mudstone successions (e.g. Ghadeer and Macquaker 2011, 2012), suspension settling is locally significant, although is never the sole depositional mechanism. A combination of suspension settling, sediment-gravity flows, and bottom water currents distribute sediment throughout the basin. Near reef complexes, downslope sediment-gravity deposits are common, as seen by limestone breccias and packstones. Turbidite beds are much more minor and uncommon further into the basin but are present as thin fossiliferous beds. Siliciclastic sediment is transported into the basin from the north by slope-parallel currents (Stoakes, 1980; Chapter 2). Sediment is remobilized and sorted by contour currents whose position and strength are in part determined by basin morphology. Contour currents even act within areas of the basin where organic-rich mudstones are dominant, creating interbedded muddy and silty/sandy successions which may still contain significant TOC values. Organic matter and clay minerals deposited from suspension are commonly observed as aggregates.

Total organic carbon varies systematically within a lithofacies framework and organic-enrichment is attributed to a variety of factors. The highest TOC values are observed in planar-

laminated, siliceous mudstones, deposited in generally anoxic bottom waters, where dilution of organic matter by clastic or carbonate sediment is minimal. However, significant organic-rich deposits also occur where contourites are interbedded with siliceous, organic-rich mudstone. Periodic fluctuations in current energy and bottom water oxygenation generally act to reduce TOC values, but not necessarily enough to exclude the strata from being prospective for hydrocarbon exploration. Organic enrichment also occurs in dysoxic bottom waters where sediment composition and increased sedimentation rate are key to organic matter preservation. Clay minerals may aid in the formation of organo-minerallic aggregates which decreases the time organic matter is exposed to oxygenated water. Where bottom water anoxia is not present, an ideal sedimentation rate may be key to preserving but not significantly diluting organic matter. Organic enrichment in a variety of depositional settings illustrates the interplay of bottom water oxygen concentrations, sedimentation rates, and sediment composition. The relative importance of each factor varies, even within a single succession of mudstones.

The character and distribution of lithofacies depends heavily on type and proximity of sediment sources, which are not consistent throughout deposition. The relative importance of carbonate, clastic, and biogenic sediment varies through time and geographic location. Changes in basin morphology, water circulation, and sea level act to increase or reduce the significance of each sediment source, and thus the character of sediments deposited.

## CHAPTER 2: SEA LEVEL AND BASIN MORPHOLOGY CONTROL ON DISTRIBUTION AND CHARACTER OF ORGANIC-RICH MUDSTONES: A SEQUENCE STRATIGRAPHIC MODEL FOR THE DUVERNAY FORMATION, ALBERTA, CANADA

### **2.1 Introduction:**

Sequence stratigraphy is a powerful tool for predicting the distribution of sediment bodies. For shallow-water sedimentary units, the sequence stratigraphic method is widely-employed; however the application of sequence stratigraphy to fine-grained, basinal sediments is much less developed. The challenges of applying sequence stratigraphy to basinal sediments stems from 1) the reduced effect of sea level change on basinal sediments compared to shallow water deposits, 2) the difficulty in identifying sequence stratigraphic surfaces and systems tracts in fine-grained deposits, and 3) a lack of understanding of depositional processes and controls for organic-rich mudstone deposition

The effects of sea level change on basinal lithofacies are more subtle than on shallow water deposits (Hemmesch et al., 2014). A sea level fall or rise represents a much smaller fraction of total water depth in deep water realms as compared to shallow water, and as such, the effect on lithofacies character is reduced in deep water. A minimized change in basinal lithofacies character may also mean a minimized change in wireline log signatures, which are a fundamental component of subsurface sequence stratigraphic analyses.

Identification of sequence stratigraphic surfaces and systems tracts in fine-grained sediments has been hindered by the difficulty in observing important features, fabrics, and surfaces. Mudstone outcrops have a tendency to weather significantly due to the fissility of shale, making it very difficult to observe sedimentary structures on a fine enough scale to study mudstone sequence stratigraphy. Even in slabbed and polished drill core, critical changes in lithofacies character may be very difficult to observe without the use of thin sections and a petrographic microscope.

Compared to organic-lean mudstones, the sequence stratigraphic analysis of organic-rich mudstones or black shales comes with additional challenges. Organic matter and hydrocarbons alter the wireline signature of the rock (Creaney and Passey, 1993; Bohacs, 1998; Lüning and

Kolonic, 2003; Hemmesch et al., 2014), which needs to be understood and accounted for when using wireline logs to build a sequence stratigraphic framework.

Application of sequence stratigraphy to organic-rich mudstone formations has potentially significant benefits for oil and gas exploration and production due to the ability to predict variations in critical rock properties such as organic richness, porosity, permeability, and fracturability. Petrophysical properties depend on small-scale variations in components such as total organic carbon (TOC) content, biogenic silica and carbonate minerals (Schieber, 1996; Schröder-Adams et al., 1996; Loucks and Ruppel, 2007; Dong et al., 2015)

This study investigates the geographic and stratigraphic response of lithofacies distribution to sea level change during deposition of organic-rich mudstones of the Duvernay Formation. The Duvernay Formation has been the target of exploration for unconventional gas and liquids since 2009, but very little literature exists on the sedimentological and stratigraphic characteristics of the Duvernay Formation. Sequence stratigraphic studies have been carried out on time-equivalent Leduc Formation reef strata (e.g. Chow et al., 1995; Potma et al., 2001; and Van Buchem, 1996a, 2000a), but no detailed sequence stratigraphic framework for the Duvernay Formation has been published. The sequence stratigraphic framework presented here is built on detailed lithofacies analyses from drill core (Chapter 1) and correlation through an extensive network of wireline logs.

## **2.2 Geological Setting:**

The Duvernay Formation was deposited during the Late Devonian in Western Canada (Fig. 2.1, Fig. 2.2), roughly time-equivalent to several other major black shale deposits across North America. During the Middle to Late Devonian, global sea level was significantly higher than present day (Johnson et al., 1985; Savoy and Mountjoy, 1995; Haq and Schutter, 2008), resulting in widespread flooding of continental margins. It is within these epicontinental settings that many organic-rich Devonian successions were deposited, such the Duvernay, Horn River, Bakken, Marcellus, Chattanooga, Ohio, New Albany, and Woodford shales.

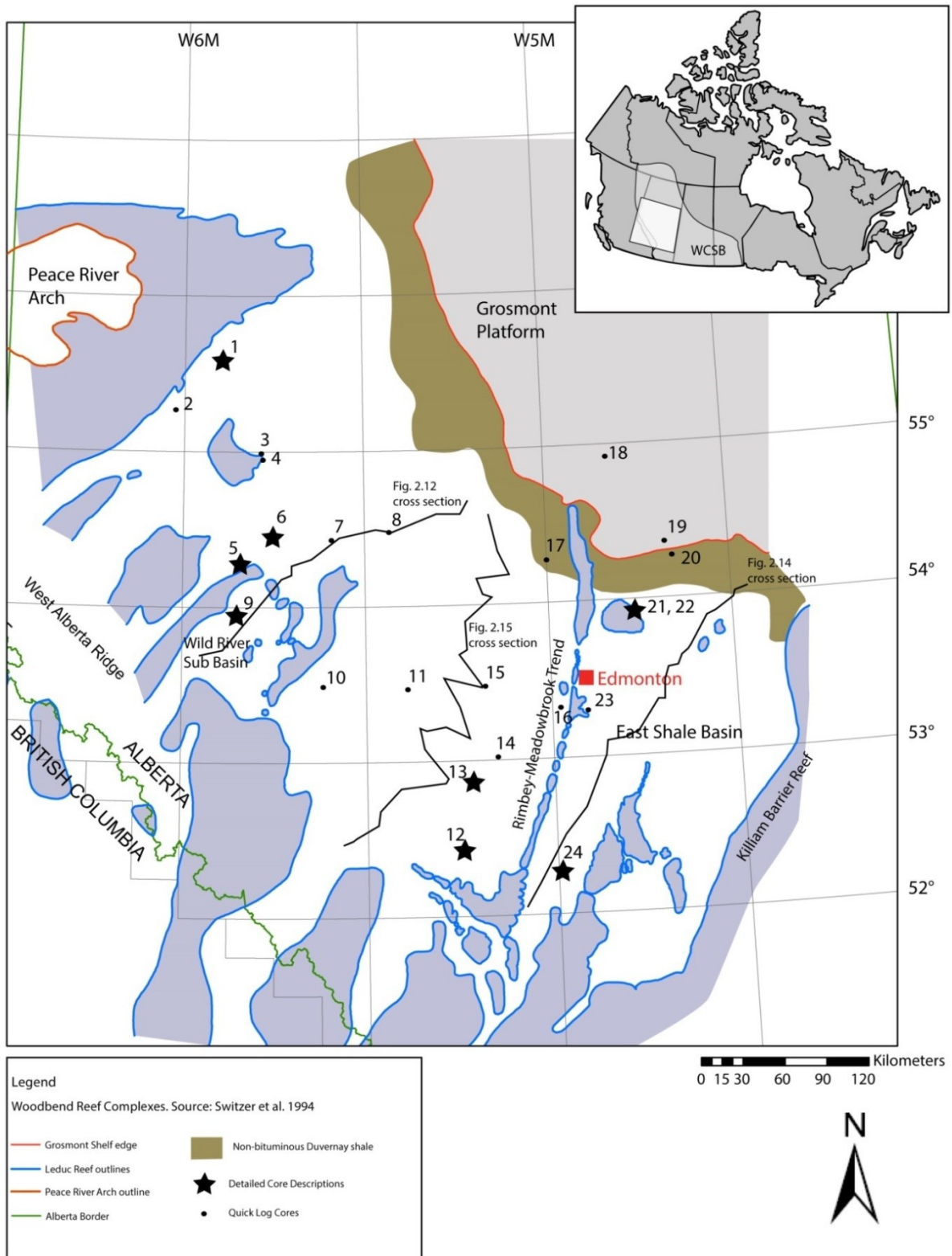


Figure 2.1: Map of study area. Duvernay Formation organic-rich mudstones are the basinal equivalent of Leduc Formation reefs. Numbers correspond to described cores listed in Table 2.1. Cross section locations are indicated on map.

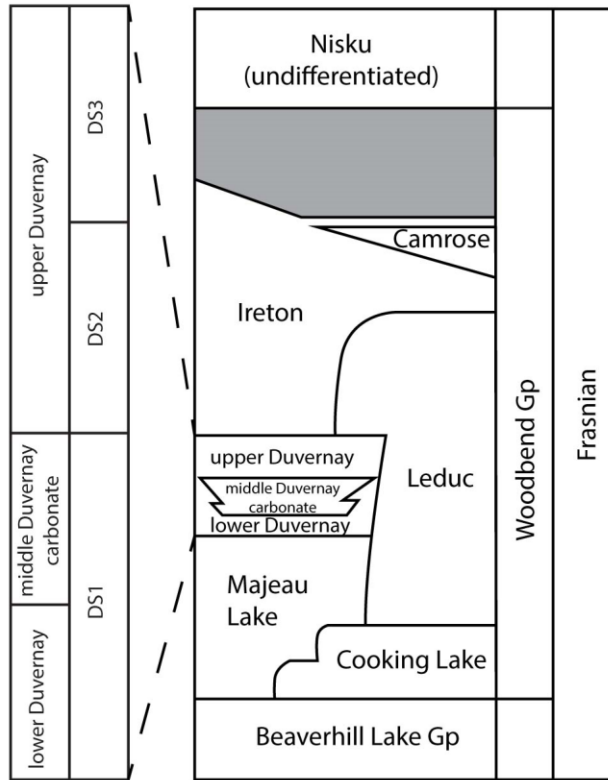


Figure 2.2: Late Devonian stratigraphy of the Western Canadian Sedimentary Basin in central Alberta. The Duvernay Formation is divided into lower, middle, and upper members. Three third order depositional sequences (DS1-3) are identified on the left. Modified from Switzer et al., 1994.

During the Frasnian, the Western Canadian Sedimentary Basin was a passive margin at the western edge of North America. Sedimentation on this margin of North America was dominated by open marine shales in British Columbia and the Northwest Territories, transitioning to shallow water carbonates in Alberta, and restricted dolomites and evaporites in Saskatchewan and

Manitoba to the southeast (Ziegler, 1967; Switzer et al., 1994). During deposition of the Woodbend Group, the rate of accumulation and preservation of sediment increased dramatically (Switzer et al., 1994). In Alberta, the section is characterized by thick accumulations of basin-filling shales, including hydrocarbon source rocks, and thick and extensive reef complexes (Switzer et al., 1994).

Duvernay Formation sediments were deposited during the time of maximum flooding within a second order depositional sequence (Potma et al., 2001). The late Givetian to Frasnian second order depositional sequence is bound by regional unconformities. Overlying the unconformities are regional clastics of the Gilwood Formation (base of sequence) and Graminia Formation (top of sequence) (Potma et al., 2001). Within this sequence, deposition within the Alberta Basin was characterized by platform carbonates (Slave Point Formation and Swan Hills Formation) and organic-lean shales (Waterways Formation) during early transgression. During late transgression and early highstand, platform carbonates (Cooking Lake Formation) are backstepped and transition into pinnacle reefs of the Leduc Formation. Stratigraphically equivalent to these carbonates are source rocks of the Majeau Lake Formation (only locally organic-rich) and Duvernay Formation, respectively. The Duvernay Formation conformably

overlies the Majeau Lake Formation throughout most of the basin (Fig. 2.2). In the far south and west, Majeau Lake Formation sediments were not deposited and Duvernay Formation strata onlap Swan Hills Formation platform carbonates and older Devonian strata (Switzer et al., 1994). An informal stratigraphy, introduced by Andrichuk (1961) and used by industry, separates the Duvernay Formation into lower, middle, and upper members. Member boundaries are lithostratigraphic, as the upper and lower members are siliceous units that overlie and underlie a middle calcareous member. Thick, basin-filling, organic-lean highstand shales of the Ireton Formation conformably overlie the Duvernay Formation across much of the basin. Near reef complexes and the Grosmont Platform, Leduc Formation reef-margin strata and Grosmont Formation platform carbonates, respectively, overlie the Duvernay Formation. Ireton Formation shale clinofolds are capped by platform carbonates of the Nisku Formation and siliciclastic siltstones of the Calmar Formation and Graminia Formation (Switzer et al., 1994; Potma et al., 2001).

Tectonic features that influenced deposition of the Duvernay Formation include the Peace River Arch, West Alberta Ridge, Rimbey Arc, and Meadow Lake Escarpment (Fig. 2.1). The Peace River Arch was an emergent landmass on the west side of the basin, fringed by Leduc Formation reefs (Dix, 1990; O'Connell et al., 1990). The West Alberta Ridge was flooded at the start of Woodbend Group deposition, but formed a base for extensive Leduc reef complexes (Switzer et al., 1994). The Rimbey Arc was a southwest-northeast trending basement lineament that had a strong control on accommodation space during Woodbend Group deposition (Ross and Stephenson, 1989). During deposition of Duvernay Formation sediments, the lineament was marked by a chain of Leduc Formation reefs called the Rimbey-Meadowbrook trend. The reef chain divides the Alberta Basin into a West Shale Basin (WSB) and East Shale Basin (ESB). Accommodation space was limited in the ESB compared to the WSB as a result of the underlying Cooking Lake Platform which developed on the tectonically-higher eastern side of the Rimbey Arc (Switzer et al., 1994). The Meadow Lake Escarpment is a pre-Devonian erosional and structural feature (Oldale and Munday, 1994). During deposition of Duvernay Formation sediments, the Killiam Barrier Reef roughly coincided with the underlying Meadow Lake Escarpment, and marks the furthest eastward extent of Duvernay Formation shales and argillaceous limestones (Switzer et al., 1994).

### 2.3 Methods:

Eight drill cores (Table 2.1) were selected for detailed description. Cores were described at a scale of 1:10, paying special attention to lithologies and sedimentary structures. Core selection was primarily based on total thickness of formation cored, core quality, and geographic distribution across the basin. An additional 16 cores were described in less detail to observe facies variations and stratigraphic surfaces over a greater extent of the basin. Few of the 16 additional cores covered the entire Duvernay Formation interval. A total of 108 thin sections were cut from 4 cores, covering the major lithofacies and intervals of interest. Thin sections were cut to 20 $\mu$ m rather than the standard 30 $\mu$ m so that finer detail could be observed in fine-grained facies. Most thin sections were cut perpendicular to bedding but a subset was selected for bed-parallel thin sections to further examine the nature of potential bioturbation features. Thin sections were scanned using a Nikon Super Coolscan 5000 ED scanner to observe centimeter- to millimeter-scale features. Millimeter- to micrometer-scale features were analyzed under transmitted and reflected white light using a Zeiss Axio Scope.A1 petrographic microscope.

Samples for geochemical analysis were cut every 1 meter from 5 of the 8 cores. These 5 cores were chosen to for their geographic coverage of the basin and range of thermal maturity. Detailed analysis of these samples is presented in McMillan (2016). A 10 cm long by 2 cm thick slab was cut from the back of the core at each sample location. Vertical splits were cut along the length of the slabs for separate analyses. Samples were sent to Weatherford Geochemical Services Group in Shanandoah, TX for Leco-TOC analysis. Total organic carbon values reported here are averages for each sampled facies from the SCL Kaybob 02-22, ECA Cecilia 11-04, GuideX Gvillee 09-06, and EOG Cygnet 08-20 cores. Esso Redwater 16-28 was also sampled for TOC but was removed from average TOC calculations because it is much less thermally mature than the other sampled wells and as such has much higher TOC values for all facies.

Depositional units identified in core were correlated through an extensive network of wireline logs. Correlations represent sequence stratigraphic surfaces rather than lithostratigraphic boundaries. Correlations were made in Geoscout, primarily using gamma radiation and

resistivity logs, but also sonic and density logs where necessary. A total of 759 wells with wireline logs were used in creation of cross sections and maps.

<b>Map #</b>	<b>Well Name</b>	<b>UWI</b>	<b>Sampled</b>	<b>Detailed Description</b>
<b>1</b>	GuideX Gvillee 09-06	100/09-06-076-23W5/00	Y	Y
<b>2</b>	BPC et al. Smoky HT 04-36	100/05-36-072-01W6/00	N	N
<b>3</b>	Xerex SturLks 07-22	100/07-22-069-21W5/00	N	N
<b>4</b>	Enermax Panther SturLs 14-02	100/14-02-069-21W5/00	N	N
<b>5</b>	AOSC Grizzly 01-24	100/01-24-061-23W5/00	N	Y
<b>6</b>	SCL HZ Kaybob 02-22	100/02-22-063-20W5/00	Y	Y
<b>7</b>	Chevron Chickadee 03-05	100/03-05-062-16W5/00	N	N
<b>8</b>	Imperial Virginia Hills 06-36	100/06-36-063-12W5/00	N	N
<b>9</b>	ECA Cecilia 11-04	100/11-04-058-23W5/00	Y	Y
<b>10</b>	CNRL HZ Edson 01-10	100/01-10-052-17W5/00	N	N
<b>11</b>	Imperial Cynthia No. 09-06	100/09-06-052-11W5/00	N	N
<b>12</b>	SCL HZ Ferrier 03-21	100/03-21-040-07W5/00	N	Y
<b>13</b>	Penn West Pembina 10-17	100/10-17-045-06W5/00	N	Y
<b>14</b>	Imp Cdn-Sup Norbuck 02-06	100/02-06-047-04W5/00	N	N
<b>15</b>	Imp Cdn-Sup Tomahawk 16-18	100/16-18-052-05W5/00	N	N
<b>16</b>	Forgotson Burk SGSpoke 10-04	100/10-04-051-27W4/00	N	N
<b>17</b>	Sarcee et al. Pibroch 10-16	100/10-16-061-26W4/00	N	N
<b>18</b>	Imperial Deep Creek 04-33	100/04-33-068-22W4/00	N	N
<b>19</b>	Imperial Figure Lake 11-19	100/11-19-062-18W4/00	N	N

20	Tex et al. Lucky 09-09	100/09-09-061-18W4/00	N	N
21	Esso Redwater 10-27	102/10-27-057-21W4/00	N	N
22	Esso Redwater 16-28	102/16-28-057-21W4/00	Y	Y
23	Nexxtep 07-05	102/07-05-050-25W4/00	N	N
24	EOG Cygnet 08-20	100/08-20-038-28W4/00	Y	Y

Table 2.1: Name and location of described cores.

## 2.4 Results:

### 2.4.1 Lithofacies Analysis

A detailed lithofacies analysis was presented in Chapter 1 of this thesis. A summary of the major lithofacies is presented in Table 2.2 and Figure 2.3.

### 2.4.2 Lithofacies Stacking Patterns and Cyclicality

Lithofacies stack to form depositional packages that are typically 25-60cm thick. In stratigraphically ascending order within individual depositional packages, 5 general trends were observed: 1) decreasing quality of lamination; 2) siliceous lithofacies (LF1-3) are most abundant at the bases of depositional packages, with more abundant calcareous lithofacies (LF4-8) upwards; 3) decreasing TOC; 4) more common *in-situ* benthic macrofossils; and 5) increasing grain size. Depositional packages are typically bound by flooding surfaces that may be sharp or gradational over a few centimeters. Flooding surfaces are recognized by a sharp or rapid shift to deeper water lithofacies (lithofacies interpretation in Chapter 1 of this thesis). The tops of depositional packages are sometimes heavily cemented and may be burrowed and/or scoured. This scale of lithofacies cyclicality is not observable on wireline logs.

The nature of individual depositional packages varies both geographically and stratigraphically. For example, in platform-margin deposits, individual depositional packages are

	Bedding	Other Sed. Struct.	Grain Size	Silt-Sand Grains	Clay-Size Grains	Bioturbation	Common Taxa	Cements	Avg. TOC	TS
LF1	Planar lamination	-	Mudstone	Calcite, dolomite silt, less common quartz, rare chert	Siliceous, organic-rich	Absent to minor	Radiolaria, styliolinids, tentaculitids	Variable calcite, silica cement in laminae	3.6 wt%	Y
LF2	Planar lamination	-	Mudstone	Calcite, dolomite silt, less common quartz, rare chert	Siliceous, organic-rich	Absent to minor	Radiolaria, styliolinids, tentaculitids	Framboidal pyrite and pyrite-replaced carbonate grains in laminae	3.2 wt%	Y
LF3	Planar lamination	normal, inverse grading	Silty mudstone	Calcite, dolomite silt, less common quartz, rare chert	Siliceous-calcareous, organic-rich	Absent to minor	Radiolaria, styliolinids, tentaculitids	Variable calcite, silica cement in laminae	3.2 wt%	Y
LF4	Wavy/lenticular bedding	planar parallel lam, low angle cross lam, starved ripples, loading/flame structures	Silty mudstone	Calcite, dolomite silt-sand, less common quartz, rare chert	Siliceous-calcareous, organic-rich	Minor to moderate	Radiolaria, styliolinids, tentaculitids	Common calcite cement in laminae	2.4 wt%	Y
LF5	Poorly bedded to structureless	Uncommon normal grading	Wackestone-floatstone	Variable. Most commonly calcite, dolomite silt	Calcareous, variably organic-rich	Minor to intense	Radiolaria, styliolinids, tentaculitids, <i>brachiopods</i> , <i>bivalves</i> , <i>crinoids</i>	Variable calcite cement	2.3 wt%	Y
LF6	Structureless to wispy	-	Mudstone	Calcite, dolomite, quartz silt	Siliceous-calcareous, increased clays. Variably organic-rich	Moderate to intense	Styliolinids, tentaculitids, conodonts, <i>brachiopods</i> , <i>bivalves</i> , <i>gastropods</i> , <i>agglutinated forams</i>	Pyrite concentrated in traces	2.1 wt%	Y
LF7	Poorly bedded, wispy/wavy	-	Mudstone	Calcite, dolomite silt, uncommon quartz	Calcareous, less organic matter	Moderate to intense	Styliolinids, tentaculitids, arthropods, conodonts, <i>agglutinated forams</i>	Variable calcite cement	1.8 wt%	Y
LF8	Nodular to burrow-mottled	-	Mudstone-wackestone	Calcite, dolomite silt, less common quartz	Calcareous, low but variable organic-richness	Moderate to intense	Styliolinids, tentaculitids, <i>crinoids</i> , <i>brachiopods</i> , <i>bivalves</i>	Heavily calcite-cemented nodules, spar-filled fractures	1.1 wt%	Y

<b>LF9</b>	Structureless to planar laminated	Normal grading, uncommon current ripples, cross lam	Packstone	Calcite clasts, fossil frags. Less common quartz, dolomite silt, siliceous/pyritic/phosphatic clasts and fossil frags. Common mud rip ups	-	Minor to intense	Styliolinids, tentaculitids, brachiopods, bivalves, crinoids, gastropods,, amphipora	Calcite, dolomite, minor evaporites	N.A.	Y
<b>LF10</b>	-	Normal grading, poor sorting	Pebble to boulder	Calcite	Calcite	Absent	-	Calcite	N.A.	N
<b>LF11</b>	Poorly laminated	-	Mudstone	Clay mineral aggregates? Calcite/dolomite silt	Clay minerals, dolomite, calcite?	Moderate to intense	-	Minor-moderate anhydrite in laminae	N.A.	N
<b>LF12</b>	Nodular to burrow-mottled	-	Mudstone-packstone	Dolomite, calcite	Dolomite, calcite, clay minerals?	Moderate to intense	Brachiopods, crinoids	Abundant anhydrite as burrow fills and nodules	N.A.	N

Table 2.2: Lithofacies characteristics for LF1-12. Text in italics indicates that taxa may be present *in-situ*. TS=thin section.

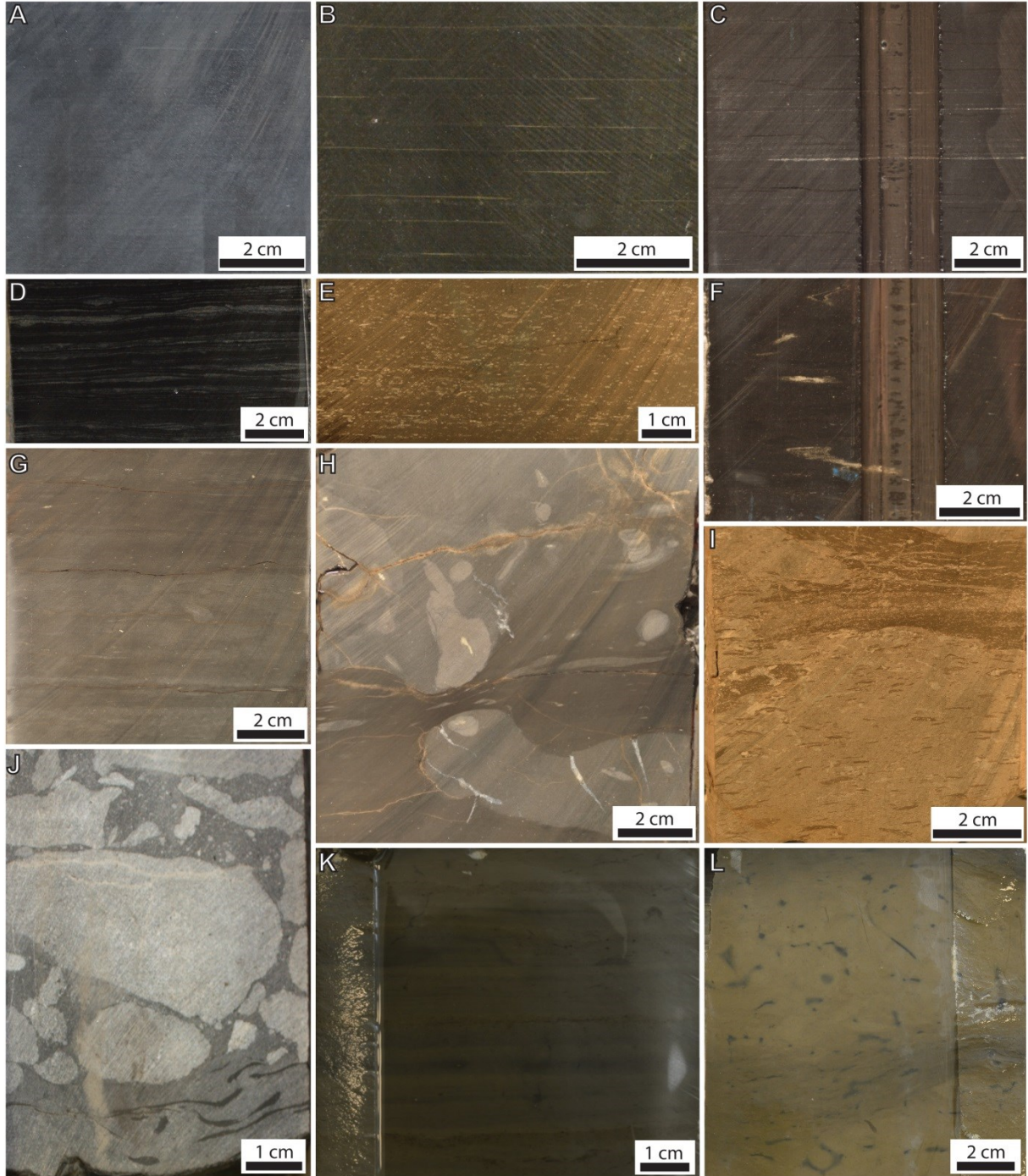


Figure 2.3: Photo plate summary of lithofacies. A) LF1 planar laminated siliceous mudstone. B) LF2 planar laminated pyritic mudstone. C) LF3 planar laminated silty mudstone. D) LF4 wavy-laminated silty mudstone. E) LF5 siliceous-calcareous wackestones and floatstones. F) LF6 bioturbated pyritic mudstone. G) LF7 bioturbated calcareous mudstone. H) LF8 nodular limestone. I) LF9 intraclastic packstone. J) LF10 limestone breccia. K) LF11 argillaceous-dolomitic mudstone. L) LF12 nodular dolostone.

often composed entirely of LF11 and LF12 in which case, there are no siliceous, organic-rich deposits and packages grade upwards from argillaceous, variably laminated mudstones to burrow mottled, nodular, dolomitic mudstones. Stratigraphically, the dominance of siliceous, calcareous, or argillaceous lithofacies within successive depositional packages is variable and is used to describe larger scale cycles (see following sections).

Depositional packages stack to form larger, meso-scale cyclic units that are typically 2-6m thick. Within these larger units, stacked depositional packages display the same 5 general trends. Each individual depositional package contains thinner siliceous, organic-rich deposits at their base and more common silty or calcareous deposits than the depositional package underlying it. At the top of the meso-scale cyclic units there is a sharp shift to deeper water facies. Cycle tops are locally cemented, sometimes forming hardground surfaces. This type of cyclicity is most common in the lower and middle Duvernay members (Fig. 2.4 – Interval A). In the upper Duvernay member, the character of meso-scale cycles is more variable. Meso-scale cycles in the upper Duvernay less commonly have sharp tops and more commonly show a more gradational shift to deeper water facies; the top portions of the cycles show a reversal of the 5 general trends (Fig. 2.4- Interval B). Hardgrounds are not common in this scenario. Meso-scale cyclic units are the lowest level of cyclicity observable on wireline logs.

The largest level of cyclicity observed was three cyclic units, designated DS1-3, which make up the entire thickness of the Duvernay Formation. DS1 is composed of the lower and middle Duvernay members while DS2 and DS3 both occur within the upper Duvernay member. Cyclicity was recognized by trends in lithofacies character and distribution. These three units are bounded by regionally-mappable surfaces which are presented in the following section.

### *Major Surfaces*

The three cyclic units (DS1-3) that comprise the entire thickness of the Duvernay Formation are bound by 4 major surfaces that can be mapped across the basin. From oldest to youngest, these bounding surfaces are: top Majeau Lake Formation / base of Duvernay Formation, top of middle Duvernay member, a surface in the upper Duvernay member above which lithofacies rapidly become more argillaceous, and the top of the Duvernay Formation.

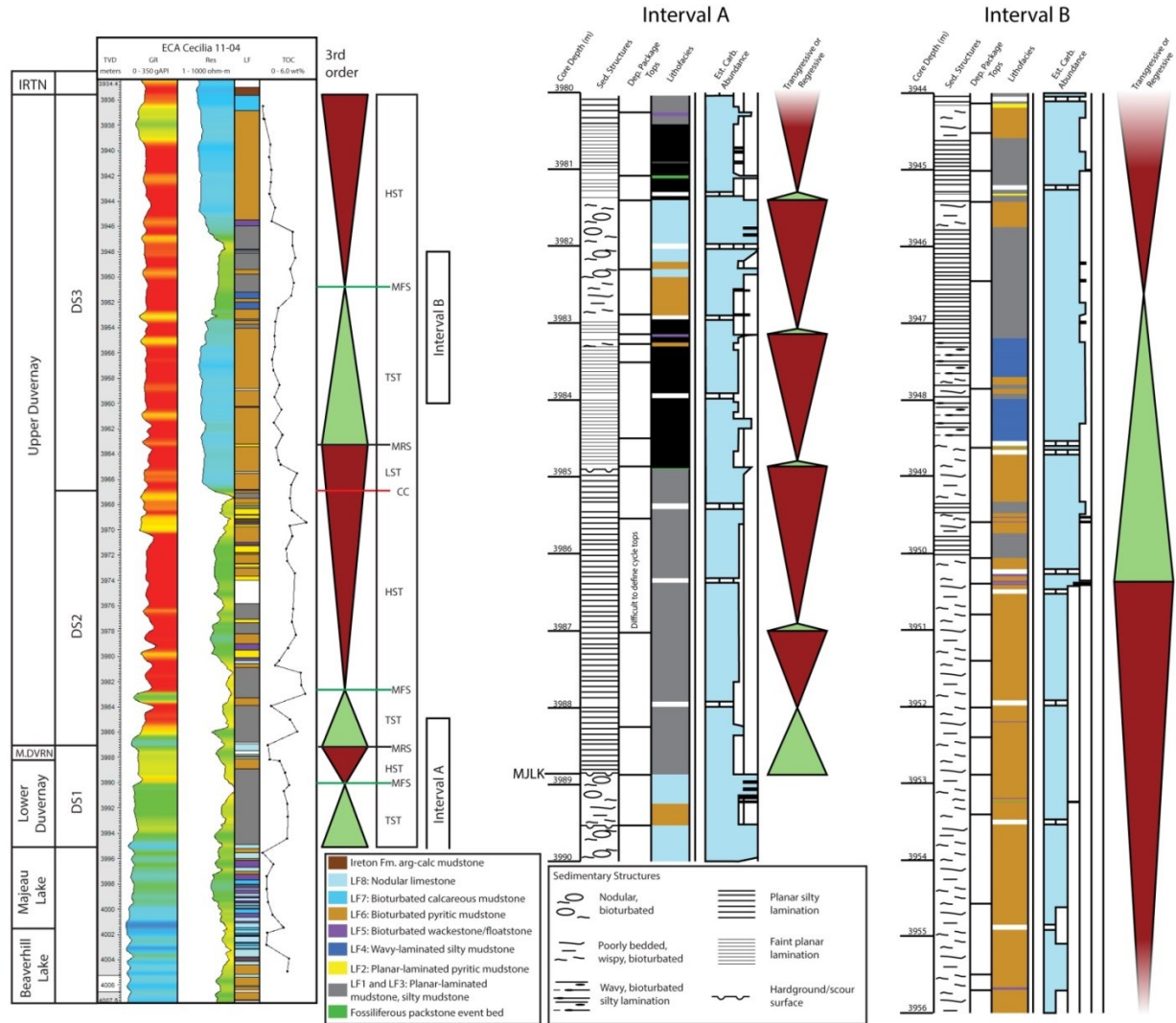


Figure 2.4: Core description and cyclicity summary of ECA Cecilia 11-04. Left) Gamma log, deep resistivity, lithofacies, TOC, and sequence stratigraphic interpretation. Nodular limestones of LF8 are only a minor facies and form a thin unit at the top of DS1. Bioturbated pyritic mudstones of LF6 become dominant in DS3 and upper DS2. (TST = highstand systems tract; TST = transgressive systems tract; LST = lowstand/stillstand systems trace; MRS = maximum regressive surface; MFS = maximum flooding surface; CC = correlative conformity). Middle) Meso-scale cyclicity in DS1 and lower DS2. Transgressive intervals are relatively thin and hardground/scour surfaces are common at the top of regressive intervals. Right) Meso-scale cyclicity in DS3. Both transgressive and regressive intervals are relatively thick and hardground surfaces are not observed.

The oldest surface, the Majeau Lake Formation – Duvernay Formation contact, is defined by a sudden shift from argillaceous, generally organic-lean mudstones to more siliceous, laminated, organic-rich mudstones of LF1-3 (Fig. 2.5). Across most of the West Shale Basin (WSB), the Majeau Lake Formation – Duvernay Formation contact is marked by a shift from

argillaceous mudstones to siliceous, organic-rich mudstones of LF1-3. The contact is easily identified on wireline logs as a sharp increase in resistivity. In the East Shale Basin (ESB) and along the western and southern margins of the WSB, the top of the Majeau Lake Formation is more commonly composed of argillaceous limestones, which reduce the resistivity contrast at the contact. The contact is conformable over most of the WSB; however, the surface is more commonly erosive near basin margins, near reef complexes, and in the ESB. Where the surface is erosive, it is commonly overlain by a fossil lag on the millimeter to centimeter scale (e.g. ECA Cecilia 11-04, Enermax Panther Sturls 14-02, Nexxstep 07-05).

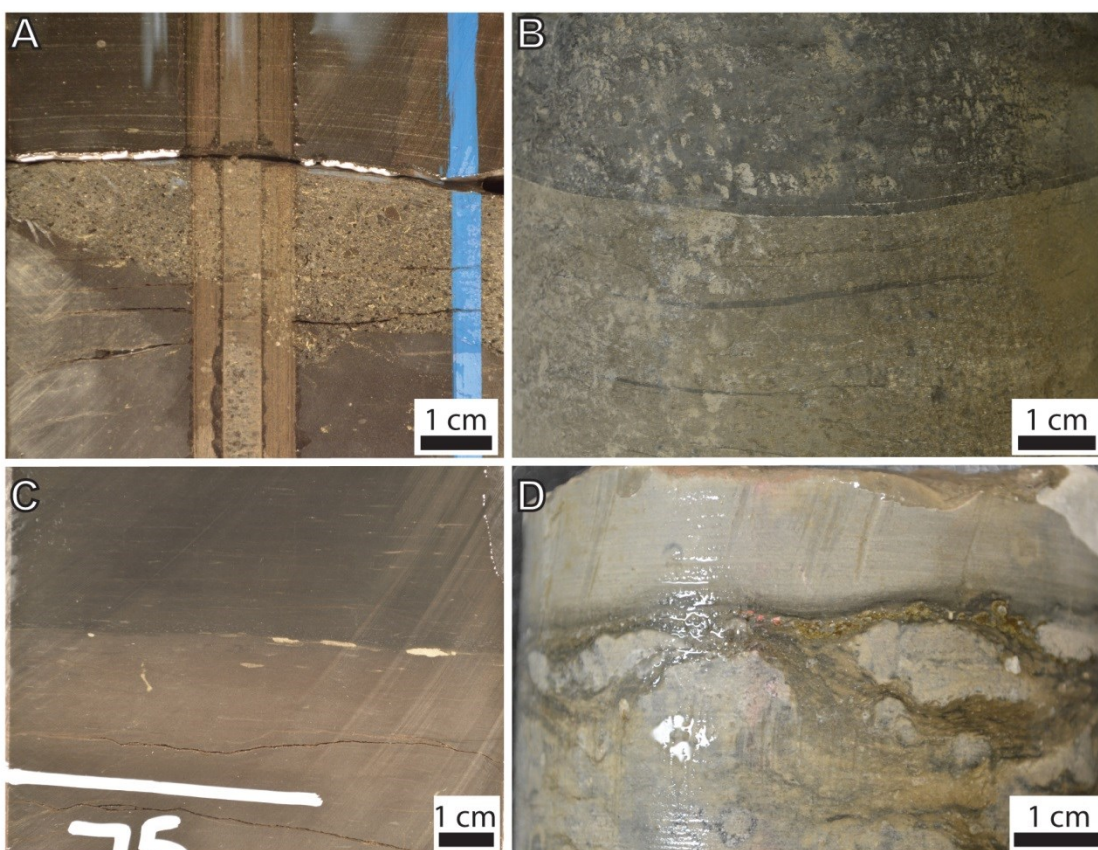


Figure 2.5: Core photos of the top Majeau Lake Formation / base Duvernay Formation surface. The contact is conformable to unconformable with minor erosion evident in some cores as sharp surfaces and thin lags of clasts and fossil fragments. A) ECA Cecilia 11-04. B) Enermax Panther Sturls 14-02. C) EOG Cecilia 08-20. D) Amoco Cache 03-01.

The next major surface is the top of the middle Duvernay member. The middle Duvernay member in the WSB and southern ESB is dominated by limestones of LF8, and its upper bounding surface is characterized as a sharp, erosive shift to organic-rich mudstone facies of

LF1-4 (Fig. 2.6). Fossiliferous lags are common at the contact, but may be as thin as 1mm. Over much of the basin, the contact appears on gamma logs as a sharp, significant increase in gamma radiation. This contrast in gamma ray is reduced in areas of more significant carbonate deposition such as the ESB.

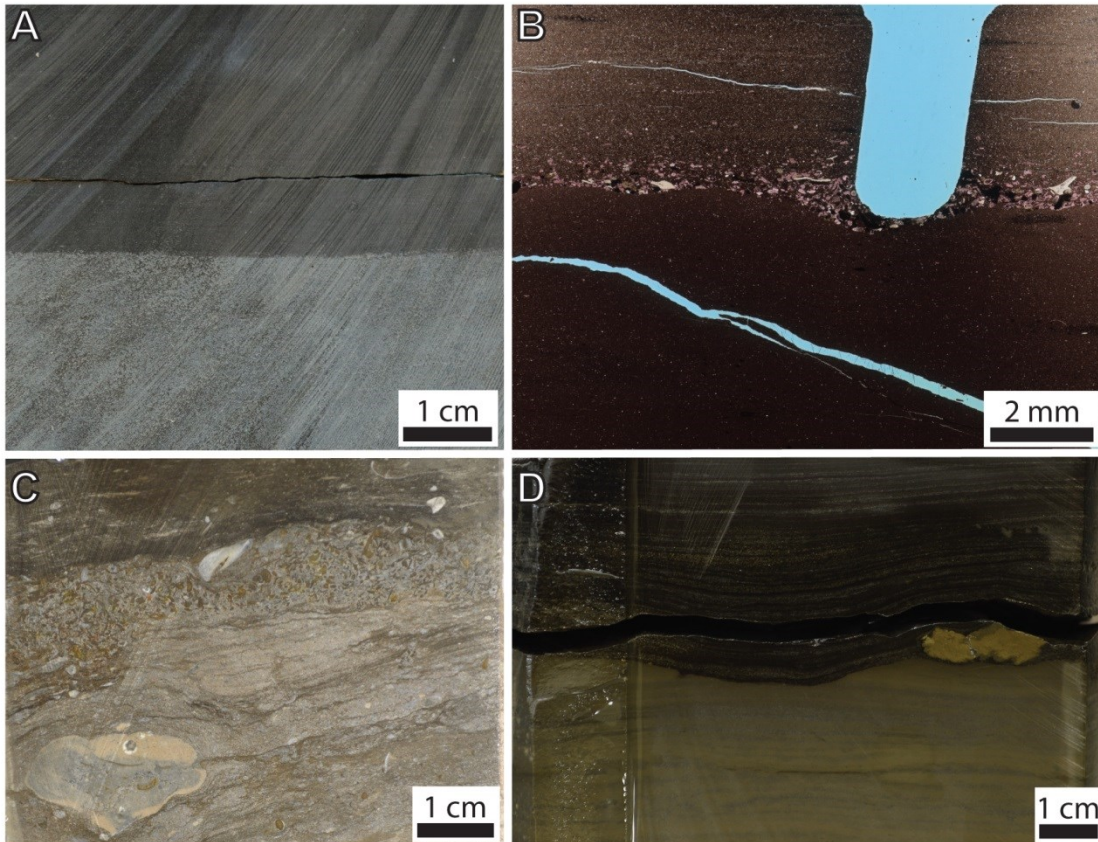


Figure 2.6: DS1-DS2 contact. The surface commonly shows at least minor erosion. Thin lags of clasts and fossil fragments are common overlying the contact. A) Core photo, SCL Kaybob 02-22. B) Thin section photomicrograph, SCL Kaybob 02-22. C) Core photo, Esso Redwater 10-27. D) Core photo, Imperial Virginia Hills 06-36.

Upwards, the next major surface is within the upper Duvernay member. This surface marks a rapid, basin-wide shift to more argillaceous, bioturbated facies (commonly LF6) (Fig. 2.7). Erosion at this surface is not always evident in deep water, organic-rich portions of the basin, but near reef complexes, the surface is locally characterized by coarse, erosively based limestone breccias or fossiliferous to intraclastic packstone through rudstone beds. Across much of the basin, the surface is picked on wireline logs at the base of a significant drop in resistivity.

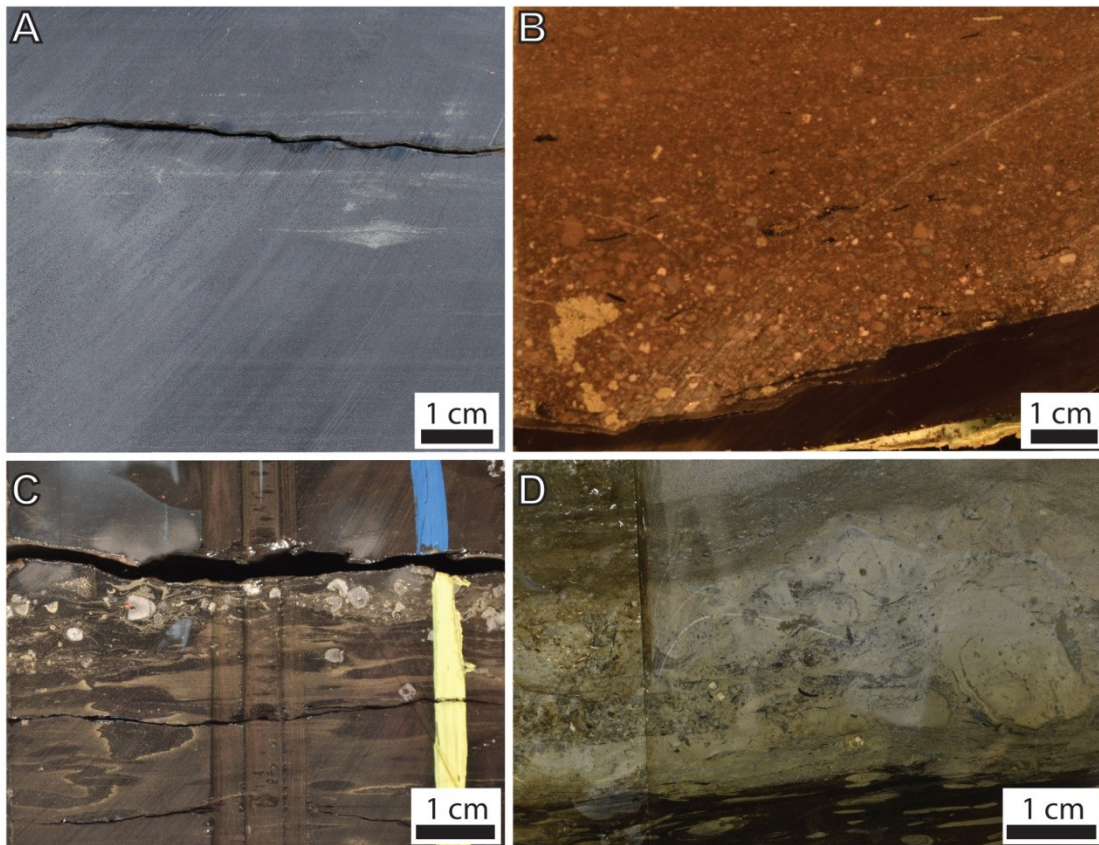


Figure 2.7: Core photos of DS2-DS3 contact. The surface is quite variable. In areas of the basin dominated by organic-rich siliceous mudstones, the surface is often subtle in core, often as a thin, bed of shell fragments (A, C). Closer to reef complexes, the surface is commonly marked by a coarse-grained, erosive-based packstone-grainstone bed (B). Towards the Grosmont Platform, the surface is commonly marked by an argillaceous-calcareous shell debris bed and is significantly bioturbated (D). A) SCL Kaybob 02-22. B) GuideX Gvillee 09-06. C) ECA Cecilia 11-04. D) Sarcee et al. Pibroch 10-16

The uppermost major bounding surface is the top of the Duvernay Formation. Across most of the basin, the contact is underlain by organic-rich Duvernay Formation mudstones and overlain by organic-lean Ireton Formation mudstones (Fig. 2.8). Duvernay Formation mudstones below the contact are typically more siliceous while Ireton Formation mudstones above the contact are more argillaceous and calcareous. In the Wild River Sub Basin and near the Peace River Arch, upper Duvernay member mudstones are more argillaceous than in basinal locations and the contrast with argillaceous Ireton Formation mudstones is reduced. Near reef complexes and the Grosmont platform, reef and platform carbonates overlie the contact rather than Ireton Formation mudstones. The surface is conformable. Across most of the basin, the top of the Duvernay members is picked at a sudden drop in resistivity. The change in resistivity is more

gradual in the Wild River Sub Basin and near the Peace River Arch, and the contact is picked at the top of the resistivity decline.

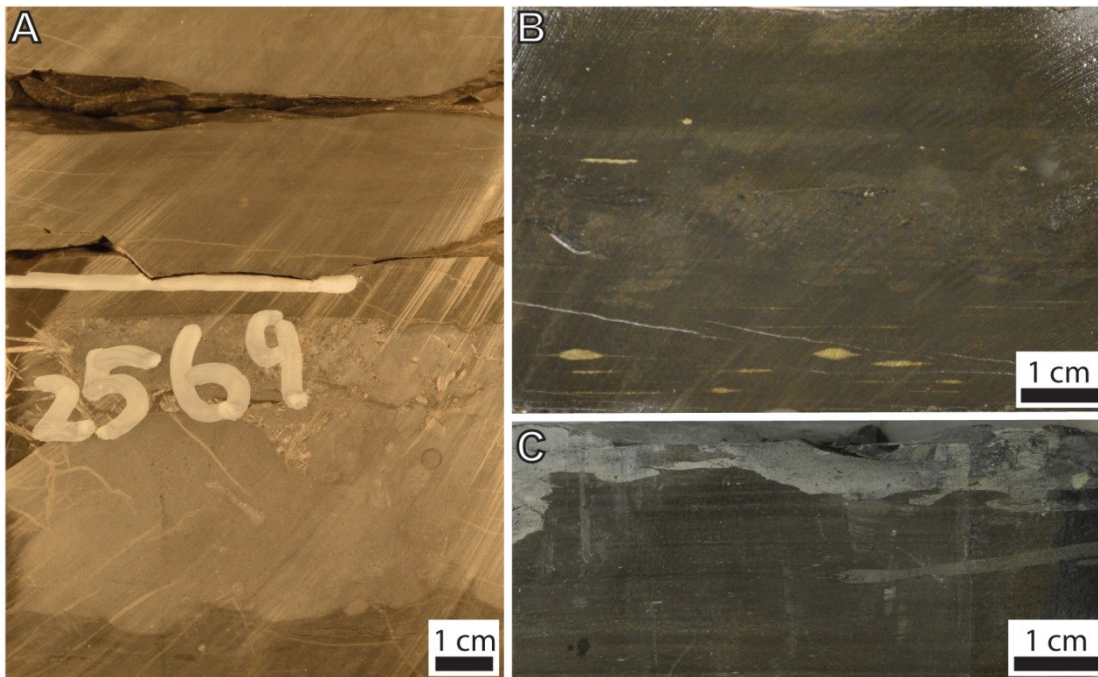


Figure 2.8: Core photos of the top of DS3, which is also the Duvernay Formation - Ireton Formation contact. Ireton Formation mudstones above the contact are always more argillaceous than underlying Duvernay Formation deposits. The contact is consistently bioturbated, often marked by a shell debris bed, and sometimes forms a hardground surface. A) EOG Cygnet 08-20. B) CNRL Edson 01-10. C) Sarcee et al. Pibroch 10-16.

### ***2.4.3 Geographic Variation in Lithofacies and Stratal Thickness Variations***

Correlation of major surfaces through a network of wells containing wireline logs allows for the recognition of lateral facies transitions and stratal thickness variations. This section describes geographic variations in sedimentation within cyclic units DS1-3.

#### ***DS1***

Lithofacies of DS1 show distinct transitions with increasing distance from the Grosmont Platform. Directly adjacent to the platform, DS1 is dominantly composed of LF12 organic-lean, nodular argillaceous dolostones (Fig. 2.9) that are locally enriched in anhydrite (Fig. 2.3L). South and west from the platform, dolostones grade into LF11 organic-lean argillaceous-

dolomitic mudstones. Further from the platform, LF8 nodular limestones dominate most of the WSB during DS1 (Fig. 2.10). Towards the western margins of the WSB nodular limestones are only present as thin beds at the top of the DS1 interval and most of the interval is composed of laminated, organic-rich mudstones of LF1-3 (Fig. 2.4) The northern ESB shows similar facies transitions away from the platform, but the full suite of facies was not documented due to a lack of data. The ESB is more calcareous than the WSB, with LF8 nodular limestone and LF7 bioturbated calcareous mudstone dominating (Fig. 2.11).

Changes in thickness of DS1 strata coincide with lithofacies transitions. The DS1 interval is thickest adjacent to the Grosmont Platform (Fig. 2.12, Fig. 2.13) where LF12 nodular dolostones cap thick packages of LF11 argillaceous-dolomitic mudstone. The interval thins to the south and west as sediments become less argillaceous and nodular limestones become dominant. The thinnest DS1 strata occur in the far west of the WSB where nodular limestones are minor and most of the interval is composed of laminated, organic-rich mudstones. The DS1 interval in the ESB similarly thins southward away from the Grosmont Platform (Fig. 2.13, Fig. 2.14), as LF11 argillaceous dolomitic mudstones grade into LF8 nodular limestones and LF7 bioturbated calcareous mudstones.

## *DS2*

Near the Grosmont Platform, lithofacies of DS2 show similar distribution to DS1, but further into the basin, lithofacies distribution between the two intervals is significantly different. Adjacent to the Grosmont Platform, the DS2 interval is composed of LF12 organic-lean nodular argillaceous dolostone, with local evaporites. To the south and west in the WSB and to the south in the ESB, dolostones grade into LF11 organic-lean argillaceous-dolomitic mudstones. The area of argillaceous mudstone deposition is much narrower than in DS1, but extends southward along the west side of the Rimbey-Meadowbrook reef trend. Further basinward from the platform in the northern WSB, a zone of non-deposition or very minimal deposition developed (Fig. 2.12). In the eastern WSB, a zone of non-deposition did not develop, but DS2 strata thin southward (Fig. 2.15), basinward of LF11 argillaceous mudstone deposition. The basinward margin of the zone of non-deposition is dominated by silty mudstones of LF4 (Fig. 2.16). The rest of the WSB, south and west of silty mudstone deposition, is dominated by laminated, organic-rich mudstones of LF1-3 (Fig. 2.10). The areal extent of organic-rich mudstone deposition during DS2 is greatly

expanded with respect to the DS1 interval. In the Wild River Sub Basin, on the western edge of the WSB, the top of the DS2 interval is dominated by LF6 bioturbated pyritic mudstones (Fig. 2.4), which are not observed in abundance elsewhere during DS2.

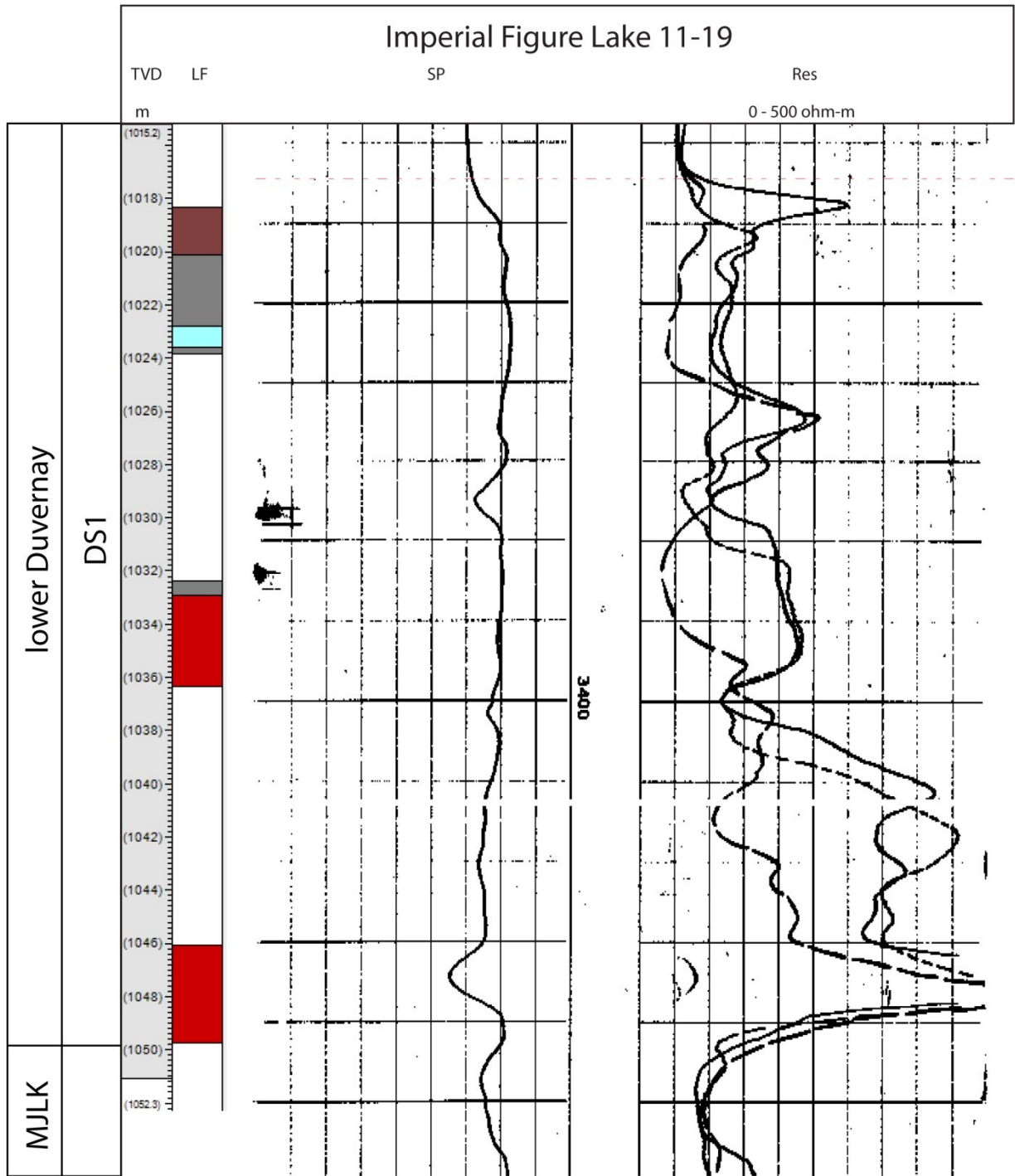
An isopach of the DS2 interval (Fig. 2.17) shows that the sediment distribution during DS2 is distinctly different than during DS1. The DS2 interval is much thinner than DS1 in the northeastern area of the basin. In the WSB, DS2 thins southwestward from 20 meters adjacent to the Grosmont Platform to less than 2 meters in a northwest-southeast trending corridor. The northeast edge of this corridor marks the basinward edge of LF11 argillaceous-dolomitic mudstone deposition. The southwest edge of this corridor, where strata begin to thicken westward, is dominated by LF4 silty mudstones. DS2 strata thicken substantially westward towards the Wild River Sub Basin. The DS2 interval in the ESB is generally less than 10 meters thick, but thickens to 15-20 meters adjacent to the Grosmont Platform and Leduc Formation reef complexes.

### *DS3*

At the base of the DS3 interval, a rapid shift in facies occurred across the basin. Nodular argillaceous dolostones of LF12 have a much greater western and southern extent than in most of the DS2 interval. On the eastern margin of the WSB, LF12 nodular argillaceous dolostones were deposited on top of LF11 argillaceous-dolomitic mudstones. The area of LF11 mudstone deposition shifted only slightly westward and southward. Silty mudstones of LF4 are not well-developed and are finer-grained than similar deposits of DS2 (Fig. 2.4). Bioturbated, pyritic mudstones of LF6 were deposited across most of the WSB, where planar-laminated, organic-rich mudstones of LF1-3 were previously deposited during DS2 (Fig. 2.10). In the southern ESB, LF6 bioturbated pyritic mudstones overlie LF7 bioturbated calcareous mudstones and nodular limestones (Fig. 2.12). *In-situ* benthic macrofossils become abundant in the Wild River Sub Basin and the ESB.

Above the basal DS3 beds, backstepping occurred and basinal lithofacies were deposited over a greater areal extent (Fig. 2.12). LF12 nodular argillaceous dolostones were deposited adjacent to the Grosmont Platform and southward along the eastern margin of the WSB. To the south and west, LF12 nodular argillaceous dolostones grade into LF11 argillaceous-dolomitic

# Imperial Figure Lake 11-19



- LF12: Nodular dolostone
- LF11: Argillaceous-dolomitic mudstone
- LF8: Nodular limestone
- LF1 and LF3: Planar-laminated mudstone, silty mudstone

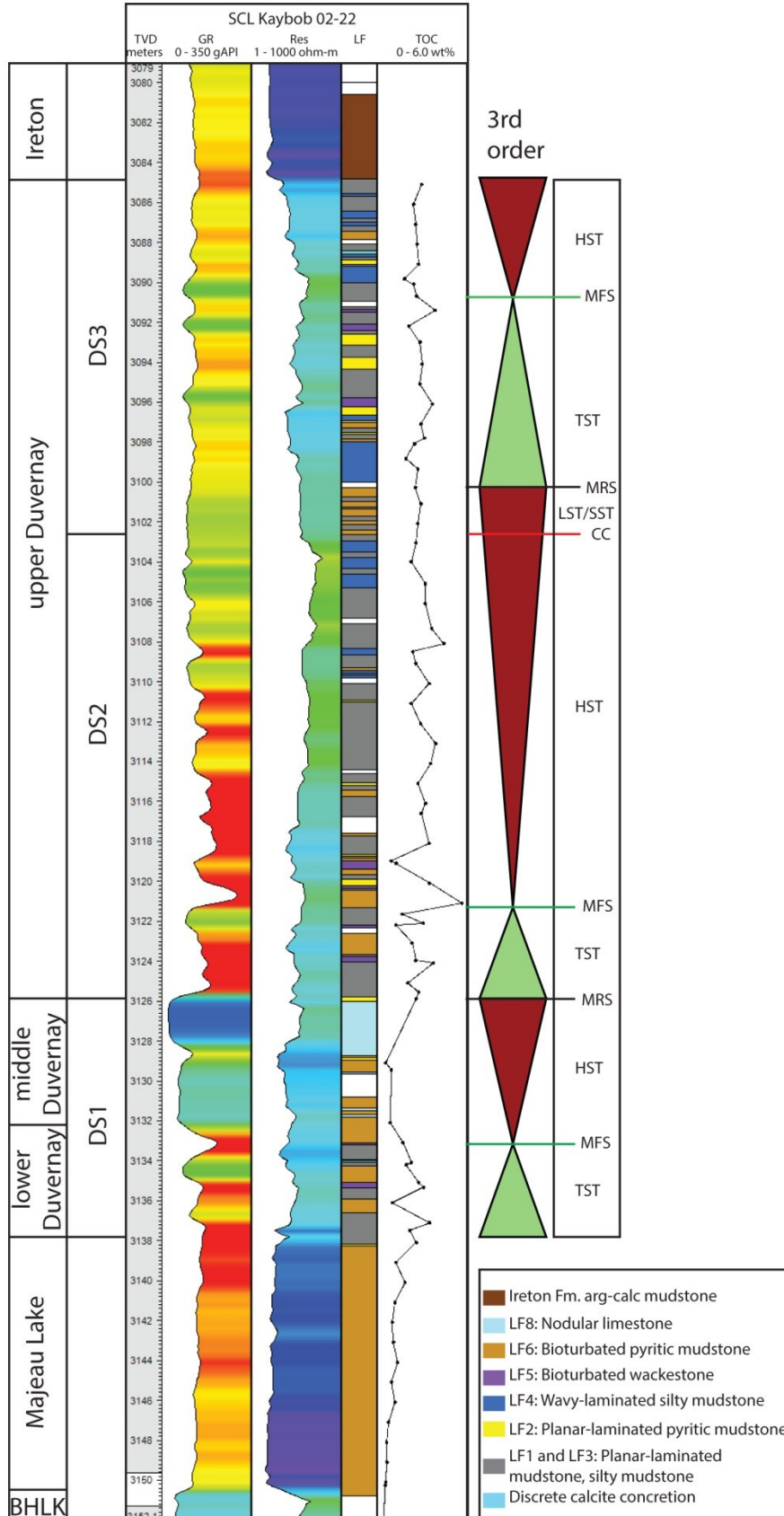


Figure 2.9: Imperial Figure Lake 11-19 core description. LF12 is the dominant lithofacies near the Grosmont Platform during DS1.

Figure 2.10: Gamma log, deep resistivity, lithofacies, TOC, and sequence stratigraphic interpretation for SCL Kaybob 02-22. LF1-3 laminated mudstones and laminated silty mudstones are dominant throughout much of the core. (TST = highstand systems tract; TST = transgressive systems tract; LST/SST = lowstand/stillstand systems trace; MRS = maximum regressive surface; MFS = maximum flooding surface; CC = correlative conformity). Red triangle = regression; Green triangle = transgression

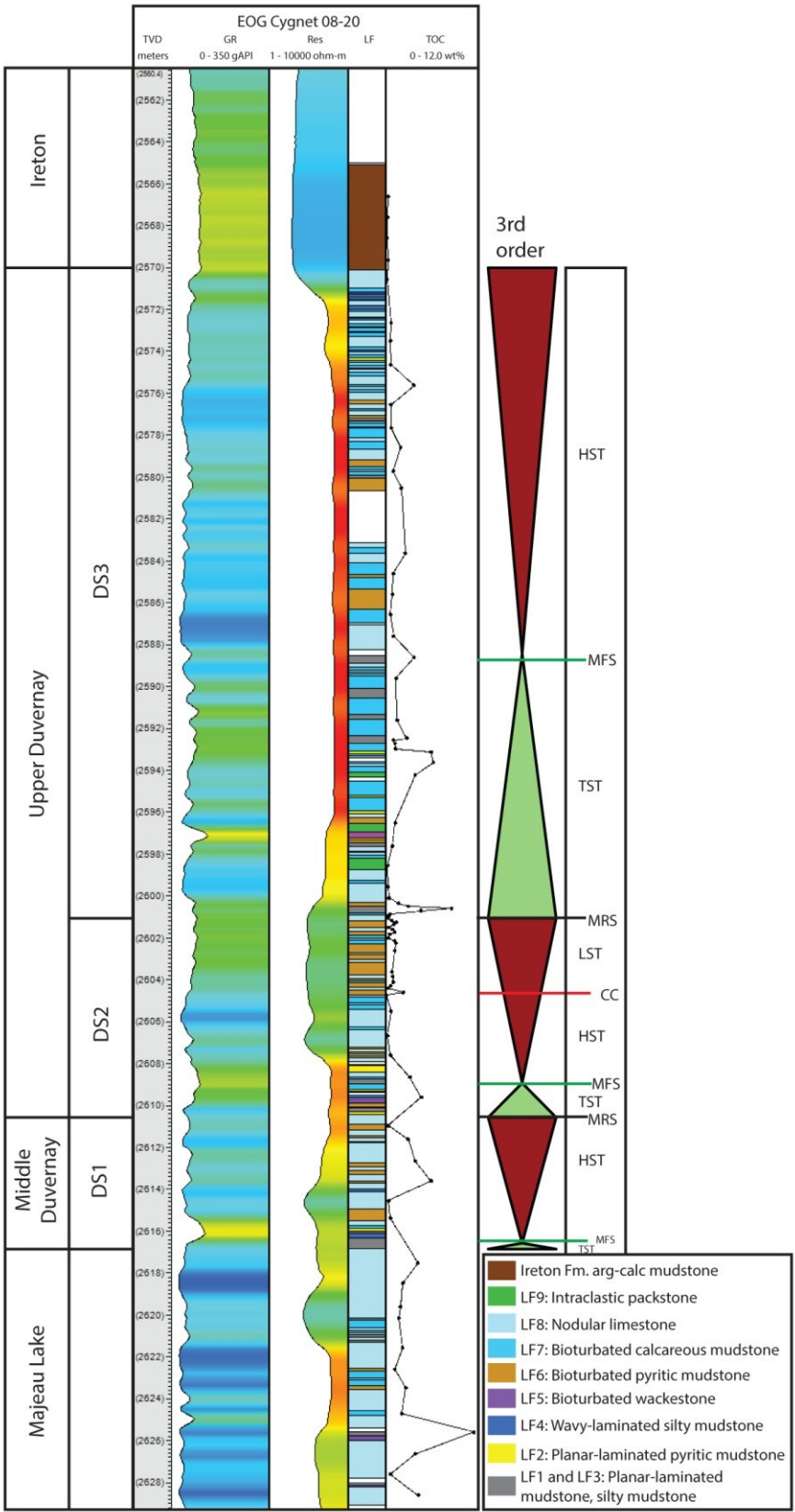


Figure 2.11: Gamma log, deep resistivity, lithofacies, TOC, and sequence stratigraphic interpretation for EOG Cygnet 08-28. The East Shale Basin is much more calcareous than the West Shale Basin. LF7 and LF8 are dominant in this location. (TST = highstand systems tract; TST = transgressive systems tract; LST = lowstand/stillstand systems trace; MRS = maximum regressive surface; MFS = maximum flooding surface; CC = correlative conformity)

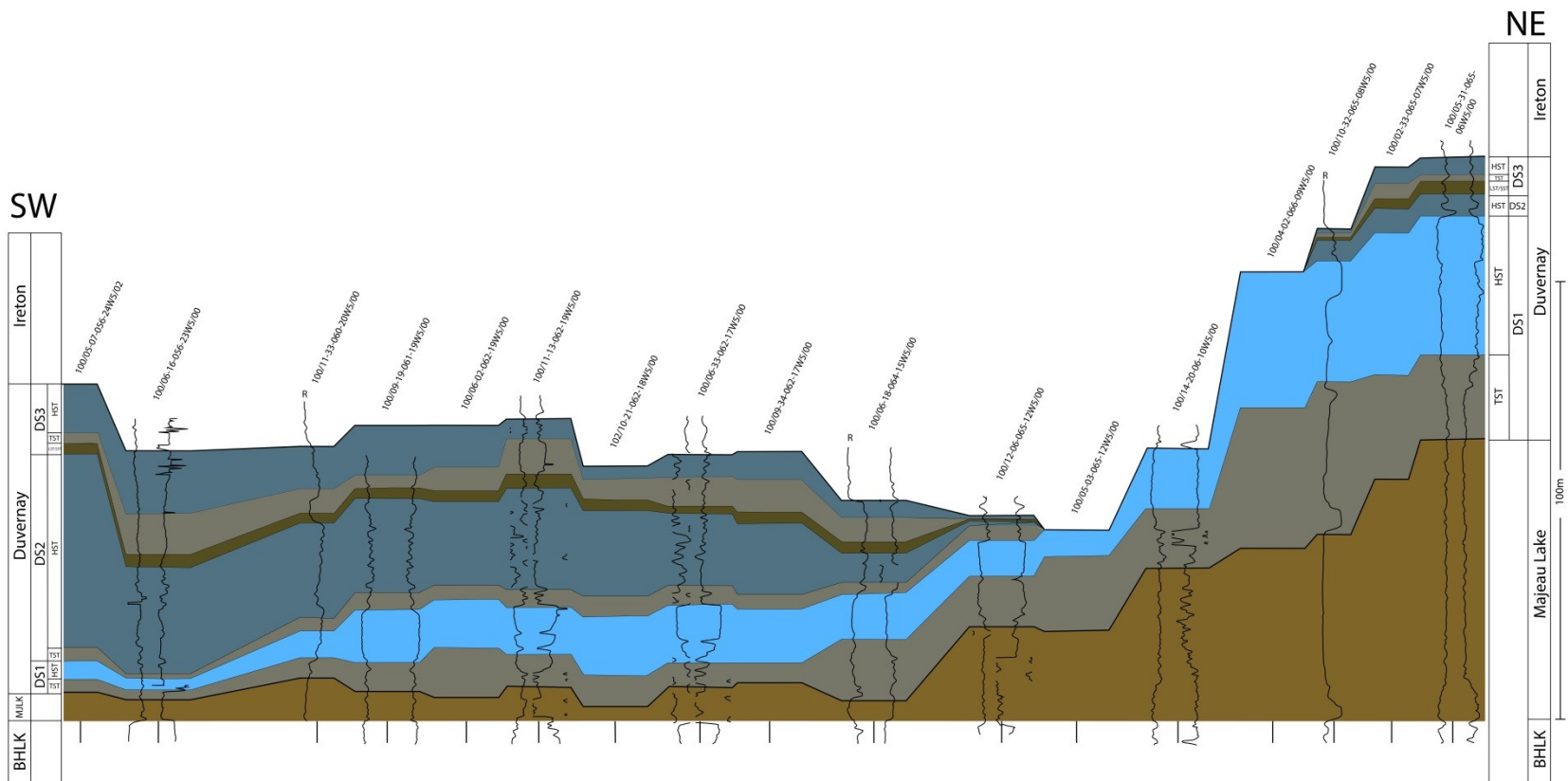


Figure 2.12: Dip section from Wild River Sub Basin, through Kaybob, towards Grosmont. DS1 strata thin from the Grosmont Platform into the basin. DS2 and DS3 strata are thickest in the Wild River Sub Basin to the west, and thin eastward. DS1 slope break and slope sediments are exposed during DS2 and DS3 due to backstepping of northeasterly derived argillaceous sediments. Datum: top of Beaverhill Lake Group. Most wells show gamma and sonic or density logs. R= resistivity log.

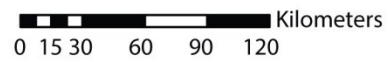
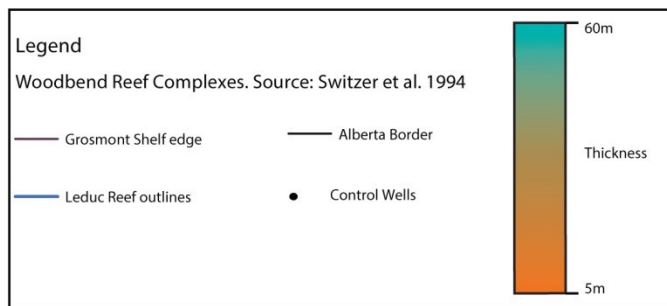
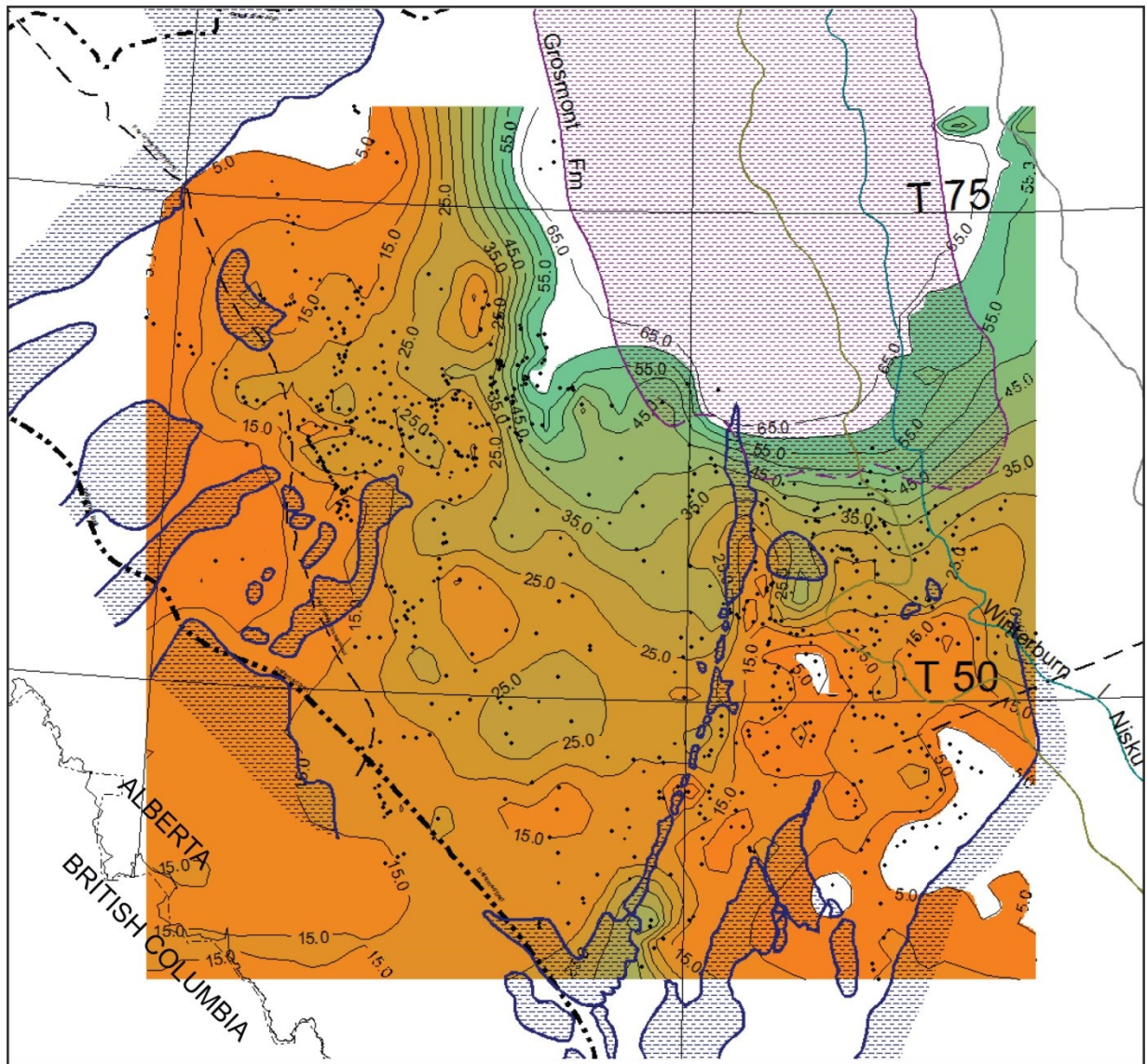


Figure 2.13: DS1 isopach.

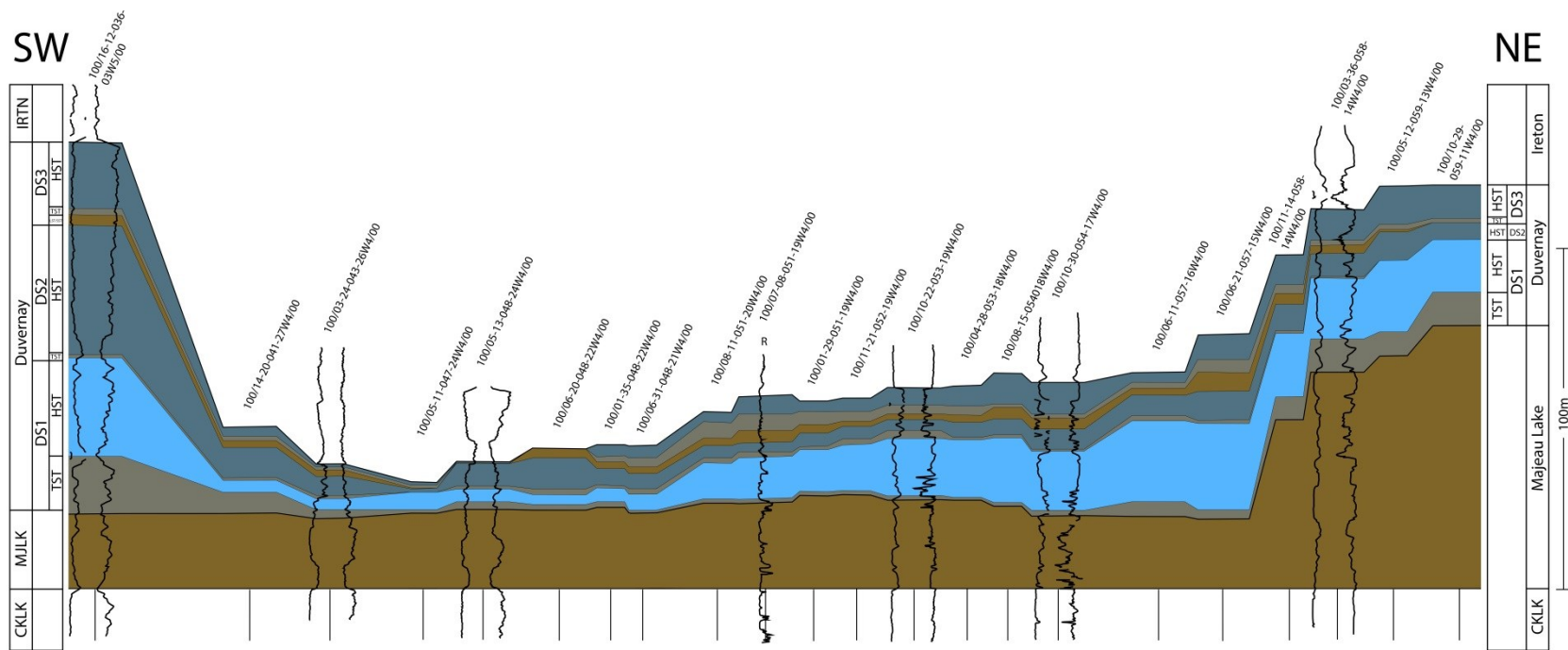


Figure 2.14: Dip section through the East Shale Basin. East Shale Basin strata thin from the north, adjacent to the Grosmont Platform, towards the south, with significant thickening near reef complexes and in the south end of the basin. Datum: top of Cooking Lake Formation. Most wells show gamma and sonic or density logs. R= resistivity log.

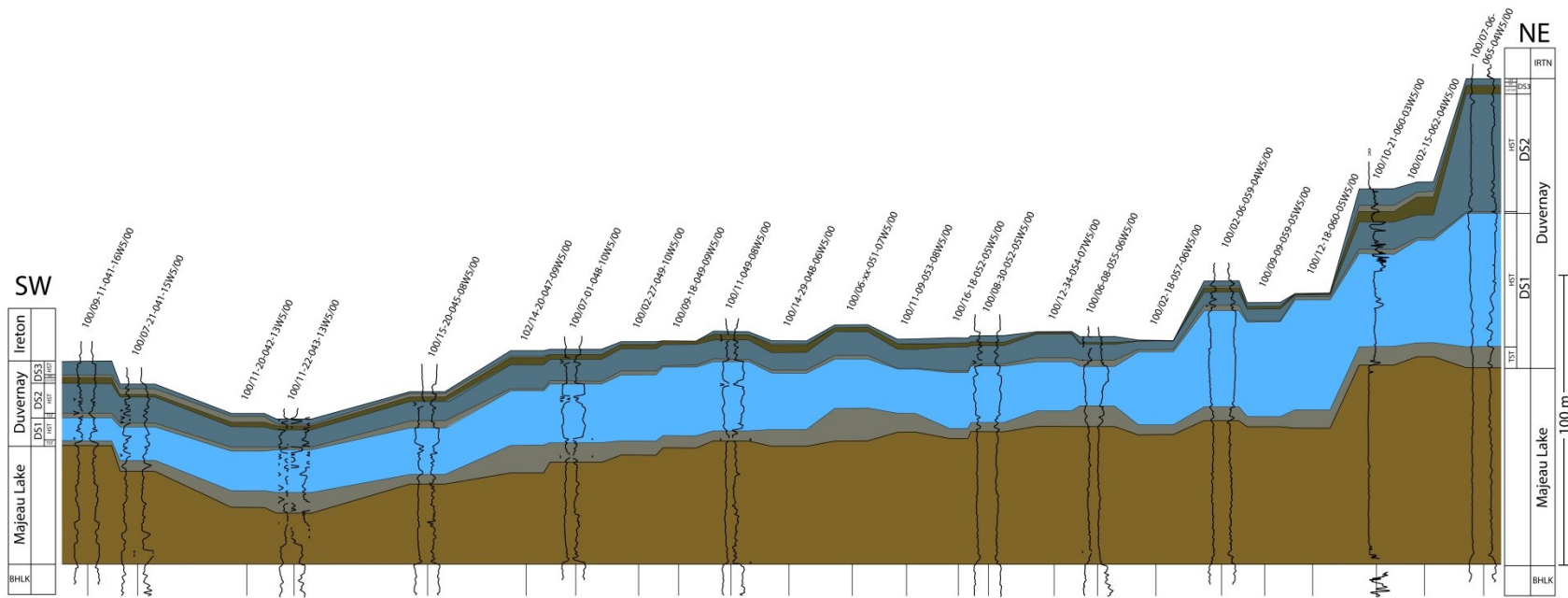


Figure 2.15: Dip section through the eastern West Shale Basin. Strata thin from the northeast to the southwest, with minor thickening at the far south end of the basin. DS1 strata thin consistently towards the southwest. DS2 and DS3 strata thin rapidly in the northeast to a zone of least deposition and then thicken minimally to the southwest. Datum: top of Beaverhill Lake Group. Most wells show gamma and sonic or density logs. R= resistivity log.

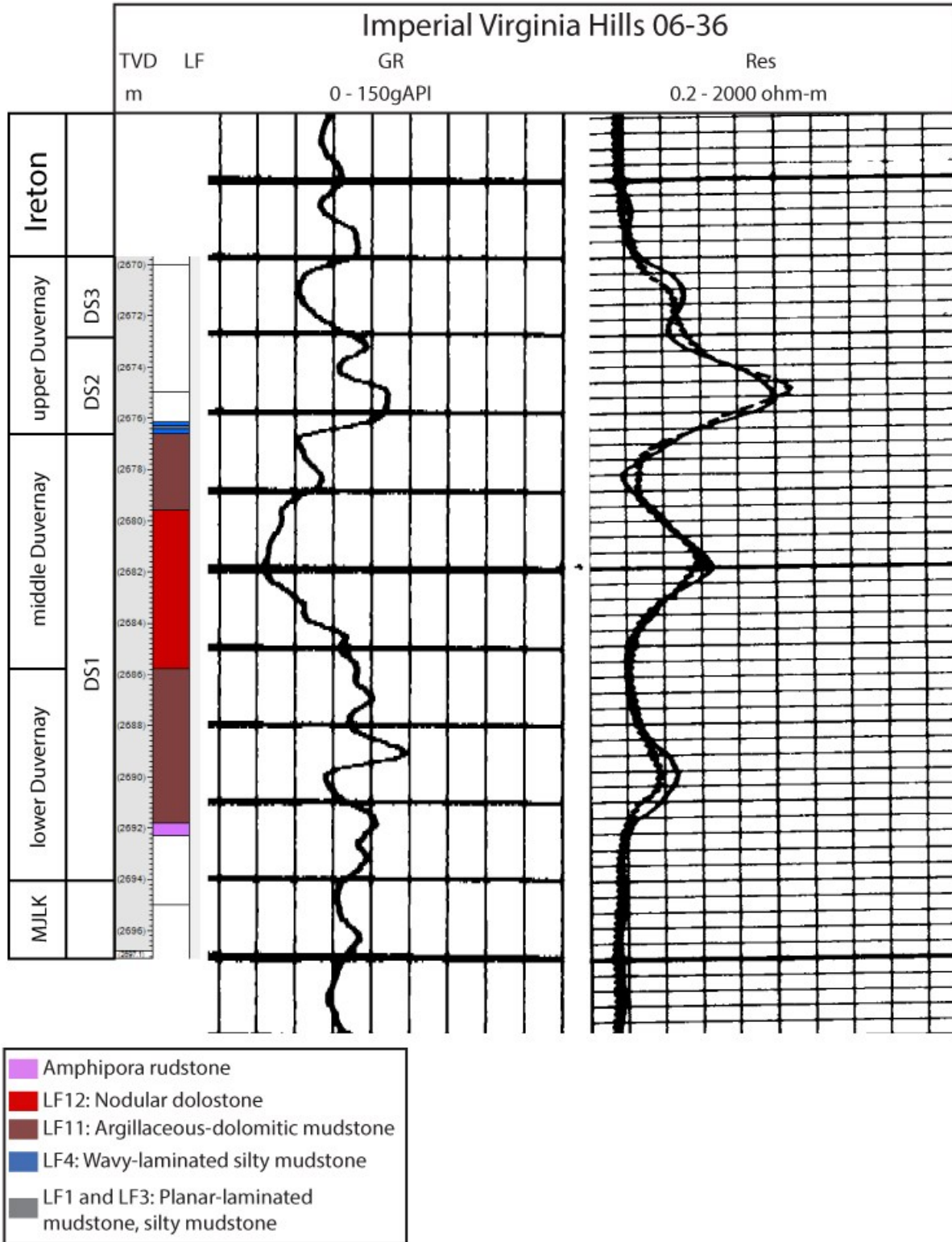


Figure 2.16: Imperial Virginia Hills 06-36 core description. LF11 and LF12 are dominant during DS1 but are sharply overlain by LF4 silty mudstones at the DS1-DS2 boundary.

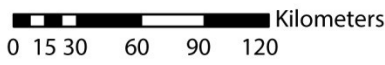
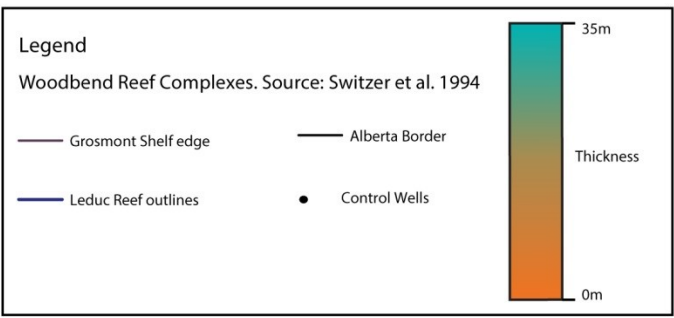
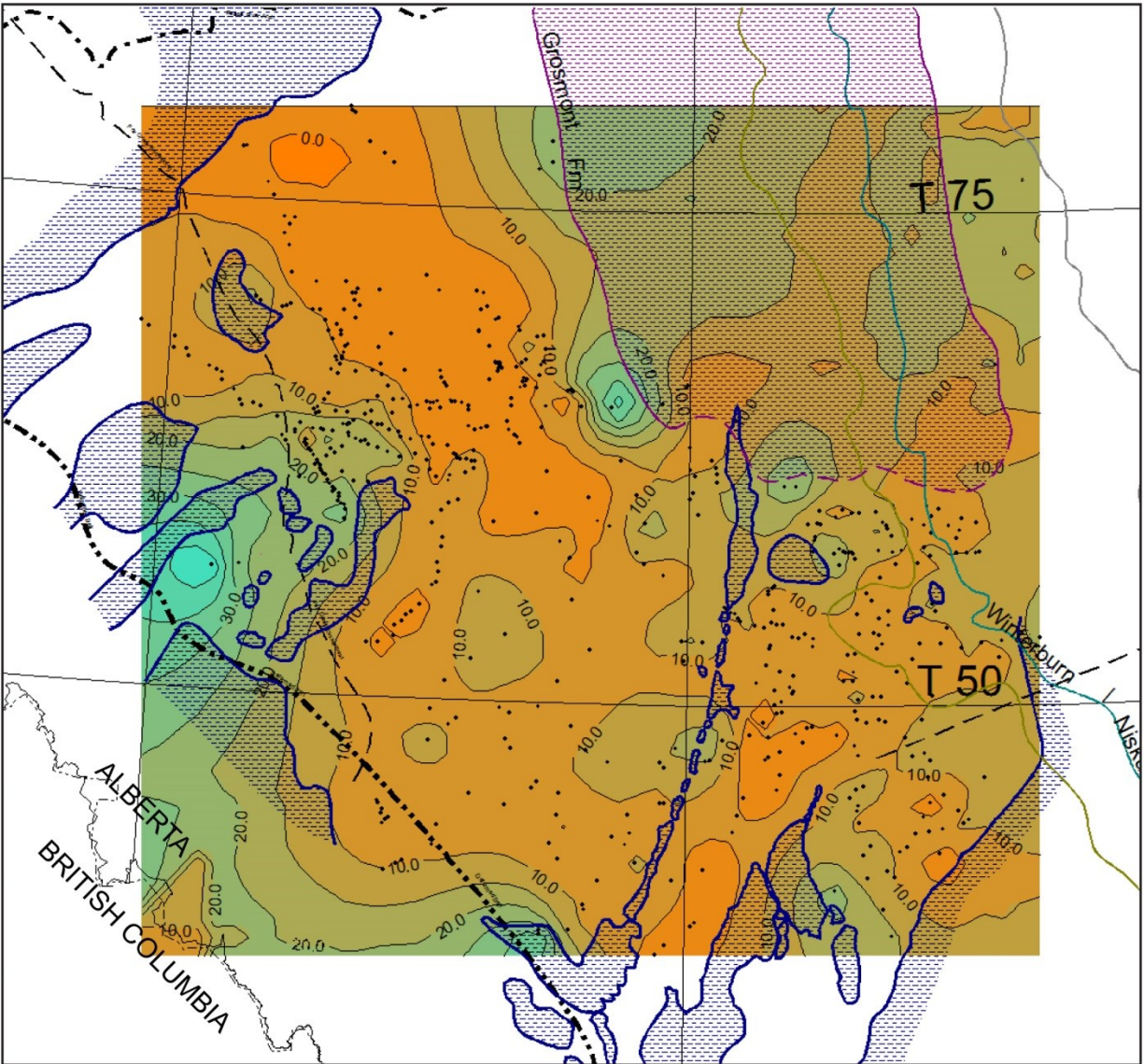


Figure 2.17: DS2 isopach.

mudstones. A zone of non-deposition to minimal deposition developed to the SW of LF11 deposition over much of the WSB. LF4 silty mudstones are the dominant lithofacies near the southwest margin of this zone. Much of the western and southern WSB is dominated by planar-laminated, organic-rich mudstones of LF1-3 (Fig. 2.10), except in the Wild River Sub Basin where bioturbated pyritic mudstones are the dominant lithofacies (Fig4). Bioturbated calcareous mudstones of LF7 are the dominant lithofacies in the ESB during DS3 time (Fig. 2.11)

An isopach map of the DS3 interval shows that variations in sediment thickness coincide with lithofacies variations (Fig. 2.18). Adjacent to the Grosmont Platform and along the eastern margin of the WSB, the DS3 interval is 10-20 meters thick, coinciding with areas of LF11 argillaceous-dolomitic mudstone and LF12 dolostone deposition. To the west and southwest, DS3 strata thin to less than 2 meters at the basinward margin of LF11 argillaceous-dolomitic mudstone deposition. A corridor of very minimal DS3 deposition extends from the eastern tip of the Peace River Arch, southeast through much of the WSB. The southwest margin of this corridor coincides with deposits of LF4 silty mudstones. Towards the Wild River Sub Basin, DS3 strata thicken to 20 meters where LF6 bioturbated pyritic mudstones become dominant (Fig. 2.4). In the ESB, DS3 strata are generally less than 10 meters thick but thicken to 40 meters near reef complexes in the south and southeast.

## **2.5 Discussion:**

### ***2.5.1 Sequence Stratigraphic Method***

The building blocks of a sequence stratigraphic model are the sequence, systems tract, and parasequence, which are bounded by sequence stratigraphic surfaces such as the surface of maximum regression, surface of maximum flooding, basal surface of forced regression, and sequence boundary or correlative conformity (Catuneanu et al., 2011). The recognition of these units and surfaces in outcrop, drill core, wireline logs, and seismic profiles allows for the characterization of the hierarchical levels of cyclicity of the depositional system.

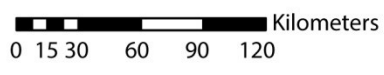
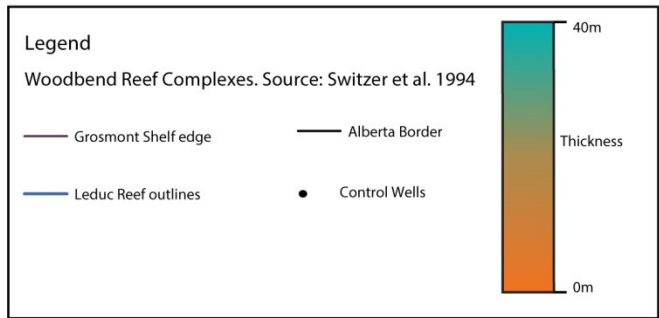
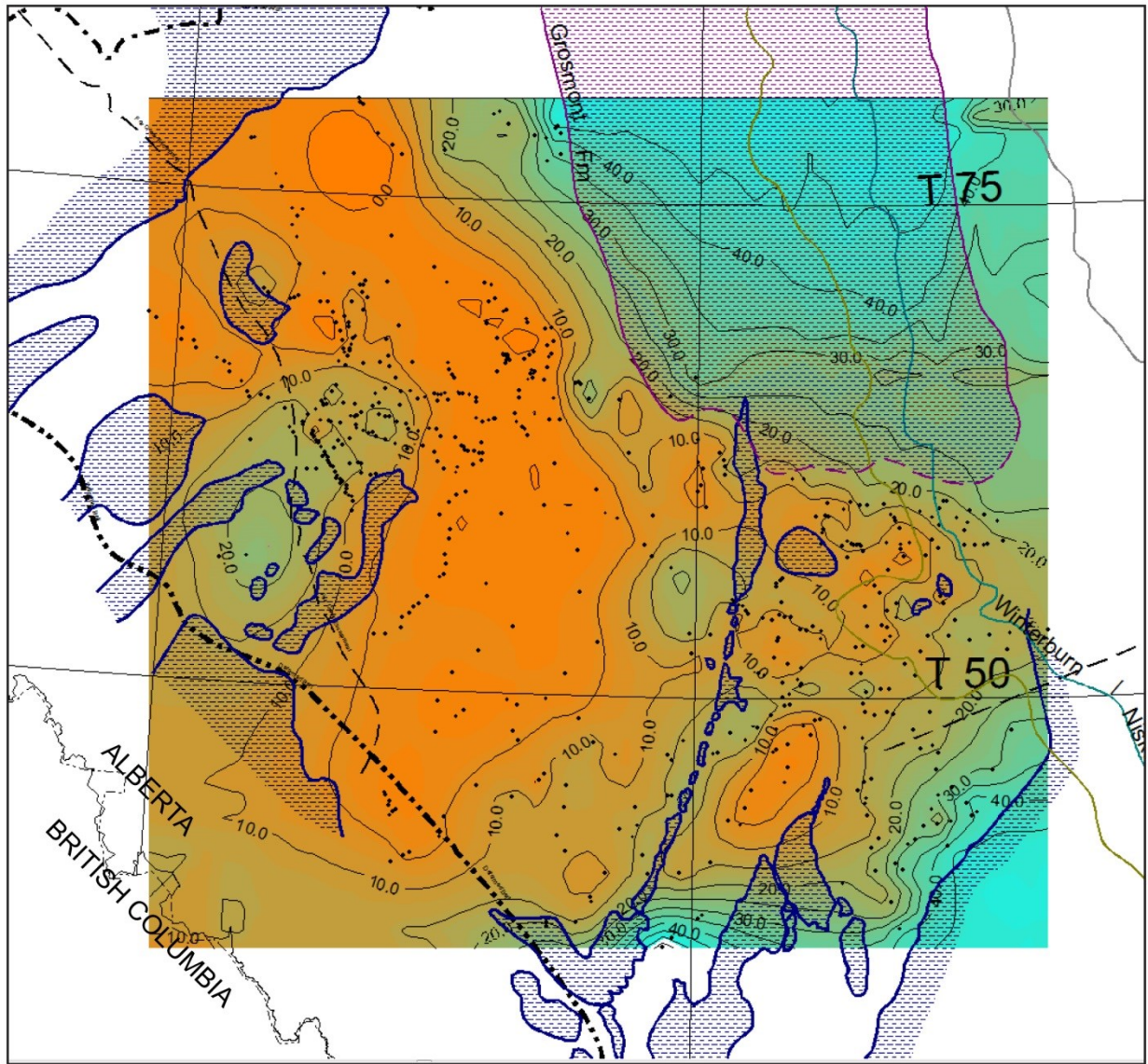


Figure 2.18: DS3 isopach.

This study follows Catuneanu et al. (2009) in defining a sequence as “a succession of strata deposited during a full cycle of change in accommodation or sediment supply”. Systems tracts were characterized based on type of bounding surface, stratal stacking pattern, and position within the sequence (Van Wagoner et al., 1987, 1988, 1990; Posamentier et al., 1988; Van Wagoner, 1995; Posamentier and Allen, 1999). The systems tracts identified in this study are the transgressive systems tract (TST), highstand systems tract (HST) and lowstand or stillstand systems tract (LST/SST). Transgressive systems tracts are defined as the sediment deposited from the onset of transgression until the onset of regression (Catuneanu et al., 2011). Transgressive systems tracts overlie a surface of maximum regression which caps the lowstand systems tract. In the absence of lowstand and falling-stage deposits, the TST directly overlies the HST and correlative conformity *sensu* Posamentier and Allen (1999). The TST is overlain by a maximum flooding surface which marks the maximum landward deposition of marine deposits (Catuneanu et al., 2011). The highstand systems tract marks the beginning of normal regression and overlies the maximum flooding surface. The HST is capped by a correlative conformity (Posamentier and Allen 1999) which is a conformable surface in basinal deposits. No forced regressive units were recognized in Duvernay Formation strata, which is the reason no falling stage systems tracts were identified. As such, lowstand or stillstand deposits directly overlie the highstand systems tract and correlative conformity. Lowstand/stillstand systems tracts are capped by a surface of maximum regression.

### ***2.5.2 Sequence Stratigraphy in Mudstones***

Application of the sequence stratigraphic method to fine-grained sediments can be challenging. Recognition of sequence stratigraphic surfaces can be much more difficult in fine-grained sediments compared to coarser shallower water deposits because drastic contrasts in lithology do not always occur across sequence stratigraphic surfaces. The scale of observation often must be much finer in fine-grained sediments in order to observe the necessary detail to create a sequence stratigraphic model.

Sequence stratigraphic analysis of fine-grained sediments, especially organic-rich mudstones has become increasingly common in recent years, but challenges still remain in

understanding the depositional processes and controls on lithofacies character and distribution. A growing number of published studies have attempted to apply the sequence stratigraphic method to organic-rich mudstones, with a resultant realization that the same set of rules does not apply to all organic-rich mudstones. The gamma radiation log for example, which has been used extensively in sequence stratigraphic analysis of shallow water strata, is not necessarily correlative to sea level changes (Bohacs, 1998). In some cases, TOC covaries with gamma radiation while in other cases, the correlation is only moderate to poor (Lüning and Kolonic, 2003). Additionally, organic-matter enrichment may occur during maximum transgression (Creaney and Passey, 1993) or other intervals of a sequence (Hemmesch et al., 2014). Detailed sedimentological observations have proven vital in some studies in order to recognize key sequence stratigraphic surfaces (e.g. Macquaker and Taylor, 1996; Williams et al., 2001; Schieber and Riciputi, 2004; Ver Straeten et al., 2011). Schieber and Riciputi (2004) for example, identified pyritized ooids within a succession of Upper Devonian black shales of the Eastern United States, and from that observation inferred periods of significant sea level fall.

### ***2.5.3 Duvernay Formation Sequence Stratigraphic Model***

#### *The relationship between lithofacies and sea level*

Detailed core description allows for the recognition of systematic changes in lithofacies, providing the basis for interpreting variations in sea level. Three orders of cyclicity were observed in Duvernay Formation strata. The smallest scale of cyclicity was observed in individual depositional packages and was based on 5 general trends: 1) decreasing quality of lamination; 2) siliceous bases (i.e. LF1-3) that become more calcareous and/or argillaceous upwards (i.e. LF4-8); 3) decreasing TOC; 4) more common *in-situ* benthic macrofossils; and 5) increasing grain size. Based on these trends, individual depositional packages are interpreted as shallowing-upwards packages.

Decreasing quality of lamination upwards in individual depositional packages is the result of increased bioturbation, indicating an increase in bottom water oxygen concentration. While this can be caused by changing circulation patterns, it is most likely the result of decreasing water depth and more efficient oxygenation of the sea floor.

An upwards change in lithology from siliceous to calcareous/argillaceous in individual depositional packages reflects changes in influx of carbonate and clastic detritus to the basin, also a result of sea level changes. During transgression, clastic sediment is trapped upslope, and reef complexes and carbonate platforms backstep, reducing the supply of both clastic and carbonate detritus to the basin. This results in an increased proportion of biogenic sediment at the bases of shallowing-upwards depositional packages. During regression, biogenic sediment is increasingly diluted by carbonate and/or clastic sediment. Organic matter is enriched and diluted by the same mechanism. In formations with high productivity, this mechanism may fail to concentrate organic matter because the sedimentation rate of inorganic biogenic sediment is high enough to “autodilute” organic matter (Bohacs et al., 2005; Tyson, 2005). In this scenario, the tests of planktonic organisms should be abundant, which is not the case in the Duvernay Formation. The right amount of autodilution may also act to preserve organic matter by burying it more efficiently (Tyson, 2005).

During transgression, bottom water anoxia is generally more widespread due to increased water depth and less efficient circulation of the water column. Anoxia allows for the preservation of gradually deposited organic matter. During regression, organic matter is more completely degraded due to increased dissolved oxygen concentration in the water column. An increase in the abundance of *in-situ* benthic macrofossils upwards in a depositional package also suggests that conditions at the sediment-water interface, particularly oxygen concentrations, are becoming more consistently conducive to life for aerobes. This may be a result of more efficient circulation of the water column or more frequent downslope sedimentation events that transport oxygen into the basin. This trend is not observable where LF1-5 make up the entirety of a depositional package, as none of these lithofacies contain *in-situ* benthic macrofossils.

Increasing grain size upwards in a depositional package is the result of increasing proximity of sediment sources and increasing carbonate production. Over much of the basin, most of the silt- and sand-sized material is calcareous. An increase in calcite detritus can occur due to erosion and more efficient transport into the basin during lowstand and also as a result of increased carbonate production during highstand shedding (Schlager et al., 1994; Vecsei and Sanders, 1997). Increased carbonate silt and sand upwards in depositional packages in the Duvernay Formation is interpreted primarily to be caused by highstand shedding rather than

lowstand transport because eroded material is generally not observed, and terrigenous sedimentation does not increase where carbonate material becomes coarser. During lowstand, carbonate platforms and reefs experience reduced carbonate production due to decreased geographic area suitable for platform carbonates, and reduced accommodation space for upwards growth of reefs (Schlager, 1994). However, carbonate material can be eroded from platforms and reefs and decreased accommodation space typically results in more efficient transport into the basin (Vecsei and Sanders, 1997). Eroded intraclasts are not observed in combination with increased carbonate silt and sand in the Duvernay Formation. Additionally, lowstand is conducive for clastic transport into the basin, but clastics are not observed to increase in combination with increased carbonate silt and sand abundance in the Duvernay Formation.

Lower order (i.e. thicker packages of sediment) sea level fluctuations are recognized by the stacking of individual depositional packages. This scale of cyclicity is described in the results section as meso-scale, 2-6m thick intervals containing successions of depositional packages (Fig. 2.4) that show the same 5 general trends observed above, or those same trends in reverse. Regressive intervals have decreasing thicknesses of siliceous, organic-rich mudstones in each overlying depositional package and show the same 5 trends as discussed above. These intervals represent an overall shallowing over several successive depositional packages. The reverse is true for transgressive intervals. These intervals represent an overall deepening over several successive depositional packages. Each successive depositional package contains a greater thickness of siliceous, organic-rich mudstones at its base and the overall interval displays the 5 general trends in reverse.

Not every regressive interval is overlain by a transgressive package of sediments. Transgressions are commonly represented by surfaces that separate two regressive intervals. In this case, carbonate cementation and hardground formation locally occurs. Hardground formation in Duvernay Formation and Ireton Formation deposits was ascribed by Stoakes (1980) to the reduction of terrigenous influx to the basin during transgression and cementation due to low sedimentation rates and a dominance of pelagic carbonate cementation. In the upper Duvernay member, above the DS2 maximum flooding surface, transgressive intervals are generally thicker than below the DS2 MFS, and regressive intervals less commonly have sharp, cemented tops. This change in the nature of flooding surfaces and transgressive sedimentation is

interpreted to be influenced by the 2<sup>nd</sup> order deposition sequence outlined by Potma et al. (2001). The 2<sup>nd</sup> order maximum flooding surface coincides with the DS2 maximum flooding surface. Sharp flooding surfaces and thin transgressive deposits are more common below the DS2 MFS because they occur within a 2<sup>nd</sup> order TST and clastic sedimentation into the basin was limited. Above the DS2 MFS, in the 2<sup>nd</sup> order HST, transgressive deposits are thicker and sharp, cemented flooding surfaces are less common because overall clastic influx to the basin is higher.

### *3<sup>rd</sup> order sequence stratigraphic framework*

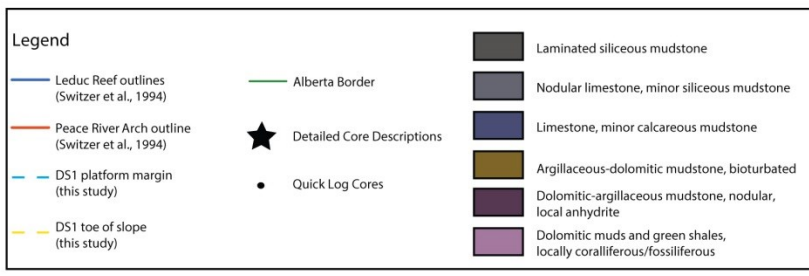
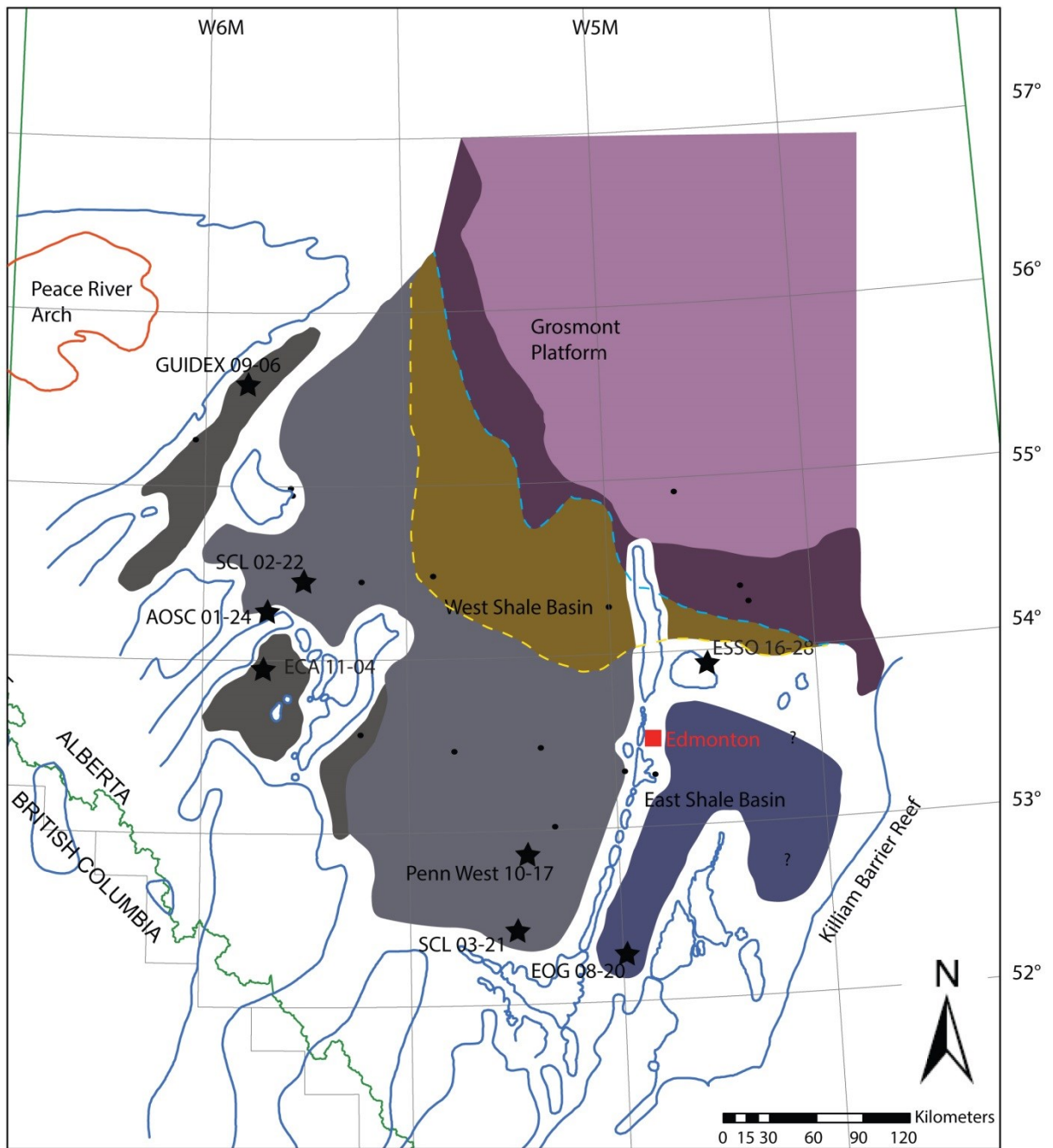
This study recognizes three 3<sup>rd</sup> order depositional sequences (as per Hunt and Tucker, 1992; Catuneanu, 2009) that comprise the entire thickness of the Duvernay Formation. Third order sequences were defined by cyclical vertical facies distribution in described cores, and by stratal stacking patterns defined through wireline mapping. By combining observations from core, wireline cross sections, and isopach maps, basin-scale lithofacies maps were created for specific stratigraphic intervals. These maps illustrate the changes in the distribution of lithofacies through time

The lower and middle Duvernay members compose the first depositional sequence (DS1); organic-rich mudstones (LF1-3) and nodular limestones (LF8) dominate much of this interval (Fig. 2.19). The base of DS1 is marked by a major transgression, with basal Duvernay Formation sediments interpreted to have been deposited in deeper water than sediments of the underlying Majeau Lake Formation. The end of transgression (maximum flooding surface) often occurs where the most basinal set of lithofacies occurs in a given core, and is commonly marked by a spike in gamma radiation and TOC. Above this surface, basinal lithofacies become less common. Subsequent regression during DS1 is interpreted as highstand normal regression because stratal geometries are aggradational (Fig. 2.12), and the vertical progression in lithofacies does not show lowstand style sedimentation such as rapid clastic influx. A cross section from the Wild River Sub Basin, northeast towards the Grosmont Platform, shows a steepening of depositional slope from Majeau Lake time through DS1 (Fig. 2.12). This pattern of aggradation and steepening was a result of thick packages of LF11 argillaceous-dolomitic mudstones being deposited in the northeast part of the basin during highstand normal regression. Argillaceous sediments of LF11 are capped by LF12 nodular dolostones that are interpreted to be platform-margin deposits. Aggradation during DS1 is equivalent to Grosmont Platform stages

G1 and G2 as defined by Cutler (1983). Dix (1990) recognized a similar pattern of ramp- to platform-style evolution of Leduc Formation sediments that fringe the Peace River Arch. Many authors have studied time-equivalent Leduc Formation reefs, and document a period of backstepping, followed by significant aggradation (e.g. Klovan, 1964; Chow et al., 1995; Potma et al., 2001; and Van Buchem, 1996a, 2000a), which is interpreted to be equivalent to transgression and highstand normal regression during DS1 time.

The second depositional sequence (DS2) starts at the top of the middle Duvernay member, which is capped by a significant flooding surface. In core, the contact is commonly sharp, locally overlain by a thin transgressive lag of coarse calcareous fossil fragments, conodonts and phosphatic clasts. Transgression during lower DS2 is reflected in core as a shift to deeper water, more organic-rich facies, and in lithofacies maps as a greatly expanded zone of planar-laminated, organic-rich mudstone (LF1-3) deposition (Fig. 2.20). Transgression during deposition of the basal section of DS2 resulted in the creation of upslope accommodation space and significant backstepping of argillaceous sediments (Fig. 2.12). Platform development during DS1, followed by early DS2 transgression resulted in the accumulation of argillaceous deposits upslope of the platform margin. During DS2, an area of non-deposition to minimal deposition was developed over the DS1 sediments that make up the DS1 platform slope break and much of the slope because nearly all of the argillaceous sediment was deposited towards the inner platform. Evidence for this is seen in the scarcity of argillaceous facies in the basin (Fig. 2.12) and a dominance of LF11 and LF12 in cores such as Imperial Deep Creek 04-33 which is located northeast of the DS1 platform slope break.

Basinward of the DS1 platform and zone of no DS2 deposition, DS2 strata are very clay-poor, and siliceous mudstones of LF1-3 predominate. The thickest accumulation and greatest areal expanse of planar-laminated organic-rich mudstones occurs during DS2 transgression and early highstand. Near the base of the DS1 slope, DS2 silty mudstones are deposited by turbidity currents and contour currents (Chapter 1). Carbonate silt and sand is sourced from reef and platform carbonates as well as erosion of exposed and cemented DS1 sediments.



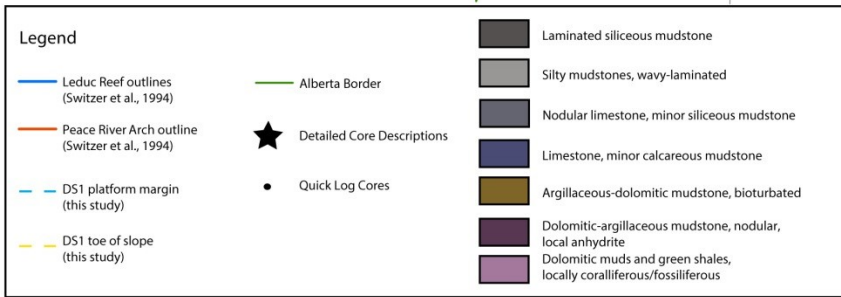
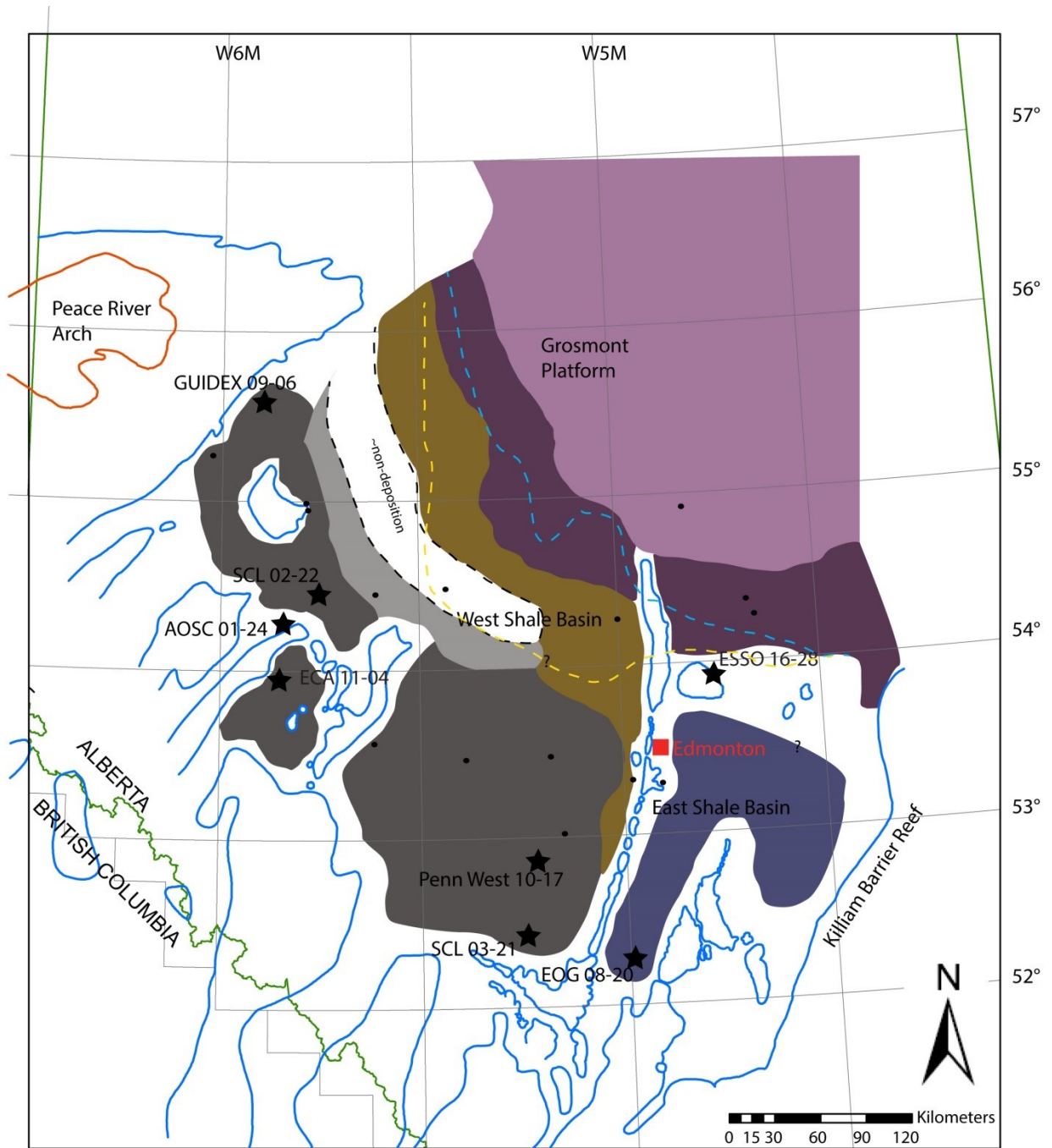


Figure 2.19: DS1 lithofacies distribution. Argillaceous-dolomitic LF11 and LF12 are dominant adjacent to the Grosmont Platform. Much of the DS1 interval in the West Shale Basin is composed of nodular limestone with minor laminated, organic-rich mudstone.

Figure 2.20: DS2 lithofacies distribution. During DS2 time, argillaceous sediments are deposited landward of the slope break that was formed during DS1. A NW-SE trending corridor of very minimal deposition formed on the basinward edge of argillaceous mudstone deposition. Silty mudstones (dominantly LF4) were deposited on the basinward edge of the non-deposition zone. Much of the West Shale Basin is dominated by planar laminated, organic-rich mudstones of LF1-3.

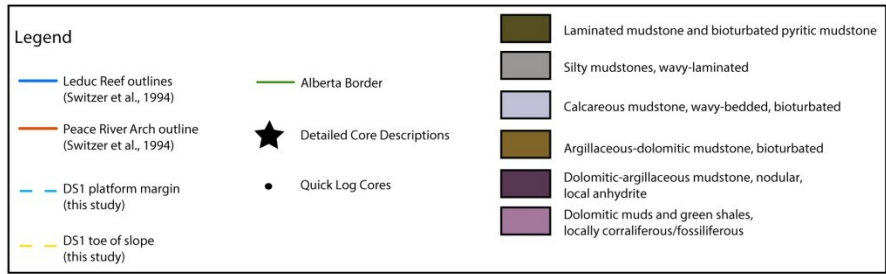
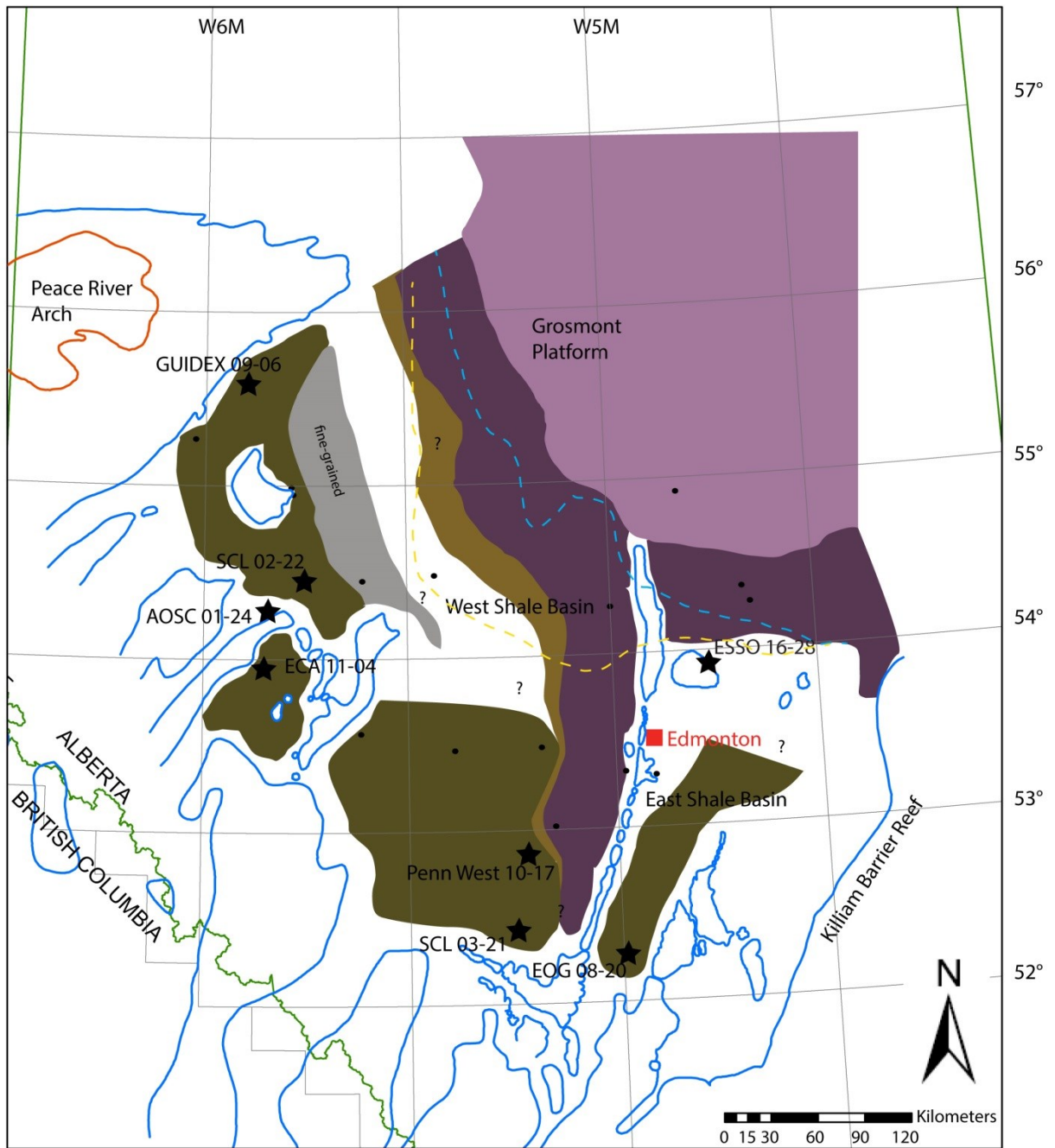
Regression during upper DS2 is interpreted as highstand normal regression. In the northwest WSB, planar-laminated mudstones become siltier upwards as a result of increased carbonate detritus being shed into the basin during highstand shedding of reefs (Fig. 2.10.) Additionally, silty mudstones of LF4 prograde basinward from the base of the DS1 slope. In the Wild River Sub Basin, the upper DS2 section becomes pyritic and bioturbated upwards (Fig. 2.4). The increase in pyrite was observed both macroscopically in core and microscopically in thin section (Chapter 1). An increase in pyrite is associated with an increase in iron-rich clay minerals (Chapter 1; McMillan et al., 2016). We propose that the increase in argillaceous sediments on the western side of the basin (i.e. dominance of LF6) (Fig. 2.12) is the result of clastic input from the exposed Peace River Arch.

Strata significantly thicken to the west during DS2 regression (Fig. 2.12.), which is opposite of the isopach patterns observed in DS1. The reversal in stratal thickening from DS1 to DS2 is a result of transgression at the base of DS2. This transgression resulted in upslope trapping of northeast-derived clastics above the platform slope break. During the subsequent highstand normal regression, the northeast-derived clastics did not prograde all the way back to the platform slope break created during DS1 deposition, thus creating a zone of non-deposition during DS2. The absence of these northeast-derived clastic sediments in basinal areas led to westward thickening of DS2 strata. Clastics sourced from the Peace River Arch did not have a broad platform to travel across and were deposited in abundance on the west side of the WSB. This relationship is best developed in the Wild River Sub Basin where increased sedimentation rates compared to elsewhere in the West Shale Basin (based on sediment thickness) resulted in significant shallowing of the sea floor into more oxygenated bottom waters, as evidenced by the dominance of bioturbated facies such as LF6. In the eastern part of the WSB, a zone of non-deposition did not develop (Fig. 2.15), which is interpreted to the result of less significant DS1 platform development in that area. The southern WSB is far removed from any clastic source so

there is no significant southward or southwestward stratal thickening during DS2 in the southern WSB. Minor thickening is a result of carbonate detritus being shed from the Rimbey Meadowbrook chain of reefs and the carbonate complexes on the West Alberta Ridge.

The base of DS3 is marked by a rapid basinward shift of lithofacies (Fig. 2.21), interpreted to be the result of lowstand or stillstand progradation. The base of DS3 differs from that of DS1 and DS2 in that it is marked by a negative change in accommodation space. The bases of DS1 and DS2 do not show evidence for any significant reduction in accommodation space and no lowstand or stillstands were recognized in these units. However, the bases of all three cycles sit above highstand (HST) units. At the base of DS3, sediments across the basin become more argillaceous (i.e. a shift from LF1-3 to LF6), indicating that clastic sediments were more effectively being transported into the basin. While some of the argillaceous sediment may have been sourced from the northeast, lithofacies distributions, specifically the increased abundance of LF6 in the Wild River Sub Basin with respect to the Kaybob area (Fig. 2.4 vs Fig. 2.10), suggest that the Peace River Arch was a more important source of clastic sediment, at least to the WSB. Additionally, LF6 is significantly bioturbated, suggesting that water depths in western areas such as the Wild River Sub Basin were shallower during the DS3 lowstand than to the northeast at the base of the DS1 slope. No significant accumulation of sediment occurred over the exposed DS1 slope break or slope during the DS3 lowstand/stillstand, suggesting that northeast-derived argillaceous sediments did not prograde into basinal areas. The area of maximum progradation of northeast-derived sediments was along the eastern margin of the WSB (Fig. 2.21). In this part of the basin, LF12 nodular argillaceous dolostones were deposited on top of LF11 argillaceous-dolomitic mudstones in a north-south trending belt.

At the end of DS3 lowstand, lithofacies begin shifting landward (Fig. 2.12). The transition is not abrupt and no major flooding surfaces exist, suggesting that transgression during DS3 was not as sudden or significant as transgression during DS1 and DS2. During DS3 transgression, the zone of deposition of organic-rich mudstones of LF1-3 expands again, although not to the extent of DS2 (Fig. 2.22). During DS3 highstand normal regression, LF11 argillaceous mudstones and LF12 nodular dolostones prograde above the DS1 platform and along the eastern margin of the WSB. Throughout DS3, sedimentation was still very minimal



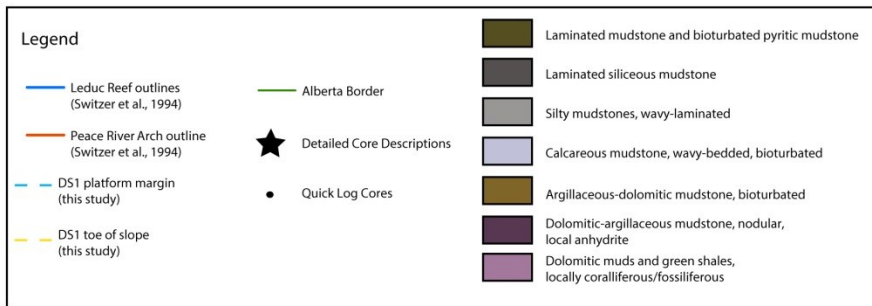
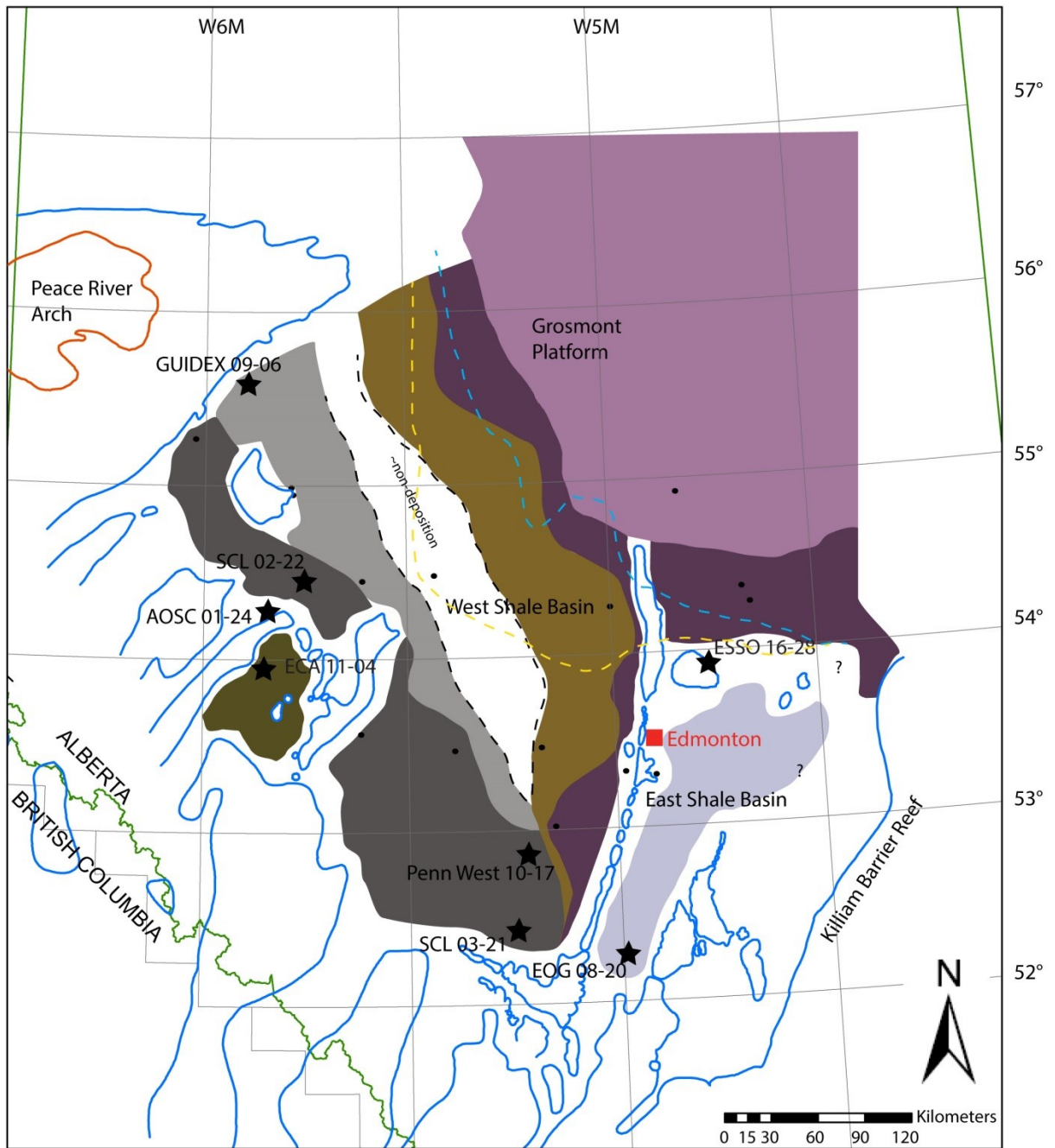


Figure 2.21: DS3 lowstand/stillstand lithofacies distribution. Bioturbated pyritic mudstones of LF6 are deposited over much of the basin, indicating an increase in clay mineral flux to the basin and increase in bottom water oxygenation. Argillaceous mudstones and nodular argillaceous dolostones prograde southward along the eastern margin of the West Shale Basin.

Figure 2.22: DS3 TST and HST lithofacies distribution. A landward shift of lithofacies occurs after the DS3 lowstand/stillstand. LF6 bioturbated pyritic mudstones are only prominent in the Wild River Sub Basin, while the zone of LF1-3 organic-rich siliceous mudstone deposition is expanded. Silty mudstones, primarily LF4, are deposited at the basinward edge of a non-deposition zone that has expanded southeastward through the West Shale Basin.

overlying the DS1 platform slope break and slope (Fig. 2.12). Westerly-derived sedimentation continued, as seen by thickening of strata to the west.

#### ***2.5.4 Recognizing Sequence Stratigraphic Surfaces and Systems Tracts in Organic-Rich Mudstones***

While each individual surface or tract has its own unique expression, certain common features can be identified that define major sequence stratigraphic surfaces.

##### *Maximum Regressive Surface and Transgressive Systems Tract*

The transgressive systems tract is the stratigraphic interval deposited from the onset of transgression (maximum regressive surface) until the onset of highstand normal regression (maximum flooding surface) (Catuneanu et al., 2011). During transgression, facies shift landward and basinal sedimentation occurs over a greater geographic expanse. Transgressive strata onlap previously deposited sediments.

The transgressive systems tract has been recognized in some black shale formations as the interval of maximum organic enrichment (Creaney and Passey, 1993). This is due to sediment starvation in the basin, and the concentration of organic-rich sediment at a potentially anoxic sea floor. In some instances, transgression results in the flooding of intracratonic basins and the deposition of black shales within those basins due to restriction of circulation with open ocean waters (e.g. Lüning et al., 2000; Algeo et al., 2007). In other formations, transgression may result in the flooding of palaeo-highs, resulting in greater connection to open ocean waters and a decreased potential for organic matter preservation (Röhl et al. 2001). Transgression can

also be detrimental to organic matter enrichment when the sedimentation rate of inorganic biogenic sediment is high, resulting in “autodilution” of organic-rich sediment (Tyson, 2005).

This study has identified transgressive systems tracts in the Duvernay Formation primarily on the recognition of flooding surfaces and by the increasing presence of deeper water lithofacies. The onset of transgression is commonly marked by a major flooding surface (maximum regressive surface). The most prominent examples of this type of surface are the Majeau Lake Formation – Duvernay Formation contact (Fig. 2.5), and the top of DS1 (Fig. 2.6). At these surfaces, deeper water facies sharply overlie shallower water facies. Over much of the West Shale Basin, organic-rich, siliceous mudstones of LF1-3 overlie bioturbated, organic-lean nodular limestones of LF8 at the DS1-DS2 contact. Maximum regressive surfaces are often heavily calcite-cemented due to very low sedimentation rates and the reduction of clastic influx into the basin (Stoakes, 1980). These surfaces may represent a significant amount of time (e.g. “hiatal surface” of Galloway, 1989)

Above these major flooding surfaces, transgressive systems tracts are identified by the increasing proportion of deep water facies in successive depositional packages (Fig. 2.4). The interpretation of deeper vs shallower black shale lithofacies depends heavily on a robust lithofacies analysis (Chapter 1). A transgressive systems tract will not always be preserved. Often, the maximum flooding surface very closely overlies the maximum regressive surface, separated by only a thin interval of transgressive deposits.

Third order transgressions within the Duvernay Formation have different characteristics depending on whether they occur above or below the 2<sup>nd</sup> order MFS that coincides with the DS3 3<sup>rd</sup> order MFS. The Duvernay Formation was deposited within the late transgressive and early highstand systems tracts of a second order depositional sequence (Potma et al., 2001). The 3<sup>rd</sup> order transgressions within DS1 and DS2 occur below the 2<sup>nd</sup> order MFS, thus during a second order transgression. The two 3<sup>rd</sup> order transgressions overlie sharp flooding surfaces, and are represented by only thin sets of transgressive deposits. In contrast, the DS3 transgressive systems tract, deposited during a second order highstand, is much thicker over much of the basin and no significant, sharp flooding surface (maximum regressive surface) is observed. The change in the character of TSTs above and below the 2<sup>nd</sup> order MFS appears to reflect fundamental differences

in accommodation space and sediment supply. During the 2<sup>nd</sup> order transgression, the influx of clastic minerals into the basin is progressively decreased, and carbonate platforms transition into more isolated reef complexes (Switzer et al., 1994; Potma et al., 2001). These processes reduce the overall supply of sediment to the basin, resulting in sharper maximum regressive surfaces and thinner 3<sup>rd</sup> order transgressive deposits. In contrast, the 2<sup>nd</sup> order highstand results in increased sediment supply to the basin and is reflected in the 3<sup>rd</sup> order TST as thicker deposits and a lack of a sharp, cemented maximum regressive surface.

The bimodal character of transgressive systems tracts is also observable on wireline logs (Fig. 2.23). The gamma log is a measure of the radiation emitted by U, Th, and K (Dypvik and Eriksen, 1983). For thin, sharp based TSTs deposited during the second order transgression, the gamma log often increases sharply and dramatically and shows an overall increase over the interval. This dramatic increase in gamma radiation is driven by an increase in uranium that is associated with organic matter (Schmoker, 1981; Meyer and Nederlof, 1984; Zelt, 1985; Mann et al., 1986; Wignall and Myers, 1988; Stocks and Lawrence, 1980; Arthur and Sageman, 1994; Lüning and Kolonic, 2003; Dean, 2007), rather than an increase in K- or Th- rich terrigenous minerals. The thin transgressive deposits are generally siliceous and very depleted in clay-minerals due to upslope trapping of clastics, minimizing the effect of K and Th as drivers for increases in gamma radiation.

For thicker TSTs deposited during the second order high stand, in our study the DS3 TST, the overall in gamma ray signal is much smaller, even decreasing over the transgression. The reason behind this is the increased presence of clay minerals. The increased presence of K-rich terrigenous clay minerals at the top of shallowing upwards intervals means that the difference between the gamma signature of clay-rich regressive deposits and siliceous, organic-rich transgressive deposits is minimized. Clay-rich regressive deposits may even have higher gamma radiation than transgressive deposits if the deeper water lithofacies are not significantly enriched in organic-matter (for example: ECA Cecilia 11-04, DS3 MRS; Fig. 2.4)

Phosphatic deposits have also been shown to alter the wireline signature of organic-rich mudstone successions (e.g. Abouelresh and Slatt, 2012; Hemmesch et al., 2014) but phosphate is not abundant in Duvernay Formation sediments.

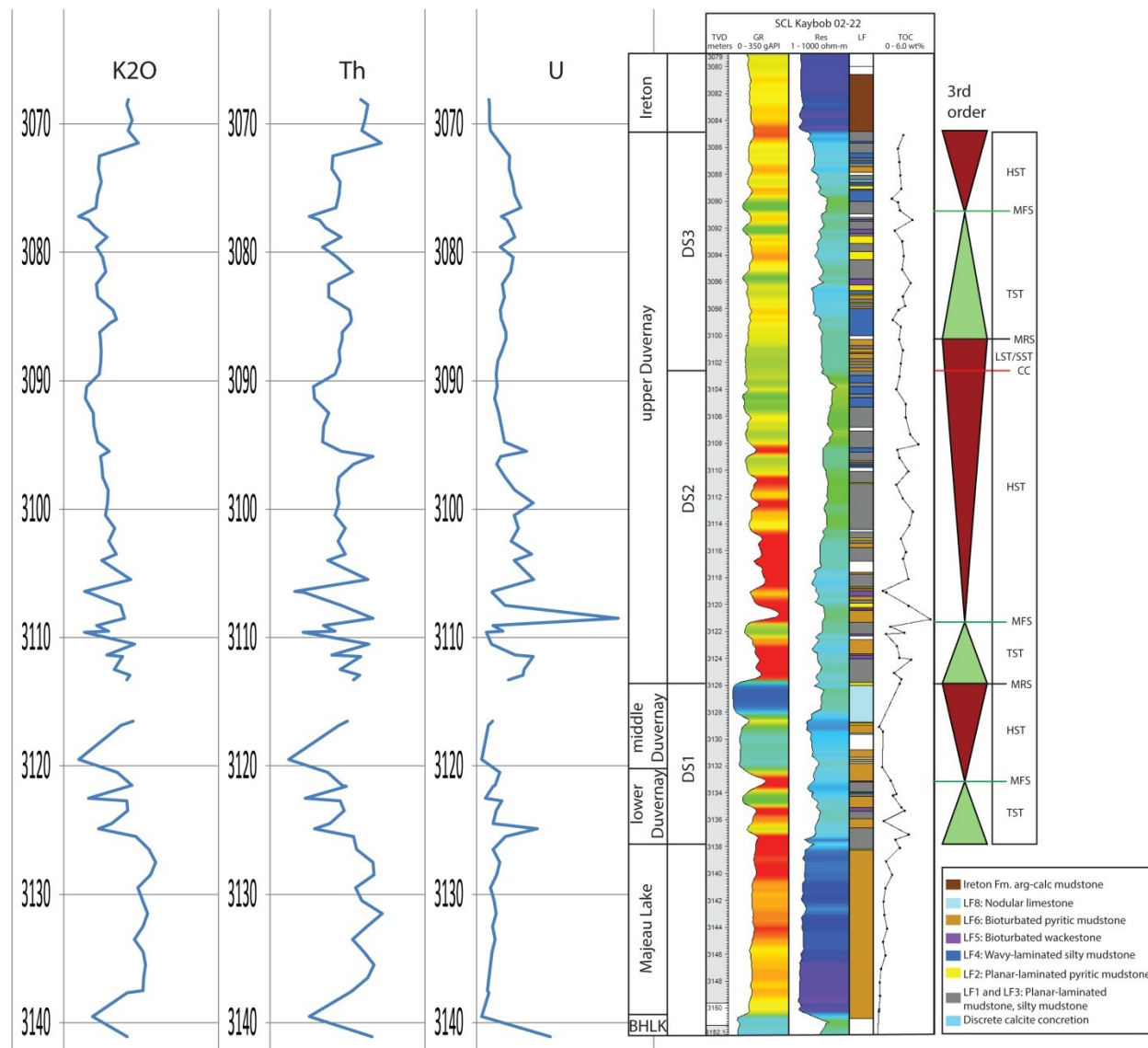


Figure 2.23: SCL Kaybob 02-22 core description with potassium, thorium and uranium abundances. Uranium spikes disproportionately to potassium and thorium during transgression (e.g. DS2 MFS). During regression, potassium and thorium are enriched while uranium is not (e.g. DS3 lowstand/stillstand). In both scenarios, total gamma radiation increases, evidence that gamma radiation does not always co-vary with sea level fluctuations.

Resistivity curves in transgressive deposits commonly increase upwards, which is most evident when clay minerals are present. (e.g. DS3 TST, Fig. 2.23). The difference in the abundance of clay minerals in very clay-poor deep water lithofacies and more clay-rich shallower, regressive facies has a significant impact on the resistivity log. Clay-rich sediments have a much lower resistivity signal, driven by increased pore water (Archie, 1942; Waxman-Smits, 1968; Clavier et al., 1984), decreased organic matter content (due to more oxygenated conditions during regression) (Meyer and Nederlof, 1984; Passey et al., 1990; Creaney and

Passey, 1993; Passey et al., 2010), and potentially increased pyrite (Passey et al., 2010; Kethireddy et al., 2014). During transgression, clay minerals and pyrite typically decrease in abundance in Duvernay Formation mudstones while organic matter content increases which drives the resistivity signal upwards.

### *Maximum flooding surface*

The end of transgression is marked by the maximum flooding surface. This surface represents the period of maximum landward deposition of basinal facies and the onset of highstand normal regression (Catuneanu et al., 2011).

The maximum flooding surface is represented by a condensed section in some black shale formations. In a condensed section, detrital sediment input is low and the interval is dominated by pelagic, biogenic sediment. The sediment may be very organic-rich if inorganic biogenic sedimentation rate is low, but increasing sedimentation rate of inorganic biogenic sediment causes “autodilution” (Tyson, 2005), and can significantly reduce TOC values at the maximum flooding surface. Conversely, low rates of inorganic sedimentation can decrease organic matter preservation due to prolonged exposure to sea water (Tyson, 2005). In drill core, the point of maximum flooding may not be easily distinguishable as a single surface; rather it occurs within a section of black shale lithofacies and is picked at the point where a transgressive succession of lithofacies switches to a regressive succession of lithofacies (Fig. 2.4). Often the MFS closely overlies a flooding surface. When the MFS is identifiable as an observable surface, it is commonly evident because of early diagenetic processes. Slow sedimentation rates allow for early diagenetic cements to precipitate in minimally compacted sediments. This results in hardground surfaces and horizons containing large, discrete concretions (Fischer and Garrison, 1967; Kennedy and Garrison, 1975; Scholle, 1977; Mullins et al., 1980; Stoakes, 1980).

The wireline character of a maximum flooding surface is variable. In the Duvernay Formation, maximum flooding surfaces are marked by gamma and TOC spikes, although are not as pronounced in DS3 where terrestrial input is higher (Fig. 2.23). Significant gamma radiation spikes are most common where terrestrial input is low (most notably at the 2<sup>nd</sup> order MFS in DS2). In these settings, the main driver of the gamma log is uranium associated with organic matter (e.g. Lüning and Kolonic, 2003). Organic-rich, high gamma mudstones above flooding

surfaces contrast strikingly with low-gamma calcareous sediments below the surface. Within intervals of higher terrestrial input, above the second order maximum flooding surface, the gamma contrast above and below the third order maximum flooding surfaces is dampened because regressive sediments below a flooding surface may have moderately high gamma signatures due to the abundance of K-rich clay minerals.

### *Highstand Systems Tract*

The highstand systems tract represents a period of normal regression after the transgressive systems tract and before forced regression of the falling stage systems tract (Catuneanu et al., 2011).

During highstands in carbonate systems, reefs catch up to sea level and carbonate production is high, resulting in an increased supply of detrital carbonate sediment to adjacent basins (“highstand shedding”; Schlager et al., 1994). Highstand shedding is reflected in basinal mudstones as an increasing siltiness and grain size or as discrete turbidites (Droxler and Schlager, 1985; Glaser and Droxler, 1993; Hemmesch et al., 2014). In clastic-dominated systems, highstands are times of aggradation and progradation of clastic clinoforms (Catuneanu et al., 2011). Basinal mudstones become more clastic-enriched through the highstand.

In mixed clastic-carbonate systems like the Duvernay Formation, the character of highstand intervals varies by geographic location and stratigraphic interval. The DS2 highstand, for example is more a carbonate dominated system in the West Shale Basin (SCL Kaybob 02-22 for example; Fig. 2.10), as deposition of northeast-derived clastics backstepped during the preceding DS2 transgression. Organic-rich, siliceous mudstones become increasingly enriched in carbonate silt and sand upwards through the highstand. LF1-3 are dominant at the base of the highstand and LF3 and LF4 become dominant upwards. During the DS3 highstand, over much of the basin, clastics are more prominent as clastic sources prograded into the basin. In the west and northeast, closer to clastic sources, the highstand interval becomes more clay-rich upwards (ECA Cecilia 11-04 for example; Fig. 2.4). Further from clastic sources, at the SCL Kaybob 02-22 well for example, the highstand interval is a mixture of clastic-enriched lithofacies (LF6) and carbonate-enriched lithofacies (LF4). In areas surrounded by reef complexes (e.g. southern East

Shale Basin; EOG Cygnet 08-20; Fig. 2.11), DS3 highstand is still carbonate-dominated due to a large distance from clastic sources and highstand shedding of nearby reef complexes.

Wireline signatures of the highstand vary significantly, depending on whether sedimentation is dominated by clastics or carbonates. Where clastics are more prominent than carbonates, the resistivity log tends to slowly decrease throughout the highstand as sediments become more clay-rich (Fig. 2.4). Where carbonates are more prominent, resistivity values increase as sediment becomes more and more enriched in carbonate detritus and commonly in calcite cement (Fig. 2.10).

### *Basal Surface of Forced Regression*

The basal surface of forced regression marks the onset of sea level fall (Catuneanu et al., 2011). In the Duvernay Formation, no forced regressive deposits were observed so the highstand systems tracts are overlain by a correlative conformity where lowstand deposits exist (top DS2), and a maximum regressive surface where no lowstand deposits are present (top DS1).

### *Correlative Conformity*

The correlative conformity (*sensu* Posamentier and Allen (1999)) occurs at the base of the lowstand systems tract and marks the onset of sea level rise. The correlative conformity marks the maximum extent of sea level fall, however, during the subsequent lowstand, progradation rather than retrogradation occurs because sedimentation rate is greater than the rate of accommodation space creation (Catuneanu et al., 2011). The presence of a correlative conformity implies that a time-equivalent upslope subaerial unconformity exists as a result of sea level fall.

In organic-rich mudstones the correlative conformity may be over- and underlain by black shale lithofacies. Evidence for sea level fall may require highly detailed observation (Macquaker and Taylor, 1996; Williams et al., 2001; Schieber and Riciputi, 2004; Ver Straeten et al., 2011). Scheiber and Riciputi (2004) identified pyritized ooids within a succession of Devonian black shales, and interpreted their presence as the product of sea level fall and subsequent transgression. Shallowing to the point of ooid formation is not observed in areas of the Duvernay Formation where organic-rich mudstones are dominant. In the Duvernay

Formation, a correlative conformity is recognized at a point where LF6 bioturbated pyritic mudstones suddenly overlie laminated, organic-rich, siliceous mudstones of LF1-3 over much of the Basin. This shift in facies reflects a sudden increase in clastic sedimentation, and at least a minor increase in bottom water oxygenation. The correlative conformity, especially near basin margins and reef complexes, is often marked by an erosive turbidite or debris flow bed containing coarse-grained carbonate clasts (Fig. 2.7B). In more distal parts of the basin, equivalent turbidite beds are thinner and finer-grained or non-existent (Fig. 2.7A). The rapid progradation of shallower water lithofacies and emplacement of erosive turbidite beds is the result of reduced accommodation space and reef slope instability during sea level fall or stillstand.

The wireline signature of a correlative conformity reflects the juxtaposition of lithofacies that results from a decrease in accommodation space. Where calcareous turbidite beds overlie the surface, a sharp drop in gamma radiation occurs. Because transport of clastics into the basin is efficient during lowstand (Catuneanu et al., 2011), clay-mineral-rich mudstones commonly directly overlie the erosive calciturbidite beds, resulting in decreased resistivity. Because clays may also contain K, a correlative unconformity is commonly expressed by a sharp drop in gamma (calciturbidites), followed by an increase in gamma (clay-rich section). Where calciturbidite beds are not present, the gamma log may show very little change at the correlative conformity, but the resistivity log still decreases as a result of clay-mineral-rich mudstones overlying clay-mineral-poor, siliceous mudstones (Fig. 2.23).

#### *Lowstand Systems Tract*

The lowstand systems tract immediately overlies the correlative conformity, and represents a return to normal regression subsequent to forced regression (Catuneanu et al., 2011).

Recognition of the lowstand system tract in core depends upon the recognition of the correlative conformity (as outlined above). During lowstand normal regression, an overall shallowing trend is observed in core. Clastic sediments are efficiently transported into the basin during this time; as a result, mudstones tend to become increasingly rich in terrigenous material, although the shallowing trend may not be recognized as a grain size increase if the clastic source is very fine grained, as in the Duvernay Formation.

The wireline response of the lowstand systems tract varies considerably, based on lithology and organic-richness. Resistivity logs may display a considerable decrease if lowstand clay-rich mudstones overlie siliceous-calcareous highstand mudstones, but this signal may be dampened in formations where organic enrichment primarily occurs during lowstand. In some black shale formations, sea level lowstands are periods of minimal connection to open ocean and restricted circulation, which can be beneficial for the preservation of organic matter (Röhl et al. 2001). The presence of organic matter and hydrocarbons in a rock increase the resistivity of that rock (Meyer and Nederlof, 1984; Passey et al., 1990; Creaney and Passey, 1993; Passey et al., 2010). This resistivity increase may negate or minimize the decrease in resistivity driven by an increase in clay minerals deposited in the basin during lowstand.

The gamma log responds similarly to the concentrations of organic matter and clay minerals in most mudstones. The gamma response of the lowstand systems tract may not significantly contrast with that of the underlying highstand systems tract, where medium to high gamma K-rich lowstand mudstones overlie medium to high gamma U-rich mudstones (Fig. 2.23). In the Duvernay Formation the gamma log slowly increases upwards though the lowstand as the sediments become more clay-rich (Fig. 2.23). This trend may not be observed in formations with a coarser grained clastic source, as quartz sand will decrease the gamma response. In those black shale formations that are preferentially organic-enriched in the lowstand systems tract, the gamma response is likely to be highest during the lowstand, as the sediment is rich in U (associated with organic matter) and K (in terrigenous clay minerals). The gamma response may also be altered by the presence of redeposited phosphatic material (Abouelresh and Slatt, 2012).

## **2.6 Conclusion:**

Sequence stratigraphy has an increasingly important role in the characterization of fine-grained, organic-rich strata. In the Duvernay Formation, a sequence stratigraphic model defines mappable units and explains facies variability. Through a sequence stratigraphic analysis of the Duvernay Formation, we have identified criteria for identifying sequence stratigraphic tracts and

surfaces in organic-rich mudstones, and examined the processes that are responsible for diagnostic characteristics.

The Duvernay Formation was deposited during three 3<sup>rd</sup> order depositional sequences. The lower Duvernay member and middle Duvernay member comprise DS1. Duvernay Formation strata of DS1 are equivalent to Grosmont Platform stages G1 and G2. During DS1, highstand normal regression resulted in the aggradation of thick platform margin and slope deposits in the northeast part of the basin, which thinned to the south and west into the basin. A major transgression marks the beginning of DS2. The creation of accommodation space during transgression, combined with slope-parallel currents significantly reduced the amount of sediment supplied to the basin from the northeast, and as a result, basinal sediments are very clay-poor. Lowstand or stillstand at the base of DS3 resulted in progradation of clastic material into the basin, with LF6 bioturbated pyritic mudstones deposited throughout much of the basin over previously deposited siliceous, organic-rich mudstones of LF1-3. Coarse carbonate detritus was locally enhanced near reef complexes.

Basin morphology plays a considerable role in lithofacies distribution and stratal stacking. During platform construction, strata thin away from the platform margin and become increasingly organic-rich with decreasing detrital sediment contribution. When the platform is flooded, backstepping of platform-building sediments results in areas of non-deposition on the outer platform and slope. This upslope trapping results in enhanced sediment starvation in the basin and deposition of siliceous, organic-rich deposits. Basin morphology at least partially governs circulation patterns, as currents are directed parallel to slope. Circulation patterns strongly influence sediment distribution.

Transgressive systems tracts have a strong potential for the deposition of organic-rich, siliceous mudstones as the influx of both clastic and carbonate sediment is minimized. Organic enrichment in transgressive deposits is significant when bottom waters are anoxic and the sedimentation rate of inorganic biogenic sediment is low. The character of transgressive deposits and flooding surfaces are influenced by lower order sequences. Third order transgressive deposits that occur within a 2<sup>nd</sup> order transgression are often thin and have sharp, cemented flooding surfaces as a result of sediment starvation. Third order transgressive deposits that occur

within a 2<sup>nd</sup> order highstand, are thicker, and less commonly have sharp, cemented flooding surfaces because overall sedimentation rates are higher than during 2<sup>nd</sup> order transgression.

During highstands, calcareous detrital flux to the basin is enhanced due to highstand shedding from reef complexes. Turbidity currents and contour currents have the ability to transport silt- and sand-sized material into and throughout the basin, even in areas where anoxic bottom waters are persistent and organic-rich mudstone deposition is the norm. Deposition of organic-rich mudstones within a highstand systems tract is greatest where clastic influx is weak.

Lowstands are recognized in black shale successions by an increased flux of terrigenous clastics to the basin. Significant sea level fall is not necessary to significantly change the composition of basinal mudstones. A minor sea level fall or pause in sea level rise (stillstand) causes rapid progradation of clastics into the basin.

Sequence stratigraphic surfaces and systems tracts have distinctive wireline log responses, although the interpretation is complicated by geographic location (proximity to sediment sources) and stratigraphic location within larger scale (lower order) depositional sequences.

## CHAPTER 3: CONCLUSIONS

This study sheds light on the processes and conditions responsible for organic-rich mudstone deposition, and key criteria for interpreting similar deposits. Chapter 1 demonstrates the variability in mudstone lithofacies and describes the depositional processes and conditions responsible for this variation. Chapter 2 presents a sequence stratigraphic analysis of the Duvernay Formation that demonstrates the relationship between sea level, basin morphology, and lithofacies distribution and character, and describes the expression of sequence stratigraphic tract and surfaces in organic-rich mudstone successions.

### **3.1 Sediment Transport Mechanisms and Organic Enrichment**

Duvernay Formation mudstones were deposited in an epicontinental seaway on the western margin of North America, coeval with basin-fringing Leduc reef complexes and Grosmont Platform carbonates in the northeast part of the basin. A combination of suspension settling, sediment-gravity flows, and bottom water currents distributed sediment throughout the mudstone-dominated areas of the basin. Sediment-gravity flows transported carbonate detritus, which is most abundant during highstand shedding of reefs. Contour currents transported clay-through sand-sized material and redistributed sediments deposited by turbidites. The position of these contour currents was in part governed by basin morphology. Contourite deposits are interbedded with organic-rich mudstones indicating variable bottom water energy in areas of organic-rich mudstone deposition. Organic matter and clay minerals were deposited as aggregates that formed higher in the water column and settled from suspension.

Lithofacies were deposited in a range of bottom water oxygen concentrations from anoxic to oxic and total organic carbon varied systematically within a lithofacies framework. The highest TOC values are observed in planar-laminated, siliceous mudstones, deposited in generally anoxic bottom waters, where dilution of organic matter by clastic or carbonate sediment was minimal. Significant organic-rich deposits also occur in facies in which contourites are interbedded with siliceous, organic-rich mudstone. Periodic fluctuations in current energy

and bottom water oxygenation minimally to moderately reduced TOC values. Mudstone lithofacies deposited under dysoxic conditions are moderately to intensely bioturbated and generally contain significantly reduced levels of organic carbon. Bioturbated pyritic mudstones are an exception, as they contain greater abundances of organic carbon than other similarly bioturbated lithofacies. In this case, sediment composition and sedimentation rate may have enhanced organic matter deposition and preservation. Clay minerals may aid in the formation of organo-mineralic aggregates which decreased the time organic matter was exposed to oxygenated water. Where bottom water anoxia was not present, a moderately increased sedimentation rate may have preserved organic matter where it was not enough to dilute organic matter significantly. Mudstone lithofacies deposited under oxic conditions are intensely bioturbated and organic lean.

### **3.2 Lithofacies Variation in a Sequence Stratigraphic Context**

The Duvernay Formation was deposited during three 3<sup>rd</sup> order depositional sequences, during late transgression and early highstand of a 2<sup>nd</sup> order depositional sequence. The first of the 3<sup>rd</sup> order sequences (DS1) is equivalent to a phase of major aggradation of the Grosmont Platform. During early DS1, siliceous, organic-rich mudstones are extensively deposited in the basin, but become increasingly calcareous and organic-lean, as nodular limestones are dominant across much of the basin by the end of DS1. The creation of accommodation space during DS2 transgression significantly reduced the amount of sediment supplied to the basin from the northeast, and as a result, basinal sediments are very clay-poor. Lowstand or stillstand at the base of DS3 resulted in progradation of clastic material into the basin, with more argillaceous mudstones deposited throughout much of the basin over previously deposited siliceous, organic-rich mudstones. The recognition of cyclicity and identification of systems tracts in mudstone successions generates a predictive capability for lithofacies distribution and character.

The deposition of organic-rich, siliceous mudstone was common in transgressive systems tracts, as the influx of both clastic and carbonate sediment was minimized and bottom waters were often anoxic. Third order transgressive deposits that occurred within a 2<sup>nd</sup> order transgression are often thin, and have sharp, cemented flooding surfaces as a result of sediment

starvation. Third order transgressive deposits that occur within a 2<sup>nd</sup> order highstand are thicker and less commonly have sharp, cemented flooding surfaces because overall sedimentation rates were higher than during the 2<sup>nd</sup> order transgression. In parts of the basin where platform development was greatest, transgression resulted in the creation of non-deposition zones, as clastics were trapped upslope, and did not prograde all the way across the previously formed platform and slope. The geographic extent of basinal mudstone deposition is greatest at the end of the transgressive systems tract (maximum flooding surface).

During highstands, calcareous detrital flux to the basin was enhanced due to highstand shedding from reef complexes. Deposition of organic-rich mudstones within a highstand systems tract was greatest where clastic influx was weak. Highstands were also periods of time when platform aggradation was maximized. Platform carbonates cap thick packages of argillaceous sediment that were deposited near basin margins during highstand regressions.

Lowstands are recognized by an increased flux of terrigenous clastics to the basin. Significant sea level fall was not necessary to significantly change the composition of basinal mudstones, as even minor sea level falls or pauses in sea level rise (stillstand) caused rapid progradation of clastics into the basin. Potassium-rich clay minerals can cause an increase in the gamma response, especially when the terrigenous source was especially fine-grained, as in the Duvernay Formation. The potential for increasing gamma radiation during regression needs to be recognized in order to properly identify sea level fluctuations and to differentiate high-gamma, clay-rich regressive deposits from high-gamma U-rich, high-TOC transgressive deposits. A significant drop in resistivity coincides with clay-rich lowstand deposits in formations where low stands were not intervals of preferential organic-enrichment.

#### ACKNOWLEDGEMENTS:

This research could not have been completed without the funding we have received from Imperial Oil, Shell Canada, ConocoPhillips, Nexen, Devon Energy, Husky Energy, and the Natural Sciences and Engineering Research Council of Canada.

Throughout the project, technical discussions with a number of individuals helped me form and evaluate my interpretations, teach me how to think critically, and teach me how to communicate my ideas. These people are Korhan Ayranci, Julia McMillan, Tian Dong, Noga Vaisblat, Chris Schnieder, Murray Gingras, Matthew Fay, Hugh Alley, John Weissenberger, and of course my supervisor, Dr. Nick Harris . Thank you to the staff at Shell Canada. During my summer term on the exploration team, you helped me understand the oil and gas industry's interests in shale research and its impact on the business.

## REFERENCES:

Abouelresh, M. O., Slatt, R. M., 2012. Lithofacies and sequence stratigraphy of the Barnett Shale in east-central Fort Worth Basin, Texas. *AAPG Bulletin* 96(1), 1–22.

Aller, R.C., 1978. The effects of animal-sediment interactions on geochemical processes near the sediment water interface. In: Wiley, M.L. (Ed.), *Estuarine interactions*. Academic Press, New York, pp. 157-172.

Allredge, A.L., 1976. Discarded appendicularian houses as sources of food, surface habitats, and particulate organic matter in planktonic environments. *Limnology and Oceanography* 21, 14–23.

Allredge, A. L., and M. W. Silver, 1988. Characteristics, dynamics and significance of marine snow. *Progress in Oceanography* 20, 41–82.

Algeo, T.J., Lyons, T.W., Blakey, R.C., and Over D.J., 2007. Hydrographic conditions of the Devonian-Carboniferous North American Seaway inferred from sedimentary Mo-TOC relationships: *Palaeogeography, Palaeoclimatology, Palaeoecology*, v.256, p.204-230

Andrichuk, J.M. 1958. Cooking Lake and Duvernay (Late Devonian) sedimentation in Edmonton area of central Alberta, Canada. *AAPG Bulletin* 42, 2189-2222.

Andrichuk, J.M. 1961. Stratigraphic evidence for tectonic and current control of Upper Devonian reef sedimentation Duhamel area, Alberta, Canada. AAPG Bulletin 45, 612-632.

Andrichuk, J.M. and Wonfor, J.S. 1954. Late Devonian geologic history in Stettler area, Alberta, Canada. AAPG Bulletin, 38, 2500-2536.

Aplin, A.C. and Macquaker J.H.S., 2011. Mudstone diversity: Origin and implications for source, seal, and reservoir properties in petroleum systems. AAPG Bulletin 95(12), 2031-2059.

Aoudia, K., Miskimmins, J.L., Harris, N.B., and Mních, C.A., 2010. Statistical Analysis of the Effects of Mineralogy on Rock Mechanical Properties of the Woodford Shale and the Associated Impacts for Hydraulic Fracture Treatment Design. 44th US Rock Mechanics Symposium. American Rock Mechanics Association, Alexandria, Virginia, USA.

Archie, G.E., 1942, The Electrical Resistivity Log as an Aid in Determining Some Reservoir Characteristics, Paper SPE-942054-G, *Petroleum Transactions, AIME*, 146, 54–62.

Arthur, M.A., and Sageman, B.B., 1994. Marine black shales: Depositional mechanisms and environments of ancient deposits: Annual Reviews in Earth and Planetary Sciences, v.22, p.499-551

Barron, J.A. 1993. Diatoms. In: J. Lipps (Ed.), Fossil Prokaryotes and Protists. Blackwell Scientific Publications, p. 155-168.

Berner, R.A., 1970. Sedimentary pyrite formation. Am. J. Sci. 268, 1–23.

Bernhard, J.M., Reimers, C.E., 1991. Benthic foraminiferal population fluctuations related to anoxia: Santa Barbara Basin. Biogeochemistry 15, 127–149.

Bernhard, J.M., Visscher, P.T., Bowser, S.S., 2003. Sub-millimeter life positions of bacteria, protists, and metazoans in laminated sediments of the Santa Barbara Basin. *Limnology and Oceanography* 48, 813–828.

Billett, D.S.M., Lampitt, R.S., Rice, A.L., and Mantoura, R.F.C., 1983. Seasonal sedimentation of phytoplankton to the deep-sea benthos. *Nature* 302(5908), 520-522.

Bohacs, K.M., 1998. Contrasting expressions of depositional sequences in mudrocks from marine to nonmarine environs. In: Schieber, J., Zimmerle, W., and Sethi, P.S. (Eds.), *Shales and Mudstones I*. Stuttgart, E. Schweizerbart'sche Verlagsbuchhandlung, pp. 33-78

Bohacs, K.M., G. J. Grabowski, A. R. Carroll, P. J. Mankiewicz, K. J. Miskell-Gerhardt, and J. R. Schwalbach, 2005. Production, destruction, and dilution: The many paths to source rock development. In N. B. Harris (Ed.), *The deposition of organic carbon-rich sediments: Models, mechanisms, and consequences*. Society for Sedimentary Geology Special Publication 82, pp. 61–101.

Bouma, A. H. (1962). In: *Sedimentology of some flych deposits: a graphic approach to facies interpretation* (pp. 168). Amsterdam: Elsevier.

Braithwaite, C.J.R., 2014. Reef talus: A popular misconception. *Earth Science Reviews* 128, 169-180.

Bromley, R.G., Ekdale, A.A., 1984. Chondrites: a trace fossil indicator of anoxia in sediments. *Science* 224, 872–874.

Byers, C.W., 1977. Biofacies patterns in euxinic basins: a general model. *SEPM Special Publication* 25, 5-17.

Catuneanu, O., Abreu, V., Bhattacharya, J.P., Blum, M. D., Dalrymple, R.W., Eriksson, P. G., Fielding, C. R., Fisher, W. L., Galloway, W. E., Gibling, M. R., Giles, K. A., Holbrook, J. M., Jordan, R., Kendall, C. G. St. C., Macurda, B., Martinsen, O. J., Miall, A. D., Neal, J. E., Nummedal, D., Pomar, L., Posamentier, H.W., Pratt, B. R., Sarg, J.F., Shanley, K.W., Steel, R.

J., Strasser, A., Tucker, M. E., Winker, C., 2009. Towards the standardization of sequence stratigraphy. *Earth-Science Reviews*, vol. 92, 1–33.

Catuneanu, O., Galloway, W.E., Kendall, C.G.St.C, Miall, A.D., Posamentier, H.W., Strasser, A., and Tucker, M.E. 2011. Sequence stratigraphy: methodology and nomenclature. *Newspapers on stratigraphy*, v.44/3, p.173-245.

Chow, N., Wendte, J., and Stasiuk, D., 1995. Productivity versus preservation controls on two organic-rich carbonate facies in the Devonian of Alberta: sedimentological and organic petrological evidence: *Bulletin of Canadian Petroleum Geology* 43, pp.433-460.

Clavier, C., Coates, G., and Dumanoir, J., 1984, Theoretical and Experimental Bases for the Dual-Water Model for Interpretation of Shaly Sands, Paper SPE-6859, *SPE Journal*, 24(2), 153–168.

Creaney, S., and Passey, Q. R., 1993. Recurring patterns of total organic carbon and source rock quality within a sequence stratigraphic framework: *AAPG Bulletin*, v.77, no. 3, p. 386-401.

Cutler, D.W.G. 1983. Stratigraphy and sedimentology of the Upper Devonian Grosmont Formation, northern Alberta. *Bulletin of Canadian Petroleum Geology* 31, 282-325.

Cuomo, M.C., and Bartholomew, P.R., 1991. Pelletal black shale fabrics: their origin and significance. In: Tyson, R.V., and Pearson, T.H. (Eds.), *Modern and Ancient Continental Shelf Anoxia*. Geological Society of London, Special Publication 58, pp.221–232.

Dalrymple, R.W., Narbonne, G.M., 1996. Continental slope sedimentation in the Sheepbed Formation (Neoproterozoic, Windermere Supergroup), Mackenzie Mountains, N.W.T. *Can. J. Earth Sci.* 33, 848 -862.

Dean, W.E., 2007. Sediment geochemical records of productivity and oxygen depletion along the margin of western North America during the past 60,000 yr. Teleconnections with Greenland Ice and Cariaco Basin: *Quaternary Science Reviews*, v.26, p.98-114

Demaison, G.I., Moore, G.T., 1980. Anoxic environments and oil source bed genesis. AAPG Bulletin 64, 1179-1209.

Dix, G.R. 1990. Stages of platform development in the Upper Devonian (Frasnian) Leduc Formation, Peace River Arch, Alberta. In: S.C. O'Connell and J.S. Bell (Eds.), Geology of the Peace River Arch. Bulletin of Canadian Petroleum Geology 38A, pp. 66-92.

Dong, T., Harris, N.B., Ayranci, K., Twemlow, C.E., and Nassichuk, B.R., 2015. Porosity characteristics of the Devonian Horn River shale, Canada: Insights from lithofacies classification and shale composition.

Droxler, A. W., and W. Schlager, 1985. Glacial versus interglacial sedimentation rates and turbidite frequency in the Bahamas: Geology 13, pp. 799–802.

Dypvik, H. and Eriksen, D. Ø., 1983. Natural radioactivity of clastic sediments and the contributions of U, Th and K. *Journ. Petrol. Geol.*, 5, 409-416.

Egenhoff, S.O. and Fishman, N.S. 2013. Traces in the dark – sedimentary processes and facies gradients in the upper shale member of the Upper Devonian-Lower Mississippian Bakken Formation, Williston Basin, North Dakota, U.S.A. *Journal of Sedimentary Research* 83, 803–824.

Ekdale, A.A., Mason, T.R., 1988. Characteristic trace-fossil associations in oxygen-poor sedimentary environments. *Geology (Boulder)* 16, 720–723.

Fischer, A. G. and Garrison, R. E., 1967. Carbonate lithification on the sea floor: *Journal of Geology*, v. 75, p. 488-496.

Fortier, M., Fortier, L., Michel, C., and Legendre, L., 2002. Climatic and biological forcing of the vertical flux of biogenic particles under seasonal arctic sea ice. *Marine Ecology, Progress Series* 225, 1–16.

Fowler, M.G., Stasiuk, L.D., Hearn, M., and Obermajer, M., 2001. Devonian hydrocarbon source rocks and their derived oils in the Western Canada Sedimentary Basin. *Bulletin of Canadian Petroleum Geology* 49, 117-148.

Gao, Z., Luo, S., He, Y., Zhang, J., Tang, Z., 1995. The Middle Ordovician contourite on the west margin of Ordos. *Acta Sedimentol. Sin.* 13(4), 16–26. (in Chinese with English abstract).

Galloway, W. E., 1989. Genetic stratigraphic sequences in basin analysis, I. Architecture and genesis of flooding surface bounded depositional units. *American Association of Petroleum Geologists Bulletin* 73, 125–142.

Ghadeer, S.G., and Macquaker, J.H.S., 2011. Sediment transport processes in an ancient mud-dominated succession: a comparison of processes operating in marine offshore settings and anoxic basinal environments. *Journal of the Geological Society London* 168, 835-846.

Ghadeer, S.G., and Macquaker, J.H.S., 2012. The role of event beds in the preservation of organic carbon in fine-grained sediments: Analyses of the sedimentological processes operating during deposition of the Whitby Mudstone Formation (Toarcian, Lower Jurassic) preserved in northeast England. *Marine and Petroleum Geology* 35, 309-320.

Glaser, K. S., and A. W. Droxler, 1993. Controls and development of late Quaternary periplatform carbonate stratigraphy in Walton Basin (northeastern Nicaragua Rise, Caribbean Sea). *Paleoceanography* 8, pp. 243–274.

Gonthier, E., Faugères, J.-C., Stow, D.A.V., 1984. Contourite facies of the Faro Drift, Gulf of Cadiz. In: Stow, D.A.V., Piper, D.J.W. (Eds.), *Fine-Grained Sediments, Deep-Water Processes and Facies*. *Geol. Soc. London Spec. Publ.* 15, pp. 275–292.

Grabowski, R.C., Droppo, I.G., and Wharton G, 2011. Erodibility of cohesive sediment: the importance of sediment properties. *Earth-Science Reviews* 105, 101–120.

Grimm, K.A., Lange, C.B., and Gill, A.S., 1997. Self-sedimentation of phytoplankton blooms in the geologic record. *Sedimentary Geology* 110, 151–161.

Haq, B.U., and Schutter, S.R., 2008. A chronology of Paleozoic sea level changes. *Science* 322, 64-68.

He, Y., Duan, T., Gao, Z., 2008. Sediment entrainment. In: Rebesco, M., Camerlenghi, A. (Eds.), *Contourites. Developments in Sedimentology* 60, Elsevier, Amsterdam, pp. 99–120.

Hemmesch, N.T., Harris, N.B., Mnich, C.A., and Selby, D., 2014. A sequence-stratigraphic framework for the Upper Devonian Woodford Shale, Permian Basin, west Texas. *AAPG Bulletin* 98, 23-47.

Hernández-Molina, F.J., Stow, D.A.V., Alvarez-Zarikian, C., Expedition IODP 339 Scientists, 2013. IODP Expedition 339 in the Gulf of Cadiz and off West Iberia: decoding the environmental significance of the Mediterranean Outflow Water and its global influence. *Scientific Drilling* 16, 1–11.

Hunt, D., Tucker, M. E., 1992. Stranded parasequences and the forced regressive wedge systems tract: deposition during base-level fall. *Sedimentary Geology* 81, 1–9.

Ito, M., 1996. Sandy contourites of the Lower Kazusa Group in the Boso Peninsula, Japan: Kuroshio current influenced deep-sea sedimentation in a Plio-Pleistocene forearc basin. *J. Sediment. Res.* 66, 587–598.

Johnson, J.G., Klapper, G., Sandberg, C.A., 1985. Devonian eustatic fluctuations in Euramerica. *Geol. Soc. Amer. Bull.* 96, 567–587.

Jones, R.W., 1996. Siliceous microfossils. In: Jones, R.W. (Ed.), *Micropaleontology in Petroleum Exploration*. Clarendon Press, Oxford, pp. 92-106.

Kennedy, W. J. and Garrison, R. E., 1975. Morphology and genesis of nodular chinks and hardgrounds in the Upper Cretaceous of southern England. *Sedimentology* 22, 311-386.

Kennedy, M.J., Pevear, D.R., and Hill, R.J., 2002. Mineral surface control of organic carbon in black shale. *Science* 295, 657–660.

Kethireddy, N., Chen, H., and Heidari, Z., 2014. Quantifying the effect of kerogen on resistivity measurements in organic-rich mudrocks: *Petrophysics*, v.55, p.136-146

Klovan, J.E. 1964. Facies analysis of the Redwater Reef Complex; Alberta, Canada: *Bulletin of Canadian Petroleum Geology*, v. 12, p. 1-100.

Knapp, L.J., 2016. Controls on organic-rich mudstone deposition: The Devonian Duvernay Formation, Alberta, Canada. M.Sc. thesis, University of Alberta, Edmonton, Canada.

Könitzer, S.F., Davies, S.J., Stephenson, M.H., and Leng, M.J., 2014. Depositional controls on mudstone lithofacies in a basinal setting: implications for the delivery of sedimentary organic matter. *Journal of Sedimentary Research* 84, 198-214.

Kump, L.R., and Slingerland, R.L, 1999. Circulation and stratification of the early Turonian Western Interior Seaway: Sensitivity to a variety of forcings. *Geological Society of America Special Paper* 332, 181-190.

Lampitt, R. S., 1985. Evidence for the seasonal deposition of detritus to the deep-sea floor and its subsequent resuspension. *Deep-Sea Research* 32, 885–897.

Loucks, R. G., and S. C. Ruppel, 2007. Mississippian Barnett Shale: Lithofacies and depositional setting of a deepwater shale-gas succession in the Fort Worth Basin, Texas. *AAPG Bulletin* 91, 579–601.

Lüning, S, Craig, J., Loydell, D.K., Štorch, P., and Fitches, B., 2000. Lower Silurian ‘hot shales’ in North Africa and Arabia: regional distribution and depositional model: *Earth-Science Reviews*, v.49, p121-200

Lüning, S., and Kolonic, S., 2003. Uranium spectral gamma-ray response as a proxy for organic richness in black shales: applicability and limitations. *Journal of Petroleum Geology*, v.26 (2), p.153-174

Macquaker, J. H. S., and K. G. Taylor, 1996. A sequence stratigraphic interpretation of a mudstone-dominated succession: The Lower Jurassic Cleveland Ironstone Formation, United Kingdom: *Journal of the Geological Society*, v. 153, p. 759–770.

Macquaker, J. H. S., S. J. Bentley, and K. M. Bohacs, 2010a. Wave-enhanced sediment-gravity flows and mud dispersal across continental shelves: Reappraising sediment transport processes operating in ancient mudstone successions. *Geology* 38, 947–950.

Macquaker, J. H. S., and K. M. Bohacs, 2007. On the accumulation of mud. *Science* 318, 1734–1735.

Macquaker, J. H. S., and M. A. Keller, 2005. Mudstone sedimentation at high latitudes: Ice as a transport medium for mud and supplier of nutrients. *Journal of Sedimentary Research* 75, 696–709.

Macquaker, J. H. S., M. A. Keller, and S. J. Davies, 2010b. Algal blooms and “marine snow”: Mechanisms that enhance preservation of organic carbon in ancient fine-grained sediments. *Journal of Sedimentary Research* 80, 934–942.

Macquaker, J.H.S., and Gawthorpe, R.L., 1993. Mudstone lithofacies in the Kimmeridge Clay Formation, Wessex Basin: implications for the origin and controls on the distribution of mudstones. *Journal of Sedimentary Petrology* 63, 1129–1143.

Macquaker, J.H.S., and Howell, J.K., 1999. Small-scale (< 5.0 m) vertical heterogeneity in mudstones: implications for high-resolution stratigraphy in siliciclastic mudstone successions. *Geological Society of London Journal* 156, 105–112.

Macquaker, J. H. S., Taylor, K. G., and Gawthorpe, R. L., 2007. High-resolution facies analyses of mudstones: Implications for paleoenvironmental and sequence-stratigraphic interpretations of offshore ancient mud-dominated successions. *Journal of Sedimentary Research* 77, 324–339.

Mallamo, M.P., 1995. Paleooceanography of the Upper Devonian Fairholme Carbonate Complex, Kananaskis – Banff area, Alberta. Ph.D. Thesis, McGill University, Montreal, Canada

Mann, U., Leythaeuser, D. and Muller, P.J., 1986. Relation between source rock properties and wireline log parameters. An example from Lower Jurassic Posidonia Shale, NW-Germany. In: *Advances in Organic Geochemistry 1985*, Leythaeuser D. and Rullkötter J. (Eds.), Oxford (Pergamon Press), pp. 1105-1112.

Martin-Chivelet, J., Fregenal-Martinez, M.A., Chacòn, B., 2008. Traction structures in contourites. In: Rebesco, M., Camerlenghi, A. (Eds.), *Contourites. Developments in Sedimentology* 60, Elsevier, Amsterdam, pp. 159–182.

McCave, I. N., 1984. Erosion, transport and deposition of fine-grained marine sediments, in D. A. V. Stow and D. J. W. Piper, eds., *Fine-grained sediments: Deepwater processes and facies*. Geological Society (London) Special Publication 15, 35–69.

McCrossan, R.G., 1961. Resistivity mapping and petrophysical study of upper Devonian inter-reef calcareous shales of central Alberta, Canada: *AAPG Bulletin* 45, 441-470.

McLean, D.J., and Mountjoy, E.W., 1993. Upper Devonian buildup-margin and slope development in the southern Canadian Rocky Mountains. *Geological Society of America Bulletin* 105, 1263-1283.

McMillan, J.M., 2016. Expression of major and trace element signatures of the Frasnian Duvernay Formation within a sea level context: insights into the processes that control mudstone composition, paleoredox conditions and organic matter enrichment. M.Sc. thesis, University of Alberta, Canada.

- Meyer, B. L. and Nederlof, M. H., 1984. Identification of source rocks on wireline logs by density/ resistivity and sonic transit time/resistivity crossplots. *AAPG Bull.*, 68, 121-129
- Milliken, K.L., Choh, S.-J., Papazis, P., Schieber, J., 2007. “Cherty” stringers in the Barnett Shale are agglutinated foraminifera. *Sedimentary Geology* 198, 221–232.
- Moraes, M.A.S., Maciel, W.B., Braga, M.S.S., Viana, A.R., 2007. Bottom-current reworked Palaeocene- Eocene deep-water reservoirs of the Campos basin, Brazil. In: Viana, A.R., Rebesco, M. (Eds.), *Economic and Palaeoceanographic Significance of Contourite Deposits*. Geol. Soc. London Spec. Publ. 276, pp. 81–94.
- Mountjoy, E.W. 1980. Some questions about the development of Upper Devonian carbonate buildups (reefs) Western Canada. *Bulletin of Canadian Petroleum Geology* 28, 315-344.
- Mulder, T., Faugères, J.-C., Gonthier, E., 2008. Mixed turbidite-contourite systems. In: Rebesco, M., Camerlenghi, A. (Eds.), *Contourites. Developments in Sedimentology* 60, Elsevier, Amsterdam, pp. 435–456.
- Mullins, H. T., Neumann, A. C., Wilbur, R. J. and Boardman, M. R., 1980. Nodular carbonate sediment on Bahamian slopes: Possible precursors to nodular limestones. *Journal of Sedimentary Petrology* 50, 117-131.
- Newland, J.B, 1954. Interpretation of Alberta reefs based on experience in Texas and Alberta. *Alberta Society of Petroleum Geologists, Bulletin* 2, 2-6.
- Nittrouer, C.A., and Sternberg, R.W., 1981. The formation of sedimentary strata in an allochthonous shelf environment—the Washington continental-shelf. *Marine Geology* 42, 201–232.
- Noble, J. P. A. and Howells, K. D. M., 1974. Early marine lithification of the nodular limestones in the Silurian of New Brunswick. *Sedimentology* 21, 597-609.

O'Connell, S.C., Dix, G.R., and Barclay, J.E. 1990. The origin, history and regional structural development of the Peace River Arch, Western Canada. *Bulletin of Canadian Petroleum Geology* 38A, 4-24.

Oldale H.S. and Munday R.J.C., 1994. Devonian Beaverhill Lake Group of the Western Canada Sedimentary Basin. In: G.D. Mossop and I. Shetsen (comps.), *Geological Atlas of the Western Canada Sedimentary Basin*. Calgary, Canadian Society of Petroleum Geologists and Alberta Research Council, chapter 11.

Passey, Q.R., Creaney, S., Kulla, J.B., Moretti, F.J., and Stroud, J.D., 1990, A Practical Model for Organic Richness from Porosity and Resistivity Logs, *AAPG Bulletin*, 74(12), 1777–1794. Posamentier, H.W., Allen, G. P., 1999. Siliciclastic sequence stratigraphy: concepts and applications. *SEPM Concepts in Sedimentology and Paleontology* no. 7, 210 pp.

Passey, Q.R., Bohacs, K.M., Esch, W.L., Klimentidis, R., and Sinha, S., 2010. From Oil-Prone Source Rock to Gas-Producing Shale Reservoir: Geologic and Petrophysical Characterization of Unconventional Shale-Gas Reservoirs. *Society of Petroleum Engineers* 131350, 29 pp.

Pedersen, T. F., and S. E. Calvert, 1990. Anoxia vs productivity: What controls the formation of organic-carbon-rich sediments and sedimentary-rocks. *AAPG Bulletin* 74, 454–466.

Posamentier, H.W., Jervey, M.T., Vail, P. R., 1988. Eustatic controls on clastic deposition. I. Conceptual framework. In: Wilgus, C. K., Hastings, B. S., Kendall, C. G. St. C., Posamentier, H.W., Ross, C. A., Van Wagoner, J. C. (Eds.), *Sea Level Changes – An Integrated Approach*. *SEPM Special Publication* 42, p. 110-124.

Posamentier, H.W., Allen, G. P., 1999. Siliciclastic sequence stratigraphy: concepts and applications. *SEPM Concepts in Sedimentology and Paleontology* no. 7, 210 pp.

Potma, K., Weissenberger, J.A.W., Wong, P.K., and Gilhooly, M, G., 2001. Toward a sequence stratigraphic framework for the Frasnian of the Western Canada Basin. *Bulletin of Canadian Petroleum Geology* 49, 37-85.

Rebesco, M., Camerlenghi, A., 2008. Late Pliocene margin development and mega debris flow deposits on the Antarctic continental margins: Evidence of the onset of the modern Antarctic Ice Sheet? *Palaeogeogr. Palaeoclimatol. Palaeoecol.* 260, 149–167.

Rebesco, M., Pudsey, C.J., Canals, M., Camerlenghi, A., Barker, P.F., Estrada, F., Giorgetti, A., 2002. Sediment drifts and deep-sea channel systems, Antarctic Peninsula Pacific Margin. In: Stow, D.A.V., Pudsey, C.J., Howe, J.A., Fauge`res, J.-C., Viana, A.R. (Eds.), *Deep-Water Contourite Systems: Modern Drifts and Ancient Series, Seismic and Sedimentary Characteristics*. *Geol. Soc. London Mem.* 22, pp. 353–371.

Rebesco, M., Camerlenghi, A., Volpi, V., Neagu, C., Accettella, D., Lindberg, B., Cova, A., Zgur, F., The Magico Party, 2007. Interaction of processes and importance of contourites: Insights from the detailed morphology of sediment Drift 7, Antarctica. In: Viana, A.R., Rebesco, M. (Eds.), *Economic and Palaeoceanographic Significance of Contourite Deposits*. *Geol. Soc. London Spec. Publ.* 276, pp. 95–110.

Rebesco, M., Hernández-Molina, F.J., Van Rooij, D., and Wåhlin, A., 2014. Contourites and associated sediments controlled by deep-water circulation processes: State-of-the-art and future considerations. *Marine Geology* 352, 111-154.

Rhoads, D. C., 1974. Organism-sediment relationship on the muddy sea floor. *Oceanogr. Marine Biology Ann. Rev.* 12, 263-300.

Rhoads, D.C., and Morse, I.W., 1971. Evolutionary and ecologic significance of oxygen-deficient marine basins. *Lethaia* 4, 413-428.

Rine, J., and R. Ginsburg, 1985. Depositional facies of a mud shoreface in Suriname, South America: A mud analog to sandy shallow-marine deposits. *Journal of Sedimentary Petrology* 55, 633–652.

Röhl, H.J., Schmid-Röhl, A., Oschmann, W., Frimmel, A., and Schwark, L., 2001. The Posidonia Shale (Lower Toarcian) of SW-Germany: an oxygen-depleted ecosystem controlled by sea level and paleoclimate. *Palaeogeography, Palaeoclimatology, Palaeoecology* 165, 27–52.

Rokosh, C.D., Lyster, S., Anderson, S.D.A., Beaton, A.P., Berhane, H., Brazzoni, T., Chen, D., Cheng, Y., Mack, T., Pana, C., and Pawlowicz, J.G. 2012. Summary of Alberta's shale- and siltstone-hosted hydrocarbons. ERCB/AGS Open File Report 2012-06

Ross, G.M. and Stephenson, R.A., 1989. Crystalline basement: the foundation for the Western Canadian Sedimentary Basin. In: B.D. Ricketts (Ed.), *The Western Canadian Sedimentary Basin - A Case Study*. Calgary, Canadian Society of Petroleum Geologists, p. 33-46.

Savoy, L.E., Mountjoy, E.W., 1995. Cratonic-margin and Antler-age foreland basin strata (Middle Devonian to Lower Carboniferous) of the southern Canadian Rocky Mountains and adjacent plains. In: Dorobek, S.L., Ross, G.M. (Eds.), *Stratigraphic Evolution of Foreland Basins*. Soc. Sediment. Geol. Spec. Publ. 52, pp. 213–231.

Savrda, C.E., 1995. Ichnologic applications in paleoceanographic, paleoclimatic, and sea level studies. *Palaios* 10, 565–577.

Savrda, C.E., 2007. Trace fossils and benthic oxygenation. In: Miller III, W. (Ed.), *Trace Fossils: Concepts, Problems, Prospects*. Elsevier, pp. 149–158.

Savrda, C.E., Bottjer, D.J., and Gorsline, D.S., 1984. Development of a comprehensive oxygen-deficient marine biofacies model: evidence from Santa Monica, San Pedro and Santa Barbara Basins, California Continental Borderland. *AAPG Bulletin* 68,1179-1192.

Savrda, C.E., Bottjer, D.J., 1987. The exaerobic zone, a new oxygen-deficient marine biofacies. *Nature* 327, 54–56.

Savrda, C.E., Bottjer, D.J., 1989. Trace-fossil model for reconstructing oxygenation histories of ancient marine bottom waters: application to Upper Cretaceous Niobrara Formation, Colorado. *Palaeogeography, Palaeoclimatology, Palaeoecology* 74, 49–74.

Schieber, J., 1996. Early diagenetic silica deposition in algal cysts and spores: A source of sand in black shales? *Journal of Sedimentary Research* 66, 175–183.

Schieber, J., 1999. Distribution and deposition of mudstone facies in the Upper Devonian Sonyea Group of New York. *Journal of Sedimentary Research* 69, 909–925.

Schieber, J., 2003. Simple gifts and hidden treasures — implications of finding bioturbation and erosion surfaces in black shales. *The Sedimentary Record* 1(2), 4–8.

Schieber, J., 2009. Discovery of agglutinated benthic foraminifera in Devonian black shales and their relevance for the redox state of ancient seas: *Palaeogeography, Palaeoclimatology, Palaeoecology* 271, 292-300.

Schieber, J., 2011. Reverse engineering mother nature – Shale sedimentology from an experimental perspective. *Sedimentary Geology* 238, 1-22.

Schieber, J., and Riciputi, L., 2004. Pyrite ooids in Devonian black shales record intermittent sea-level drop and shallow water conditions: *Geology*, v. 32, p. 305-308.

Schieber, J., J. B. Southard, and K. Thaisen, 2007b. Accretion of mudstone beds from migrating floccule ripples. *Science* 318, 1760–1763.

Schieber, J., and Southard, J. B., 2009. Bedload transport of mud by floccule ripples – Direct observation of ripple migration processes and their implications. *Geology* 37, 483-486.

Schieber, J., J. B. Southard, and A. Schimmelmann, 2010. Lenticular shale fabrics resulting from intermittent erosion of water-rich muds: Interpreting the rock record in the light of recent flume experiments. *Journal of Sedimentary Research* 80, 119–128.

- Schlager, W., Reijmer, J.J.G., and Droxler, A., 1994. Highstand Shedding of Carbonate Platforms: *Journal of Sedimentary Research*, v.64, p.270-281
- Schmoker, J. W., 1981. Determination of organic-matter content of Appalachian Devonian shales from gamma-ray logs. *AAPG Bull.*, 65, 1285-1298.
- Scholle, P.A., 1977. Chalk diagenesis and its relation to petroleum exploration: oil from chalks, a modern miracle?: *AAPG Bulletin*, v.61, p.982-1009
- Schröder-Adams, C. J., D. A. Leckie, J. Bloch, J. Craig, D. J. McIntyre, and P. J. Adams, 1996. Paleoenvironmental changes in the Cretaceous (Albian to Turonian) Colorado Group of western Canada: Microfossil, sedimentological and geochemical evidence. *Cretaceous Research* 17, 311–365.
- Shanks, A. L., 2002. The abundance, vertical flux, and stillwater and apparent sinking rates of marine snow in a shallow coastal water column. *Continental Shelf Research* 22, 2045–2064.
- Shanmugam, G., 2000. 50 years of the turbidite paradigm (1950s–1990s): deep-water processes and facies models—a critical perspective. *Marine and Petroleum Geology* 17, 285–342.
- Shanmugam, G., 2008. Deep-water bottom currents and their deposits. In: Rebesco, M., Camerlenghi (Eds.), *Contourites. Developments in Sedimentology* 60, Elsevier, Amsterdam, pp. 59–81.
- Slingerland, R. L., Kump, L. R., Arthur, M. A., Sageman, B. B., and Barron, E. J., 1996. Estuarine circulation in the Turonian Western Interior Seaway of North America: *Geological Society of America Bulletin* 108, 941–952.
- Staplin, F. L., 1961. Reef-controlled distribution of Devonian microplankton in Alberta: *Palaeontology* 4, 392-424.

Stasiuk, L.D., and Fowler, M.G., 2004. Organic facies in Devonian and Mississippian strata of Western Canada Sedimentary Basin: relation to kerogen type, paleoenvironment, and paleogeography. *Bulletin of Canadian Petroleum Geology* 52, 234-255.

Stoakes, F.A., 1980. Nature and control of shale basin fill and its effect on reef growth and termination: Upper Devonian Duvernay and Ireton formations of Alberta, Canada. *Bulletin of Canadian Petroleum Geology* 28, 345-410.

Stocks, A. E. and Lawrence, S. R., 1990. Identification of source rocks from wireline logs. In: Hurst, A., Lovell, M. A. and Morton, A. C. (Eds), *Geological applications of wireline logs. Geol. Soc. Sp. Publ.*, 48, 241-252.

Stow, D.A.V., Faugères, J.C., 2008. Contourite facies and the facies model. In: Rebesco, M., Camerlenghi, A. (Eds.), *Contourites. Developments in Sedimentology* 60. Elsevier, Amsterdam, pp. 223–256.

Stow, D.A.V., Hernández-Molina, F.J., Alvarez Zarikian, C.A., the Expedition 339 Scientists, 2013b. Proceedings IODP, 339. Integrated Ocean Drilling Program Management International, Tokyo.

Stow, D.A.V., Holbrook, J.A., 1984. North Atlantic contourites: An overview. In: Stow, D.A.V., Piper, D.J.W. (Eds.), *Fine-grained sediments, Deep-water Processes and Facies. Geol. Soc. London Spec. Publ.* 15, pp. 245–256.

Stow, D.A.V., Piper, D.J.W., 1984. Deep-water fine-grained sediments: Facies models. In: Stow, D.A.V., Piper, D.J.W. (Eds.), *Fine-grained sediments: Deep-Water Processes and Facies. Geol. Soc. London Spec. Publ.* 15, pp. 611–646.

Stow, D.A.V., Kahler, G., Reeder, M., 2002d. Fossil contourites: Type example from an Oligocene palaeoslope system, Cyprus. In: Stow, D.A.V., Pudsey, C.J., Howe, J.A., Faugères, J.-C., Viana, A.R. (Eds.), *Deep-Water Contourite Systems: Modern Drifts and Ancient Series, Seismic and Sedimentary Characteristics. Geol. Soc. London Mem.* 22, 443–455.

Stow, D.A.V., Pudsey, C.J., Howe, J.A., Faugères, J.-C., Viana, A.R. (Eds.), 2002f. Deep-Water Contourite Systems: Modern Drifts and Ancient Series, Seismic and Sedimentary Characteristics. Geol. Soc. London Mem., Vol. 22, 464 pp.

Stow, D.A.V., Hunter, S., Wilkinson, D., Hernández-Molina, J., 2008. The nature of contourite deposition. In: Rebesco, M., Camerlenghi, A. (Eds.), Contourites. Developments in Sedimentology 60, pp. 143–156.

Switzer, S.B., Holland, W.G., Christie, D.S., Graf, G.C., Hedinger, A.S., McAuley, R.J., Wierzbicki, R.A., and Packard, J.J., 1994. The Woodbend-Winterburn strata of the Western Canada Sedimentary Basin. In: G.D. Mossop and I. Shetsen (comps), Geological Atlas of the Western Canada Sedimentary Basin. Geological Survey of Canada, Chapter 12

Thiel, H., 1995. Ocean cleaning and marine snow. Marine Pollution Bulletin 30, 490–491.

Tucker, M. E., 1973. Sedimentology and diagenesis of Devonian pelagic limestones (Cephalopodenkalk) and associated sediments of the Rheno-Hercynian Geosyncline, West Germany: Neues Jahrbuch f. Geologie u. Palaontologie Abhandlungen Bd. 142, 320-350.

Tyson, R V., 2005. The "productivity versus preservation" controversy; cause, flaws, and resolution. In: Harris, N.B. (Ed.), The deposition of organic-carbon-rich sediments: models, mechanisms, and consequences. Special Publication - Society for Sedimentary Geology 82, pp. 17-33.

Van Buchem, F.S.P., Eberli, G.P., Whalen, M.T., Mountjoy, E.W., and Homewood, P.W., 1996a. Basinal geochemical cycles and platform margin geometries in the Upper Devonian carbonate system of western Canada: Société Géologique de France, Bulletin 167, 685–699.

Van Buchem, F.S.P., Chaix, M., Eberli, G.P., Whalen, M.T., Masse, P., and Mountjoy, E.W., 2000a. Outcrop to subsurface correlation of the Upper Devonian (Frasnian) based on the comparison of the Miette and Redwater carbonate buildup margins. In: Homewood, P.W., and

Eberli, G.P. (Eds.), Genetic Stratigraphy on the Exploration and Production Scales—Case Studies from the Pennsylvanian of the Paradox Basin and the Upper Devonian of Alberta. Bulletin Centre de Recherche Elf Exploration Production, Mémoire 24, pp. 139–175.

Van Wagoner, J. C., 1995. Sequence Stratigraphy and Marine to Nonmarine Facies Architecture of Foreland Basin Strata, Book Cliffs, Utah, U.S.A. In: Van Wagoner, J. C., Bertram, G.T. (Eds.), Sequence Stratigraphy of Foreland Basin Deposits. American Association Petroleum Geologists Memoir 64, 137–223.

Van Wagoner, J. C., Mitchum, R. M., Posamentier, H.W., Vail, P. R., 1987. An overview of sequence stratigraphy and key definitions. In: Bally, A.W. (Ed.), Atlas of Seismic Stratigraphy, volume 1. AAPG Studies in Geology 27, 11–14.

Van Wagoner, J. C., Posamentier, H.W., Mitchum, R. M., Vail, P. R., Sarg, J. F., Loutit, T. S., Hardenbol, J., 1988. An overview of sequence stratigraphy and key definitions. In: Wilgus, C. K., Hastings, B. S., Kendall, C. G. St. C., Posamentier, H.W., Ross, C. A., Van Wagoner, J. C. (Eds.), Sea Level Changes – An Integrated Approach SEPM Special Publication 42, 39–45.

Van Wagoner, J. C., Mitchum Jr., R. M., Champion, K. M., Rahmanian, V. D., 1990. Siliciclastic sequence stratigraphy in well logs, core, and outcrops: concepts for high resolution correlation of time and facies. American Association of Petroleum Geologists Methods in Exploration Series 7, 55 pp.

Vecsei, A, and Sanders, D.G.K, 1997. Sea-level highstand and lowstand shedding related to shelf margin aggradation and emersion, Upper Eocene-Oligocene of Maiella carbonate platform, Italy: Sedimentary Geology, v.112, p.219-234

Ver Straeten, C.A., Brett, C.E., and Sageman, B.B., 2011. Mudrock sequence stratigraphy: A multi-proxy (sedimentological, paleobiological and geochemical) approach, Devonian Appalachian Basin. Palaeogeography, Palaeoclimatology, Palaeoecology, v.304, p.54-73

Viana, A.R., Rebesco, M. (Eds.), 2007. Economic and Palaeoceanographic Significance of Contourite Deposits. Geol. Soc. London, Spec. Publ. 276, 350 pp.

Waxman, M.H., and Smits, L.J., 1968, Electrical Conductivities in Oil-Bearing Shaly Sand, Paper SPE-1863, *SPE Journal*, 8(2), 107–122.

Weissenberger, J.A.W., 1994. Frasnian reef and basinal strata of West-Central Alberta: a combined sedimentological and biostratigraphic analysis. *Bulletin of Canadian Petroleum Geology* 42, 1-25.

Wendte, J. C., 1974, Sedimentation and diagenesis of the Cooking Lake platform and lower Leduc reef facies, upper Devonian, Redwater, Alberta. Ph.D. dissertation, University of California, Santa Cruz, 222p.

Wetzel, A., Werner, F., Stow, D.A.V., 2008. Bioturbation and biogenic sedimentary structures in contourites. In: Rebesco, M., Camerlenghi, A. (Eds.), *Contourites. Developments in Sedimentology* 60, Elsevier, Amsterdam, pp. 183–202.

Wetzel, A., 2010. Deep-sea ichnology: Observations in modern sediments to interpret fossil counterparts. *Acta Geologica Polonica* 60, 125-138.

Whalen, M.T., Eberli, G.P., Van Buchem, F.S.P., Mountjoy, E.W., Homewood, P.W., 2000. Bypass margins, basin-restricted wedges, and platform-to-basin correlation, Upper Devonian, Canadian Rocky Mountains: Implications for sequence stratigraphy of carbonate platform systems. *Journal of Sedimentary Research* 70, 913-936.

Wignall, P.B., 1991. Dysaerobic trace fossils and ichnofabric in the Upper Jurassic Kimmeridge Clay of southern England. *Palaios* 6, 264–270.

Wignall, P.B., 1993. Distinguishing between oxygen and substrate control in fossil benthic assemblages. *Journal of the Geological Society of London* 150, 193-196.

Wignall, P.B., 1994. *Black shales*: Oxford, United Kingdom, Clarendon Press, v. ix, 127 pp.

Wignall, P.B. and Myers, K.J., 1988. Interpreting benthic oxygen levels in mudrocks: a new approach. *Geology* 16, 452-455.

Wignall, P.B., and Pickering, K.T., 1993. Paleoecology and sedimentology across a Jurassic fault scarp, northeast Scotland. *Journal of the Geological Society of London* 150, 323–340.

Williams, C. J., Hesselbo, S. P., Jenkyns, H. C., and Morgan-Bell, H. S., 2001. Quartz silt in mudrocks as a key to sequence stratigraphy (Kimmeridge Clay Formation, Late Jurassic, Wessex Basin, UK): *Terra Nova*, v. 13, no. 6, p. 449-455

Zelt, F. B., 1985. Natural gamma-ray spectrometry, lithofacies, and depositional environments of selected Upper Cretaceous marine mudrocks, western United States, including Tropic Shale and Tununk Member of Mancos Shale. Ph.D thesis, Princeton University, 284 p.

Zeigler, P.A. 1967. International Symposium on the Devonian System, Guidebook for Canadian Cordilleran Field Trip. Alberta Society of Petroleum Geologists, Map: Upper Devonian 345-359 m.y., pp.13

## Appendix A: Thin Section Descriptions

TS = thin section; BP = bed-parallel thin section; TOC = total organic carbon; OM = organic matter

TOC values from McMillan (2016).

### **SCL Kaybob 02-22**

#1 3068.10m: This section is from the Ireton Formation. Poorly laminated to structureless, organic-lean, argillaceous mudstone. Fissile. Mudstone is light to medium grey-brown, clay rich, moderately abundant clay- and very fine silt-sized calcite, minor quartz. Radiolaria sparsely dispersed at top of section. Low to moderate abundance of OM aggregates. Whole sample TOC = 0.479 wt%

#10 3075.85m: Laminated mudstone draped around a discrete calcite concretion. Laminae can be traced from mudstone into concretion, showing much greater compaction in mudstone than concretion. Silt laminae are composed of quartz, calcite, dolomite and chert clasts. Mudstone is very siliceous with abundant chert stringers. Authigenic chert is observed in matrix and inside styliolinid tests. Rare phosphatic clasts. Rare clay aggregates. Calcite concretion has a rim of sparry calcite. Whole sample TOC = 2.643 wt%

#12 3077.22m: Very silty wavy-laminated mudstone. Silt laminae can have sharp or gradational contacts and show normal or inverse grading. Silt lenses are likely silt-filled burrows but some may be starved ripples. Silt laminae are grain supported, and may contain quartz, calcite and dolomite cement. Low abundance of fossil fragments. One silicified crinoid oscicle found. Silt-poor laminae are organic rich, with common OM aggregates and abundant chert stringers. A fracture runs through the whole section and is filled with authigenic calcite, dolomite, and barite. Whole sample TOC = 1.792 wt%.

#17 3080.40m: Bottom of section is organic-rich siliceous mudstone. Similar to previous section although tentaculitids are more common. Rare conodonts. Discontinuous pyritic laminae.

Moderately abundant OM aggregates. Uncommon agglutinated foraminifera. Top of section is bioturbated wackestone with abundant radiolarian, styliolinid, and tentaculitid tests. Moderately common clay aggregates. Whole sample TOC = 2.835 wt%.

#19 3082.50m: Bottom 1/3 of section is laminated mudstone. Organic-rich mudstone with faint silt laminae. Uncommon cherty stringers, rare clay aggregates. Possible agglutinated foraminifera. Upper 2/3 of section is laminated wackestone. Abundant radiolaria and styliolinid fossils. Abundant fine fossil fragments. Laminated at base of section but becoming structureless towards top. Rare clay aggregates. Lenses of framboidal pyrite are common in finer laminae. Pyrite also replaces fine fossil fragments. Horizontal calcite spar-filled fracture(?). Whole sample TOC = 2.828 wt%.

#21 3084.50m: Structureless to faintly laminated mudstone. Rare distinct laminae but also no distinct bioturbation features. Thin, discontinuous silty laminae have gaps. Low to moderate abundance of clay aggregates. Common OM aggregates. Cross polars show variations in clay abundance in laminae by differences in extinction. Laminae with more clays are show stronger parallel extinction. Whole sample TOC = 2.898%.

#23 3085.50m: Bioturbated, wavy laminated silty mudstone. Discontinuous and disturbed silty laminae. Laminae are composed of quartz with subsequent calcite, minor dolomite and uncommon chert clasts. Common pyrite replacement of spine-type fossils (sponge spicules?). Pyrite less commonly observed as framboid-rich pellets. Uncommon conodont fragments. Fine-grained laminae are organic-rich, with OM aggregates and unaggregated OM in matrix. No chert stringers observed. Whole sample TOC = 2.463 wt%.

#27 3088.50m: Moderately well laminated silty mudstone. Laminae are commonly discontinuous and disturbed. Chert stringers are rare. Moderately abundant mica. Moderately abundant dolomite rhombs. Moderately abundant dark brown OM aggregates. Uncommon agglutinated foraminifera (siliceous), some with observable central cavity or suture. Common pellet shapes filled with framboidal pyrite. Pyritic pellets common in finer, less silty laminae but not exclusive to finer-grained laminae. Whole sample TOC = 2.905 wt%

#27 BP 3088.50m: Pyritic pellets are equant to ovoid (not bioturbation features).

#28 3089.50m: Laminated to structureless silty mudstone. Variation in lamination quality from moderately well laminated to structureless. Fine to coarse silt in silty laminae, clay to fine silt in silt-poor laminae. Minor dolomite, sometimes with visibility zoned overgrowths. Large, irregular pyrite accumulation in upper half of thin section. Lower portion of pyrite enrichment is mostly pyrite-replaced fossil fragments (sponge spicules?) with a less amount of framboids. Framboids become dominant towards the middle of the accumulation, and euhedral pyrite is dominant in the top half. Rare phosphate clasts. Matrix is organic-rich although well-defined OM aggregates are not common. Whole sample TOC = 2.682 wt%

#28 BP 3089.50m: No new information. Silt laminae intersect bedding plane producing silt-rich wavy/linear features.

#30 3091.40m: Wavy laminated silty mudstone. Coarse silt to very fine sand in coarsest laminae. Lamina sets may have sharp bases and/or sharp tops. Normal and inverse grading. Quartz silt is abundant with lesser abundance of calcite silt. Minor dolomite, rare chert clasts, very rare feldspar. Moderately abundant fine grained fossil debris although there is significant variability from lamina to lamina. Minor to moderate bioturbation. Bedding is still well preserved but silt filled burrows are common. Calcite and quartz cement in coarse-grained laminae. Abundant chert stringers. Whole sample TOC = 2.246 wt%.

#33 3094.75m: Laminated siliceous silty mudstone. Uncommon crushed calcareous styliolinids. Abundant cherty stringers. Dark brown OM aggregates are moderately common but most OM is mixed into groundmass. Low to moderate abundance of calcite silt, fine fossil debris. Some calcite looks dissolved or silica-replaced. Whole sample TOC = 3.614 wt%.

#34 3095.50m: Base of section is styliolinid wackestone with irregular, erosive base. Dominated by styliolinids but conodonts are also abundant. Silty pellet-forms with light colored matrix are abundant. Pellet forms commonly lined with dark-brown, organic-rich, pyritic, fine-grained material. Potential mud-lined burrows. Other pellet/burrows are finer grained, dominantly calcareous. Rare clay mineral aggregates. Upwards, styliolinids become less abundant, radiolaria become the dominant fossil type. Planar parallel silty laminae are present although silt enrichment is minor. Fossils are much less bedded and do not show enrichment where silt is enriched. Less common silty pellet-forms upwards, more common clay aggregates. Top of thin

section is laminated silty mudstone with very rare fossils. Calcareous material is much less abundant and siliceous material increases. Moderately abundant cherty stringers. More common OM in top of section. Whole sample TOC = 4.429 wt%.

#35 3095.90m: Silty mudstone. Silt is medium to coarse. Planar lamination with minor to moderate disruption of laminae due to bioturbation. Possible dipping bedding in lower half, but possibly bioturbation features. Some silt laminae show normal grading, fine into silt-bearing mudstone. Fine calcareous fossil fragments are common. Styliolinids are often crushed. Rare phosphatic clasts. Abundant very small lenses and streaks of framboidal pyrite. Low abundance of chert stringers. Whole sample TOC = 2.353 wt%.

#38 3098.50m: Laminated silty mudstone. Similar to previous but siltier, more abundant clay aggregates. Silt is quartz and calcite. Silty laminae have minor authigenic quartz. Chert stringers are common. Rare styliolinid fragments. Whole sample TOC = 2.239 wt%.

#42 3102.50m: Laminated silty mudstone. Organic-rich matrix. Some silty laminae are sharp-based. Radiolaria, styliolinids and foraminifera are commonly silica-replaced. Cherty stringers are moderately common. Uncommon light brown clay aggregates. Whole sample TOC = 2.691 wt%

#42 BP 3102.50m: Pellets/aggregates are rare but appear ~equant to ovoid in plan view. Section looks structureless with dispersed OM aggregates.

#44 3104.00m: Silty mudstone with abundant calcite muds clasts, fine-grained calcite shell debris. Common radiolaria. Laminated lower portion of TS, structureless upper portion. Laminae pinch and swell and are discontinuous. Rare conodonts. This sample is part of a sharp-based, normally graded bed. Some authigenic quartz in coarse laminae. Whole sample TOC = 2.914 wt%

#46 3106.39m: Bioturbated styliolinid wackestone. Intense bioturbation, abundant pyrite in burrows. Randomly oriented styliolinids are very abundant, with minor coarser fossil fragments of brachiopods. Very calcareous, fine-grained matrix. Minor phosphatic clasts. Whole sample TOC = 0.904 wt%

#47 3106.50m: Bioturbated styliolinid wackestone. No bedding evident. Styliolinids in bed-parallel and random orientation. Very abundant, fine-grained calcareous shell fragments. Pyrite accumulations associated with burrows. Pyrite is also common within styliolinid tests. Whole sample TOC = 1.248 wt%.

#52 3109.60m: Silty radiolarian wackestone. Laminated to structureless. Medium to coarse quartz and dolomite silt. Heavily calcite cemented. Radiolaria are dominant, low abundance of styliolinids. Radiolaria are confined to definable laminae. Radiolaria are recrystallized. Rare calcite mud clasts(?). Whole sample TOC = 1.227 wt%

#53 3110.50m: Fully bioturbated. No bedding evident. Small, very finely granular pellet shapes are very abundant (likely burrows). Very rare styliolinid fragments. Moderately common agglutinated foraminifera (siliceous). Matrix is composed of silt- and clay-sized quartz and mica. No strong orientation direction. Clay-size calcite in low to moderate abundance. Rare phosphatic clasts. Whole sample TOC = 2.301 wt%.

#53 BP 3110.50m: Clay aggregates are common and are ~equant in bed-parallel section.

#54 3111.37m: Silty mudstone. Bottom ¼ of TS is very silty and poorly laminated. Silt is mostly quartz with some calcite. Rare very fine sand-sized grains. Common phosphatic clasts, uncommon conodonts/fish debris(?). Very rare calcareous fossils. Very rich in pellet forms. Silt pellets are mostly calcite silt with some quartz, no clay material or amorphous OM. Light brown pellets are clay-rich with a minor to moderate quartz/calcite silt component. Some have very little silt. Light brown pellets have cross-hatched texture visible in cross polars (card house structure of floccule?). Middle half of thin section is structureless mudstone with abundant very fine calcite, moderately abundant quartz silt, low to moderate abundance of styliolinids, very rare pellets, rare conodonts, phosphatic grains, and radiolaria. Top ¼ of TS similar to middle but with greater styliolinid abundance. Whole sample TOC = 2.545 wt%.

#54 BP 3111.37m: Poorly-prepared section. Taken from bottom ¼ of bed normal section. Abundant pellets, phosphatic clasts, some conodonts.

#58 3113.30m: Middle-upper Duvernay contact. Below contact is calcareous-argillaceous, with vary abundant clay-sized calcite, low to moderate abundance of styliolinid fragments, and

abundant burrow-mottling. Contact is sharp and erosive, overlain by a lag of coarse fossil debris (calcareous, siliceous, and phosphatic), phosphatic and pyritic clasts, and uncommon green mud clasts. Above contact, clay minerals and quartz silt become more abundant, organic matter becomes moderately abundant, and calcareous sediment becomes much less abundant. Some pyrite-enriched streaks, rare light brown pellets. Sediment above contact is structureless with some faint, discontinuous laminae. Whole sample TOC = 2.582 wt%.

#58 BP 3113.30m: Bed parallel section located just below contact. Structureless-looking, with irregular pyritic accumulations, abundant fine calcite and calcareous fossil fragments. Some organic-matter aggregates, phosphatic clasts, and conodonts.

#59 3113.50m: Nodular limestone. Burrow mottled. One potential boring (vertical, sharp walls). Abundant fine calcareous fossil debris.

#60 3114.50m: Nodular limestone. Burrow mottled. Abundant fine fossil debris. Wedge-shaped fractures in nodules are filled with sparry calcite. Pyrite occurs disseminated throughout the matrix and as irregular accumulations associated with burrows. Matrix pyrite is mostly framboidal. Irregular pyrite accumulations, framboids are larger and euhedral crystals are common. Another white-reflecting mineral is present (but minor) and has tabular to acicular habit. Other reflective minerals are in lesser abundance with white, gold, and purple reflected light colors. Colored minerals are associated with large pyrite framboids.

#61 3115.40m: Nodular limestone. Burrow-mottled and fossiliferous. Abundant calcareous fossil fragments. Mostly styliolinids but some brachiopods and other shallow water fossil fragments. Large burrows destroy bedding. Wedge-shaped fractures in nodules are filled with sparry calcite. I think calcareous mud clasts (peloids) are a significant component of the sediment but are difficult to identify because they don't contrast much in color with cemented nodules.

#62 3116.60m: Nodular limestone. Abundant authigenic calcite. Coalescing crystals form nodules. Crystal size is finest in the center of the bed with little to no matrix visible. Outwards, both up and down, crystals become larger and more matrix is present between them. Matrix visible between crystals is the same as the sediment outside the nodules. Detrital sediment is light brown and organic-lean. Irregular pyrite throughout sample. Whole sample TOC = 0.53 wt%

#62 BP 3116.60m: Bed=parallel section is dominated by authigenic calcite. Linear features can be several millimeters in length and are recognized by variations in cement abundance.

#65 3118.50m: Micritic mudstone and micritic radiolarian wackestone. Lamination is characterized by micrite-rich and micrite-poor laminae. Very minimal visible organic matter. Upper section of TS is radiolarian-rich. Radiolaria-rich laminae do not have sharp bases or tops and some contacts are visibly bioturbated. No grading evident. Rare pyritization of radiolaria.

#68 3121.50m: Bioturbated silty mudstone. Argillaceous. Laminae are continuous to discontinuous, often disturbed. Laminae are characterized by variation in silt abundance. Less silty laminae are darker, more organic-rich. Low abundance of intact styliolinids. Most fossils are in the form of silt-sized fragments. Rare chert. Whole sample TOC = 2.257 wt%

#69 3121.60m: Burrow-mottled base with pyrite-filled burrows. Erosively overlain by wackestone-packstone event bed. Event bed clasts are dominantly styliolinids but also moderately abundant conodonts, low to moderately abundant phosphatic clasts, abundant green clay clasts (glaucitic?). Event bed is overlain by bioturbated silty mudstone/wackestone. Moderately abundant calcite and quartz silt, low to moderately abundant calcareous microfossils (mostly styliolinids, rare conodonts). At least one minor erosional contact with coarser silt, microfossils, green mud clasts, and phosphatic clasts. Laminae are disturbed, wavy, and discontinuous. Whole sample TOC = 1.917 wt%

#70 3122.50m: Structureless to burrow-mottled calcareous silty mudstone. Abundant calcite silt, calcareous fossil debris. Abundant styliolinids, less common radiolaria, brachiopod fragments. Quartz silt in moderate abundance. Most pyrite is framboidal. Whole sample TOC = 2.734 wt%

#71 3122.74m: Well laminated silty mudstone. Some laminae have sharp boundaries and do not show any visible burrows. Other lamina contacts have irregularities due to bioturbation. Silt is a mixture of calcite and quartz. Mica flakes are in low to moderate abundance. Distinct parallel extinction in fine-grained laminae. Extinction less notable in silty laminae. Large (>2mm) burrows near top of section filled with lighter colored sediment and coarse fossil debris. Minor irregular pyrite, almost exclusively framboidal. Rare light brown pellets. Greater abundance of organic matter aggregates in fine-grained laminae. Whole sample TOC = 3.073 wt%

## GuideX Gvillee 09-06

#6 2552.93m: Styliolinid wackestone. Structureless. Styliolinids randomly oriented. Calcite silt is abundant. Calcite mud clasts are common but not abundant. Whole sample TOC = 2.02%

#8 2555.09m: Intraclastic wackestone-packstone (or muddy siltstone). Section fines upwards. Some lamination at base but becomes structureless upwards. Calcareous mud clasts abundant at base and decrease to minor at top. Quartz and calcite silt become dominant grain type in upper 2/3 of section. Whole sample TOC = 2.30 wt%.

#8 BP 2555.09m: Calcareous mud clasts are ~equant in bed parallel section.

#9 2556.52m: Structureless packstone. 70% of clasts are calcareous mud clasts (coarse silt to medium sand sized). Other grains are fossils fragments (similar assemblage to previous section but less shallow water taxa and finer grained). Rare feldspar, conodonts. Minor silicification. More mud than previous section but still grain supported. No obvious bedding at thin section scale. Rare, discontinuous shale partings. Mudstone is pyritic, dark brown. Whole sample TOC = 4.12 wt%.

#11 2558.20m: Erosively-based grainstone-rudstone bed. Shallower water taxa than other sections (brachiopods, echinoderms(?), placoderm(?) cephalopod(?), crinoid oscicles, bryozoans, conodonts. Common silicification of calcareous fossil fragments. Abundant intraclasts (rounded mud clasts and larger, lithified, more angular mud clasts). Uncommon phosphatic clasts (some rounded, some have overgrowths). Whole sample TOC = 0.56 wt%.

#13 2558.71m: Laminated mudstone. Laminae defined by varying silt abundance. Silty laminae are composed of fine to coarse silt, mostly quartz, less abundant calcite and dolomite. Rare feldspar. Silt-poor laminae have more abundant OM aggregates. Clay aggregates are moderately common. Uncommon silty pellets containing quartz silt, and randomly oriented mica flakes. Conodonts are rare. Whole sample TOC = 5.54 wt%.

#13 BP 2558.71m: Bed-parallel section shows an abundance of clay aggregates and OM aggregates that are ~equant to ovoid.

#14 2559.77m: Bioturbated silty mudstone. Irregular, disturbed bedding due to bioturbation. Silty but mud-supported. Silt-sized peloids are common and approximately as abundant as quartz and calcite silt (not composed of mud). Calcite silt is more common than quartz. Phosphatic clasts are moderately common. Uncommon clay aggregates. Conodonts are moderately common. Minor to moderate abundance of OM aggregates. Whole sample TOC = 2.11 wt%.

#16 2561.06m: Lower portion of section is styliolinid wackestone-packstone and is normally graded. Upper section is dominated by silt (calcite, quartz, dolomite) and is grain-supported (or very close to it). Difficult to pick out bedding. Phosphatic clasts are rare. Uncommon conodonts, rare agglutinated foraminifera (siliceous), common calcareous mud clasts (peloids). Mudstone matrix is minor and is medium to dark brown, composed of clay and OM. Whole sample TOC = 1.36 wt%.

#18A 2563.07: Mudstone with erosive-based wackestone-packstone beds. Wackestone-packstone beds are dominantly composed of styliolinids, but also contain tentaculitids, brachiopod fragments, and conodonts. Matrix contains common clay aggregates, but abundance is variable across section. Intervals with less clay aggregates have more silt, are lighter colored. Silt accumulations may be bioturbation features or remnants of agglutinated foraminifera (although silt is calcite not quartz). Whole sample TOC = 5.46 wt%.

#18B 2563.07: Styliolinid wackestone-packstone. Most of sample is mud supported but especially fossiliferous beds are grain-supported. Laminae are composed of styliolinid tests up to 1mm long. Fossiliferous laminae also contain fine to very fine silt (mostly calcite, less common quartz and dolomite). Matrix is organic-rich with rare mica. Pyrite commonly forms as euhedral crystals, less commonly as framboids. Non-fossiliferous mudstone laminae contain fine to medium calcite silt, euhedral and framboidal pyrite. Non-fossiliferous laminae have a greater abundance of OM aggregates. Clay aggregates are moderately common. Rare phosphatic clasts. Bioturbation disrupts lamina contacts. Whole sample TOC = 5.46 wt%.

#19 2563.64m: Laminated mudstone. Faintly laminated. Laminae are defined by minor color change which reflects varying silt, clay, and OM abundance. Dark laminae contain more abundant OM aggregates, more pyrite. Clay mineral aggregates are moderately abundant throughout the sample. Fossils are uncommon, mostly styliolinids and brachiopod fragments.

Rare phosphatic clasts. Pyrite is dominantly framboidal. Rare peloids. Whole sample TOC = 5.26 wt%

#19 BP 2563.64: Bed parallel section shows much the sediment is in the form of clay aggregates and OM aggregates. Aggregates are ~equant to ovoid in plan view. OM aggregates have wispy edges.

#21 2565.91m: Laminated to structureless silty mudstone. Planar-parallel lamination. Minor lamina disruption, pinching/swelling. Laminae composed of calcite silt, some dolomite. Laminae commonly present in pairs. Rare fossils. Most are styliolinids, minor to moderate thin brachiopod fragments, rare conodonts, and rare echinoderm(?) fragments. Fossils commonly have calcite overgrowths. Moderately common silty pellets. Common clay aggregates (light brown). Clay mineral aggregates are more elongate/thinner than silty pellets. Uncommon calcareous mud pellets. Framboidal and euhedral pyrite forms and lenses and is disseminated. A minor proportion of pyrite is fossil replacement. Whole sample TOC = 2.42 wt%/

#21 BP 2565.91m: Aggregates and pellets observed in bed-normal section are equant to ovoid in plan view, suggesting they are not burrows or burrow-fills.

#### **ECA Cecilia 11-04**

#8 3942.42m: Planar laminated mudstone. Continuous to discontinuous laminae are composed of calcite and dolomite silt and calcareous fossil fragments. Most of section is dark brown mudstone (although, section seems to be >20 $\mu$ m thick), organic-rich, and contains dispersed calcite, dolomite, and quartz fine silt and fine fossil fragments. Whole sample TOC = 3.45 wt%.

#8 BP 3942.42m: Linear silt accumulations are likely burrows. Larger fossil fragments with ridges (Brachiopod? Bivalve? Cephalopod aptychus?)

#22 3956.48m: Poorly bedded to structureless silty mudstone. Abundant radiolaria. Minor tentaculitids. Minor pyritic pellets, minor mud pellets. Whole sample TOC = 2.25 wt%.

#37 3971.47m: Bioturbated pyritic mudstone. Very abundant pyritic pellets, radiolaria. Moderately common agglutinated foraminifera (siliceous). Whole sample TOC = 3.36 wt%.

#51 3985.47: Planar laminated silty mudstone. Very calcareous. Abundant peloidal calcite, fossil fragments. Possible low angle cross lamination (but could be a bioturbation feature). Fossil fragments are dominantly styliolinids but also some brachiopod fragments. Matrix is organic-rich, dark-brown, pyritic. Whole sample TOC = 2.52 wt%.

#66 3960.84m: Bioturbated pyritic mudstone. Irregular to sub horizontal pyrite accumulations. Low fossil abundance. Rare clay aggregates. Minor parallel extinction of matrix due to clays. Whole sample TOC = 2.19 wt%.

#66 BP 3960.84: ~Homogenous. Irregular pyrite. Silt lined lineaments are likely traces. Mantle and swirl(?) style traces are enriched in clay minerals and poor in OM (similar birefringence to clay aggregates). Color/composition look similar to clay aggregate-rich mudstone but distinct aggregates are rare.

#67 3965.67: Structureless silty mudstone. Uncommon discontinuous silt laminae. Rare inclined laminae. Most silt is calcite/dolomite. Base of section is wackestone with abundant styliolinids, less common brachiopod, bivalve fragments. Irregular pyrite. Possible agglutinated foraminifera (siliceous). Whole sample TOC = 3.15 wt%.

#67 BP 3963.67m: Bed-parallel section through wackestone. Styliolinid-rich, a few large brachiopods. Moderately common clay aggregates. Linear mud-filled, silt-lined burrows.

#68 lower 3974.91m: Bioturbated pyritic mudstone. Contains a contact with bioturbated pyritic mudstone below. Inclined pyrite-filled burrows. Structureless, more calcareous above contact. Abundant fossil debris, mostly styliolinids. Rare conodonts, rare and angular phosphatic clasts, pyritic clasts in fossiliferous laminae. Whole sample TOC = 1.60 wt%.

#68 upper 3974.91m: Calcareous mudstone below a contact. Discontinuous, silty, fossiliferous laminae. Abundant fossil fragments. Bioturbated pyritic mudstone above contact. Contact is gradational. Whole sample TOC = 1.60 wt%.

#69 lower 3982.57m: Bioturbated pyritic mudstone. Structureless with abundant fine calcite/dolomite silt. Whole sample TOC = 2.06 wt%.

#69 upper 3982.57m: Erosive lag containing coarse calcareous, siliceous, phosphatic, and pyritic fossil fragments. Some rounded phosphatic clasts. Silty mudstone above lag with abundant fine fossil fragments and calcite/dolomite/quartz silt. Authigenic calcite/dolomite/pyrite nodules. Whole sample TOC = 2.06 wt%.

#69 BP: Structureless mudstone. No readily identifiable bioturbation structures. Dark brown, organic-rich, pyritic matrix.

### **EOG Cygnet 08-20**

#6 2569.47m: Nodular limestone. Lower half of section is composed of a calcite nodule containing common styliolinid tests. The silty mudstone above the nodule is poorly bedded, and contains common styliolinid fossils. Silt is calcite and dolomite with lesser amounts of quartz. Whole sample TOC = 0.08 wt%.

#7 2570.44m: Nodular limestone overlain by silty mudstone. Silt abundance is greatest just above the nodular limestone and is mostly dolomite, with lesser quartz and calcite. Upwards, silt content decreases and becomes more calcareous. Fine calcite fossil fragments are abundant. ~30-50% of the calcite silt is peloidal. Organic matter is very minimal in the nodular limestone, but becomes more abundant upwards through the silty mudstone. Bioturbation is intense at the base of the section and decreases upwards. Moderately common conodonts and phosphatic grains. Dolomite replacement of calcareous fossils is common where silt content is high (directly overlying calcite nodule).

#10 2573.54m: Intensely bioturbated silty wackestone. Most of the rock is composed of silt-sized calcite detritus. Dolomite and quartz silt are abundant in the middle of the section. Larger fossil fragments (>0.5mm) are abundant. Fossils are mostly styliolinids and tentaculitids but brachiopod, bivalve, bryozoan(?), echinoderm(?), placoderm(?) fragments are present as well. Dolomite replacement of fossils and dolomite cement is common in the middle part of the section. Whole sample TOC = 0.56 wt%.

#17 2582.53m: Structureless to poorly bedded calcareous mudstone-siltstone. Generally unbedded but faint, discontinuous, wispy laminae are present. The rock is dominated by silt-

sized calcite detritus (calcite silt, fine fossil fragments, and silt-sized peloids). Uncommon larger fossils and fragments are primarily styliolinids. Organic matter is minimal. Whole sample TOC = 2.42 wt%.

#19 2584.50m: Poorly bedded calcareous mudstone. Bioturbation is intense. Remnant bedding is in the form of wispy laminae. Much of the rock is composed of clay- and silt-sized calcite. Dolomite is secondary. Quartz is minor. Minor abundance of dark brown organic matter. Whole sample TOC = 0.80 wt%.

#21 2586.50m: Nodular limestone. Heavily calcite cemented at top and bottom of section, with poorly bedded calcareous mudstone between. Bioturbation is intense. Remnant bedding is in the form of wispy laminae. Much of the rock is composed of clay- and silt-sized calcite. Dolomite is secondary. Quartz is minor. Minor abundance of dark brown organic matter. Whole sample TOC = 0.93 wt%.

#22 2587.50m: Wackestone. Faint planar lamination but most of fabric is defined by fossil orientation parallel to bedding. Fossil and fossil fragments are abundant and include styliolinids, tentaculitids, radiolaria, minor brachiopod and bivalve fragments, and possible agglutinated foraminifera. Moderately abundant dark brown organic matter. Whole sample TOC = 3.59 wt%.

#22 BP 2587.50: Bed-parallel section shows abundant fossil debris on bedding plane. Conodonts(?) and radiolaria are common.

#24 2589.60m: Structureless calcareous mudstone. Very rich in clay- and silt-sized and calcite cement. Burrow mottled. Pyrite enrichment is associated with burrows. Uncommon styliolinid tests.

#26 2591.30m: Moderately well laminated wackestone. Lamina contacts are often disrupted due to bioturbation. Lamination reflects varying silt abundance. Most of the rock is composed of clay- and silt-sized calcite detritus with less common dolomite silt. Styliolinids are abundant. Dark brown organic matter is moderately abundant.

#28 2591.61m: Moderately well laminated wackestone. Lamina contacts are often disrupted due to bioturbation. Lamination reflects varying silt abundance. Most of the rock is composed of

clay- and silt-sized calcite detritus with less common dolomite silt. Styliolinids are abundant. Dark brown organic matter is moderately abundant. Whole sample TOC = 1.15 wt%.

#30 2592.03m: Planar laminated wackestone. Very abundant styliolinid and tentaculitid fossil fossils and fossil fragments along with calcite and dolomite silt. Moderately common phosphatic clasts, calcareous intraclasts.

#32 2593.12m: Structureless calcareous mudstone with faint remnants of wispy laminae. Intensely bioturbated. Rock is dominated by clay- and silt-sized calcite silt and fossil fragments. Dolomite silt is less common. Quartz is minor. Dark brown organic-rich matrix is minimal. Whole sample TOC = 3.71 wt%.

#34 2595.50m: Packstone composed of coarse fossil fragments, intraclasts and peloidal silt and sand. A wide variety of fossil taxa are present including brachiopods, bivalves, echinoderms(?), bryozoans(?), and unidentified fragments. Abundant nodules of dolomite and gypsum(?), ~ovoid, <2mm in diameter.

#36a 2596.45: Packstone composed of peloidal silt, and fine fossil fragments. Intensely bioturbated. Burrows are preferentially cemented. Many ovoid to irregular dolomite nodules (or replacements?), usually less than 0.5x0.25mm. Whole sample TOC = 0.79 wt%.

#36b 2596.45: Packstone. Rock is composed of coarse fossil fragments and intraclasts and contains very little mud matrix. A wide variety of fossil taxa are present including brachiopods, bivalves, echinoderms(?), bryozoans(?), and unidentified fragments. Peloidal silt and sand is abundant. The section is calcite-cemented. Partial dolomitization of fossil fragments is common. The top of the section contains several irregular fractures filled with calcite spar. Whole sample TOC = 0.79 wt%.

#41 2599.39m: Styliolinid-tentaculitid wackestone. Very abundant styliolinid and tentaculitid tests (some greater than 2mm in length). Matrix is dominated by fine calcareous fossil fragments and dark brown organic matter. Whole sample TOC = 2.83 wt%.

#45 2599.86m: Nodular limestone. Very calcareous. Intensely bioturbated. Large fossil fragments (up to 5mm) are brachiopod and bivalve tests. Whole sample TOC = 0.30 wt%.

#54 2600.90m: Nodular limestone. Bioturbated calcareous mudstone in lower half of section, calcite nodule in upper part of section. Nodule has gradational contact. Mudstone composed of clay- and silt-sized calcite with less common dolomite and quartz. Uncommon fossils include styliolinids, tentaculitids, and conodonts. Whole sample TOC = 0.27 wt%.

#55 2601.04m: Bioturbated calcareous mudstone. Most bedding gone, with remnant wispy laminae (variations in silt abundance). Rock composed of clay- and silt-sized calcite and dolomite with minor quartz. Matrix is medium brown with uncommon organic matter aggregates. Common styliolinid and tentaculitid tests, rare conodonts, agglutinated foraminifera(?). Whole sample TOC = 1.09 wt%.

#56 2601.14m: Bioturbated calcareous mudstone. Most bedding gone, with remnant wispy laminae (variations in silt abundance). Rock composed of clay- and silt-sized calcite and dolomite with minor quartz. Matrix is medium brown with uncommon organic matter aggregates. Common styliolinid and tentaculitid tests, rare conodonts, agglutinated foraminifera(?). Whole sample TOC = 1.27 wt%.

#57 2601.24m: Bioturbated calcareous mudstone. Most bedding gone, with remnant wispy laminae (variations in silt abundance). Rock composed of clay- and silt-sized calcite and dolomite with minor quartz. Matrix is dark brown with common organic matter aggregates. Common styliolinid and tentaculitid tests, rare conodonts.

#57 BP 2601.24m: Bed parallel section shows common organic matter aggregates that are ~equant to ovoid in plan view. Less common clay pellets. Linear to arcuate features show minor variations in grain size, often contain more pyrite than surrounding section. These features are interpreted to be burrows.

#59 2602.51m: Bioturbated calcareous mudstone. Moderately bioturbated. Discontinuous wispy silty laminae. Abundant calcite, dolomite silt, less abundant quartz. Light brown matrix, appear organic-lean. Burrows often associated with an increase in pyrite (within or surrounding burrow). Uncommon fossil fragments are primarily tentaculitids and styliolinids. Whole sample TOC = 0.70 wt%.

#61 2602.85m: Bioturbated calcareous mudstone. Moderately bioturbated. Discontinuous, wispy, silty laminae. Rock composed of clay- and silt-sized calcite and dolomite with minor quartz. Matrix is dark brown with common organic matter aggregates. Styliolinids and tentaculitids are common, minor brachiopod fragments.

#62 2603.00m: Structureless mudstone, intensely bioturbated. Rock composed of clay- and silt-sized calcite and dolomite with minor quartz. Matrix is dark brown with common organic matter aggregates. Uncommon fossils include styliolinid and conodont fragments. Burrows often associated with an increase in pyrite (within or surrounding burrow). Whole sample TOC = 0.90 wt%.

#65 2603.40m: Structureless mudstone, intensely bioturbated. Rock composed of clay- and silt-sized calcite and dolomite with minor quartz. Matrix is dark brown with common organic matter aggregates. Uncommon fossils include styliolinid, brachiopod, and conodont fragments. Burrows often associated with an increase in pyrite (within or surrounding burrow).

#66 2603.50m: Structureless mudstone, intensely bioturbated. Rock composed of clay- and silt-sized calcite and dolomite with minor quartz. Matrix is dark brown with common organic matter aggregates. Uncommon fossils include styliolinid and conodont fragments. Whole sample TOC = 2.17 wt%.

#67 2603.62m: Structureless calcareous mudstone. Rock is dominated by silt-sized calcite detritus with very little matrix material. No bedding evident other than very subtle, subhorizontal, discontinuous laminae that are only one to two silt grains thick. Rare identifiable fossil fragments include styliolinids, tentaculitids, and bivalves(?). Whole sample TOC = 0.04 wt%.

#68 2604.41m: Nodular limestone. Calcite nodule has irregular to undulatory, gradational boundaries. Most of rock is composed of silt-sized calcite detritus. No bedding is evident. Calcite nodule contains spar-filled, wedge-shaped fractures. Whole sample TOC = 0.61 wt%.

#71 2607.55m: Structureless calcareous mudstone. Most of rock is composed of silt-sized calcite, dolomite, and quartz. Uncommon larger fossil fragments include brachiopods, styliolinids, and conodonts. Not much for organic-rich matrix. Two dolomite nodules in upper

part of section. Nodules have irregular edges and also contain euhedral pyrite. Whole sample TOC = 3.03 wt%.

#72 2608.50m: Laminated wackestone-packstone. Very abundant styliolinids define lamination. Some laminae are grain-supported. Most fossils are crushed. Matrix is composed of clay-silt sized calcite, dolomite and dark brown organic matter. Whole sample TOC = 4.51 wt%.

#74 2610.51m: Nodular limestone. Abundant sub-millimeter fossil debris, abundant calcite cement. Tentaculitid and styliolinid fossils are most abundant but much of the fine fossil debris is not identifiable. Whole sample TOC = 2.81 wt%.

#75 2611.64m: Calcareous mudstone. Laminated to structureless. Common pyrite lenses in upper portion of section. Lamination, where present is defined by increased abundance of styliolinid tests. Calcite cement is common throughout sample. Whole sample TOC = 3.74 wt%.

#75 BP 2611.64m: Bed-parallel section appears generally structureless with some silt-filled linear structures that are likely to be burrows

#77 2613.46m: Nodular limestone. Millimeter-scale fossil fragments (mostly brachiopods) common but not abundant. One brachiopod appears in situ and shows stalactitic pyrite cement within fossil. Pyrite lenses are common throughout sample. Most of the rock is composed of clay-silt sized calcite detritus. Whole sample TOC = 0.30 wt%.

#79 2615.59m: Laminated calcareous mudstone. Lamination defined by increased abundance of styliolinid tests. Lamina contacts are not sharp. Styliolinid tests are sometimes partially replaced with silica or filled with silica cement. Matrix is very dark with abundant lighter colored pellet-like structures. Pellets often contain silt-sized grains. Uncommon sand-sized calcareous intraclasts.

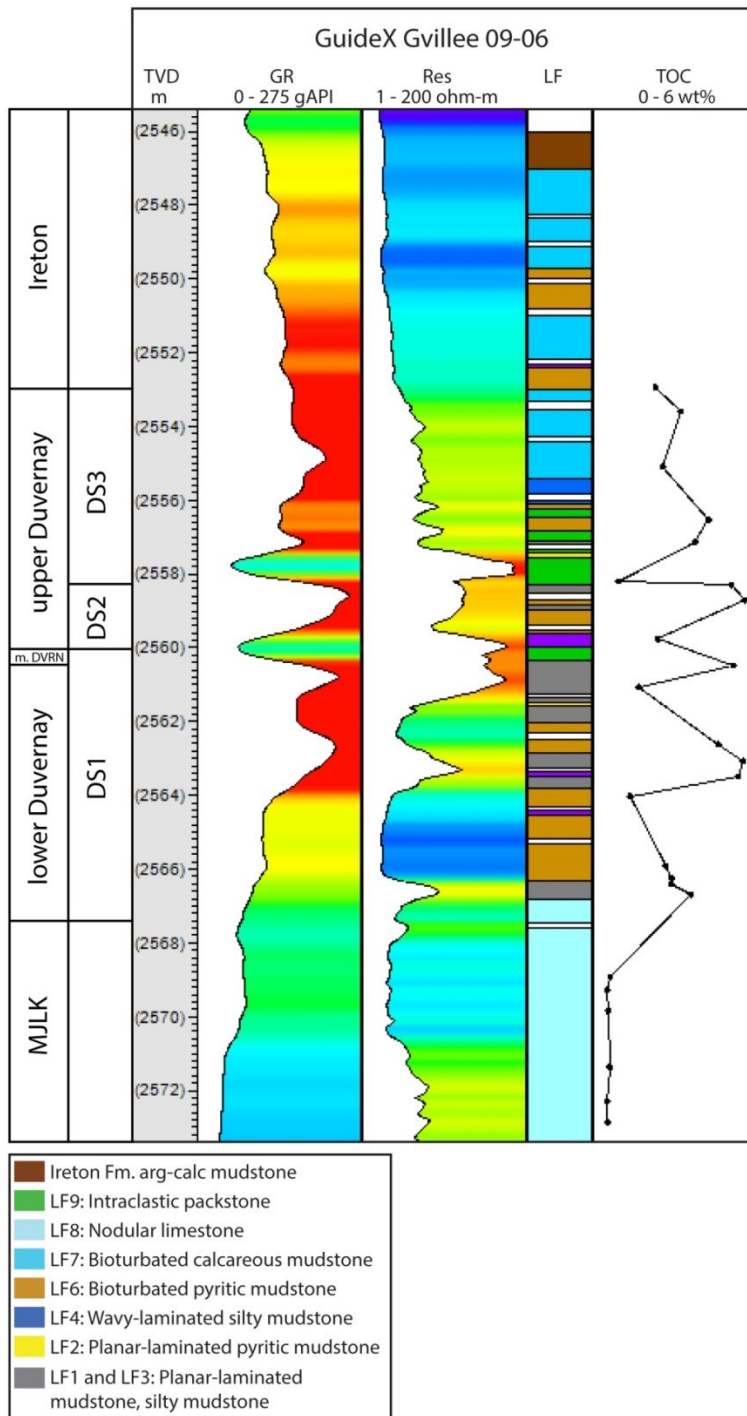
#87 2623.62m: Lower portion of thin section is mudstone with discontinuous silty lamination, clay-silt sized calcite and dolomite matrix, abundant organic matter in matrix, uncommon phosphatic grains and conodont fragments. Upper section is a packstone bed dominated by silt-sized calcite debris. Packstone bed also contains larger (~1-3mm) fossil fragments (mostly brachiopods, less common bivalves, styliolinids, tentaculitids, conodonts). Packstone bed is

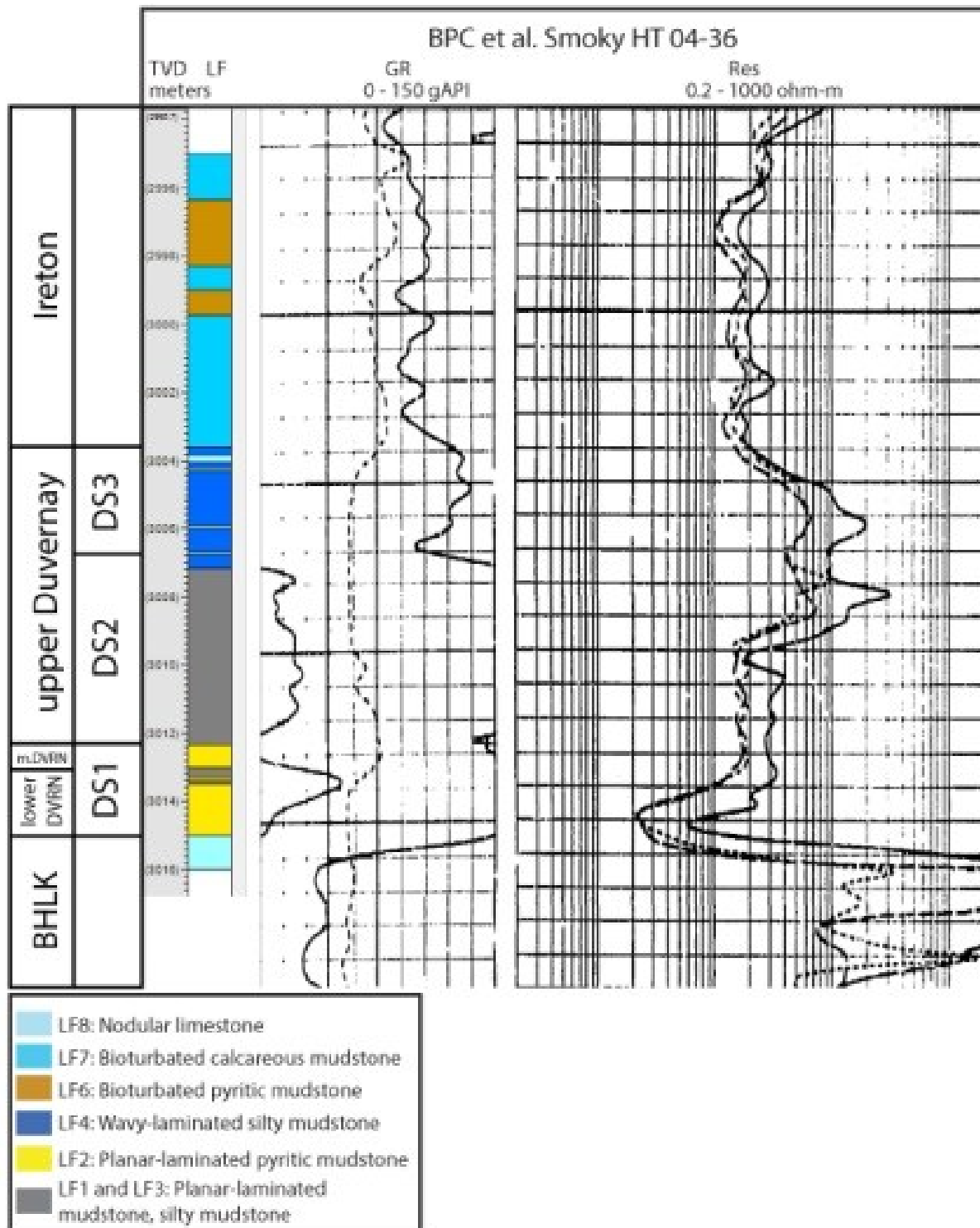
intensely bioturbated and packstone-filled burrows extend down into underlying mudstone.  
Whole sample TOC = 2.00 wt%.

#88 2624.50m: Laminated calcareous mudstone. Abundant fine calcite detritus. Common phosphatic clasts (shell/bone material? Don't look like phosphatic intraclasts). Abundant tentaculitid and styliolinid fragments. Abundant dark brown organic matter mixed into matrix.  
Whole sample TOC = 12.80 wt%.

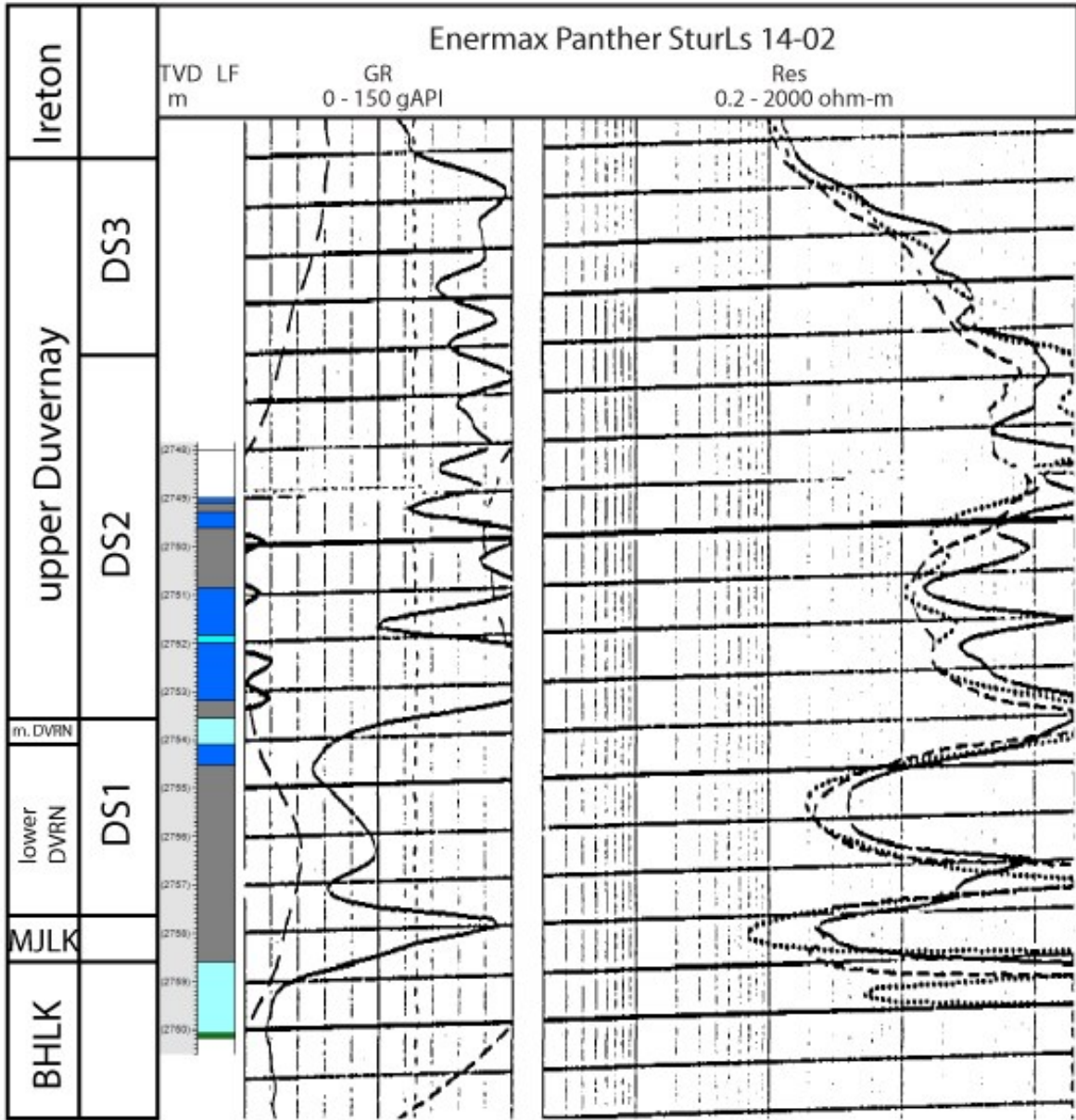
#91 2627.50m: Fossiliferous wackestone-packstone. Intensely bioturbated. Abundant large fossil fragments. Dominantly brachiopods, with lesser bivalves, styliolinids, tentaculitids, echinoderms(?), bryozoans(?). Matrix is clay-sand sized calcite, common recrystallization and cementation. Low abundance of organic matter in matrix. Whole sample TOC = 4.14 wt%.

## Appendix B: Additional Core Descriptions

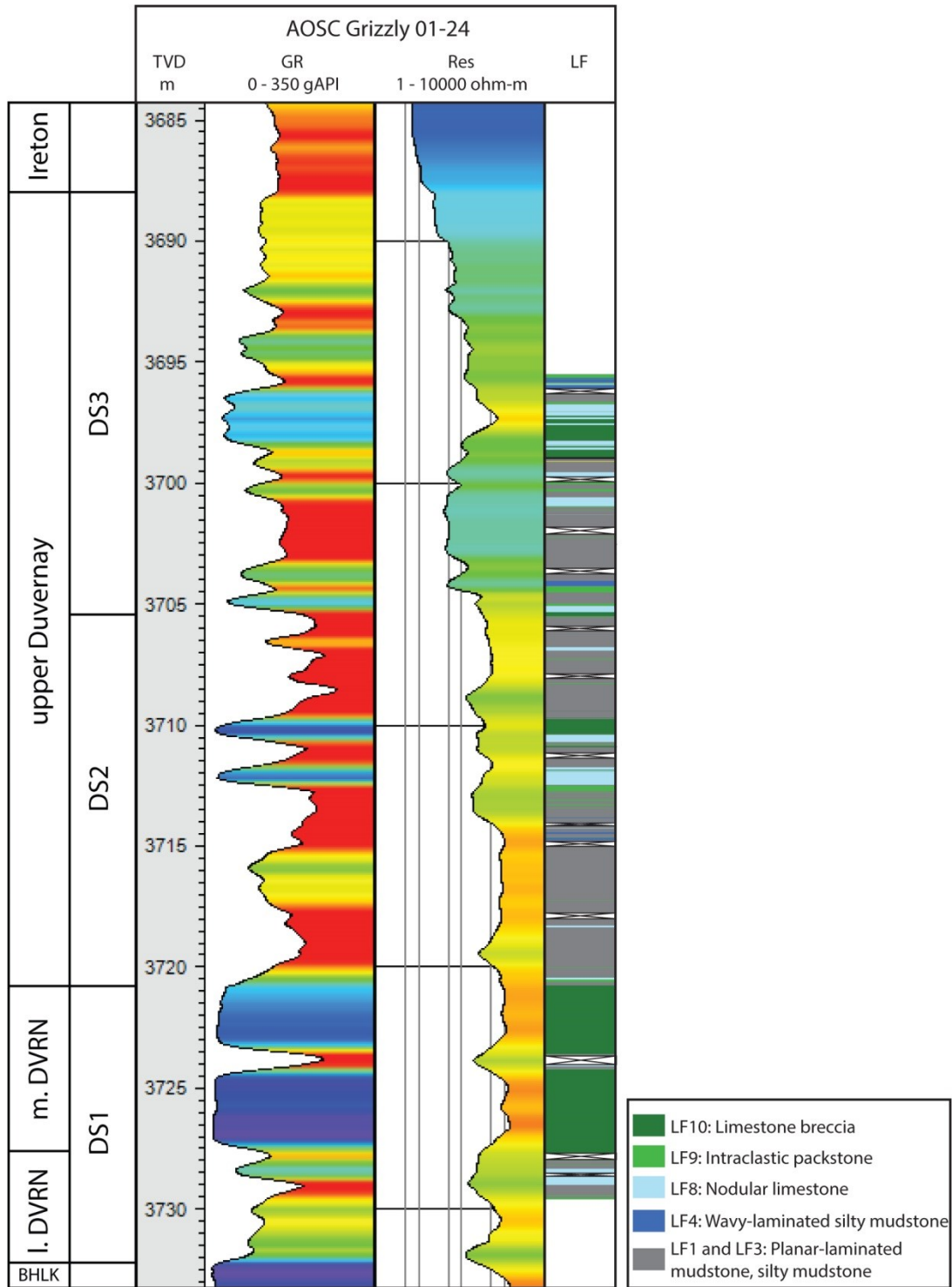


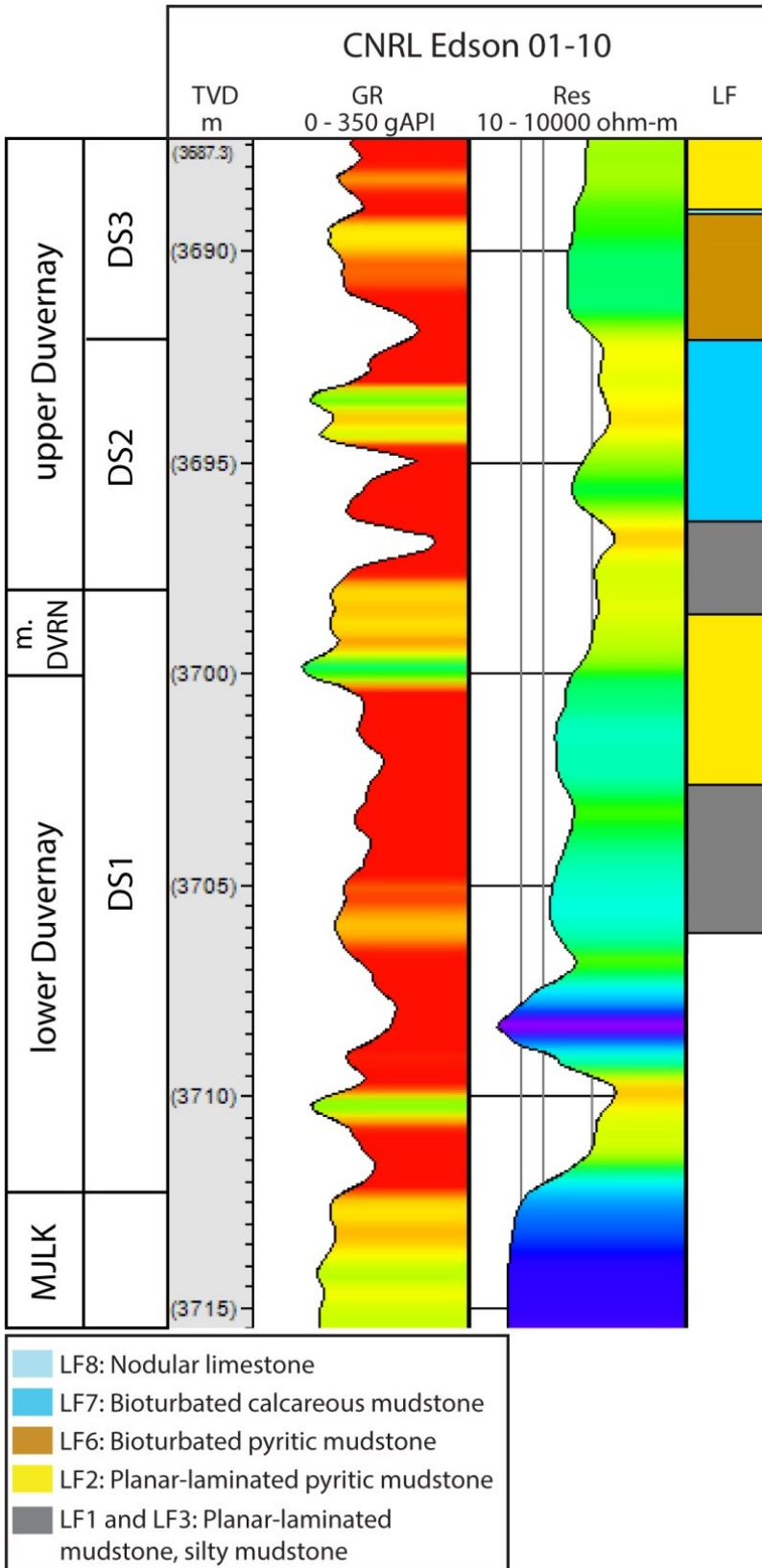


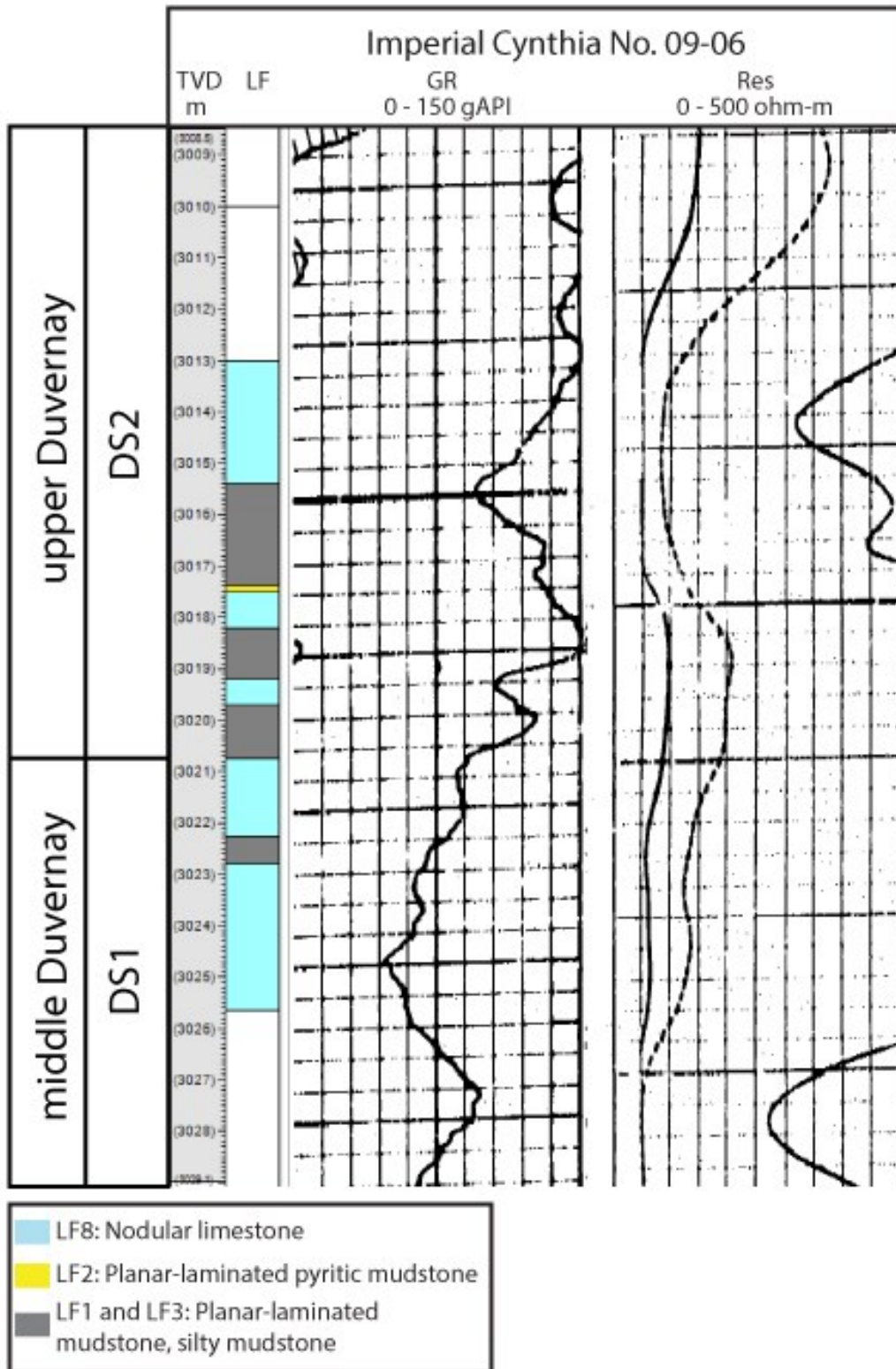


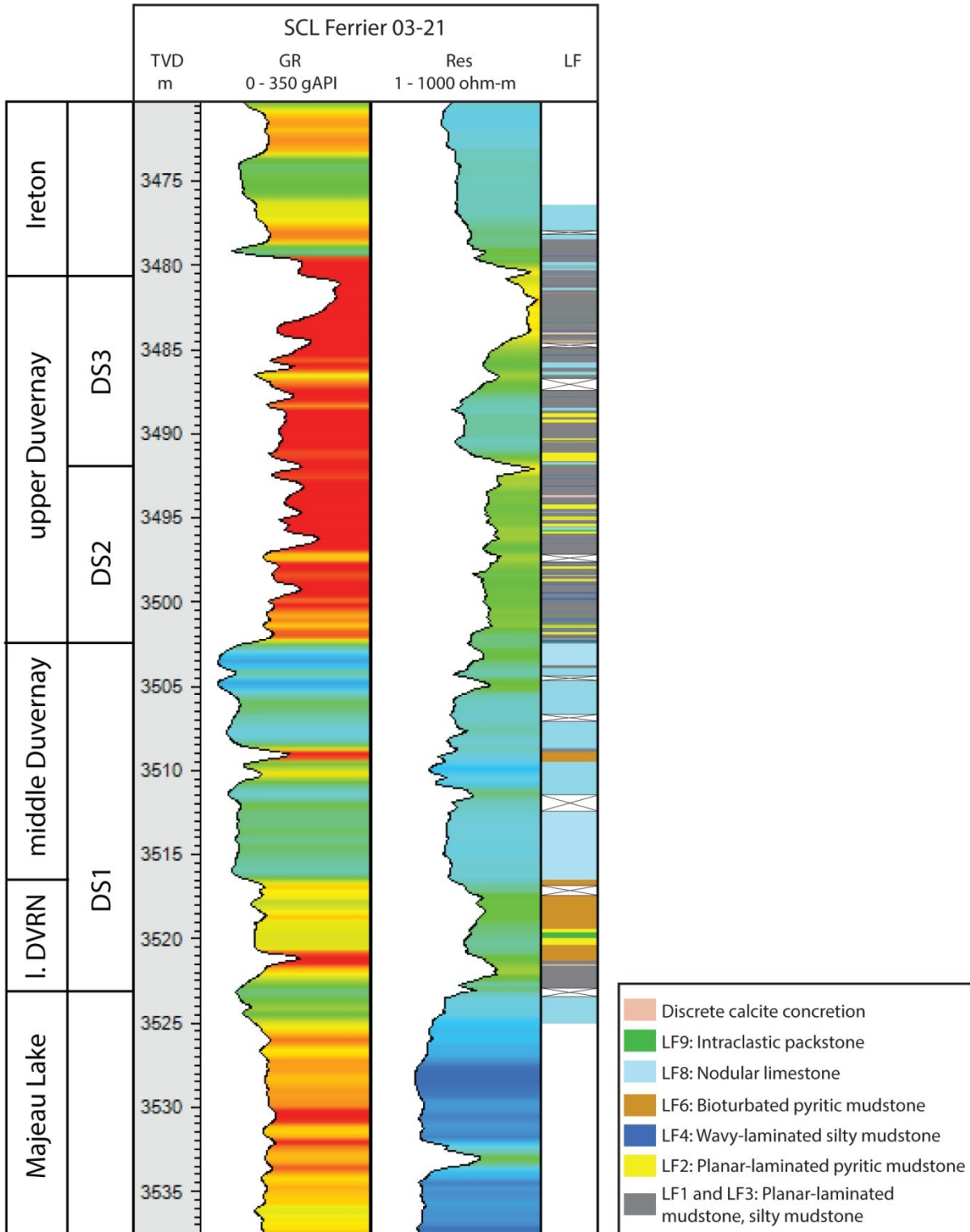


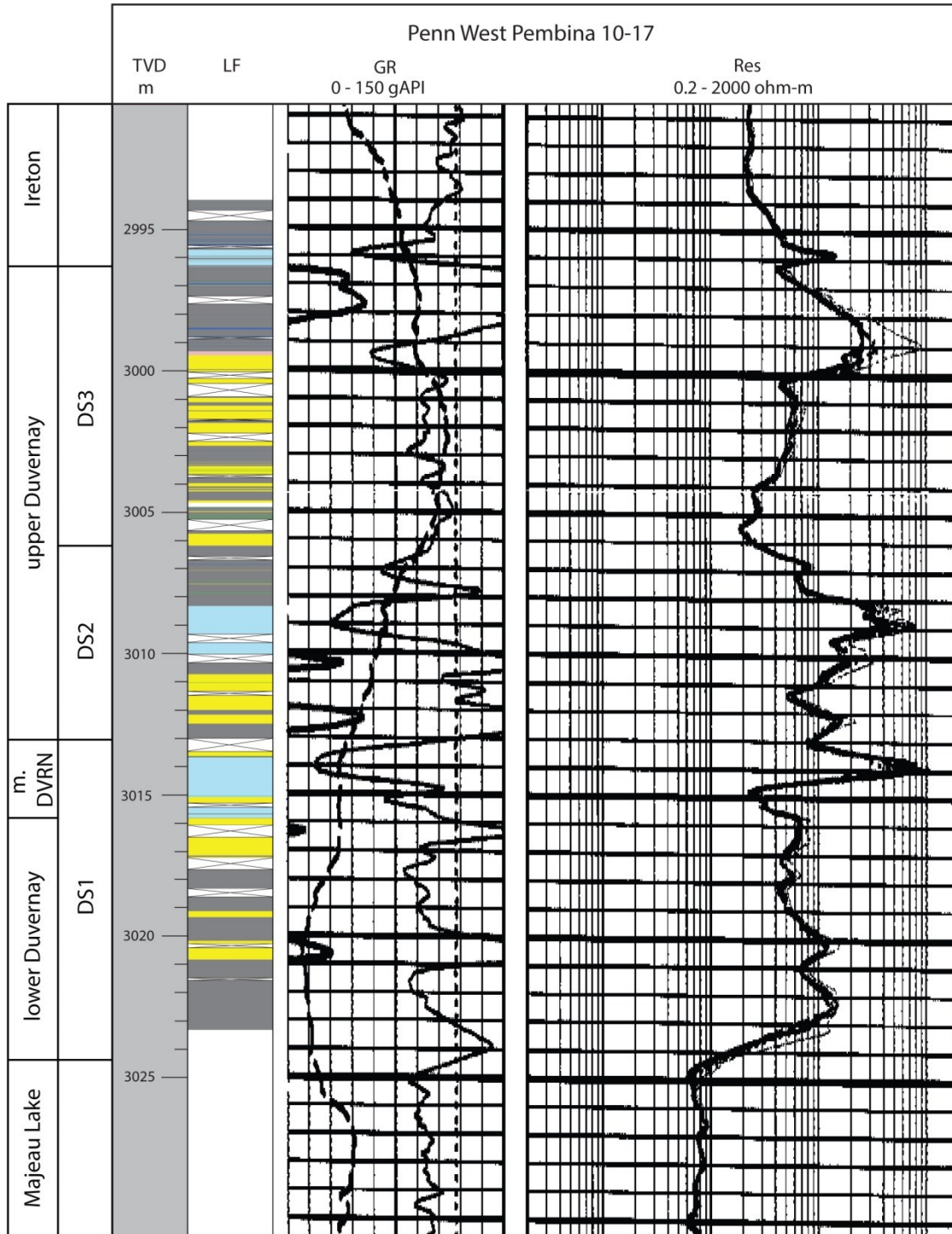
- LF10: Limestone breccia
- LF8: Nodular limestone
- LF7: Bioturbated calcareous mudstone
- LF4: Wavy-laminated silty mudstone
- LF1 and LF3: Planar-laminated mudstone, silty mudstone











- Discrete calcite concretion
- LF9: Intraclastic packstone
- LF8: Nodular limestone
- LF4: Wavy-laminated silty mudstone
- LF2: Planar-laminated pyritic mudstone
- LF1 and LF3: Planar-laminated mudstone, silty mudstone

